POLYMER BLENDS FOR DRUG RELEASE SYSTEMS

EDITED BY: Nafisa Gull, Shahzad Maqsood Khan, Aman Ullah and Rafi Ullah Khan

PUBLISHED IN: Frontiers in Materials

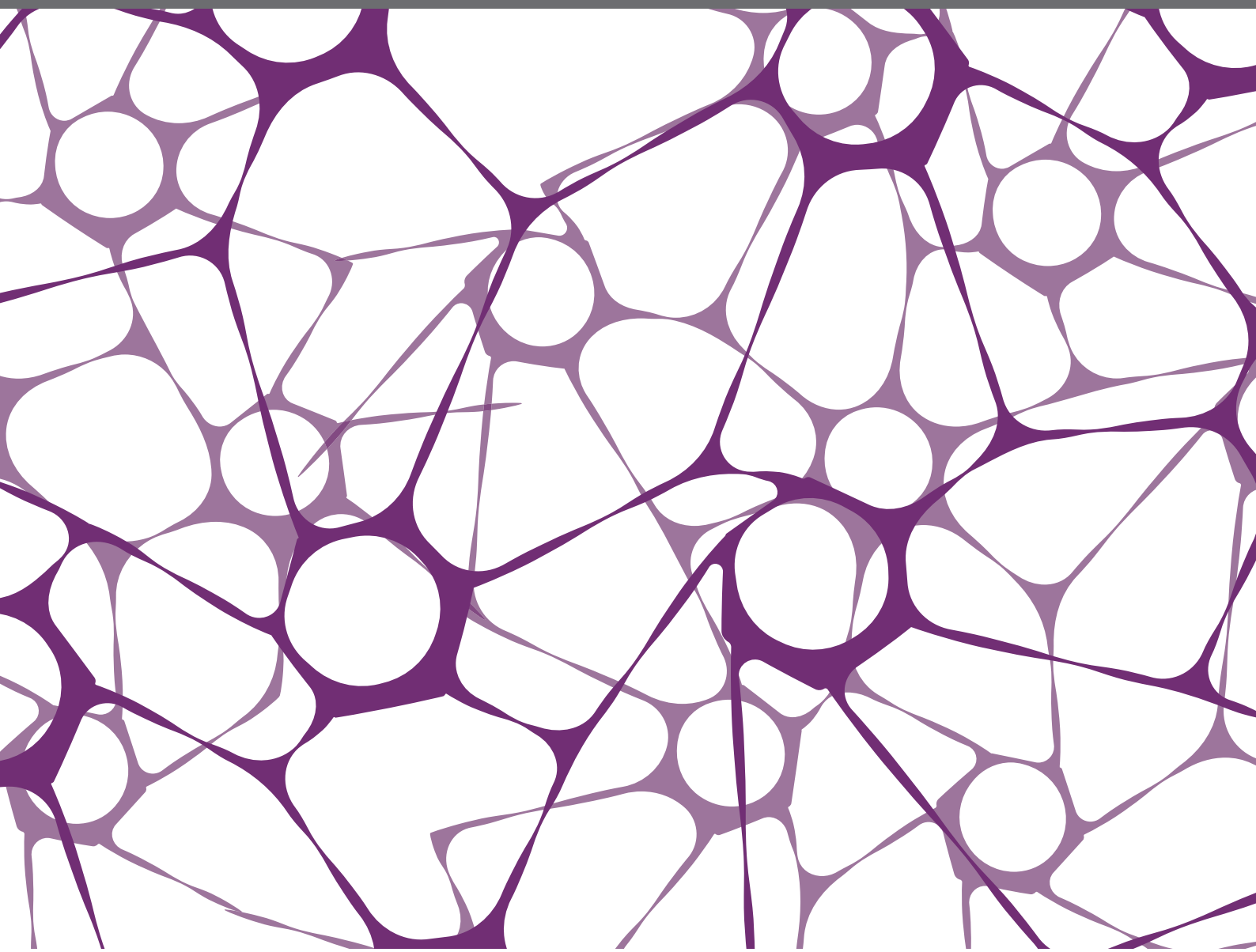

frontiers Research Topics

ISSN 1664-8714
ISBN 978-2-83250-805-3
DOI 10.3389/978-2-83250-805-3

About Frontiers

Frontiers is more than just an open-access publisher of scholarly articles: it is a pioneering approach to the world of academia, radically improving the way scholarly research is managed. The grand vision of Frontiers is a world where all people have an equal opportunity to seek, share and generate knowledge. Frontiers provides immediate and permanent online open access to all its publications, but this alone is not enough to realize our grand goals.

Frontiers Journal Series

The Frontiers Journal Series is a multi-tier and interdisciplinary set of open-access, online journals, promising a paradigm shift from the current review, selection and dissemination processes in academic publishing. All Frontiers journals are driven by researchers for researchers; therefore, they constitute a service to the scholarly community. At the same time, the Frontiers Journal Series operates on a revolutionary invention, the tiered publishing system, initially addressing specific communities of scholars, and gradually climbing up to broader public understanding, thus serving the interests of the lay society, too.

Dedication to Quality

Each Frontiers article is a landmark of the highest quality, thanks to genuinely collaborative interactions between authors and review editors, who include some of the world's best academicians. Research must be certified by peers before entering a stream of knowledge that may eventually reach the public - and shape society; therefore, Frontiers only applies the most rigorous and unbiased reviews.
Frontiers revolutionizes research publishing by freely delivering the most outstanding research, evaluated with no bias from both the academic and social point of view. By applying the most advanced information technologies, Frontiers is catapulting scholarly publishing into a new generation.

What are Frontiers Research Topics?

Frontiers Research Topics are very popular trademarks of the Frontiers Journals Series: they are collections of at least ten articles, all centered on a particular subject. With their unique mix of varied contributions from Original Research to Review Articles, Frontiers Research Topics unify the most influential researchers, the latest key findings and historical advances in a hot research area! Find out more on how to host your own Frontiers Research Topic or contribute to one as an author by contacting the Frontiers Editorial Office: frontiersin.org/about/contact

POLYMER BLENDS FOR DRUG RELEASE SYSTEMS

Topic Editors:
Nafisa Gull, University of the Punjab, Pakistan
Shahzad Maqsood Khan, University of the Punjab, Pakistan
Aman Ullah, University of Alberta, Canada
Rafi Ullah Khan, Independent researcher, Pakistan

Citation: Gull, N., Khan, S. M., Ullah, A., Khan, R. U., eds. (2023). Polymer Blends for Drug Release Systems. Lausanne: Frontiers Media SA.
doi: 10.3389/978-2-83250-805-3

Table of Contents

frontiers | Frontiers in Materials

TYPE Editorial
PUBLISHED 03 November 2022
DOI 10.3389/fmats.2022.1059009

OPEN ACCESS

EDITED AND REVIEWED BY
Robert Li,
City University of Hong Kong, Hong Kong SAR, China

*CORRESPONDENCE
Nafisa Gull,
nafisagull@gmail.com,
nafisagull.ipte@pu.edu.pk

SPECIALTY SECTION
This article was submitted to Polymeric and Composite Materials, a section of the journal Frontiers in Materials

RECEIVED 30 September 2022
ACCEPTED 06 October 2022
PUBLISHED 03 November 2022

CITATION
Gull N, Khan SM, Ullah A and Khan RU (2022), Editorial: Polymer blends for drug release systems.
Front. Mater. 9:1059009.
doi: 10.3389/fmats.2022.1059009

Editorial: Polymer blends for drug release systems

Nafisa Gull[1]*, Shahzad Maqsood Khan[1], Aman Ullah[2] and Rafi Ullah Khan[1]

[1]Institute of Polymer and Textile Engineering, University of the Punjab, Lahore, Pakistan, [2]Department of Agricultural, Food and Nutritional Science, Faculty of Agricultural, Life & Environmental Sciences, University of Alberta, Edmonton, AB, Canada

KEYWORDS

polymers, blend, drug release, crosslinking, hydrogel

Editorial on the Research Topic
Polymer blends for drug release systems

Controlled drug release is considered a new approach in pharmaceutical fields to reduce recurrent, severe drug reactions and to optimize efficiencies by reducing fluctuations in both the concentration and dosage of drugs. In this regard, polymer blending, where the properties of the blends are different from the individual polymers, is considered to be an attractive approach. This Research Topic presents six research articles, two mini-reviews, and one review, providing insight into this field and offering a basis for further studies.

Shirazi et al. extracted keratin from protein-based chicken feathers using reduction hydrolysis (sodium sulfide). Nanogel composites comprising different ratios of keratin and Tragacanth gum were produced using a chemical crosslinking method. Cinnamon (5 and 10%), as an antibacterial herbal extract, was subsequently added to the nanogels which were then coated on cotton fabric. Finally, different properties of the prepared nanogels were evaluated to assess their suitability for drug delivery in wound dressings and medical textiles. Ghasemiyeh et al. provided an overview on polymer blends that can be used as release-modulating tools in drug delivery. Firstly, different types of polymers and their various applications in biomedical sciences were discussed, and smart or stimuli-responsive polymers were introduced and categorized based on their nature. Secondly, the rationale for polymer blending in drug delivery systems was discussed. Different types of polymer blends, including physical mixtures, core-shell polymeric carriers, and block copolymers were summarized, with a focus on the effect of polymer blending on encapsulated drug release profiles. Finally, the impact of each blending approach on the drug release profiles and the kinetics of drug release were discussed in tabular format.

Raza et al. proposed a state-of-the-art irradiation technology for the fabrication of hydrogels and studied their applications in drug release systems. Irradiation crosslinking of polymers is considered to be a safe method for the fabrication of hydrogels because crosslinking occurs without the addition of unnecessary toxic reagents such as initiators

or crosslinkers. This technology is a useful way to sterilize and crosslink in a single step. Several different combinations of natural and synthetic polymers can be crosslinked using high-energy ionizing radiation such as electron-beam and gamma-ray irradiation. Polymeric hydrogels prepared using these techniques exhibit excellent gel fractions, swelling ratios, mechanical properties, drug loading and release characteristics, antimicrobial characteristics, and *in-vivo*/*in-vitro* cytocompatibilities. This mini-review on irradiation-crosslinked hydrogels provides excellent guidelines for new researchers to proceed further in this field.

Redondo et al. discussed the use of a composite poly (dimethylsiloxane-*block*-ε-caprolactone) copolymer coating and tricalcium phosphate as precursors for the electrophoretic deposition of compact and homogenous coatings, yielding useful substrates for hydroxyapatite growth. The authors argued that the obtained coatings exhibited an enhanced capacity to induce the precipitation of tricalcium phosphate and suggested that the chemical transformation of tricalcium phosphate into hydroxyapatite occurred *via* a dissolution–precipitation mechanism.

Buntum et al. explored the potential of a drug delivery system based on longan seed extract (LSE) incorporated in alginate/chitosan (Alg/CS) beads. The beads were prepared using an ionic gelation method *via* the interaction between protonated amino groups in CS and negatively charged carboxylic groups in Alg. The properties of the LSE-loaded Alg/CS beads, including the morphology of the beads, particle sizes, encapsulation efficiency (%EE), controlled release profile, cytotoxicity, and biocompatibility, were investigated. Based on the results, the beads can be used as drug carriers for biomedical applications. Rehmat et al. developed novel pH-sensitive, biodegradable, and antimicrobial hydrogels from the bio-macromolecule pectin, polyvinyl pyrrolidone (PVP), 3-aminopropyl (diethoxy) methylsilane (3-APDEMS), and sepiolite clay using a blending and solution-casting technique. The purified sepiolite (40 μm) was functionalized with the crosslinker 3-APDEMS (*ex-situ* modification) followed by hydrogel fabrication.

Naz et al. prepared nanofiber mats consisting of a chitosan (CTS)/polyvinyl alcohol (PVA)/halloysite nanoclay. Drug-loaded CTS/PVA/halloysite nanoclay//3-glycidyoxypropyl trimethoxysilane nanofibers were fabricated using an electrospinning method. The electrospun nanofiber samples were characterized using Fourier transform infrared spectroscopy (FTIR), scanning electron microscopy (SEM), and thermogravimetric analysis (TGA). These drug-loaded nanofibers are proposed to be used in different clinical applications.

Manna et al. synthesized matrix-type transdermal glibenclamide patches using a combination of hydrophilic and hydrophobic polymers and utilized them to investigate the efficacy of transdermal carriers. The matrix-type transdermal patches were developed using a solvent-casting technique by dissolving a hydrophilic and a hydrophobic polymer. HPMC E50 was selected as the hydrophilic matrix-forming polymer and was combined with the hydrophobic Eudragit RS 100. The authors concluded that the developed formulations may be superior alternatives to the conventional oral delivery of glibenclamide. Aktas et al. explored the specific pathways associated with the fabrication of polymeric organic hydrogels in order to develop novel biomaterials for pharmaceutical, medical, and drug-delivery platforms. This short review focused on a number of pioneering, prospective organo-hydrogels, particularly those useful in clinical therapy. The review also discussed their biodegradable, target-responsive properties for use as sensing components in novel microscale apertures. The authors expect that these organogels will be increasingly utilized in the coming years because of their unique characteristics such as biocompatibility, facile tunability, and tailorability using chemical modifications. These properties enable organogels to be potentially applied in a vast array of applications such as drug delivery, anti-icing, anti-fouling, food processing, and so on.

Author contributions

All authors listed have made a substantial, direct, and intellectual contribution to the work and approved it for publication.

Conflict of Interest

The authors declare that the research was conducted in the absence of any commercial or financial relationships that could be construed as a potential conflict of interest.

Publisher's note

frontiers in Materials

ORIGINAL RESEARCH
published: 16 September 2021
doi: 10.3389/fmats.2021.720385

Production and Characterization of Keratin/Tragacanth Gum Nanohydrogels for Drug Delivery in Medical Textiles

Nazanin Mansouri Shirazi, Niloofar Eslahi and Adeleh Gholipour-Kanani*

Department of Textile Engineering, Science and Research Branch, Islamic Azad University, Tehran, Iran

Keratin protein has been applied for biomedical applications due to its biocompatibility, biodegradability, mechanical resistance, and bioavailability. Tragacanth gum (TG) as a polysaccharide-based biopolymer has wound healing and antimicrobial properties. In this study, keratin was extracted from protein-based chicken feather by using reduction hydrolysis (sodium sulfide), and nanogels of keratin and TG composites at different ratios were produced by using the chemical cross-linking method. Then, cinnamon (5 and 10%) as an antibacterial herbal extract was added to the nanogels and coated on cotton fabric. The morphology and size of the composite nanogels, chemical structure, biological, and antibacterial properties were evaluated. According to DLS results, TGK2:1 (ratio of TG to keratin = 2:1) had the minimum size (80 nm) and PDI (0.1), and therefore, this sample was chosen as the optimum one. FESEM and TEM images showed the semi-spherical shape of the produced nanogels. FTIR spectra revealed the possible hydrogen bonding between the components, and the formation of disulfide bonds after the addition of hydrogen peroxide was confirmed by XPS. After loading cinnamon into the nanogels, an increase in size was observed from 80 nm for free-nanogel to 85 and 105 nm for 5 and 10% extract-loaded nanogels, respectively. Besides, more cinnamon was released from the treated fabrics by increasing time and cinnamon concentration. The antibacterial test exhibited good antibacterial properties against both Gram-positive and Gram-negative bacteria. Finally, MTT assay approved the biocompatibility of the produced nanogels for potential use in medical textiles.

Keywords: keratin, tragacanth gum, nanogel, drug delivery, medical textiles

OPEN ACCESS

Edited by:
Nafisa Gull,
University of the Punjab, Pakistan

Reviewed by:
Sharjeel Abid,
National Textile University, Pakistan
Hossam Elsayed Emam,
National Research Centre, Egypt

****Correspondence:***
Niloofar Eslahi
niloofar.eslahi@srbiau.ac.ir

Specialty section:
This article was submitted to Polymeric and Composite Materials, a section of the journal Frontiers in Materials

Received: *04 June 2021*
Accepted: *23 August 2021*
Published: *16 September 2021*

Citation:
Mansouri Shirazi N, Eslahi N and Gholipour-Kanani A (2021) Production and Characterization of Keratin/Tragacanth Gum Nanohydrogels for Drug Delivery in Medical Textiles. Front. Mater. 8:720385. doi: 10.3389/fmats.2021.720385

INTRODUCTION

Hydrogels are hydrophilic three-dimensional networks that swell in contact with water but do not dissolve. They come in many forms, including sheets, microparticles, nanoparticles, coating structures, and films. For this reason, hydrogels can be used in diverse research areas including sensors, tissue engineering, and biomolecular separation (Amin et al., 2009). Nanogels or hydrogel nanoparticles are ideal candidates for target-specific delivery of drugs due to their high drug loading capacity, biocompatibility, biodegradability, and improved cellular uptake efficiency (Chacko et al., 2012; Cheng et al., 2013; McKenzie et al., 2015). Nanogels could be used as drug delivery vehicles capable of protecting the encapsulated drugs from the physiological environment and releasing them in the targeted tissues with meliorated permeability and retention effect (Sun et al., 2017).

Keratin is a natural protein with a cysteine-rich structure. It is found in different sources such as human hair, wool, feathers, horns, and nails and produced in various forms such as film, sponge, powder, and hydrogel. Bird feathers, as one of the important sources of keratin having disulfide bonds, hydrogen bonds, and hydrophobic interactions, can be used in biomedical applications (Eslahi et al., 2013). In addition, due to the presence of various functional groups, such as carboxyl, amid, or sulfhydryl, keratin could be easily modified with biomolecules to enhance its stability, solubility, as well as biocompatibility for drug carrier applications (Cilurzo et al., 2013). For instance, Li et al. (2012) synthesized keratin-g-PEG copolymers with dual triggerable release properties for cancer therapy. Cheng et al. (2018) studied keratin nanoparticles for controlled mucoadhesion and drug release. In another study, Sun et al. (2017) produced stimuli-responsive keratin-alginate nanogels as a drug carrier for doxorubicin hydrochloride (DOX). Zhang & Lui (2019) also investigated keratin-based nanoparticles for tumor intracellular DOX delivery. The results showed pH and reduction of dual-triggered drug release with enhanced antitumor efficacy.

In recent years, tragacanth gum (TG) has been used as a superabsorbent hydrogel, antimicrobial nanocapsules, wound dressings, skin scaffolds, and drug release systems (Meghdadi & Boddohi 2019; Zare et al., 2019). Tragacanth gum is a natural polysaccharide obtained from different species of *Astragalus* plant. This polysaccharide comprises an insoluble but a water-swellable fraction called bassorin and a water-soluble fraction called tragacanthin. In addition, the active ingredients in TG help to produce collagen and improve wound healing (Ghayempour et al., 2016). Pathania et al. (2018) fabricated TG nanohydrogels using microwave radiations for the controlled release of ampicillin. Besides, Verma et al. (2020) evaluated TG-lecithin core-shell nanogels by nanoemulsion process, in which cisplatin was encapsulated into the TG core of the nanogels.

Cinnamon is a natural preservative and flavoring material, which can be used as an interesting substitute for other chemical preservatives. Literature review showed that cinnamon can inhibit the growth of molds, yeasts, and bacteria (Matan et al., 2006). Cinnamon extract (CE) has diverse biological functions including antimicrobial, anti-inflammation, antioxidant, antidiabetic, and antitumor activity (Kwon et al., 2010). In spite of the significant antibacterial activity of CE, it is highly unstable and volatile. To overcome this issue, CE is encapsulated in composite hydrogels as promising long-term antibacterial materials with a sustained release profile. It is worth mentioning that although essential oils are prominent inhibitors of microorganisms, there is a limitation in their application due to their uncontrollable release. Some approaches such as designing mesoporous composites have been performed for the controlled release of essential oils (Abdelhameed at al. 2021).

Promoting the textile properties in different fields such as protective textile is of an interest and has been progressively considered especially in medical textiles. Recently, a novel technique has been reported by Emam et al. (2020) in which multifunctional textiles were prepared *via* incorporation of silicate and zeolitic imidazole frameworks on cotton fabric with durable protective activity against solar radiation as well as microbial pathogens.

The main goal of this research is to improve the drug-releasing property of textiles with the help of smart nanohydrogels. Despite several studies on keratin and polysaccharides, the fabrication of keratinpolysaccharide nanogels is still a challenge owing to the long molecular chains and strong hydrophilic interactions involved, which result in troubles in the formation of uniform-sized nanoparticles. To the best of our knowledge, the production of keratin and TG composite nanogels has not been reported yet. In this study, keratin was extracted from protein-based chicken feather by using reduction hydrolysis, and nanogel of keratin and TG was produced by using the chemical cross-linking method. Then, cinnamon as an antibacterial herbal extract was added to the nanogels, and the loaded nanogels were padded onto the cotton fabric. Finally, the fabricated composite hydrogels were tested by different analyses.

MATERIALS AND METHODS

Materials

White broiler chicken feathers were provided by a slaughterhouse in Iran. TG and cinnamon extract were supplied by the domestic market and Morvarid Farm Co. (Iran), respectively. Other chemicals such as sodium sulfide and hydrogen peroxide were of analytical grade and obtained from Merck Co., (Germany). 100% cotton fabric (145 g/m2) was also utilized as the textile substrate.

Extraction of Keratin

At first, feathers were washed with 1 g/L nonionic detergent and 1% sodium carbonate at liquid-to-goods ratio (L:G) of 40:1at 60°C for 30 min. Afterwards, they were treated with 80% methanol for 2 h to remove grease, then dried, and cut to 2–5 mm. Keratin was extracted from the cleaned feathers by using 10 g/L sodium sulfide for 3 h at 60°C (L:G = 30:1). After filtration, the keratin solution was dialyzed against distilled water with a cellulose tube (molecular weight cutoff = 3.5 KD) for 48 h with frequent water replacement. The purified keratin solution was concentrated by a rotary evaporator and finally freeze-dried to get feather keratin powder.

Fabrication of Composite Nanohydrogels

The produced keratin powder was mixed with TG in 40 ml distilled water under N_2 atmosphere at different mass ratios of 1:1, 1:2, and 2:1 (TG: keratin) for 1 h. Hydrogen peroxide (2 ml) was then added to the mixtures drop by drop to induce chemical cross-linking, and the mixtures were stirred for 24 h at 37°C. Then, the samples were dialyzed against distilled water for 48 h to remove excess H_2O_2 and finally freeze-dried.

CE Loading Into Nanohydrogels and Coating on Cotton Fabric

After determining the optimum ratio of the components, two different amounts of CE (5 and 10%) as an antibacterial herbal extract were added to the blend of TG and keratin before chemical

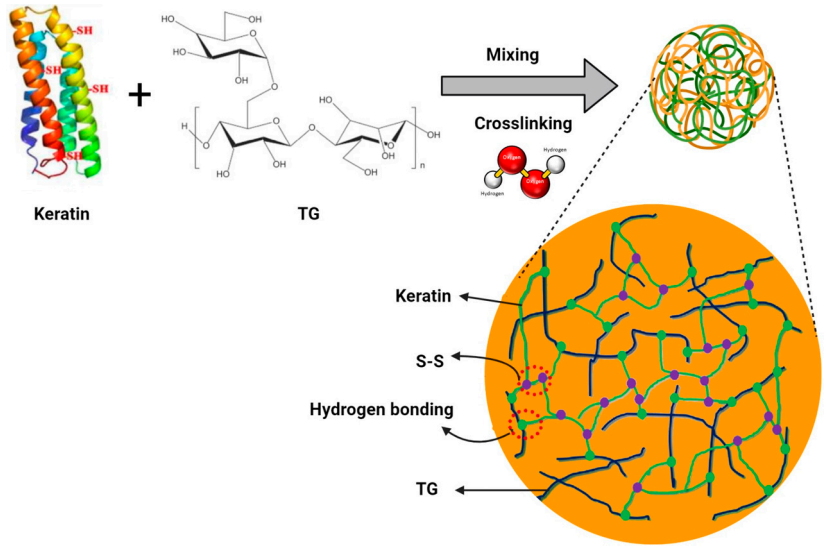

SCHEME 1 | Schematic illustration of TGK nanogels synthesized by chemical cross-linking.

cross-linking. The rest of steps were done according to the same procedure for the fabrication of composite nanogels. The supernatant was characterized *via* absorption spectra by UVVis spectroscopy (DR 5000™ UVVis Spectrophotometer, United States) at λ = 674 nm. CE loading content (CL) and encapsulation efficiency (E) of the nanogels were calculated by using the following equations:

$$CL = W_{CE.L}/W_{CE.TGK} \times 100 \quad (1)$$

$$E = W_{CE.L}/W_{CE.F} \times 100 \quad (2)$$

where $W_{CE.L}$, $W_{CE.TGK}$, and $W_{CE.F}$ are the weight of CE in the nanogels, the total weight of CE-loaded TGK nanogels, and the weight of feeding CE, respectively (Sun et al., 2018). Finally, the cotton fabrics (5 × 5 cm) were immersed in the prepared CE-loaded nanogels for 24 h and then dried in open air.

Characterization of Nanohydrogels

Physicochemical Properties

Morphological investigation of the prepared nanohydrogels was performed by field emission scanning electron microscopy (FESEM, Zeiss EM900, Germany) at an acceleration voltage of 20 kV as well as TEM (Zeiss, EM10C, Germany) at 100 kV. The size distribution and zeta potential of the nanoparticles were examined by dynamic light scattering (ZEN3600, Malvern, United Kingdom). For this test, the samples were dispersed in PBS (1 mg/ml) and sonicated with Ultrasonic Homogenizer (Misonix, S3000) at 20 kHz for 10 min. The chemical structure of the nanohydrogels was also investigated by Fourier transform infrared spectroscopy (FTIR, Thermo Nicolet Nexus 870, United States) using KBr pellets in the wavenumber range of 4,000–400 cm^{-1}. XPS was performed using an X-ray photoelectron spectrometer (Bes Tec, Germany) with Al Kα X-ray source (1,486.6 eV), and high-resolution binding energy regions for carbon (C1s) and sulfur (S2p) were investigated.

Release Study

To study the release percentage of the CE from the treated fabrics, the samples (3 × 3 cm) were precisely cut and then immersed in PBS (pH 7.4). At certain time intervals (0.5, 1, 2, 4, 8, 12, 24, 48, 72, 96, 120, 144, 168, 192 h), the incubation medium (2 ml) was removed and replaced with fresh PBS. This procedure was repeated twice. The amount of released cinnamon was then quantified by UVVis spectroscopy (DR 5000™ UVVis Spectrophotometer, United States) at λ = 674 nm.

Antibacterial Test

The antimicrobial activity of the CE-loaded nanohydrogel was assessed by agar well diffusion method. For this purpose, bacteria were transported to Mueller Hinton Broth medium and put in an incubator at 37°C for 3 h to obtain 0.5 McFarland. Then, 500 ml suspension of 1.5 × 108 CFU/ml was transported to Mueller Hinton agar and cultured. Then, a hole with a diameter of 6–8 mm was punched aseptically with a sterile cork bore, and a volume (100 µl) of the nanogel was introduced into the well and incubated at 37°C. The antimicrobial agent diffused in the agar medium and inhibited the growth of the microbial strain tested. Finally, the zone of inhibition was calculated after 24 h where bacteria growth is inhibited (Debalke et al., 2018).

In vitro Assay

The biocompatibility of free and CE-loaded nanogels was assessed using the 3-(4,5-dimethylthiazol-2-yl)-2,5-diphenylte-trazolium bromide (MTT) method. L929 fibroblast cells were cultured in

TABLE 1 | Average size and PDI of different samples.

Sample codes	Size (nm)	PDI
TGK11	88	0.521
TGK12	171	0.509
TGK21	80	0.100

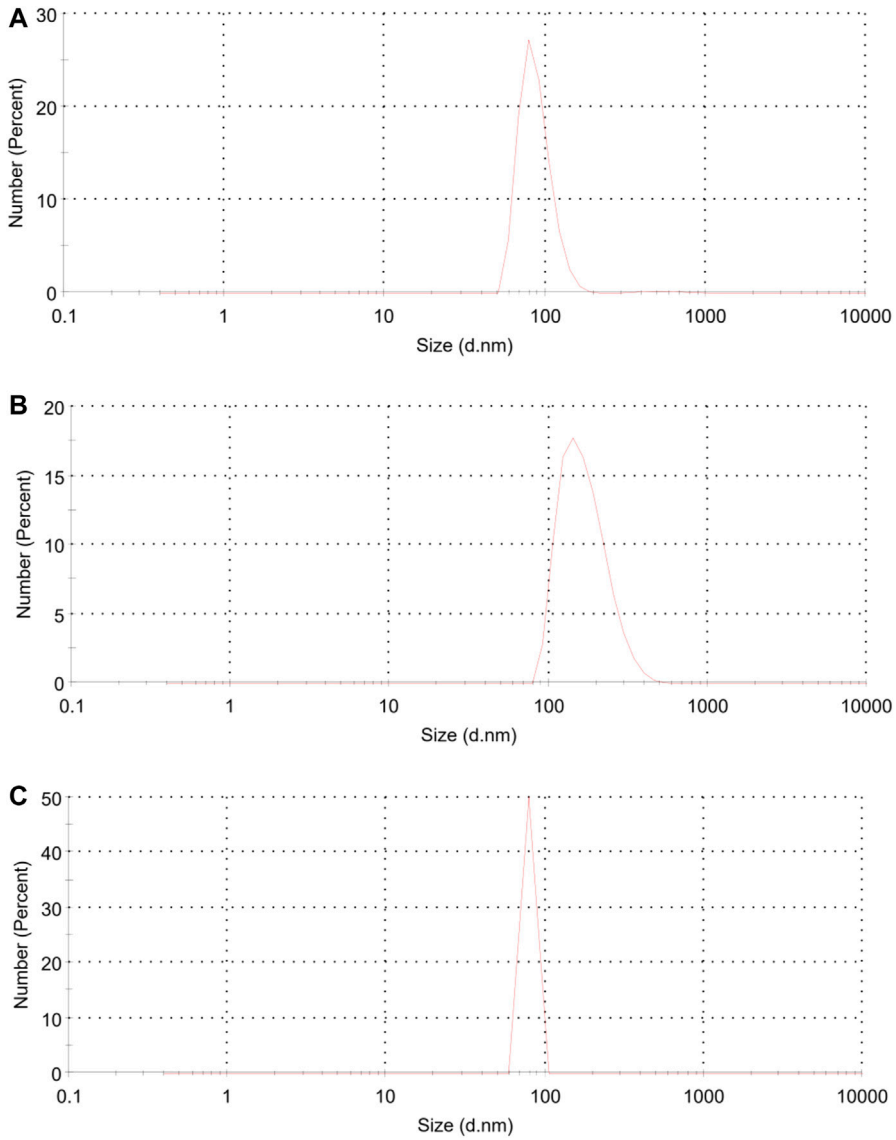

FIGURE 1 | Particle size distribution of different formulations: **(A)** TGK11, **(B)** TGK12, **(C)** TGK21.

RPMI-1640 medium containing 10% FBS, 50 U/ml penicillin, and 50 U/ml streptomycin and kept for 24 h at 37°C in a 5% CO2 humidified sterile incubator. After incubation at different times, 20 µl of 5 mg/ml MTT solution was added to each well containing the sample. Then, the MTT solution was replaced with 150 µl dimethyl sulfoxide (DMSO) and shacked for 10 min. Finally, the optical density of each well was measured at 570 nm using ELISA reader at 24, 48, and 72 h. Cell viability percentage was calculated in comparison to control sample by using the following equations:

$$\text{Toxicity } \% = \left(1 - \frac{\text{mean OD of sample}}{\text{mean OD of control}}\right) \times 100 \quad (3)$$

$$\text{Viability } \% = 100 - \text{Toxicity } \% \quad (4)$$

RESULTS AND DISCUSSION

Characterization of TG-Keratin Composite Nanohydrogels

TG-keratin composite nanohydrogels were synthesized in an aqueous solution *via* an oxidative cross-linking reaction with H_2O_2 (**Scheme 1**). The hydroxyl, carboxyl, and amino groups on keratin could form hydrogen bonds with carboxyl and hydroxyl groups on TG. After the addition of hydrogen peroxide, the thiol groups (-SH) of keratin were oxidized to form disulfide bonds, leading to keratin chain assembled, and TGK nanogels were consequently obtained. A similar mechanism was reported by Sun et al. (2018) for the formation of keratin and hyaluronan nanogels.

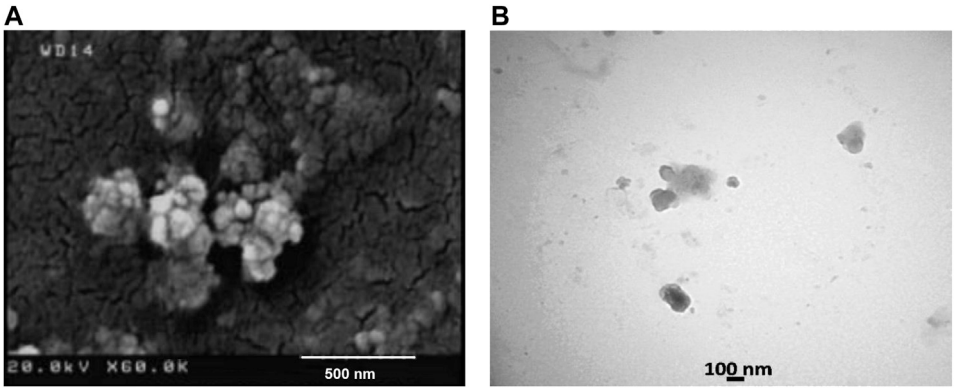

FIGURE 2 | (A): FESEM and **(B)**: TEM images of TGK21.

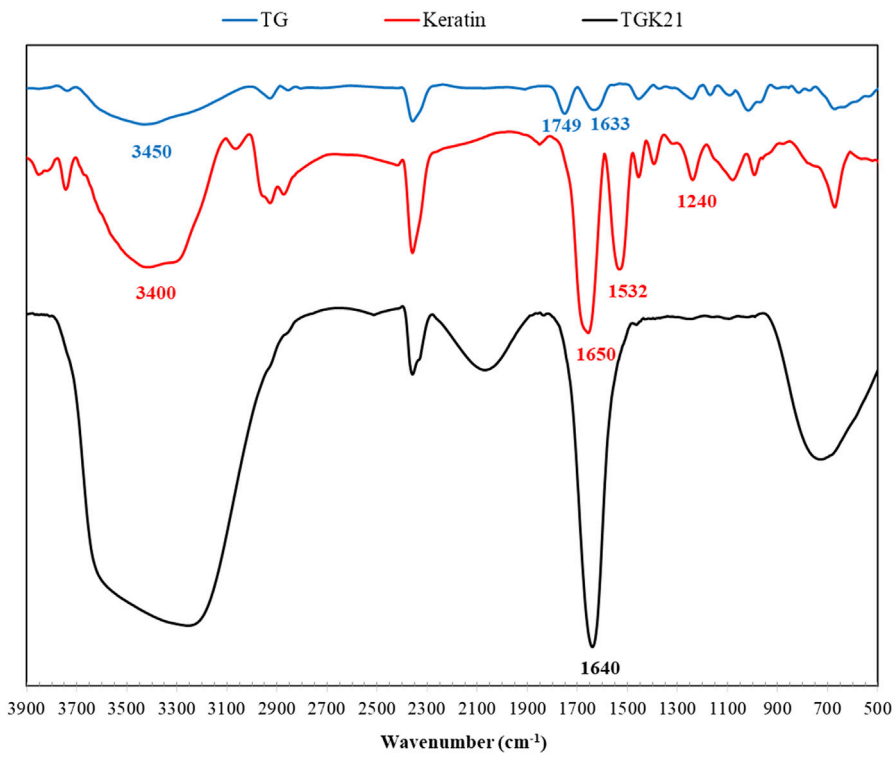

FIGURE 3 | FTIR spectra of keratin, TG, and TGK composite.

Size and Morphological Investigation

The average size as well as polydispersity index (PDI) of different formulations was measured by dynamic light scattering (DLS). **Table 1** shows that the TGK2:1 (ratio of TG to keratin = 2:1) has the minimum size and PDI and therefore this sample is chosen as the optimum one. The greater the proportion of TG, the smaller the particle size. The measured zeta potential of the fabricated nanogel was −30.2 mV, indicating suitable colloidal stability due to electric repulsion. It was assumed that the negative charge of the nanogels could be associated with the hydroxyl and carboxyl groups of keratin and TG. **Figure 1** illustrates the particle size distribution of different nanogels. The sharp peaks in DLS graphs revealed the homogenous mono dispersion of the samples. FESEM and TEM images (**Figure 2**) also depict the semi-spherical morphology of the produced nanoparticles, validating the results of DLS.

FTIR Spectroscopy

The FTIR spectra of samples are depicted in **Figure 3**. The broad absorption band in the range of 3,100–3,700 cm^{-1} is associated with the stretching vibration of N–H and O–H bonds. The peaks around 2,900 cm^{-1} are attributed to C–H stretching modes of aliphatic

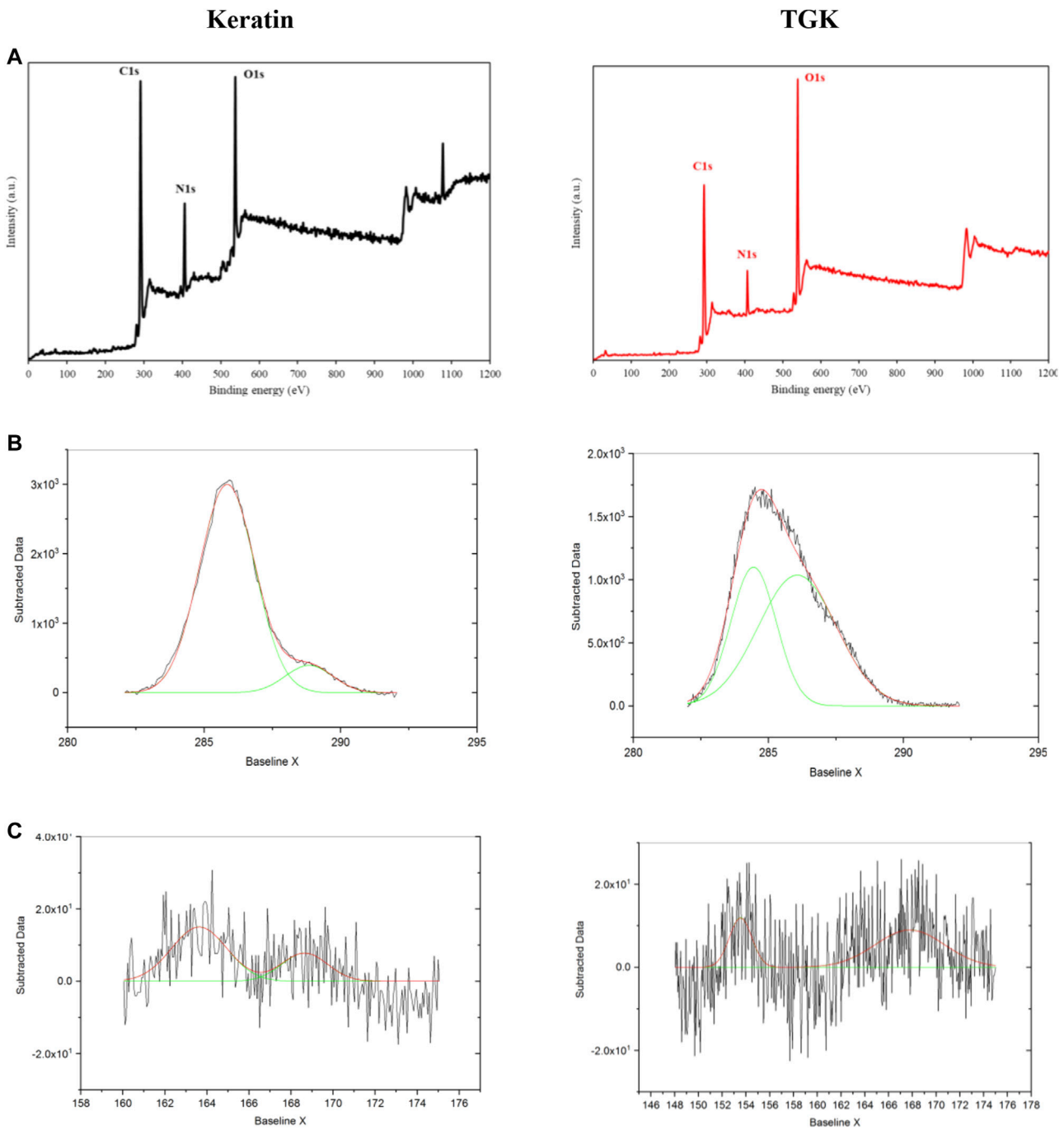

FIGURE 4 | XPS spectra of **(A)** whole regions, **(B)** C1s region, and **(C)** S2p region.

groups. As for keratin, the vibrations in the peptide bonds originate bands known as amide I, II, III. The amide I band in the range of 1700–1,600 cm^{-1} belongs to C=O stretching vibration, while the amide II appears at 1,532 cm^{-1} associated with N–H bending and C–H stretching vibration. The amide III band at 1,240 cm^{-1} is ascribed to C–N stretching and N–H in-plane bending (Eslahi et al., 2013). The spectrum of TG shows its characteristic peaks at 3,450 cm^{-1} (stretching vibration of hydroxyl groups), 2,925 cm^{-1} (the symmetric stretching of CH_2), 1749 cm^{-1} (carbonyl stretching vibration of galacturonic acid and its ester), 1,633 cm^{-1} (carboxylate stretching vibration of D-galacturonic acid), and 1,153 cm^{-1} (antisymmetric C-O-C vibrations of glycosidic groups of polysaccharides) (Fattahi et al., 2013; Singh and Sharma 2014). The FTIR spectrum of TGK composite exhibits the characteristic peaks of both TG and keratin with slight modification. For instance, the C=O stretching vibration peak at 1,650 cm^{-1} in keratin shifts to 1,640 cm^{-1}

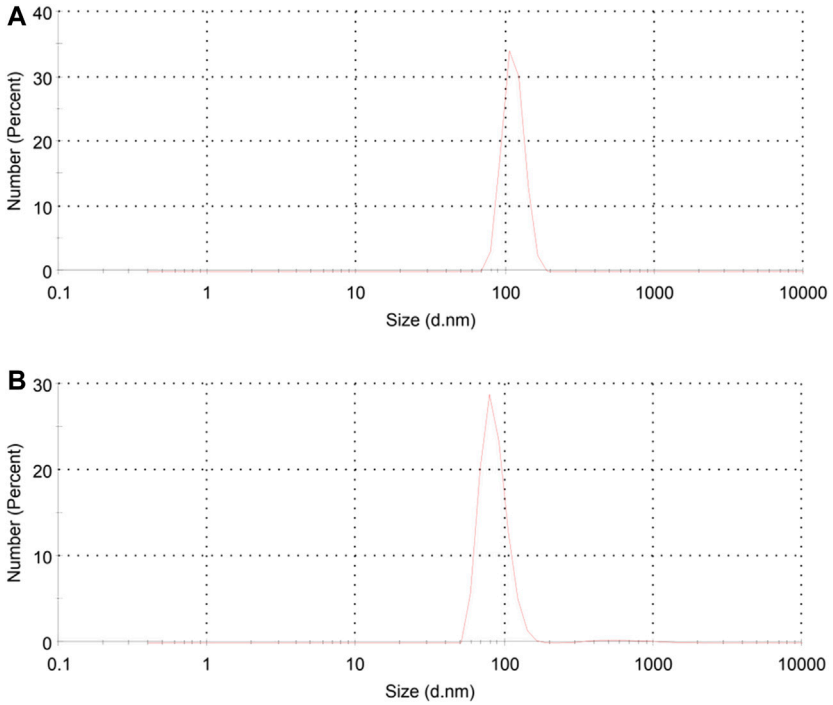

FIGURE 5 | Particle size distribution of **(A)** TGK21C5 and **(B)** TGK21C10.

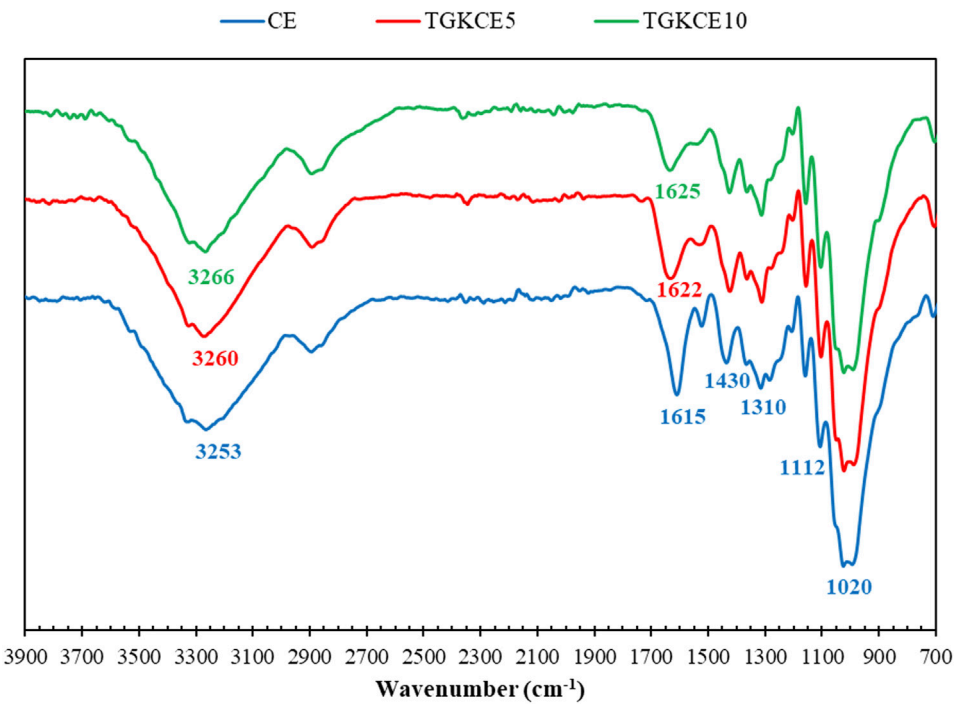

FIGURE 6 | FTIR spectra of pure CE and CE-loaded nanogels on cotton fabric.

in TGK composite. Further, the hydroxyl and carboxyl groups of TG could form hydrogen bonding with amine and carboxyl groups of keratin, which results in the broad peak in 3,000–3,700 cm^{-1} region.

XPS

XPS was employed to investigate the surface elemental composition of samples (**Figure 4**). The peaks with binding energy at 532, 400, and

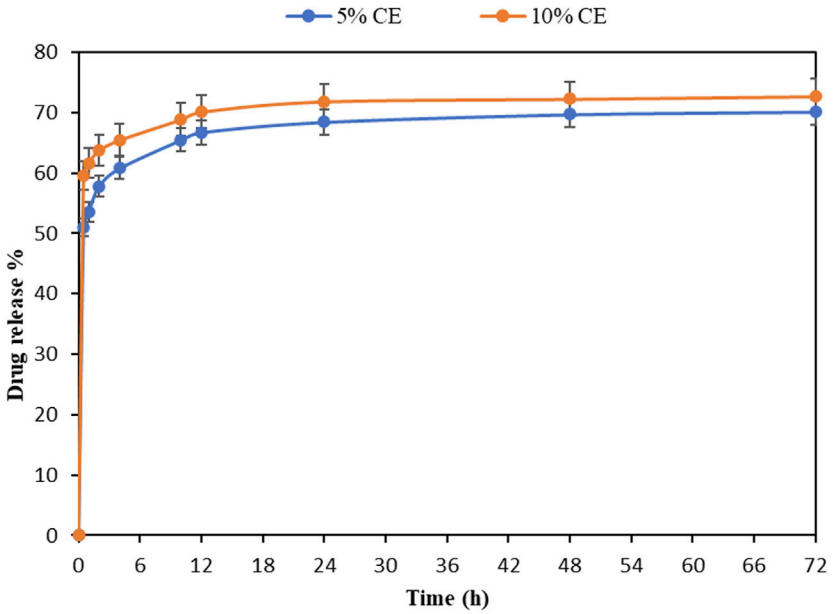

FIGURE 7 | Release profile of CE from treated cotton fabrics.

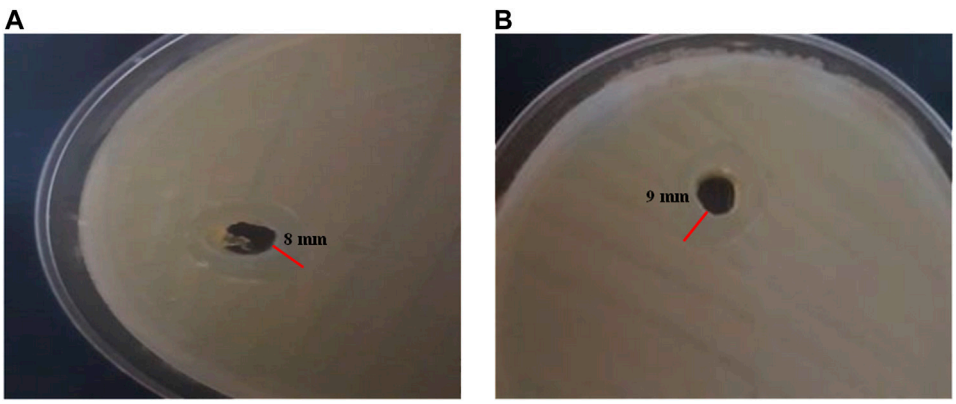

FIGURE 8 | Zone of inhibition against two bacteria: **(A)** *E. coli* and **(B)** *S. aureus*.

285 eV corresponding to oxygen (O1s), nitrogen (N1s), and carbon (C1s), respectively, represented the characteristic amino acid residues in keratin (**Figure 4A**). The distinctive elements of keratin presented in the spectra of TGK composite as well; however, the intensity of N content declined noticeably due to possible interactions of the employed polymers. An amide peak of ~288 eV (O=C–N) was observed in the high-resolution C1s region in keratin (**Figure 4B**), which was shifted to 286.1 eV in TGK. Besides, the peak at 285.8 eV (C-O, C-N) in keratin has been shifted to 284.4 (C-C, C-H) in TGK along with a decrease in the peak area (Kaur et al., 2018). In the S2p region (**Figure 4C**), a 163.6 eV peak was associated with the free thiols (-SH) in keratin (de Guzman et al., 2015). After cross-linking with H_2O_2, this peak was moved to 167.7 eV owing to the formation of disulfide bonds in TGK. It is worth mentioning that oxidative degradation of cystine disulfide S-S groups could lead to the formation of sulfur oxides -SO_3H (at ~168 eV) in keratin (Sun et al., 2017).

Characterization of CE-Loaded Nanogels

DLS

Figure 5 depicts the particle size distribution of CE-loaded TGK nanogels. The mean particle size of TGK21C5 and TGK21C10 was reported 85 and 105 nm, respectively. In comparison with the pristine TGK21 sample, it was found that the mean particles size increased after loading CE into the nanogels. The higher the amount of the extract, the bigger the sample size. This finding is in line with the study by Li et al. (2012) indicating an increase in the size of the produced nanoparticles after drug loading. It should be noted that both keratin and TG are natural macromolecules with various active groups on their molecule chain. These functional groups such as carboxyl, carbonyl, amine, and hydroxyl groups in TGK can interact

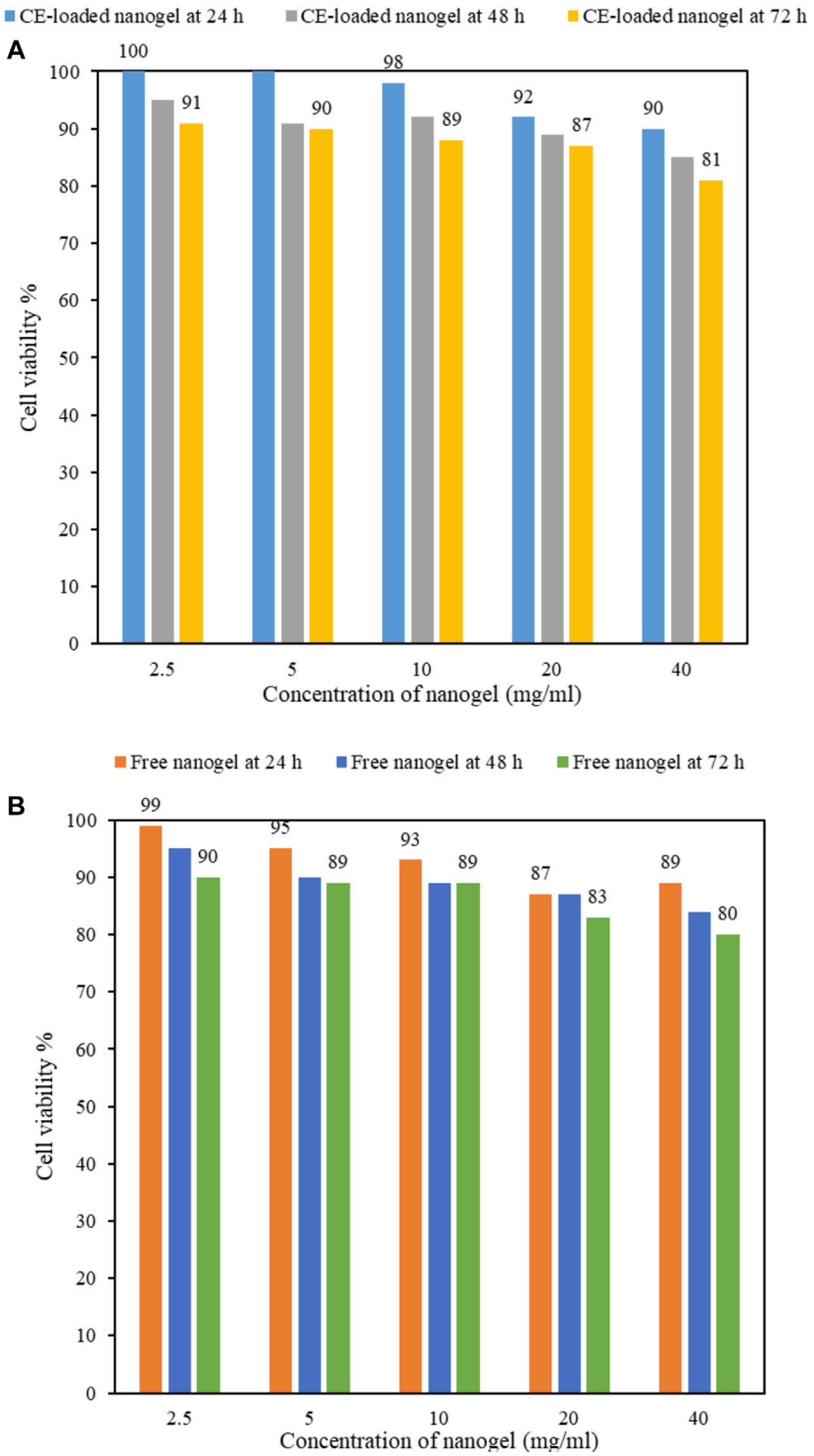

FIGURE 9 | Cell viability of nanogels **(A)** with and **(B)** without CE after 24, 48, and 72 h.

with the carbonyl and hydroxyl groups of CE *via* hydrogen bonding, which could stabilize the extract inside the nanogels leading to their growth in size. It is worth mentioning that the loading capacity of TGK nanogel was quantified by UVVis spectrophotometry, and the calculated CE loading content and encapsulation efficiency were approximately 62.7 and 42.3%, respectively. Similar results were reported by Sun et al. (2017) for keratin-alginate nanogel with enhanced drug loading efficiency.

FTIR

FTIR spectra of pure CE and CE-loaded nanogels on cotton fabrics are shown in **Figure 6**. The characteristic bands of CE exist at 1,020 cm^{-1} (deformation vibration of C-OH), 1,112 cm^{-1} (stretching vibration of C-O), 1,310 cm^{-1} (in-plane bending absorption of aromatic ring = C-H), 1,430 cm^{-1} (bending vibration of C-OH), 1,615 cm^{-1} (aromatic C=C stretching), and 3,253 cm^{-1} (O-H stretching) (Li et al., 2013; Boughendjioua et al., 2017). In the case of CE-loaded nanohydrogels, the characteristic peaks of cinnamon are vividly seen with slight movements. The peak shift from 1,615 cm^{-1} in CE to 1,622 cm^{-1} and 1,625 cm^{-1} in the nanogels loaded with 5 and 10% CE, respectively, might be owing to possible interactions between the components. The employed cotton fabric is a cellulosic-based polymer containing D-glucopyranose units linked with 1,4-glycosidic bonds. The cellulose chains are stacked together by van der Waals forces and strong intra- and/or intermolecular hydrogen bonds (Seddiqi et al., 2021). The possible hydrogen bonding between TGK, CE, and cellulose leads to the stabilization of the CE-loaded nanohydrogels on the cotton fabric.

Release Study

A good drug carrier should have the capacity to encapsulate drug molecules and release them under physiological condition sustainably (Sun et al., 2017). The release profile of encapsulated CE (5 and 10%) from treated fabrics is investigated in **Figure 7**. It can be seen that higher amount of CE was released with prolonging time, i.e., from 50 to 70% at 0.5 and 72 h for the sample containing 5% CE. Besides, more extract was released from the nanogels with higher amount of cinnamon, indicating that the release rate is related to the amount of the embedded extract. In the sample containing 10% CE, the release of about 73% occurred at the end, while in the sample containing 5% CE, 70% of CE was released at the same time point (72 h). The release curve shows a routine two-phase profile. The initial burst release may be related to the fast release of CE from the swollen nanogels, whereas the second phase (plateau after 12 h) is mainly associated with extract diffusion and hydrogel disruption. Due to the high anti-inflammatory property of the cinnamon extract (Gunawardena et al., 2015), the initial burst during the first 12 h will improve the efficiency of the nanohydrogels, especially at the first stage of wound healing. Previous studies have found that keratin-based nanogels can sustain the release of drugs and growth factors in correlation with their degradation (Li et al., 2012; Sun et al., 2017; Sun et al., 2018). In this study, as the release rate of the extract is concentration-dependent, it can be concluded that the observed release model follows the first-order kinetics model, which is in line with results obtained by Kumari and Sangal (2019). They found that the CE release from PLGA nanoparticles follows the first-order model.

Antibacterial Test

The antibacterial properties were assessed in agar medium for CE-loaded TGK nanogel against *E. coli* as a Gram-negative bacteria and *S. aureus* as a Gram-positive one. According to the obtained results in **Figure 8**, the zone of inhibition was calculated to be 9 mm for *S. aureus* and 8 mm for *E. coli*, indicating the suitable antibacterial activity of the extract in the fabricated nanogel. Literature review showed that the antibacterial activity of the CE was ascribed to the presence of cinnamaldehyde (Matan et al., 2006). It was reported that cinnamaldehyde can inhibit the production of an essential enzyme by the bacteria and disrupt the bacterial cell membrane (Helander et al., 1998; Firmino et al., 2018). Essential oils can inhibit bacterial growth activity and decrease the required active concentration of antibiotics by their synergistic activity (Sienkiewicz et al., 2014). It is worth mentioning that the L-sugars found in TG (i.e., L-arabinose and L-fucose) are responsible for the resistance to microbial attack because most organisms are unable to metabolize these foreign sugars (Ranjbar-Mohammadi and Bahrami, 2015).

Biocompatibility

The cytotoxicity of drug carriers is of great importance for their practical biomedical applications. MTT assay is one of the most commonly used colorimetric assay to evaluate cell viability through the determination of mitochondrial function of cells by measuring the activity of mitochondrial enzymes such as succinate dehydrogenase. In this assay, MTT is reduced to a purple formazan by NADH which is then quantified by its light absorbance (Aslantürk 2018). **Figure 9** exhibits the viability of nanogels with (**Figure 9A**) and without cinnamon (**Figure 9B**) at various concentrations (i.e., 2.5–40 mg/ml) using MTT assay on L929 fibroblast cells after different incubation times. As it can be seen in **Figure 9**, cell viability has decreased with increasing nanogels content, e.g., from 100 to 90% for 2.5 and 40 mg/ml CE-loaded nanogels at 24 h, respectively (**Figure 9A**); however, at all concentrations (even at relatively high concentrations up to 40 mg/ml), cell viability above 80% is obtained, implying the good biocompatibility of the fabricated TGK nanogels. This dose-dependent decrease in the viability was also studied by other researchers as well (Li et al., 2012). It is worth mentioning that both keratin and TG are biocompatible and biodegradable biopolymers that have been widely studied in biomedical applications. Keratin biomaterials have the capability to support cellular attachment and proliferation due to the presence of cell-binding motifs in the protein structure (Feroz et al., 2020). TG as a nonallergenic, nontoxic, and noncarcinogenic polysaccharide has also shown an improvement in the cell viability, attachment, and proliferation of fibroblast cells (Taghavizadeh Yazdi et al., 2021). As for cinnamon, Xie et al. (2018) reported that CE inhibited tumor cell proliferation in a dose-dependent manner. They found that anticancer properties of cinnamon were mediated by both downregulated their target cell cycle regulation molecules and mitosis regulation molecules.

As for the effect of time, with prolonging incubation time from 24 to 72 h, there is a reduction in cell viability in all the specimens, e.g., in 10 mg/ml free-nanogel from 93 to 89% at 24 and 72 h, respectively (**Figure 9B**). Moreover, an enhancement in cell viability was observed after cinnamon loading into the nanogels (e.g., at 24 h, from 93 to 98% for 10 mg/ml free-nanogel (**Figure 9B**) and CE-loaded nanogel (**Figure 9A**), respectively), owing to its high biological and antimicrobial properties (Sienkiewicz et al., 2014).

CONCLUSION

In this study, keratin was extracted from poultry feathers and mixed with TG to produce TGK nanogels at different ratios (keratin to TG: 1:1, 2:1, and 1:2). Then, CE (5 and 10%) was encapsulated into the nanogels, and the optimum sample was coated on cotton fabrics. DLS results showed an optimum sample size of approximately 80 nm for TGK21. According to TEM and FESEM images, spherical nanoparticles were formed. FTIR revealed possible interactions between the components in the composite. Moreover, the formation of disulfide bonds after cross-linking was confirmed by XPS. The mean size of the nanogel was increased from 80 to 85 and 105 nm after 5 and 10% loading of CE, respectively. The release profile of the extract from the treated fabrics was studied, and the results demonstrated a first-order release model. The antimicrobial test revealed that the incorporated extract showed proper antibacterial properties against both Gram-negative and Gram-positive bacteria. Results of MTT assay confirmed the biocompatibility of the nanogels indicating their potential applications in wound dressings and medical textiles.

DATA AVAILABILITY STATEMENT

The original contributions presented in the study are included in the article/supplementary material, further inquiries can be directed to the corresponding author.

AUTHOR CONTRIBUTIONS

NE contributed to conception and design of the study. NM performed experiments and analysis. NM and NE wrote the first draft of the manuscript. NE and AG-K performed data analysis. AG-K revised sections of the manuscript. All authors contributed to manuscript revision and approved the submitted version.

REFERENCES

Abdelhameed, R. M., Alzahrani, E., Shaltout, A. A., and Emam, H. E. (2021). Temperature-controlled-release of Essential Oil via Reusable Mesoporous Composite of Microcrystalline Cellulose and Zeolitic Imidazole Frameworks. *J. Ind. Eng. Chem.* 94, 134–144. doi:10.1016/j.jiec.2020.10.025

Amin, S., Rajabnezhad, S., and Kohli, K. (2009). Hydrogels as Potential Drug Delivery Systems. *Sci. Res. Essays.* 4, 1175–1183. doi:10.5897/SRE.9000559

Aslantürk, Ö. S. (2018). "*In Vitro* cytotoxicity and Cell Viability Assays: Principles, Advantages, and Disadvantages," in *Genotoxicity-A Predictable Risk to Our Actual World*, 64–80. doi:10.5772/intechopen.71923

Boughendjioua, H., Amoura, N., and Boughendjioua, Z. (2017). Purity Specifications of Constituents of Cinnamon Essential Oil by Fourier Transformed Infrared Spectroscopy Analysis. *Ijpbr* 5, 36–40. doi:10.30750/ijpbr.5.2.7

Chacko, R. T., Ventura, J., Zhuang, J., and Thayumanavan, S. (2012). Polymer Nanogels: A Versatile Nanoscopic Drug Delivery Platform. *Adv. Drug Deliv. Rev.* 64, 836–851. doi:10.1016/j.addr.2012.02.002

Cheng, R., Meng, F., Deng, C., Klok, H.-A., and Zhong, Z. (2013). Dual and Multi-Stimuli Responsive Polymeric Nanoparticles for Programmed Site-specific Drug Delivery. *Biomaterials* 34, 3647–3657. doi:10.1016/j.biomaterials.2013.01.084

Cheng, Z., Chen, X., Zhai, D., Gao, F., Guo, T., Li, W., et al. (2018). Development of Keratin Nanoparticles for Controlled Gastric Mucoadhesion and Drug Release. *J. Nanobiotechnol.* 16, 24. doi:10.1186/s12951-018-0353-2

Cilurzo, F., Selmin, F., Aluigi, A., and Bellosta, S. (2013). Regenerated Keratin Proteins as Potential Biomaterial for Drug Delivery. *Polym. Adv. Technol.* 24, 1025–1028. doi:10.1002/pat.3168

de Guzman, R. C., Tsuda, S. M., Ton, M.-T. N., Zhang, X., Esker, A. R., and Van Dyke, M. E. (2015). Binding Interactions of Keratin-Based Hair Fiber Extract to Gold, Keratin, and BMP-2. *PLoS One* 10, e0137233. doi:10.1371/journal.pone.0137233

Debalke, D., Birhan, M., Kinubeh, A., and Yayeh, M. (2018). Assessments of Antibacterial Effects of Aqueous-Ethanolic Extracts of Sida Rhombifolia's Aerial Part. *Scientific World J.* 2018, 1–8. doi:10.1155/2018/8429809

Emam, H. E., Darwesh, O. M., and Abdelhameed, R. M. (2020). Protective Cotton Textiles via Amalgamation of Cross-Linked Zeolitic Imidazole Frameworks. *Ind. Eng. Chem. Res.* 59, 10931–10944. doi:10.1021/acs.iecr.0c01384

Eslahi, N., Dadashian, F., and Nejad, N. H. (2013). An Investigation on Keratin Extraction from Wool and Feather Waste by Enzymatic Hydrolysis. *Prep. Biochem. Biotechnol.* 43, 624–648. doi:10.1080/10826068.2013.763826

Fattahi, A., Petrini, P., Munarin, F., Shokoohinia, Y., Golozar, M. A., Varshosaz, J., et al. (2013). Polysaccharides Derived from Tragacanth as Biocompatible Polymers and Gels. *J. Appl. Polym. Sci.* 129, 2092–2102. doi:10.1002/app.38931

Feroz, S., Muhammad, N., Ratnayake, J., and Dias, G. (2020). Keratin - Based Materials for Biomedical Applications. *Bioactive Mater.* 5, 496–509. doi:10.1016/j.bioactmat.2020.04.007

Firmino, D. F., Cavalcante, T. T. A., Gomes, G. A., Firmino, N. C. S., Rosa, L. D., de Carvalho, M. G., et al. (2018). Antibacterial and Antibiofilm Activities of Cinnamomum Sp. Essential Oil and Cinnamaldehyde: Antimicrobial Activities. *Scientific World J.* 2018, 1–9. doi:10.1155/2018/7405736

Ghayempour, S., Montazer, M., and Mahmoudi Rad, M. (2016). Encapsulation of Aloe Vera Extract into Natural Tragacanth Gum as a Novel green Wound Healing Product. *Int. J. Biol. Macromolecules* 93, 344–349. doi:10.1016/j.ijbiomac.2016.08.076

Gunawardena, D., Karunaweera, N., Lee, S., van Der Kooy, F., Harman, D. G., Raju, R., et al. (2015). Anti-inflammatory Activity of Cinnamon (C. Zeylanicum and C. cassia) Extracts - Identification of E-Cinnamaldehyde and O-Methoxy Cinnamaldehyde as the Most Potent Bioactive Compounds. *Food Funct.* 6, 910–919. doi:10.1039/c4fo00680a

Helander, I. M., Alakomi, H.-L., Latva-Kala, K., Mattila-Sandholm, T., Pol, I., Smid, E. J., et al. (1998). Characterization of the Action of Selected Essential Oil Components on Gram-Negative Bacteria. *J. Agric. Food Chem.* 46, 3590–3595. doi:10.1021/jf980154m

Kaur, M., Arshad, M., and Ullah, A. (2018). *In-Situ* Nanoreinforced Green Bionanomaterials from Natural Keratin and Montmorillonite (MMT)/Cellulose Nanocrystals (CNC). *ACS Sust. Chem. Eng.* 6, 1977–1987. doi:10.1021/acssuschemeng.7b03380

Kumari, V., and Sangal, A. (2019). Synthesis, Characterization, Antimicrobial Activity and Release Study of Cinnamon Loaded Poly (DL-Lactide-Co-Glycolide) Nanoparticles. *Rese. Jour. Pharm. Technol.* 12, 1529. doi:10.5958/0974-360X.2019.00253.1

Kwon, H.-K., Hwang, J.-S., So, J.-S., Lee, C.-G., Sahoo, A., Ryu, J.-H., et al. (2010). Cinnamon Extract Induces Tumor Cell Death through Inhibition of NFκB and AP1. *BMC Cancer* 10, 392. doi:10.1186/1471-2407-10-392

Li, Q., Zhu, L., Liu, R., Huang, D., Jin, X., Che, N., et al. (2012). Biological Stimuli Responsive Drug Carriers Based on Keratin for Triggerable Drug Delivery. *J. Mater. Chem.* 22, 19964–19973. doi:10.1039/C2JM34136K

Li, Y.-q., Kong, D.-x., and Wu, H. (2013). Analysis and Evaluation of Essential Oil Components of Cinnamon Barks Using GC-MS and FTIR Spectroscopy. *Ind. Crops Prod.* 41, 269–278. doi:10.1016/j.indcrop.2012.04.056

Matan, N., Rimkeeree, H., Mawson, A. J., Chompreeda, P., Haruthaithanasan, V., and Parker, M. (2006). Antimicrobial Activity of Cinnamon and Clove Oils under Modified Atmosphere Conditions. *Int. J. Food Microbiol.* 107, 180–185. doi:10.1016/j.ijfoodmicro.2005.07.007

McKenzie, M., BettsSuh, D. A., Suh, A., Bui, K., Kim, L., and Cho, H. (2015). Hydrogel-Based Drug Delivery Systems for Poorly Water-Soluble Drugs. *Molecules* 20, 20397–20408. doi:10.3390/molecules201119705

Meghdadi, K. R., and Boddohi, S. (2019). Preparation and Investigation of Gum Tragacanth/Gelatin Nanofibers for Antibacterial Drug Delivery Systems. Iran. *J. Polym. Sci. Technol. (Persian Ed.* 32, 145–155. doi:10.22063/JIPST.2019.1650

Nazarzadeh Zare, E., Makvandi, P., and Tay, F. R. (2019). Recent Progress in the Industrial and Biomedical Applications of Tragacanth Gum: A Review. *Carbohydr. Polym.* 212, 450–467. doi:10.1016/j.carbpol.2019.02.076

Pathania, D., Verma, C., Negi, P., Tyagi, I., Asif, M., Kumar, N. S., et al. (2018). Novel Nanohydrogel Based on Itaconic Acid Grafted Tragacanth Gum for Controlled Release of Ampicillin. *Carbohydr. Polym.* 196, 262–271. doi:10.1016/j.carbpol.2018.05.040

Ranjbar-Mohammadi, M., and Bahrami, S. H. (2015). Development of Nanofibrous Scaffolds Containing Gum Tragacanth/poly (ε-Caprolactone) for Application as Skin Scaffolds. *Mater. Sci. Eng. C.* 48, 71–79. doi:10.1016/j.msec.2014.10.020

Seddiqi, H., Oliaei, E., Honarkar, H., Jin, J., Geonzon, L. C., Bacabac, R. G., et al. (2021). Cellulose and its Derivatives: towards Biomedical Applications. *Cellulose* 28, 1893–1931. doi:10.1007/s10570-020-03674-w

Sienkiewicz, M., Głowacka, A., Kowalczyk, E., Wiktorowska-Owczarek, A., Jóźwiak-Bębenista, M., and Łysakowska, M. (2014). The Biological Activities of Cinnamon, Geranium and Lavender Essential Oils. *Molecules* 19, 20929–20940. doi:10.3390/molecules191220929

Singh, B., and Sharma, V. (2014). Influence of Polymer Network Parameters of Tragacanth Gum-Based pH Responsive Hydrogels on Drug Delivery. *Carbohydr. Polym.* 101, 928–940. doi:10.1016/j.carbpol.2013.10.022

Sun, Z., Yi, Z., Cui, X., Chen, X., Su, W., Ren, X., et al. (2018). Tumor-targeted and Nitric Oxide-Generated Nanogels of Keratin and Hyaluronan for Enhanced Cancer Therapy. *Nanoscale* 10, 12109–12122. doi:10.1039/C8NR03265C

Sun, Z., Yi, Z., Zhang, H., Ma, X., Su, W., Sun, X., et al. (2017). Bio-responsive Alginate-Keratin Composite Nanogels with Enhanced Drug Loading Efficiency for Cancer Therapy. *Carbohydr. Polym.* 175, 159–169. doi:10.1016/j.carbpol.2017.07.078

Taghavizadeh Yazdi, M. E., Nazarnezhad, S., Mousavi, S. H., Sadegh Amiri, M., Darroudi, M., Baino, F., et al. (2021). Gum Tragacanth (GT): A Versatile Biocompatible Material beyond Borders. *Molecules* 26, 1510. doi:10.3390/molecules26061510

Verma, C., Negi, P., Pathania, D., Anjum, S., and Gupta, B. (2020). Novel Tragacanth Gum-Entrapped Lecithin Nanogels for Anticancer Drug Delivery. *Int. J. Polymeric Mater. Polymeric Biomater.* 69, 604–609. doi:10.1080/00914037.2019.1596910

Xie, G. Y., Ma, J., Guan, L., Liu, X. M., Wang, A., and Hu, C. H. (2018). Proliferation Effects of Cinnamon Extract on Human Hela and HL-60 Tumor Cell Lines. *Eur. Rev. Med. Pharmacol. Sci.* 22, 5347–5354. doi:10.26355/eurrev_201808_15736

Zhang, H., and Liu, P. (2019). One-Pot Synthesis of Chicken-Feather-Keratin-Based Prodrug Nanoparticles with High Drug Content for Tumor Intracellular DOX Delivery. *Langmuir* 35, 8007–8014. doi:10.1021/acs.langmuir.9b01190

Conflict of Interest: The authors declare that the research was conducted in the absence of any commercial or financial relationships that could be construed as a potential conflict of interest.

Publisher's Note: All claims expressed in this article are solely those of the authors and do not necessarily represent those of their affiliated organizations, or those of the publisher, the editors and the reviewers. Any product that may be evaluated in this article, or claim that may be made by its manufacturer, is not guaranteed or endorsed by the publisher.

frontiers in Materials

MINI REVIEW
published: 03 November 2021
doi: 10.3389/fmats.2021.769436

State-of-the-Art Irradiation Technology for Polymeric Hydrogel Fabrication and Application in Drug Release System

Muhammad Asim Raza[1,2†], *Jin-Oh Jeong*[3,4†] *and Sang Hyun Park*[1,2*]

[1]*Advanced Radiation Technology Institute (ARTI), Korea Atomic Energy Research Institute, Jeongeup, South Korea,* [2]*Radiation Science and Technology, University of Science and Technology, Daejeon, South Korea,* [3]*Department of Biomedical Engineering, Ulsan National Institute of Science and Technology (UNIST), Ulsan, South Korea,* [4]*Wake Forest Institute for Regenerative Medicine (WFIRM), Wake Forest School of Medicine, Winston-Salem, NC, United States*

Chronic and debilitating diseases can be marginally cured by anti-inflammatory, antiseptic, and antibiotic drugs, there is still need for more efficacious delivery approaches. Biodegradable and biocompatible polymeric hydrogels are essential requirements for drug release systems due to sustained or targeted drug delivery. Irradiation crosslinking of polymers is considered a safe route for the fabrication of hydrogels because crosslinking takes place without addition of unnecessary toxic reagents such as initiators or crosslinkers. This technology is a useful way to induce sterilization and crosslinking in a single step. Several natural and synthetic polymers in different combinations are crosslinked through high energy ionizing radiation such as electron beam and gamma ray irradiation. Polymeric hydrogels prepared using these techniques exhibit good gel fraction, swelling ratio, and mechanical properties. In addition, hydrogels possess drug loading and release characteristics, antimicrobial characteristics, and *in-vivo/in-vitro* cytocompatibility. The advantage of biodegradable and biocompatible drug release systems is the controlled release of drugs without deleterious effects on targeted sites. This mini review about irradiation crosslinked hydrogels will provide sufficient guidelines for new researchers to proceed further in this field.

Keywords: hydrogels, polymeric blends, irradiation crosslinking, biomedical applications, drug release systems

OPEN ACCESS

Edited by:
Nafisa Gull,
University of the Punjab, Pakistan

Reviewed by:
Sunan Tiptipakorn,
Kasetsart University, Thailand
Goutam Thakur,
Manipal Institute of Technology, India

****Correspondence:***
Sang Hyun Park
parksh@kaeri.re.kr

†These authors have contributed equally to this work

Specialty section:
This article was submitted to Polymeric and Composite Materials, a section of the journal Frontiers in Materials

Received: *02 September 2021*
Accepted: *21 October 2021*
Published: *03 November 2021*

Citation:
Raza MA, Jeong J-O and Park SH (2021) State-of-the-Art Irradiation Technology for Polymeric Hydrogel Fabrication and Application in Drug Release System. Front. Mater. 8:769436. doi: 10.3389/fmats.2021.769436

INTRODUCTION

The term "hydrogel" was first introduced and illustrated in 1894 with inorganic salt-based colloidal gels (Buwalda et al., 2014). Irradiation technology based hydrogels were introduced in 1958, when poly (vinyl alcohol) (PVA) was crosslinked using gamma ray irradiation (Buwalda et al., 2014). Lim and Wichterle pioneered the development of poly (HEMA) hydrogels, which exhibited swollen characteristics for contact lens applications (Wichterle and Lím, 1960). Hydrogels are hydrophilic crosslinked networks with three dimensional structures that can absorb large amounts of physiological fluids or water without being dissolution due to chemical or physical interactions; they can mimic soft tissue (Hoare and Kohane, 2008). Polymeric materials from natural, semi-synthetic, and synthetic origins can be utilized for hydrogel fabrication. The preparation of hydrogels includes crosslinking of linear chains or simultaneous crosslinking and polymerization of monomers with poly functional monomers (Nugent and Higginbotham, 2007).

In polymeric hydrogels, crosslink density and hydrophilicity of the polymer are governing factors for the swelling capability and extent of swelling. Generally, mass fragments of water in the swollen state of the hydrogel are greater than mass fragments of polymer. Hydrogels can be further classified into two classes–permanent gels (chemical gels), which involve covalent linkages of chains, and pseudo gels (physical gels), which involve chain entanglements, electrostatic forces, hydrophobic interactions, or hydrogen bonds (physical gels are usually non-permanent and heating can convert them back to polymer solutions) (Benamer et al., 2006).

Currently, several crosslinking methods (chemical, physical, and irradiation) are being used (Syed K.H. Gulrez et al., 2010). Among the chemical methods, the most commonly used chemical additives are formaldehyde and glutaraldehyde. However, several studies have reported that chemical additives provoke cytotoxicity, which makes these method undesirable for pharmaceutical and biomedical applications (Yang et al., 2010). The irradiation crosslinking method is promising and clean process due to several advantages such as hydrogel fabrication and sterilization in a single step, simple process control, and absence of toxic reagents (crosslinkers and initiators), which could be difficult to remove (Benamer et al., 2006; Krklješ et al., 2007).

Stimuli responsive superabsorbents or hydrogels are triggered with even small external stimuli and undergo abrupt changes in network structure, growth, permeability, and mechanical strength due to the presence of so-called smart or environmentally sensitive hydrogels. Chemical stimuli comprising of chemical agents, ionic factors, and pH, alter the interaction at the molecular level between polymer chains, and interactions between solvents and polymer chains. On the other hand, physical stimuli include pressure, light, temperature, magnetic fields, electric fields, intensity of various energy sources, and mechanical stress, which alter interactions at the molecular level at critical onset points. Dual responsive hydrogels are another class that involves a combination of two stimuli responses in one hydrogel. Biochemical stimuli responsive hydrogels involve responses to enzyme, antigens, ligands, and several other biochemical entities. Hence, responsive hydrogels have huge potential for use as biomaterials for biotechnology, biomedical, and pharmaceutical applications (Zhang et al., 2015).

Recently, drug development has led to several controlled/targeted drug delivery approaches that consist of suitable polymer carriers containing encapsulated drugs and that deliver drugs in sustained fashion/novel route or both. Drugs can be made accessible at numerous locations within the body by choosing suitable biocompatible carriers. Targeted drug delivery to various tissues or organs can be simultaneously complemented with auxiliary benefits of obtaining both temporally and spatially controlled release, in accordance with the fundamental purpose of drug delivery. Controlled release of a drug and targeted drug delivery to diseased organs or tissues have several advantages compared to the oral (traditional) route, such as that higher drug concentration makes therapy more effective; reduction in undesired side effects and duration of therapy; and drug release sustains improved pharmacokinetics over an extended time period. In the end, convenient and simplified dosage are attributed to the wellbeing of the patient because they reduce the necessity of potentially uncomfortable repeated dosing and shorten the chances of inappropriate dispensing (Ražem and Katušin-Ražem, 2008).

In this mini review, our focus is on discussing the fabrication of natural and synthetic polymers base hydrogels for drug release systems. We explicitly describe the utilization of gamma ray and electron beam irradiation techniques for hydrogel development, the mechanism of crosslinking, the impact of crosslinking, and applications of these methods in drug release systems.

BLENDING OF POLYMERS

Natural polymer-based hydrogels can be prepared through chemical or physical crosslinking mechanisms (Ullah et al., 2015; Lou et al., 2020). The chemical crosslinking procedure induces higher mechanical strength and durability due to interconnectivity fostered through covalent bonds. The irradiation fabrication of a hydrogel is preferable as it produces sterile and pure hydrogels quickly and in the absence of toxic chemical agents (Moghaddam et al., 2019). Nevertheless, natural polymer hydrogel fabrication in aqueous solution through high ionizing energy irradiation method produces low molecular weight products, instead of good hydrogel formation, due to chain cleavage reactions (Hafezi Moghaddam et al., 2019). To overcome this issue, a blend of natural polymer and vinyl reagent or synthetic polymer has been used instead of mere natural polymers (Prusty and Swain, 2018; Moghaddam et al., 2019).

In comparison to neat polymers, polymer blends are regarded as a dominant material in the fabrication of better performance low-cost products. Composites and blends are expanding the utilization of polymers from renewable resources to recently-developed valuable products (Yu et al., 2006). The main purpose of blend formation of two or more polymers is to optimize the blend performance and to not dramatically alter the individual properties (Matveev et al., 2000). Nowadays, it is common practice to use the polymer modification process to blend two or more polymers to acquire desired properties. Polymer blends produce rare and superior properties that homo-polymers do not exhibit. Generally, chemical, physical, and irradiation techniques are used for the synthesis of polymer blends. In particular, the irradiation method is very appropriate tool that involves modification or improvement of polymeric materials through degradation, grafting, or cross-linking. Numerous research studies have been carried out in this regard (Güven et al., 1999; Bhattacharya, 2000). Natural and synthetic polymer-based blends for biomedical applications have drawn attention for their biodegradable nature (Carenza, 1992; Crescenzi et al., 1997). These blends have different material properties and can be used as hydrogels in the fields of pharmacy and biomedicine (Rosiak, 1994; Crescenzi et al., 1997; Rosiak and Ulański, 1999; Rosiak and Yoshii, 1999).

IONIZING IRRADIATION OF POLYMERIC BLENDS FOR HYDROGEL FABRICATION

On the electromagnetic spectrum, gamma rays fall in the high ionizing energy region, which has the ability to penetrate most materials. Gamma rays are radiation-source dependent high-frequency waves. Usually, radioactive nuclides such as cesium-137 and cobalt-60, are the radioactive sources used in this technology. Electron beam involve beams of energetic electrons from electron accelerators. Industrial electron beam accelerators have been categorized with respect to energy range such as high energy (>5 MeV), medium energy (300 keV–5 MeV), and low energy (80–300 keV) (Shahidi, 2019).

Unsaturated compounds are polymerized through high ionizing energy irradiation, particularly using gamma rays and electron beams. Water soluble polymers containing vinyl groups undergo hydrogel formation when exposed to high ionizing energy irradiation (Giammona et al., 1999). These irradiations generate free radicals on the polymeric chains of the water-soluble polymers through C-H bond homolytic scission. In addition, water molecules undergo radiolysis, which creates hydroxyl radicals that further interact with polymeric chains to form macroradicals (Peppas and Mikos, 1986). Then, macroradicals generate intra- and inter-molecular interactions to form covalent bonded hydrogel networks. The irradiation crosslinked hydrogel fabrication process is usually carried out in inert atmosphere (argon or nitrogen) to avoid oxygen interaction with macroradicals in the propagation stage of polymerization. Recently, poly (acrylic acid) (Jabbari and Nozari, 2000), poly (ethylene glycol) (Kofinas et al., 1996), and poly (vinyl alcohol) (Peppas and Merrill, 1977) based hydrogels were crosslinked using high ionizing energy irradiation. Also, poly (methyl vinyl ether) was synthesized using irradiation crosslinking to form a thermosensitive hydrogel (Arndt et al., 2001). The advantage of irradiation technology for hydrogel formation is that this method can be performed in aqueous phase under mild conditions (physiological pH and room temperature).

Recently, hydrogel fabrication through gamma ray irradiation has gained enormous interest. This irradiation technique is suitable for the modification of the physical and chemical properties of polymers (Jha et al., 2010; Raza and Park, 2020). Furthermore, gamma ray irradiation has several advantages as compare to the thermal activation process such as polymerization in the absence of any extra reagent and crosslinking (Park et al., 2013). Exploiting these benefits, hydrogels prepared through gamma ray irradiation are useful for medical applications, for which even minor contamination is prohibited; these materials are employed to sterilize biomedical devices for veterinary and medical applications (Gad, 2008; Juby et al., 2012). During gamma ray irradiation, the polymers crosslink such that the backbone chains of polysaccharide polymers form chemical bonds and form a three-dimensional network structure. The irradiation method of polymers promotes quantitative changes and reproducibility in the absence of chemical additives and simultaneously allows sterilization of products (Eid et al., 2009).

Similar to free radical polymerization, electron beam and gamma polymerizations also undergo initiation, propagation, and termination steps (Hennink and Nostrum, 2002). The hydrogel formation occurs when the network achieves the critical gelation point. Hydrogel fabrication and sterilization through electron beam technology in single step is a rapid and convenient method because the crosslinking process completes in a short time at ambient temperature, there is no production of radioactive waste, and process control is easy (Rosiak, 1994; Raza et al., 2021).

MECHANISM OF CROSSLINKING AND APPLICATIONS IN VARIOUS DRUG RELEASE SYSTEMS

In irradiation technology, chemical reactions initiate in aqueous mediums which starts generating series of reactive species due to radiolysis of water. Molecular products and radical species with different reactivities such as e^-_{aq}, $H^\bullet$, $HO^\bullet$, H_2O_2, H_2, and H_3O^+ are produced as given below in equation. In argon saturated or deoxygenated polymer solutions, e^-_{aq} and $HO^\bullet$ (hydroxyl radical) govern the highest yield (Spinks and Woods, 1990). The $H^\bullet$ and $HO^\bullet$ radicals interacts quickly with polymeric chains via hydrogen removal which give rise to series of macroradicals formation depending upon polymer concentration. These macroradicals undergoes inter or intra-molecular free radical recombination reactions and produce interconnected polymer networks having permanent and stable structure (Treloar, 1975).

$$H_2O \xrightarrow{E-Beam} HO^\bullet + H^\bullet + H_2 + H_2O_2 + H^+aq + HO^-aq + H_3O^-$$

Figure 1 depicts applications of hydrogels in different areas. Research on the preparation of various hydrogels (ion and electrical conductive materials, and oral patches) for effective drug release using radiation crosslinking technology has been steadily undertaken. When a hydrophilic polymer is dissolved in water and irradiated with radiation, radicals are formed on the water molecules of H and OH by the radiation to attack with low bonding strength of the hydrophilic polymer. Since this is a very unstable state, radical recombination occurs between chains in which radicals are formed and crosslinking proceeds (Park et al., 2018; Jeong et al., 2020).

Table 1 shows natural and synthetic polymer based irradiation crosslinked hydrogels with irradiation types and different irradiation doses, and release of drugs. Herein, hydrogels crosslinked with both types of irradiation (electron beam and gamma ray irradiation) are discussed. Electron beam irradiation involves beam energies (usually 2.5 or 10 MeV), and parameters such as beam power, beam current and cart speed need to be adjusted for optimum crosslinking. Hafezi et al. used electron beam irradiation for the fabrication of hydrogels for drug release applications. In case of CA-O-CMCh/PAAM, irradiation dose (10–35 kGy) was used for crosslinking and doxycycline drug was loaded for

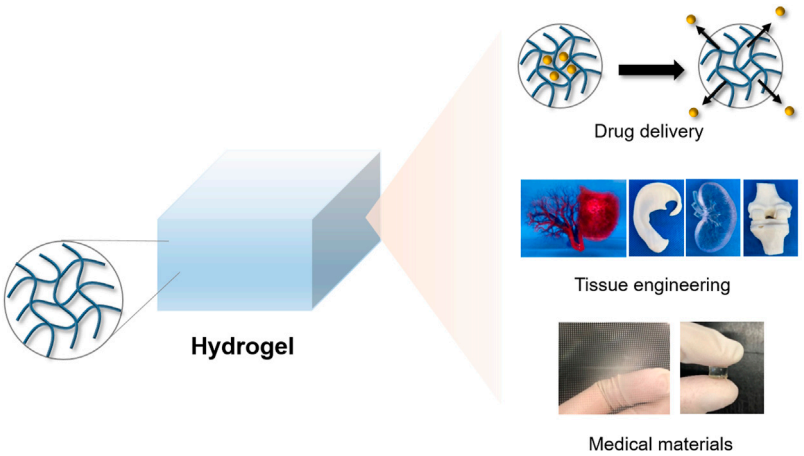

FIGURE 1 | Applications of hydrogels in different areas.

TABLE 1 | Depicting irradiation crosslinked polymers, irradiation types and dose, and used drugs.

Polymers	Irradiation types	Irradiation dose	Used drug	References
CA-O-CMCh/PAAm	E beam	10–35 kGy	doxycycline	Hafezi et al. (2020)
5-HTP/Pec	E beam	10–50 kGy	tetracycline	Hafezi et al. (2019)
Agarose	E beam	0–30 kGy	_	Krömmelbein et al. (2021)
CMSP/chitosan	E beam	25 kGy	diclofenac sodium	Tan et al. (2021)
TA-HMGT	E beam	5–90 kGy	_	Tavakol et al. (2016)
BC/AA	E beam	35 or 50 kGy	bovine serum albumin	Mohd Amin et al. (2012)
CMSP	E beam	10–20 kGy	ciprofloxacin	Lam et al. (2015)
p (HEMA/IA)	γ irradiation	25 kGy	theophylline and fenethylline hydrochloride	Tomić et al. (2007)
HA/CS/PVA	γ irradiation	5–25 kGy	Cefazoline and theophylline	Zhao et al. (2014)
HA/CS/HAP	γ irradiation	25 kGy	5-FU	Taşdelen et al. (2018)
Dextran/PNIPAAm	γ irradiation	5 kGy	ondansetron™	Almeida et al. (2013)
Cellulose/gelatin and CNCs/gelatin	γ irradiation	30 kGy	riboflavin	Ishak et al. (2018)
CS/PVA	γ irradiation	40 and 60 kGy	catechins	Sabaghi et al. (2020)
Gelatin	γ irradiation	16—20 kGy	methylene blue	Kojima et al. (2004)

release analysis. While in case of 5-HTP/Pectin, 10–50 kGy irradiation dose is utilized for tetracycline drug release. CMSP and CMSP/chitosan based hydrogels were prepared with different irradiation doses for the release of ciprofloxacin HCL and diclofenac sodium. Bacterial cellulose/acrylic acid crosslinked hydrogels were prepared at 35 or 50 kGy for the bovine serum albumin encapsulation and release. Also, Agarose and tyramine–high methoxyl content gum tragacanth based electron beam crosslinked hydrogels are prepared without involving drug loading and release.

Gamma ray irradiation involves gradual increase in dose with respect to time (k or Gy/h) to attain desired dose. Zhao et al. and Taşdelen et al. prepared different combinations of natural and synthetic polymers (HA/CS/PVA and HA/CS/HAP) using gamma irradiation for the release of cefazoline and theophylline, and 5-FU, respectively. While, Sabaghi et al. fabricated chitosan nanopartiles containing catechins and mixed with CS/PVA and crosslinked at 0, 40 and 60 kGy for drug release of catechins in different low fat and high fat simulant and studied modeling of release.

Gelatin and combination with cellulose in different forms were incorporated at lower irradiation doses and applied for methylene blue and riboflavin release analysis. Dextran/Poly (N-isopropylacrylamide) based thermo-sensitive hydrogels were irradiation crosslinked at 5 kGy and studied release pattern of ondansetron. Also, 2-hydroxyethyl methacrylate/itaconic acid copolymeric hydrogels were polymerized at 25 kGy for the drug delivery of theophylline and fenethylline hydrochloride, measured drug release kinetics and predicted drug release follows Fickian diffusion mechanism.

CURRENT CHALLENGES AND FUTURE PROSPECTIVE

Advances in the preparation of hydrogels for drug release using blending of various polymers with useful properties and radiation technology are indicating future aspects of technology. However, there are still many technical problems that need to be solved. In particular, further study on crosslinking properties related to

various polymers and/or polymer blending by irradiation are needed. Since radiation is a high energy state, it can induce various reactions such as crosslinking, degradation, polymerization, and grafting, depending on the characteristics of polymers. Therefore, to prepare a hydrogel for drug delivery, it is necessary to study the radiation crosslinking properties according to the radiation device type and radiation dose, and the type of polymer. However, it is difficult to optimize the conditions when preparing a hydrogel using radiation and time consuming due to the absence of basic research. From this point of view, research on the preparation of hydrogels for drug release after blending of polymers and drugs, and the preparation of hydrogels through irradiation (such as gamma ray and electron beam) and various polymers, all of which have been recently studied, could be said to be very noteworthy. The study of superior polymer crosslinking properties induced by irradiation is directly related to the preparation of hydrogels for drug release and could play a promising role in the development of effective drug-releasing hydrogels.

AUTHOR CONTRIBUTIONS

MR and J-OJ performed the literature survey and prepared the manuscript. SP supervised, reviewed, and revised the draft. All authors read and agreed on the final version.

FUNDING

This research was funded by the Korea Atomic Energy Research Institute (KAERI) grant number 523140-20.

REFERENCES

Almeida, J. F., Ferreira, P., Alves, P., Lopes, A., and Gil, M. H. (2013). Synthesis of a Dextran Based Thermo-Sensitive Drug Delivery System by Gamma Irradiation. *Int. J. Biol. Macromolecules* 61, 150–155. doi:10.1016/j.ijbiomac.2013.07.002

Benamer, S., Mahlous, M., Boukrif, A., Mansouri, B., and Youcef, S. L. (2006). Synthesis and Characterisation of Hydrogels Based on Poly(vinyl Pyrrolidone). *Nucl. Instr. Methods Phys. Res. Section B: Beam Interactions Mater. Atoms* 248, 284–290. doi:10.1016/j.nimb.2006.04.072

Bhattacharya, A. (2000). Radiation and Industrial Polymers. *Prog. Polym. Sci.* 25, 371–401. doi:10.1016/S0079-6700(00)00009-5

Buwalda, S. J., Boere, K. W. M., Dijkstra, P. J., Feijen, J., Vermonden, T., and Hennink, W. E. (2014). Hydrogels in a Historical Perspective: From Simple Networks to Smart Materials. *J. Controlled Release* 190, 254–273. doi:10.1016/J.JCONREL.2014.03.052

Carenza, M. (1992). Recent Achievements in the Use of Radiation Polymerization and Grafting for Biomedical Applications. *Int. J. Radiat. Appl. Instrumentation. C. Radiat. Phys. Chem.* 39, 485–493. doi:10.1016/1359-0197(92)90101-K

Crescenzi, V., Paradossi, G., Desideri, P., Dentini, M., Cavalieri, F., Amici, E., et al. (1997). New Hydrogels Based on Carbohydrate and on Carbohydrate-Synthetic Polymer Networks. *Polym. Gels Networks* 5, 225–239. doi:10.1016/S0966-7822(96)00051-2

Eid, M., Abdel-Ghaffar, M. A., and Dessouki, A. M. (2009). Effect of Maleic Acid Content on the thermal Stability, Swelling Behaviour and Network Structure of Gelatin-Based Hydrogels Prepared by Gamma Irradiation. *Nucl. Instr. Methods Phys. Res. Section B: Beam Interactions Mater. Atoms* 267, 91–98. doi:10.1016/J.NIMB.2008.11.011

Gad, Y. H. (2008). Preparation and Characterization of Poly(2-Acrylamido-2-Methylpropane-Sulfonic acid)/Chitosan Hydrogel Using Gamma Irradiation and its Application in Wastewater Treatment. *Radiat. Phys. Chem.* 77, 1101–1107. doi:10.1016/J.RADPHYSCHEM.2008.05.002

Giammona, G., Pitarresi, G., Cavallaro, G., Buscemi, S., and Saiano, F. (1999). New Biodegradable Hydrogels Based on a Photocrosslinkable Modified Polyaspartamide: Synthesis and Characterization. *Biochim. Biophys. Acta* 1428, 29–38. doi:10.1016/s0304-4165(99)00051-3

Gulrez, S. K. H., Al-Assaf, S., and Phillips, G. O. (2010). Hydrogels: Methods of Preparation. *Prog. Mol. Environ. Bioeng. Anal. Model. Technol. Appl.* 51, 1248–1259. doi:10.1016/j.jvs.2009.12.028

Güven, O., Şen, M., Karadağ, E., and Saraydın, D. (1999). A Review on the Radiation Synthesis of Copolymeric Hydrogels for Adsorption and Separation Purposes. *Radiat. Phys. Chem.* 56, 381–386. doi:10.1016/S0969-806X(99)00326-6

Hafezi Moghaddam, R., Dadfarnia, S., Shabani, A. M. H., Amraei, R., and Hafezi Moghaddam, Z. (2020). Doxycycline Drug Delivery Using Hydrogels of O-Carboxymethyl Chitosan Conjugated with Caffeic Acid and its Composite with Polyacrylamide Synthesized by Electron Beam Irradiation. *Int. J. Biol. Macromolecules* 154, 962–973. doi:10.1016/j.ijbiomac.2020.03.165

Hafezi Moghaddam, R., Dadfarnia, S., Shabani, A. M. H., Moghaddam, Z. H., and Tavakol, M. (2019). Electron Beam Irradiation Synthesis of Porous and Non-Porous Pectin Based Hydrogels for a Tetracycline Drug Delivery System. *Mater. Sci. Eng. C* 102, 391–404. doi:10.1016/j.msec.2019.04.071

Hennink, W. E., and van Nostrum, C. F. (2002). Novel Crosslinking Methods to Design Hydrogels. *Adv. Drug Deliv. Rev.* 54, 13–36. doi:10.1016/j.addr.2012.09.00910.1016/s0169-409x(01)00240-x

Hoare, T. R., and Kohane, D. S. (2008). Hydrogels in Drug Delivery: Progress and Challenges. *Polymer* 49, 1993–2007. doi:10.1016/j.polymer.2008.01.027

Jabbari, E., and Nozari, S. (2000). Swelling Behavior of Acrylic Acid Hydrogels Prepared by γ-Radiation Crosslinking of Polyacrylic Acid in Aqueous Solution. *Eur. Polym. J.* 36, 2685–2692. doi:10.1016/S0014-3057(00)00044-6

Jeong, J.-O., Park, J.-S., Kim, Y.-A., Yang, S.-J., Jeong, S.-I., Lee, J.-Y., et al. (2020). Gamma Ray-Induced Polymerization and Cross-Linking for Optimization of PPy/PVP Hydrogel as Biomaterial. *Polymers* 12, 111. doi:10.3390/polym12010111

Jha, P. K., Jha, R., Gupta, B. L., and Guha, S. K. (2010). Effect of γ-Dose Rate and Total Dose Interrelation on the Polymeric Hydrogel: A Novel Injectable Male Contraceptive. *Radiat. Phys. Chem.* 79, 663–671. doi:10.1016/J.RADPHYSCHEM.2009.11.010

Juby, K. A., Dwivedi, C., Kumar, M., Kota, S., Misra, H. S., and Bajaj, P. N. (2012). Silver Nanoparticle-Loaded PVA/Gum Acacia Hydrogel: Synthesis, Characterization and Antibacterial Study. *Carbohydr. Polym.* 89, 906–913. doi:10.1016/J.CARBPOL.2012.04.033

Arndt, K. F., Schmidt, T., and Reichelt, R. (2001). Thermo-Sensitive Poly(Methyl Vinyl Ether) Micro-Gel Formed by High Energy Radiation. *Polymer (Guildf).* 42, 6785–6791. doi:10.1016/S0032-3861(01)00164-1

Kofinas, P., Athanassiou, V., and Merrill, E. W. (1996). Hydrogels Prepared by Electron Irradiation of Poly(ethylene Oxide) in Water Solution: Unexpected Dependence of Cross-Link Density and Protein Diffusion Coefficients on Initial PEO Molecular Weight. *Biomaterials* 17, 1547–1550. doi:10.1016/0142-9612(96)89781-X

Kojima, T., Bessho, M., Furuta, M., Okuda, S., and Hara, M. (2004). Characterization of Biopolymer Hydrogels Produced by γ-ray Irradiation. *Radiat. Phys. Chem.* 71, 235–238. doi:10.1016/j.radphyschem.2004.04.069

Krklješ, A. N., Marinović-Cincović, M. T., Kacarevic-Popovic, Z. M., and Nedeljković, J. M. (2007). Radiolytic Synthesis and Characterization of Ag-PVA Nanocomposites. *Eur. Polym. J.* 43, 2171–2176. doi:10.1016/J.EURPOLYMJ.2007.03.023

Krömmelbein, C., Mütze, M., Konieczny, R., Schönherr, N., Griebel, J., Gerdes, W., et al. (2021). Impact of High-Energy Electron Irradiation on Mechanical, Structural and Chemical Properties of Agarose Hydrogels. *Carbohydr. Polym.* 263, 117970. doi:10.1016/j.carbpol.2021.117970

Lam, Y. L., Muniyandy, S., Kamaruddin, H., Mansor, A., and Janarthanan, P. (2015). Radiation Cross-Linked Carboxymethyl Sago Pulp Hydrogels Loaded

with Ciprofloxacin: Influence of Irradiation on Gel Fraction, Entrapped Drug and *In Vitro* Release. *Radiat. Phys. Chem.* 106, 213–222. doi:10.1016/j.radphyschem.2014.07.018

Lou, C., Tian, X., Deng, H., Wang, Y., and Jiang, X. (2020). Dialdehyde-β-Cyclodextrin-Crosslinked Carboxymethyl Chitosan Hydrogel for Drug Release. *Carbohydr. Polym.* 231, 115678. doi:10.1016/J.CARBPOL.2019.115678

Matveev, Y., Grinberg, V. Y., and Tolstoguzov, V. B. (2000). The Plasticizing Effect of Water on Proteins, Polysaccharides and Their Mixtures. Glassy State of Biopolymers, Food and Seeds. *Food Hydrocoll* 14, 425–437. doi:10.1016/S0268-005X(00)00020-5

Moghaddam, R. H., Dadfarnia, S., Shabani, A. M. H., and Tavakol, M. (2019). Synthesis of Composite Hydrogel of Glutamic Acid, Gum Tragacanth, and Anionic Polyacrylamide by Electron Beam Irradiation for Uranium (VI) Removal from Aqueous Samples: Equilibrium, Kinetics, and Thermodynamic Studies. *Carbohydr. Polym.* 206, 352–361. doi:10.1016/J.CARBPOL.2018.10.030

Mohd Amin, M. C. I., Ahmad, N., Halib, N., and Ahmad, I. (2012). Synthesis and Characterization of Thermo- and pH-Responsive Bacterial Cellulose/acrylic Acid Hydrogels for Drug Delivery. *Carbohydr. Polym.* 88, 465–473. doi:10.1016/j.carbpol.2011.12.022

Nugent, M. J. D., and Higginbotham, C. L. (2007). Preparation of a Novel Freeze Thawed Poly(vinyl Alcohol) Composite Hydrogel for Drug Delivery Applications. *Eur. J. Pharmaceutics Biopharmaceutics* 67, 377–386. doi:10.1016/J.EJPB.2007.02.014

Park, J.-S., Kuang, J., Gwon, H.-J., Lim, Y.-M., Jeong, S.-I., Shin, Y.-M., et al. (2013). Synthesis and Characterization of Zinc Chloride Containing Poly(acrylic Acid) Hydrogel by Gamma Irradiation. *Radiat. Phys. Chem.* 88, 60–64. doi:10.1016/J.RADPHYSCHEM.2013.03.018

Park, J.-S., Lim, Y.-M., Baik, J., Jeong, J.-O., An, S.-J., Jeong, S.-I., et al. (2018). Preparation and Evaluation of β-Glucan Hydrogel Prepared by the Radiation Technique for Drug Carrier Applications. *Int. J. Biol. Macromolecules* 118, 333–339. doi:10.1016/j.ijbiomac.2018.06.068

Peppas, N. A., and Merrill, E. W. (1977). Crosslinked Poly(vinyl Alcohol) Hydrogels as Swollen Elastic Networks. *J. Appl. Polym. Sci.* 21, 1763–1770. doi:10.1002/app.1977.070210704

Peppas, N. A., and Mikos, A. G. (1986). *Preparation Methods and Structure of Hydrogels*. 1st Edition. United States: CRC Press.

Prusty, K., and Swain, S. K. (2018). Nano Silver Decorated Polyacrylamide/Dextran Nanohydrogels Hybrid Composites for Drug Delivery Applications. *Mater. Sci. Eng. C* 85, 130–141. doi:10.1016/J.MSEC.2017.11.028

Raza, M. A., Lim, Y.-M., Lee, S.-W., Seralathan, K.-K., and Park, S. H. (2021). Synthesis and Characterization of Hydrogels Based on Carboxymethyl Chitosan and Poly(Vinylpyrrolidone) Blends Prepared by Electron Beam Irradiation Having Anticancer Efficacy, and Applications as Drug Carrier for Controlled Release of Drug. *Carbohydr. Polym.* 258, 117718. doi:10.1016/j.carbpol.2021.117718

Raza, M. A., and Park, S. H. (2020). Irradiated Ch/GG/PVP-Based Stimuli-Responsive Hydrogels for Controlled Drug Release. *J. Appl. Polym. Sci.* 137, 49041–49114. doi:10.1002/app.49041

Ražem, D., and Katušin-Ražem, B. (2008). The Effects of Irradiation on Controlled Drug Delivery/Controlled Drug Release Systems. *Radiat. Phys. Chem.* 77, 288–344. doi:10.1016/j.radphyschem.2007.06.006

Rosiak, J. M., and Ulański, P. (1999). Synthesis of Hydrogels by Irradiation of Polymers in Aqueous Solution. *Radiat. Phys. Chem.* 55, 139–151. doi:10.1016/S0969-806X(98)00319-3

Rosiak, J. M., and Yoshii, F. (1999). Hydrogels and Their Medical Applications. *Nucl. Instr. Methods Phys. Res. Section B: Beam Interactions Mater. Atoms* 151, 56–64. doi:10.1016/S0168-583X(99)00118-4

Rosiak, J. (1994). Radiation Formation of Hydrogels for Drug Delivery. *J. Controlled Release* 31, 9–19. doi:10.1016/0168-3659(94)90246-1

Sabaghi, M., Maghsoudlou, Y., Kashiri, M., and Shakeri, A. (2020). Evaluation of Release Mechanism of Catechin from Chitosan-Polyvinyl Alcohol Film by Exposure to Gamma Irradiation. *Carbohydr. Polym.* 230, 115589. doi:10.1016/j.carbpol.2019.115589

Shahidi, S. (2019). "Effect of Irradiation for Producing the Conductive and Smart Hydrogels," in *Polymers and Polymeric Composites: A Reference Series,Cellulose-Based Superabsorbent Hydrogels* (Cham: Springer), 625–653. doi:10.1007/978-3-319-77830-3_22

Spinks, J. W. T., and Woods, R. J. (1990). *An Introduction to Radiation Chemistry*. Hoboken, NJ, USA: John Wiley & Sons.

Tan, L. S., Tan, H. L., Deekonda, K., Wong, Y. Y., Muniyandy, S., Hashim, K., et al. (2021). Fabrication of Radiation Cross-Linked Diclofenac Sodium Loaded Carboxymethyl Sago Pulp/chitosan Hydrogel for Enteric and Sustained Drug Delivery. *Carbohydr. Polym. Tech. Appl.* 2, 100084. doi:10.1016/j.carpta.2021.100084

Taşdelen, B., Erdoğan, S., and Bekar, B. (2018). Radiation Synthesis and Characterization of Chitosan/Hyraluronic Acid/Hydroxyapatite Hydrogels: Drug Uptake and Drug Delivery Systems. *Mater. Today Proc.* 5, 15990–15997. doi:10.1016/j.matpr.2018.05.043

Tavakol, M., Dehshiri, S., and Vasheghani-Farahani, E. (2016). Electron Beam Irradiation Crosslinked Hydrogels Based on Tyramine Conjugated Gum Tragacanth. *Carbohydr. Polym.* 152, 504–509. doi:10.1016/j.carbpol.2016.07.044

Tomić, S. L., Mićić, M. M., Filipović, J. M., and Suljovrujić, E. H. (2007). Swelling and Drug Release Behavior of Poly(2-Hydroxyethyl Methacrylate/itaconic Acid) Copolymeric Hydrogels Obtained by Gamma Irradiation. *Radiat. Phys. Chem.* 76, 801–810. doi:10.1016/j.radphyschem.2006.05.013

Treloar, L. R. G. (1975). *The Physics of Rubber Elasticity*. (USA): New York, NY, USA: Oxford University Press.

Ullah, F., Othman, M. B. H., Javed, F., Ahmad, Z., and Akil, H. M. (2015). Classification, Processing and Application of Hydrogels: A Review. *Mater. Sci. Eng. C* 57, 414–433. doi:10.1016/J.MSEC.2015.07.053

Wan Ishak, W., Ahmad, I., Ramli, S., and Mohd Amin, M. (2018). Gamma Irradiation-Assisted Synthesis of Cellulose Nanocrystal-Reinforced Gelatin Hydrogels. *Nanomaterials* 8, 749–813. doi:10.3390/nano8100749

Wichterle, O., and Lím, D. (1960). Hydrophilic Gels for Biological Use. *Nature* 185, 117–118. doi:10.1038/185117a0

Yang, C., Xu, L., Zhou, Y., Zhang, X., Huang, X., Wang, M., et al. (2010). A Green Fabrication Approach of Gelatin/CM-Chitosan Hybrid Hydrogel for Wound Healing. *Carbohydr. Polym.* 82, 1297–1305. doi:10.1016/J.CARBPOL.2010.07.013

Yu, L., Dean, K., and Li, L. (2006). Polymer Blends and Composites from Renewable Resources. *Prog. Polym. Sci.* 31, 576–602. doi:10.1016/j.progpolymsci.2006.03.002

Zhang, W., Zhu, S., Bai, Y., Xi, N., Wang, S., Bian, Y., et al. (2015). Glow Discharge Electrolysis Plasma Initiated Preparation of temperature/pH Dual Sensitivity Reed Hemicellulose-Based Hydrogels. *Carbohydr. Polym.* 122, 11–17. doi:10.1016/J.CARBPOL.2015.01.007

Zhao, L., Gwon, H.-J., Lim, Y.-M., Nho, Y.-C., and Kim, S. Y. (2014). Hyaluronic Acid/chondroitin Sulfate-Based Hydrogel Prepared by Gamma Irradiation Technique. *Carbohydr. Polym.* 102, 598–605. doi:10.1016/j.carbpol.2013.11.048

Conflict of Interest: The authors declare that the research was conducted in the absence of any commercial or financial relationships that could be construed as a potential conflict of interest.

Publisher's Note: All claims expressed in this article are solely those of the authors and do not necessarily represent those of their affiliated organizations, or those of the publisher, the editors and the reviewers. Any product that may be evaluated in this article, or claim that may be made by its manufacturer, is not guaranteed or endorsed by the publisher.

frontiers in Materials

REVIEW
published: 09 November 2021
doi: 10.3389/fmats.2021.752813

Polymers Blending as Release Modulating Tool in Drug Delivery

Parisa Ghasemiyeh[1,2†] *and Soliman Mohammadi-Samani*[2,3*†]

[1]Department of Clinical Pharmacy, School of Pharmacy, Shiraz University of Medical Sciences, Shiraz, Iran, [2]Pharmaceutical Sciences Research Center, School of Pharmacy, Shiraz University of Medical Sciences, Shiraz, Iran, [3]Department of Pharmaceutics, School of Pharmacy, Shiraz University of Medical Sciences, Shiraz, Iran

Different polymeric materials have been used as drug delivery vehicles for decades. Natural, semisynthetic, and synthetic polymers each have their own specific characteristics and, due to the physicochemical limitations of each polymer, tuning the release rate and targeting the active ingredient to a specific organ or site of action is a complicated task for pharmaceutical scientists. In this regard, polymer blending has been considered as an attractive approach to fabricate novel and unique drug delivery systems with modified physical and/or chemical characteristics. There are three major polymer blending approaches that are used for drug delivery purposes: physical mixtures, core-shell model, and block copolymer model. Each of these types of polymer blends could significantly affect the loading capacities and the kinetics of drug release from the relevant formulations. Drug release from these blended polymers can be tuned through the changes in temperature and pH of the environment, and physiochemical properties of the target organs. Furthermore, the possible molecular interactions among polymers and drug molecules can significantly affect the drug release profile from these blended polymeric micro- and nanocarriers. In this review, first of all, different types of polymers and their various applications in biomedical sciences have been discussed and smart or stimuli responsive polymers are introduced and categorized based on their nature. Then, the purpose of polymer blending in drug delivery systems has been discussed. Different types of polymer blends including physical mixtures, core-shell polymeric carriers, and block copolymers have been summarized with focus on the effect of polymer blending on encapsulated drug release profiles. Finally, the consequence of each blending approach on drug release profile and kinetics of drug release have been mentioned in tabular format.

Keywords: polymers blending, core-shell polymeric carriers, block copolymers, physical mixtures, release profile, drug delivery

OPEN ACCESS

Edited by:
Nafisa Gull,
University of the Punjab, Pakistan

Reviewed by:
Hossam Elsayed Emam,
National Research Centre, Egypt
Shahzad Sharif,
Government College University, Lahore, Pakistan

***Correspondence:**
Soliman Mohammadi-Samani
smsamani@sums.ac.ir

†ORCID:
Parisa Ghasemiyeh
orcid.org/0000-0002-8640-5724
Soliman Mohammadi-Samani
orcid.org/0000-0002-1007-1422

Specialty section:
This article was submitted to Polymeric and Composite Materials, a section of the journal Frontiers in Materials

Received: *03 August 2021*
Accepted: *22 October 2021*
Published: *09 November 2021*

Citation:
Ghasemiyeh P and Mohammadi-Samani S (2021) Polymers Blending as Release Modulating Tool in Drug Delivery. Front. Mater. 8:752813. doi: 10.3389/fmats.2021.752813

INTRODUCTION

Controlled drug delivery systems have been considered as novel strategies in pharmaceutical sciences in order to minimize unwanted adverse drug reactions and achieve optimum efficacy by minimizing the concentration fluctuations and increasing the interval of drug administration and drug delivery to the site of action. In this regard, different types of polymeric and non-polymeric carriers with different particle size ranges have been studied (Ghasemiyeh et al., 2017; Ghasemiyeh and Mohammadi-Samani, 2018; Ghasemiyeh et al., 2019; Ghasemiyeh and Mohammadi-Samani, 2019; Ghasemiyeh and Mohammadi-Samani, 2020). Polymeric nanoparticles can be fabricated

TABLE 1 | Different applications of polymers and polymeric nanoparticles.

Polymers applications	Comments	References
Pharmaceutical and drug delivery purposes	Polymers and polymer blends with various amazing characteristics and structures are promising novel drug delivery systems with the potential for controlled and sustained drug release profile.	Pillai and Panchagnula (2001); Liechty et al. (2010); Ahmadi et al. (2015); Srivastava et al. (2015); Ghasemiyeh and Mohammadi-Samani (2019)
Cosmeceutical purposes	Different polymeric nanoparticles, especially dose with natural origin, are commonly used in cosmeceutical industries to produce novel topical formulations for skin health and beauty purposes.	Duarah et al. (2016); Aranaz et al. (2018); Asthana et al. (2021)
Tissue engineering	Smart or stimuli-responsive polymers with biocompatible and biodegradable properties are suitable candidates for tissue engineering and regenerative tissue purposes.	Guo and Ma (2018); Mohammadi et al. (2018); Doberenz et al. (2020); Wu et al. (2020)
Industrial	Removal of waste materials and pharmaceutical residues. Photo-catalytic reduction of nitro-aromatics for industrial products. Catalytic degradation and discoloration of dyes. Water treatment and removal of pesticides from waste water.	Ahmed and Emam (2019); Emam and Ahmed (2019); Abdelhameed et al. (2020); Emam et al. (2020); Abdelhameed et al. (2021); Emam et al. (2021)

using different natural and synthetic polymers (Chakravarthi et al., 2007). Polymeric nanoparticles have the advantages of biocompatibility and low toxicity in comparison to other types of nanocarriers (Ahmadi et al., 2015; Ghasemiyeh and Mohammadi-Samani, 2020). Natural polymeric nanoparticles are fabricated through the recruitment of polymers that come from natural sources such as alginate, albumin, gelatin, and chitosan. These polymers are produced through extraction followed by several purification processes. Natural polymers have the potential of hydrogel formation which makes them a suitable candidate for delivery of hydrophilic drugs, oligonucleotides, peptides, and proteins (Zhang et al., 2013). Due to the lack of purity and potential batch-to-batch variations of some of these available natural polymers, synthetic polymers were introduced. Synthetic polymers are suitable for delivery of both hydrophilic and lipophilic agents. Also, programmed drug release can be achieved through the recruitment of these polymeric nanoparticles as novel drug delivery systems. The most commonly used biodegradable synthetic polymers for drug delivery purposes are polylactide (PLA), poly (lactide-co-glycolide) (PLGA), and poly (ε-caprolactone) (PCL). While the most common non-degradable ones are polystyrene, poly (methyl methacrylate), and polyacrylate (Zhang et al., 2013). Different applications of polymers and polymeric nanoparticles are summarized in **Table 1**.

Controlled drug delivery and drug release from polymers can follow one or more of these three major mechanisms. The first is Fickian diffusion of the drug molecule through the pores or backbone of the polymer structure which is the rate limiting step of drug release from polymeric nanoparticles (Langer, 1993). The second mechanism is related to chemical reaction in term of hydrolytic or enzymatic degradation of the polymers that can result in the release of the entrapped therapeutic agents. Also, chemical reaction can appear as a bond cleavage between drug and polymer that release the encapsulated drug conjugated to the polymer. This chemical reaction can be triggered with various environmental conditions in smart or stimuli-responsive polymers (Langer, 1993). The third mechanism of drug release from polymers can be attributed to the osmotic pressure and solvent-activated drug release. In this regard, polymer will absorb large amount of solvent through a semi-permeable membrane and swell accordingly. The dissolved osmotic agent will induce osmotic pressure that can result in drug release from the polymer shell (Langer, 1993).

Polymer blending has been considered as an attractive method in which the physicochemical characteristics of these systems would be different from the characteristics of each polymer alone. Among the different types of polymeric materials as drug carrier, stimuli-responsive polymers are considered attractive polymeric carriers which undergo phase transitions in response to different environmental stimuli including temperature, pH, light, and enzymes. (Keogh et al., 2020). Thermo-responsive polymers are a common type of smart or stimuli-responsive polymeric carrier that show a change in solubility at a point called critical solution temperature (CST) (Ward and Georgiou, 2011). This trigger can be considered as a stimulus in drug release initiation. This attractive potential makes the thermo-responsive polymers suitable nanoparticles for different biomedical applications including gene delivery, drug delivery, tissue engineering, protein-ligand recognition, enzyme immobilization, and artificial organs production (Ward and Georgiou, 2011; Cirillo et al., 2015). Among these thermo-responsive polymeric nanoparticles, those that are fabricated using N-isopropylacrylamide (NIPAAm) are more popular in pharmaceutical sciences for drug delivery purposes (Cirillo et al., 2015). Most of these delivery systems are block copolymer with unique characteristics. Polymeric blends and different approaches of polymer blending could significantly affect this CST and tune the drug release profile for drug delivery purposes (Keogh et al., 2020). For biomedical applications, the trigger to form thermo-responsive hydrogels would be the change in temperature from environment to physiologic condition which is called *in situ* hydrogel formation (Klouda, 2015). Thermally-responsive polymers can be divided into two categories: natural and synthetic polymers. The detail of these thermo-responsive hydrogels are summarized in **Table 2** (Klouda, 2015).

Polymer blending approaches can result in possible molecular interactions among blended polymers which can be used in the fabrication of novel polymeric nanoparticles with unique characteristics. In this regard, it has been reported that the

TABLE 2 | Different categories of thermo-responsive polymers and characteristics.

Thermo-responsive polymers categories	Polymers		Characteristics
Natural polymers	Cellulose derivatives (Metolose®)	Methylcellulose Hydroxypropyl methylcellulose	The viscosity of Metolose® would be reduced after temperature enhancement, while further increment in temperature can form solidified hydrogels
	Chitosan	Chitosan-ß-glycerophosphate Chitosan-ß-tricalcium phosphate (ß-TCP)	Addition of either ß-glycerophosphate or ß-tricalcium phosphate (ß-TCP) can result in the formation of thermo-response hydrogel for controlled drug delivery purposes
	Xyloglucan		Xyloglucan showed thermally-responsive properties through the cleavage of galactose residues in their structure. Physical mixture of pectin with xyloglucan can result in more sustained drug release profile
	Gelatin	Gelatin cross-linked dextran Physical mixture of gelatin and chitosan/ glycerol phosphate	The thermo-responsive properties of these polymers have been used to induce porosity in polymeric nanoparticle's structure that is useful for the purpose of tissue engineering
Synthetic polymers	Poly (N-isopropylacrylamide) (pNIPAAm)	Copolymerization of NIPAAm and propylacrylic acid (PAA).	This polymer blend can result in a novel pH- and thermo-responsive hydrogel (pH < 5.5 and physiologic temperature) that would be promising for drug delivery purposes
		Copolymerization of NIPAAm and benzomethylene dioxepane	Copolymerization of NIPAAm with biodegradable monomers such as benzomethylene dioxepane can reduce the critical solution temperature of the blended polymer
		Copolymerization of NIPAAm with methacrylate polylactide and acrylic	This copolymer has been designed for protein-delivery purposes
	Poly (ethylene oxide)-b-poly (propylene oxide)-b-poly (ethylene oxide) (PEO–PPO–PEO) copolymers (Pluronic®)		These thermo-responsive tri-block copolymers are useful for different biomedical applications including drug delivery, gene delivery, and tissue engineering through the micelle formation in aqueous solution above the critical solution temperature
	Poly (ethylene glycol) (PEG)/ biodegradable polyesters	PEG-poly (lactic-co-glycolic acid) (PEG-PLGA) PEG-poly (e-caprolactone) (PCL) PEG-poly (N-(2-hydroxypropyl) methacrylamide lactate) PEG-polylactide (PLA) PEG-poly-((R)-3-hydroxybutyrate)-poly (propylene glycol) (PHB)-(PPG)	These block copolymers, in addition to their thermo-responsive properties, have the advantages of biocompatibility and biodegradability
	Poly (organophosphazenes)		The degradation products of these thermo-responsive hydrogels are biodegradable. They are suitable for gene delivery, protein drug delivery, and tissue engineering
	2-(dimethylamino) ethyl methacrylate (DMAEMA)	pDMAEMA/oxidized sodium alginate	This semi-interpenetrating polymer network showed both thermo- and pH-responsive properties
		DMAEMA and silsesquioxanes	A thermo-responsive and pH-responsive polymer blend
		Copolymerization of DMAEMA and NIPAAm	This copolymer with higher hydrophilic characteristics results in a higher critical solution temperature and slower de-swelling process would be predictable

molecular interaction between chitosan and collagen through physical mixture could result in a polymeric carrier with novel characteristics (Sionkowska et al., 2004). These molecular interactions between chitosan and collagen are polyelectrolytic interactions through the polyanion/polycation complex formation. FTIR results revealed that a new hydrogen bond (between–OH, –COOH, or–NH_2 groups of collagen and–OH or–NH_2 groups of chitosan) was formed in this blended polymers structure, which confirmed the collagen denaturation process during physical mixture with chitosan. The blended chitosan-collagen polymers were miscible, which proved the altered molecular characteristics of the blended polymers in comparison to each one alone. Further, the viscosity of the finalized blended product was higher than each component alone which also emphasized the creation of molecular interactions between chitosan and collagen (Sionkowska et al., 2004). Also, it has been reported that blending and copolymerization of chitosan with PEG can result in improved ductility properties of chitosan which can be attributed to the inter-molecular interactions between chitosan and PEG polymers (Kolhe and Kannan, 2003).

In this focused review, first of all, the purpose of polymer blending in drug delivery systems and their advantages have been discussed. After that, different methods of polymer blending including physical mixture, core-shell polymeric carriers, and block copolymer have been summarized (**Figure 1**). Finally, the consequence of each blending approach on drug release profile and kinetics of drug release have been discussed. In the

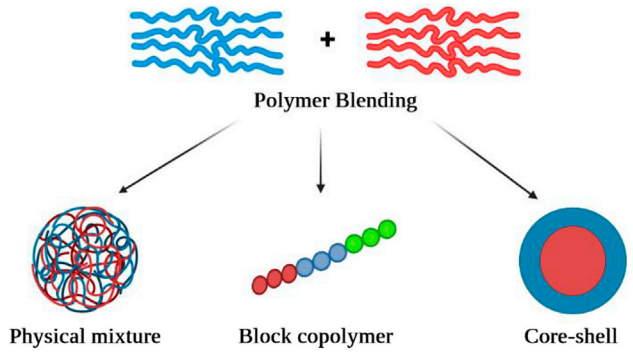

FIGURE 1 | A schematic view of different polymer blending approaches including physical mixture, block copolymer, and core-shell model.

conclusion, the recently used polymer blends, the loaded drug, and the suggested drug release profile and kinetics have been summarized in tabular format.

POLYMERS BLENDING

Drug delivery scaffolds are considered smart novel drug delivery systems that are used in controlled spatiotemporal drug release. These scaffolds are composed of various natural and/or synthetic polymer blends to fabricate novel and unique systems with improved characteristics (Calori et al., 2020). The process of polymer blending can result in changes in physicochemical characteristics of the final product in comparison to the homopolymers alone. The main advantages of polymers blending is the fabrication of miscible polymer mixtures. The physical characteristics of the blended polymers depend not only on the characteristics of each homopolymer alone but also depend on the possible intramolecular interactions among blended polymers. Furthermore, the polymer blending process can result in fabrication of a novel product with second functionality that would have potential for the formation of new interactions with other polymers and drugs (Jones et al., 2005). The most common natural polymers that are used in this field are hyaluronic acid (HA), chitosan, alginate, collagen, gelatin, elastin, keratin, and silk fibroin. Also, the most commonly available synthetic polymers used for this purpose are polylactide (PLA), polyglycolic acid (PGA), polyvinyl alcohol (PVA), and poly-ε-caprolactone (PCL) (Calori et al., 2020).

Physical Mixtures

Simply blending low molecular weight hyaluronic acid (HA) with carboxymethyl hexanoyl chitosan (CHC) under stirring without thermal treatment can result in the fabrication of *in situ* injectable hydrogels. The probable mechanisms of this hydrogel formation are hydrophilic-hydrophobic interactions, supramolecular assembly, and electrostatic micelle formation in a pH-dependent manner. The prepared hydrogel was biocompatible, biodegradable, bioadhesive, and shape-persistent. This polymer blend showed a pH-sensitive extended drug release profile at pH 6. The rate of these polymers blend degradation was accelerated at physiologic pH (pH = 7.4) (Lu et al., 2019). These injectable hydrogels are potentially applicable in tissue engineering and soft tissue repairing through a non-invasive procedure. Also, CHC can be physically mixed with thermal responsive agents including Pluronic F-127 and β-sodium glycerophosphate (β-GP) to form *in situ* temperature-sensitive injectable hydrogel (Lu et al., 2019). The major mechanism of drug release from the hydrogels would be Fickian diffusion through the pores of macromolecular chains in swollen hydrogels. However, the mechanism of drug release from these thermo-responsive hydrogels would be highly dependent on the process of drug entrapment within the hydrogel, drug-polymer affinity, and the polymeric network structure (Cirillo et al., 2015). In recent decades, chitosan has been used as a suitable carrier with mucoadhesive potential for buccal drug delivery purposes. However, chitosan polymers have some limitations including poor tensile and weak adhesion strength characteristics. These limitations can be overcome through the recruitment of polymer blending approaches (Freag et al., 2018). It has been reported that a physical mixture of chitosan and hydroxypropyl methylcellulose (HPMC) can result in a novel blended polymer with improved mucoadhesive properties for the buccal route of administration (Freag et al., 2018). Physical blending of HPMC with chitosan can result in enhanced hydration capacity which is required for controlled and uniform drug release through the buccal route (Freag et al., 2018). Furthermore, results of this study revealed that chitosan mixed with of Sodium carboxymethyl cellulose (NCMC), Sodium alginate (NALG), or hyaluronic acid (HA), respectively, fail to enhance the mucoadhesive potential while blending chitosan with either HPMC or Carbopol® (CRB) could result in significantly better mucoadhesive characteristics and residence time in the buccal cavity (Freag et al., 2018). Gelatin, agar, and κ-carrageenan are considered as suitable polymers to fabricate hydrogels with controlled drug release potential; however, the release rate of hydrophilic agents from each of these polymers would be fast. The effect of physically two-by-two blending of either gelatin, agar, or κ-carrageenan polymers (with 1:1 ratio) on the release pattern of theophylline from hydrogels has been studied (Liu et al., 2005). Results revealed that polymer blending was accompanied by sustained and prolonged drug release from hydrogels that can be attributed to the longer and more tortuous pathways that drug molecules should pass to exit from the structure of the hydrogels. Furthermore, the viscosity of the hydrogel can reduce the drug release by inducing a hindrance in molecular diffusion. Also, it has been reported that the addition of a polysaccharide including agar and κ-carrageenan to the gelatin could result in a slower release pattern in comparison to the blending of these two polysaccharides together (Liu et al., 2005). The effect of temperature on the release profile revealed that by enhancing the temperature, the release rate was increased in each studied polymer blend. Among all of these assessed polymer blends, hydrogels fabricated from agar and gelatin physical mixture (with 1:1 ratio) resulted in the slowest drug release profile (Liu et al., 2005). The miscibility studies on pairwise polymer blends revealed that physical mixture of hydroxypropyl methylcellulose

acetate succinate (HPMCAS)/PVP, HPMC/carboxymethyl cellulose acetate butyrate (CMCAB), and PVP/HPMC were miscible while Eudragit 100 (E100)/PVP and E100/HPMC had a miscibility gap. A physical mixture of these immiscible polymers can result in polymer blends with balanced amorphous solid dispersions (ASDs) that can result in controlled drug release rate and formation of polymer-polymer and polymer-drug interactions to avoid further nucleation and crystal growth of hydrophobic drugs (Marks et al., 2014).

Physical mixture of some synthetic polymers including polyethylene terephthalate (PET) and polyacrylonitrile (PAN) can result in the production of an activated carbon product with different medical, pharmaceutical, and industrial applications including pesticide removal from the liquid phase. The activated carbon can act as an efficient adsorbent agent (Belo et al., 2017). Different natural and synthetic polymers can be blended physically in order to fabricate novel polymeric micro- and nanoparticles with unique characteristics. In this regard, collagen as a natural polymer can be blended with different synthetic polymers including PVP, PEO, PVA, and PEG (Sionkowska, 2011). These blended polymers can be used for different applications including drug delivery systems, wound healing process, tissue engineering, and medical devices production (Sionkowska, 2011). Furthermore, chitosan is another natural polymer that can be blended with different synthetic polymers including PEG, PVP, PCL, PEO, and PLA, and polyacrylamide (PAAm) (Sionkowska, 2011). Other natural polymers that can blend with synthetic polymers are keratin, elastin, silk fibroin, and starch (Vaidya and Bhattacharya, 1994; Sionkowska, 2011).

Core-shell Polymeric Carriers

Polymeric nanofibers and microfibers that are composed of either synthetic or natural polymers with a diameter range of a few nanometers to several micrometers have been considered for use as drug delivery systems. A novel class of nanofibers that have a core-shell or core-sheath structure have been developed using coaxial and emulsion electrospinning techniques (Monfared et al., 2019). The most important advantages of polymeric core-shell nanofibers are their high surface area, nanoscale particle size, porous structure, simply controlled structure, flexible platform, biomimetic and biocompatible properties, high encapsulation efficiency, and sustained controlled drug release at the site of action (Monfared et al., 2019). The main drawback of these blended polymeric nanofibers for drug delivery purposes is their limited ability to sustain drug release for hydrophilic agents. Small molecule hydrophilic drugs that are highly soluble in release medium while poorly compatible with insoluble polymers with poor partitioning coefficient can result in initial burst release and overall faster release rate (Chou et al., 2015). In contrast, burst drug release would be avoided and overall prolonged drug release would be achieved for hydrophobic agents due to their poor solubility in release medium, higher compatibility with insoluble polymers, and sufficient partitioning into the hydrophobic polymers (Monfared et al., 2019; Zupančič, 2019).

In order to obtain controlled drug release, core-shell structures, also known as double wall microspheres, containing a bulk-eroding core (like PLGA) and a surface eroding sheath (like polyanhydride) has been suggested to significantly prevent initial burst release of encapsulated agents (Mohammadi-Samani and Taghipour, 2015). Drug release patterns from biodegradable core-shell nanofibers would take place based on three different mechanisms: diffusion, shell thickness, and degradation (Vashisth et al., 2016). Most of the added drug would be entrapped within the core phase of the polymeric nanofibers and molecular diffusion is the most common mechanism responsible for the extended drug release from these core-shell nanofibers. While the polymer matrix is degrading, the incorporated drug will be released from the nanofibers. Drug release from these core-shell nanofibers is almost completely a two-phasic release pattern containing an initial burst release followed by a sustained and controlled drug release. This biphasic release pattern in core-shell polymeric nanoparticles can be used as dual action drug delivery system (one dissolves in the core phase and the other in the shell) with different rates of release (Monfared et al., 2019). It has been reported that in a core-shell nanofiber fabricated from poly (methyl methacrylate) (PMMA) in the shell and PMMA/PVA blend in the core phase, the lower the ratio of PVA in the core, the lower the incidence of initial burst release (Zupančič et al., 2016). Recruitment of electrospun core-shell nanofibers can induce partition-controlled drug release especially for hydrophilic agents such as DNA, proteins, and peptides. In this regard, PVA/PCL core-shell, PVA/poly-*L*-lactide (PLLA) core-shell, and PVA/PLGA core-shell had been studied. In this study, hydrophilic drug release from each of these monolithic fibers, *ie.* PVA, PLLA, PCL, and PLGA, resulted in initial burst release which was highest for PVA and lowest for PLLA since the PVA showed immediate swelling in release medium and resulted in 90% initial burst release (Tiwari et al., 2010). However, the PLLA monoliths, with a high T_g [glass transition temperature] value, could entrap most of the insoluble drug into the fiber bulk and resulted in the least initial burst release (about 10%). Using PVA as the core phase in core-shell polymer blends could significantly reduce the initial burst release and sustain the overall drug release pattern in comparison to each monolith fiber. These observed data could be attributed to the fewer undissolved drug molecules through the recruitment of core polymer (Tiwari et al., 2010). Using PCL as the core phase of the core-shell nanofibers can result in facilitated drug release due to the nanoporous structure of PCL that can result in water sorption within the core of the nanofiber which in turn facilitates drug desorption from the surface of the core phase. Drug desorption, which is the rate-limiting step of drug release, could be bypassed through this core-shell polymeric carrier fabrication and faster drug release would be predictable (Srikar et al., 2008). Fabrication of blended core-shell PVA/PLGA nanofibers in comparison to the monolithic PLGA fibers could significantly sustain the drug release profile. The probable reason for these observed data regarding drug release from PLGA and PVA/PLGA fibers would be the ease of molecular diffusion through the monolithic PLGA

TABLE 3 | Different polymers which were used in the fabrication of core-shell polymeric carriers as novel drug delivery systems.

Core polymer	Shell polymer	Drug affinity	Advantages	Ref
Poly (styrene) (PSt)	Poly (N-isopropylacrylamide (PNIPAM)	Hydrophobic agents	A thermo-responsive shell and non-responsive core Strength against the ionic change and changing the concentration of salt environment Versatile properties	Naseem et al. (2018)
Poly (N-isopropylacrylamide (PNIPAM)	Poly (styrene) (PSt)	Affinity to hydrophilic agents below the critical solution temperature (CST) and to hydrophobic agents above the CST.	A thermo-responsive hydrogel	Zhang, (2007); Naseem et al., 2018
Poly (N-isopropylacrylamide-co-styrene) (PNIPAM-co-St)	PNIPAM	Affinity to hydrophilic agents below the critical solution temperature (CST) and to hydrophobic agents above the CST.	Mono-disperse and mono-shape nanoparticles with thermo-responsive swelling potential	Xiao et al. (2004)
PNIPAM	P(NIPAM-co-AAc)	Affinity to hydrophilic agents below the critical solution temperature (CST) and to hydrophobic agents above the CST.	A thermo-responsive and pH-responsive core-shell carrier	Jones and Lyon, (2000)
PMMA/PVA blend	Poly (methyl methacrylate) (PMMA)	Hydrophilic agents	The lower the ratio of PVA in the core phase, the lower the incidence of initial burst release	Zupančič et al. (2016)
Alginate	PLGA	Hydrophilic agents	Had the potential of higher entrapment efficiency and could prevent the unwanted leakage of encapsulated hydrophilic agents	Kong et al. (2013)
PLGA	Alginate	Hydrophobic agents	Could reduce initial burst release and provide overall extended drug release profile for encapsulated hydrophobic agents within the PLGA as core layer	Kong et al. (2013)

fiber that results in faster drug release while drug partitioning through the core-shell PVA/PLGA nanofiber was more complicated and resulted in a slower release pattern (Tiwari et al., 2010). In general, in order to obtain optimized controlled drug release using core-shell nanofibers, the core and shell layers should have different hydrophilic/hydrophobic characteristics. Furthermore, the incorporated drug should be more soluble in the core phase. In addition, sufficient polymer concentration in the shell layer is essential to avoid pore formation and initial burst release. The molecular diffusion through the shell layer should not be too slow to hinder drug release from the nanocarrier (Tiwari et al., 2010). Polymer-based microspheres have the advantage of biocompatibility, ease of fabrication, tunable physicochemical characteristics, and controlled drug release patterns. Core-shell polymeric microspheres have many additional advantages that can be attributed to the tunable properties of the shell layer. The shell phase of these core-shell microspheres can induce more control on drug release profile and release kinetics of the encapsulated drug within the core phase. Initial burst release would be avoided by drug diffusion through both core and shell layers. Using suitable shell layers can result in significantly reduced initial burst release followed by further prolonged and extended drug release. Also, the shell layer's thickness can significantly affect the drug release kinetics (Kong et al., 2013). Furthermore, other advantages of these core-shell polymeric microspheres are their potential in the protection of the fragile therapeutic agents encapsulated within the core layer from the harsh environment, targeted drug delivery through the attachment of reagents and functional groups at the surface of the shell layer, and simultaneous dual drug delivery of two distinct therapeutic agents encapsulated separately in core and shell layers (Kong et al., 2013). In this regard, alginate-PLGA core-shell microspheres had the potential of higher entrapment efficiency and could prevent the unwanted leakage of encapsulated hydrophilic agents, while PLGA-alginate core-shell microspheres could reduce initial burst release and provide overall extended drug release profile for encapsulated hydrophobic agents within the PLGA as core layer (Kong et al., 2013). In general, PLGA has been considered as a suitable polymer to control the release rate of encapsulated hydrophobic agents while alginate is a suitable candidate to provide high encapsulation efficiency of hydrophilic agents (Kong et al., 2013). A short list of several polymers used in the fabrication of core-shell polymeric carriers has been shown in **Table 3**.

Block Copolymers

Block copolymers are sophisticated compounds with two or more different chemical moieties that are linked together through chemical covalent bonding. The process of copolymerization can be tuned in order to fabricate polymer blends with different arrangements and characteristics especially for tri-block copolymers design and synthesis (Calori et al., 2020). The most common techniques used in the synthesis of di-block and/or tri-block copolymers are ionic (anionic and cationic) polymerization, free-radical polymerization, metal-catalyzed

polymerization (ring-opening metathesis polymerization (ROMP), and α-olefin polymerization) (Hillmyer, 1999). The copolymers' compositions and the length of polymers' blocks can significantly affect the degree of phase separation and transition phase (Calori et al., 2020). Block copolymers are synthesized with different purposes including enhancing the hydrophilicity that can be achieved by the addition of polyethylene oxide (PEO) moieties to the hydrophobic polymers. Also, the PEG/PCL block copolymer is a smart thermo-responsive hydrogel that gained FDA approval for local drug delivery via the parenteral route (Calori et al., 2020). Poly (lactic-co-Glycolic Acid) (PLGA) is a kind of block copolymer in which PLA and PGA moieties have been covalently bonded (Calori et al., 2020). PLGA is used in the delivery of various peptides, proteins, genes, nucleotides, and many other therapeutic agents. So, it has been considered as a favorable scaffold for drug delivery and gene delivery purposes especially in the field of biomedicine (Roointan et al., 2018a). PLGA block copolymer has the advantage of biocompatibility, biodegradability, and mechanical strength. Also, it could produce non-toxic metabolites including glycolic acid and lactic acid. Using the PLGA polymeric blend, drug release profile and release kinetics would be tuned more appropriately (Mohammadi-Samani and Taghipour, 2015). The most addressed advantage of using PLGA for drug delivery purposes are the need for less frequent drug administration due to extended drug release capability, lower total dose requirements, avoidance of unwanted fluctuations in plasma concentration, and reduced adverse drug reactions (Mohammadi-Samani and Taghipour, 2015). The PLGA polyesters exist in two forms, namely crystalline and amorphous states, which are affected by the lactide/glycolide ratio used in PLGA synthesis. The higher the lactide/glycolide ratio, the longer the time spent for block copolymer degradation, and a more sustained release profile would be expected (Mohammadi-Samani and Taghipour, 2015; Roointan et al., 2018a). Also, the hydrophilicity, drug encapsulation, degradation rate, and drug release profile are highly affected by the PLGA terminal group that can vary from COOH to COOR with different length and moieties (Mohammadi-Samani and Taghipour, 2015). The possible mechanisms of PLGA erosion are bulk (homogenous) erosion and surface (heterogeneous) erosion; the former is the dominant mechanism. One of the main drawbacks of using these block copolymers for drug delivery purposes is the possibility of burst release and irregular release profile of the encapsulated proteins that can be attributed to surface adsorption of proteins. Also, there are many water-filled pores and cracks in block copolymer structures that can induce burst release (Mohammadi-Samani and Taghipour, 2015). One of the reported efforts to overcome this drawback would be the fabrication of microparticle composite, containing PLGA and another polymer, with a core-shell structure while a hydrophilic polymer is located in the core and PLGA in the shell and results in sustained release of encapsulated hydrophilic therapeutic agents (Mohammadi-Samani and Taghipour, 2015). Also, recruitment of alginate and a surfactant in the fabrication of PLGA copolymer would be helpful to enhance drug entrapment efficiency and reduce initial burst effects (Roointan et al., 2018a). Drug release kinetics of PLGA block copolymer follows a multiphasic profile. Also, the method of drug incorporation could significantly affect the release profile. In this regard, surface adsorption of the drug to the PLGA block copolymer could result in 60–70% initial burst release (Mohammadi-Samani and Taghipour, 2015). Copolymer blending is a type of polymer blending approach in which two or more block copolymers with different characteristics, functionalities, and stimuli-responsiveness are mixed in order to form a unique polymer blend with special characteristics (Keogh et al., 2020). It has been reported that recruitment of albumin in the synthesis of block copolymers could affect drug release profile from hydrogels, while the gel consistency of the fabricated block copolymer was reduced (Perinelli et al., 2014). The possible mechanism of dissolution and drug release from Poloxamer-containing hydrogels, fabricated through the block copolymer approach, was a combination of drug diffusion and hydrogel erosion. Using bovine serum albumin (BSA) in preparation of these thermo-responsive hydrogels resulted in slower drug release with a lower terminal of release. However, the results of this study revealed that the recruitment of proteins such as BSA in the fabrication of thermo-responsive block copolymers affects Poloxamer gelation more than its micellization process. In addition, it has been emphasized that although the gel consistency of the finalized block copolymer was reduced in the presence of BSA, the rate of drug release was also reduced in this condition. These results could be attributed to different mechanisms of drug release that BSA might be involved in other than the well-recognized drug dissolution and hydrogel erosion mechanisms (Perinelli et al., 2014). Using block copolymers that are composed of PEG and PLA polymers could result in the fabrication of novel drug delivery systems with desired drug release profiles. Carboxymethyloxysuccinic acid (CMOSA), a non-toxic, hydrophilic, and biodegradable polycarboxylic acid, has been blended with the PLA-PEG-PLA tri-block copolymer through copolymerization and group modification (esterification) (Zhang et al., 2008). The novel synthesized HO_2C-PLA-PEG-PLA-CO_2H copolymer had more hydrophilic characteristics and could enhance drug encapsulation potential and improve drug release profile. Results of this study reveal that the synthesized HO_2C-PLA-PEG-PLA-CO_2H copolymer has a porous spherical shape with enhanced encapsulation efficiency and loading capacity values in comparison to the PLA-PEG-PLA tri-block copolymer for both hydrophilic and lipophilic therapeutic agents. Also, this novel copolymer showed a reduced initial burst release and a more sustained and controlled release profile in comparison to the PLA-PEG-PLA block copolymer alone. This phenomenon could be attributed to the hydrogenic bond formation between carboxyl groups of HO_2C-PLA-PEG-PLA-CO_2H and the hydroxyl group of the hydrophilic encapsulated therapeutic agents that could prevent drug adsorption to the surface of nanoparticles or microparticles and avoid faster initial burst release. Also, the same results were reported for hydrophobic drugs encapsulated in the HO_2C-PLA-PEG-PLA-CO_2H block copolymer. In general, the drug release rate from these copolymers was faster for hydrophilic drugs in comparison to

TABLE 4 | Recently used polymeric blends for drug delivery purposes, the blending type, the loaded drug, and their release kinetics.

Polymer blend	Blending type	Loaded drug	Release profile	Release kinetics	References(s)
Poly (HEMA-co-DMAEMA) nanohydrogel	Block copolymer	Doxorubicin	pH-dependent sustained drug release (higher drug release rate at acidic pH that mimics the tumor microenvironment)	-	Roointan et al. (2018b)
Lysine-modified poly (vinylcaprolactam)	Block copolymer	Doxorubicin	pH- and Temperature-responsive drug release (faster release rate at acidic pH and higher temperatures)	-	Farjadian et al. (2019)
Histidine-modified poly (aminoethyl methacrylamide)	Block copolymer	Cisplatin	pH-dependent sustained drug release (higher drug release rate at acidic pH that mimics the tumor microenvironment)	Weibull model	Entezar-Almahdi et al. (2021)
poly (2-ethyl 2-oxazoline)-b-poly (L-glutamic acid) double hydrophilic copolymer	Block copolymer	Irinotecan	-	-	Salmanpour et al. (2019)
PHEMA-st-PEG-DA Nanohydrogels	Block copolymer	Methotrexate	pH-responsive drug release which was faster at acidic pH	First-order model	Farzanfar et al. (2021)
3-(4,5-dimethylthiazol-2-yl)-2,5-diphenyl tetrazolium bromide (MTT) block copolymer	Block copolymer	Doxorubicin	pH- and thermo-responsive release profile (faster release rate at lower pH and higher temperature)	-	Biswas et al. (2021)
poly (ethylene glycol) (PEG)- and camptothecin (CPT)-conjugated poly (methacrylate) di-block copolymer	Block copolymer	Camptothecin drugs	Dual responsive drug release (faster release rate at overproduced intracellular glutathione (GSH) and high level of reactive oxygen species (ROS) at tumor microenvironment)	-	Yin et al. (2020)
Styrene–Isoprene–Styrene Block Copolymer	Block copolymer	Methyl salicylate and capsaicin (as lipophilic agents) and diphenhydramine hydrochloride (as hydrophilic agent)	Diffusion-controlled drug release for methyl salicylate and capsaicin (initial burst release followed by a sustained and continuous drug release) Diphenhydramine hydrochloride had initial fast release within the first 4 h and the release rate slowed down after that	Korsmeyer Peppas model	Wang et al. (2012)
(methyl methacrylate)-nylon6 core-shell nanofibers	Core-shell	Ampicillin	Three-phasic drug release (combination of the drug diffusion and surface erosion)	Korsmeyer Peppas model	Sohrabi et al. (2013)
PVA-PMMA core-shell nanofibers	Core-shell	Ciprofloxacin	Minimal initial burst release and strongly sustained drug release	-	Zupančič et al. (2016)
Surface-modified (oxygen dielectric barrier discharge plasma [ODBDP]) core-shell *Bombyx mori* silk/PVA nanofibers	Core-shell	Amoxicillin hydrochloride trihydrate (AMOX)	The biphasic drug release profile	Weibull model	Ojah et al. (2019)
Core-shell PVA/silk fibroin nanoparticles	Core-shell	Doxorubicin	Biphasic release profile containing an initial burst release followed by an extended drug release profile	-	Cao et al. (2017)
HA/PLGA and PLGA/HA core-shell nanoparticles	Core-shell	Bovine serum albumin	Initial burst release followed by a more sustained release profile	Zero-order model	Taghipour et al. (2014)
Injectable *in situ* forming gel based on carboxymethyl hexanoyl chitosan/ hyaluronic acid polymer blend	Physical mixture	Berberine	pH-dependent sustained drug release pattern at pH of 6 and higher polymer degradation rate and faster release rate at pH of 7.4 (Fastest drug release from this polymer blend was observed at pH of 5)	-	Lu et al. (2019)

(Continued on following page)

TABLE 4 | (*Continued*) Recently used polymeric blends for drug delivery purposes, the blending type, the loaded drug, and their release kinetics.

Polymer blend	Blending type	Loaded drug	Release profile	Release kinetics	References(s)
PLGA blended with Poloxamer/poly (ethylene oxide) (PEO)	Physical mixture	Prilocaine	Sustained drug release following water penetration through the polymer blend and PLGA degradation	-	Hamoudi-Ben Yelles et al. (2017)
Gastrointestinal tract-insoluble and enteric polymer blends (ethylcellulose and Eudragit® L polymer blend) as coating materials	Physical mixture	Propranolol hydrochloride	Controlled pH-dependent drug release pattern based on ethylcellulose: Eudragit® L ratio in the blended polymer (faster release rate at higher Eudragit® L ratios)	-	Lecomte et al. (2003)
HPMC and Carbomer 940 polymer blend	Physical mixture	Diclofenac sodium	Uniform and sustained release profile with minimal fluctuations	Zero-order model	Samani et al. (2003)

the hydrophobic ones that can be the consequence of free diffusion of hydrophilic agents through the aqueous medium of the hydrophilic block copolymers (Zhang et al., 2008). The recruitment of polyethylene glycol-b-polyaspartic acid (PEG-b-PAsp) as an interesting pH-sensitive block copolymer to sheath the lipid nanoparticles' surface could significantly enhance the systemic circulation, plasma concentration, and physiologic activity of the loaded drug that can be attributed to the protective effect of sheathed PEG. Also, the pH-responsiveness of this block copolymer could result in targeted drug release in the tumor area to achieve passive tumor-targeting potential in order to provide drug delivery to the drug-resistant cancerous cells (Tran et al., 2015). Dispersion of gancyclovir-loaded PLGA microspheres in thermo-responsive PLGA-PEG-PLGA tri-block copolymer could result in a three-phasic release pattern (sigmoidal equation) including initial drug diffusion, matrix hydration, and subsequent matrix degradation. This polymer blending approach could significantly enhance the encapsulation efficiency and reduce the initial burst release due to closer packing potential in comparison to the PLGA microspheres alone (Duvvuri et al., 2005; Duvvuri et al., 2006). The effect of physically blending PLGA with PLGA-*b*-PEG block copolymer on entrapment efficiency and release pattern of paclitaxel as a hydrophobic drug has been studied. Based on the reported results it was revealed that by enhancing the PLGA/PLGA-*b*-PEG ratio, the percentage of entrapment efficiency was enhanced due to the increment in hydrophobicity characteristics of the polymer blend that could result in higher paclitaxel (hydrophobic agent) entrapment in its structure. The mixture of PLGA-*b*-PEG block copolymer with PLGA polymer could result in the fabrication of a novel blended polymer with an enhanced rough surface area. However, the release rate from the neat PLGA-*b*-PEG copolymer was slower than the blended PLGA-*b*-PEG and PLGA polymers. This would be attributed to the much lower surface area of neat PLGA-*b*-PEG in comparison to the blended polymers or differences in hydrophobicity of these carriers. Results of this study revealed that the paclitaxel release from this novel polymer blend was much more diffusion-controlled (Fick's second law of diffusion) and polymer degradation would be less probable. Finally, these physically blended polymers showed suitable biocompatibility and cell viability that would be promising for drug and gene delivery purposes (Hussain et al., 2017).

DRUG RELEASE PROFILE AND RELEASE KINETICS

Polymer blending and the approach that has been used in this regard can significantly affect the release profile and kinetics of drug release. Each blending approach has its pros and cons that should be considered separately in order to achieve targeted drug delivery with optimal drug release kinetics. Sometimes the combination of these three principle blending methods, namely physical mixture, core-shell model, and block copolymerization, can be combined to resolve some important disadvantages of each method. A list of some recent research on polymer blending approaches used for drug delivery purposes with a focus on blending type and the consequent drug release profile and release kinetics have been summarized in **Table 4**.

DISCUSSION AND CONCLUSION

Although polymers from different origins and with different chemical natures were introduced in biomedicine as carriers in drug delivery purposes, a survey in literature reveals that, in many cases, recruitment of a single polymer does not fulfill the appropriate characteristics of a sophisticated drug delivery system in terms of site-specific and time-controlled manner of release profiles. In this regard, using different type of polymer blends from simple physical mixture to more sophisticated core-shell strategy up to recruitment of polymeric block copolymer will open new aspects in drug delivery as site-specific and rate-controlling means in pharmaceutical sciences. Although there is not any simple recommendation for all instances, in order to solve formulation limitations, application of different strategies relevant to polymers blending would be useful.

CURRENT INVESTIGATIONS LIMITATIONS

In this focused review only pharmaceutical and biomedical applications of polymer blends were considered, but different applications in chemistry and water treatment and other fields of science exist which have not been addressed in this manuscript.

FUTURE DIRECTIONS

Focus on new applications of polymer blends and attention to new polymers for modulating the rate, site, and kinetics of drug release would be necessary to maximize the drug therapy efficiency and reduce the common side effects of present drugs.

AUTHOR CONTRIBUTIONS

PG contributed to study design, data gathering, and writing-original draft, writing-reviewing and revising. S-MS contributed to conceptualization, study design, supervision, project administration, and writing-reviewing and revising. All authors have read and approved the final manuscript.

REFERENCES

Abdelhameed, R. M., Abdel-Gawad, H., and Emam, H. E. (2021). Macroporous Cu-MOF@cellulose Acetate Membrane Serviceable in Selective Removal of Dimethoate Pesticide from Wastewater. *J. Environ. Chem. Eng.* 9 (2), 105121. doi:10.1016/j.jece.2021.105121

Abdelhameed, R. M., El-Shahat, M., and Emam, H. E. (2020). Employable Metal (Ag & Pd)@MIL-125-NH2@cellulose Acetate Film for Visible-Light Driven Photocatalysis for Reduction of nitro-aromatics. *Carbohydr. Polym.* 247, 116695. doi:10.1016/j.carbpol.2020.116695

Ahmadi, F., Oveisi, Z., Samani, S. M., and Amoozgar, Z. (2015). Chitosan Based Hydrogels: Characteristics and Pharmaceutical Applications. *Res. Pharm. Sci.* 10 (1), 1–16.

Ahmed, H. B., and Emam, H. E. (2019). Synergistic Catalysis of Monometallic (Ag, Au, Pd) and Bimetallic (Ag Au, Au Pd) versus Trimetallic (Ag-Au-Pd) Nanostructures Effloresced via Analogical Techniques. *J. Mol. Liquids* 287, 110975. doi:10.1016/j.molliq.2019.110975

Aranaz, I., Acosta, N., Civera, C., Elorza, B., Mingo, J., Castro, C., et al. (2018). Cosmetics and Cosmeceutical Applications of Chitin, Chitosan and Their Derivatives. *Polymers* 10 (2), 213. doi:10.3390/polym10020213

Asthana, N., Pal, K., Aljabali, A. A. A., Tambuwala, M. M., de Souza, F. G., and Pandey, K. (2021). Polyvinyl Alcohol (PVA) Mixed green-clay and Aloe Vera Based Polymeric Membrane Optimization: Peel-Off Mask Formulation for Skin Care Cosmeceuticals in green Nanotechnology. *J. Mol. Struct.* 1229, 129592. doi:10.1016/j.molstruc.2020.129592

Belo, C. R., Cansado, I. P. d. P., and Mourão, P. A. M. (2017). Synthetic Polymers Blend Used in the Production of High Activated Carbon for Pesticides Removals from Liquid Phase. *Environ. Technol.* 38 (3), 285–296. doi:10.1080/09593330.2016.1190409

Biswas, G., Jena, B. C., Samanta, P., Mandal, M., and Dhara, D. (2021). Synthesis, Self-Assembly and Drug Release Study of a New Dual-Responsive Biocompatible Block Copolymer Containing Phenylalanine Derivative. *J. Macromolecular Sci. A*, 1–12. doi:10.1080/10601325.2021.1947748

Calori, I. R., Braga, G., de Jesus, P. d. C. C., Bi, H., and Tedesco, A. C. (2020). Polymer Scaffolds as Drug Delivery Systems. *Eur. Polym. J.* 129, 109621. doi:10.1016/j.eurpolymj.2020.109621

Cao, Y., Liu, F., Chen, Y., Yu, T., Lou, D., Guo, Y., et al. (2017). Drug Release from Core-Shell PVA/silk Fibroin Nanoparticles Fabricated by One-step Electrospraying. *Sci. Rep.* 7 (1), 11913–11919. doi:10.1038/s41598-017-12351-1

Chakravarthi, S. S., Robinson, D. H., and De, S. (2007). Nanoparticles Prepared Using Natural and Synthetic Polymers. *Nanoparticulate Drug Delivery Systems*. CRC Press, 51–60. doi:10.1201/9781420008449-3

Chou, S.-F., Carson, D., and Woodrow, K. A. (2015). Current Strategies for Sustaining Drug Release from Electrospun Nanofibers. *J. Controlled Release* 220, 584–591. doi:10.1016/j.jconrel.2015.09.008

Cirillo, G., Spataro, T., Curcio, M., Spizzirri, U. G., Nicoletta, F. P., Picci, N., et al. (2015). Tunable Thermo-Responsive Hydrogels: Synthesis, Structural Analysis and Drug Release Studies. *Mater. Sci. Eng. C* 48, 499–510. doi:10.1016/j.msec.2014.12.045

Doberenz, F., Zeng, K., Willems, C., Zhang, K., and Groth, T. (2020). Thermoresponsive Polymers and Their Biomedical Application in Tissue Engineering - a Review. *J. Mater. Chem. B* 8 (4), 607–628. doi:10.1039/c9tb02052g

Duarah, S., Pujari, K., Durai, R. D., and Narayanan, V. H. B. (2016). Nanotechnology-based Cosmeceuticals: a Review. *Int. J. Appl. Pharm.* 8 (1), 8–12. doi:10.22159/ijap.2016v8i1.10533

Duvvuri, S., Janoria, K. G., and Mitra, A. K. (2005). Development of a Novel Formulation Containing Poly(d,l-Lactide-Co-Glycolide) Microspheres Dispersed in PLGA-PEG-PLGA Gel for Sustained Delivery of Ganciclovir. *J. Control. Release* 108 (2-3), 282–293. doi:10.1016/j.jconrel.2005.09.002

Duvvuri, S., Gaurav Janoria, K., and Mitra, A. K. (2006). Effect of Polymer Blending on the Release of Ganciclovir from PLGA Microspheres. *Pharm. Res.* 23 (1), 215–223. doi:10.1007/s11095-005-9042-6

Emam, H. E., and Ahmed, H. B. (2019). Comparative Study between Homo-Metallic & Hetero-Metallic Nanostructures Based agar in Catalytic Degradation of Dyes. *Int. J. Biol. macromolecules* 138, 450–461. doi:10.1016/j.ijbiomac.2019.07.098

Emam, H. E., El-Shahat, M., and Abdelhameed, R. M. (2021). Observable Removal of Pharmaceutical Residues by Highly Porous Photoactive Cellulose Acetate@MIL-MOF Film. *J. Hazard. Mater.* 414, 125509. doi:10.1016/j.jhazmat.2021.125509

Emam, H. E., Saad, N. M., Abdallah, A. E. M., and Ahmed, H. B. (2020). Acacia Gum versus Pectin in Fabrication of Catalytically Active Palladium Nanoparticles for Dye Discoloration. *Int. J. Biol. macromolecules* 156, 829–840. doi:10.1016/j.ijbiomac.2020.04.018

Entezar-Almahdi, E., Heidari, R., Ghasemi, S., Mohammadi-Samani, S., and Farjadian, F. (2021). Integrin Receptor Mediated pH-Responsive Nano-Hydrogel Based on Histidine-Modified Poly(aminoethyl Methacrylamide) as Targeted Cisplatin Delivery System. *J. Drug Deliv. Sci. Technol.* 62, 102402. doi:10.1016/j.jddst.2021.102402

Farjadian, F., Rezaeifard, S., Naeimi, M., Ghasemi, S., Mohammadi-Samani, S., Welland, M. E., et al. (2019). Temperature and pH-Responsive Nano-Hydrogel Drug Delivery System Based on Lysine-Modified Poly (Vinylcaprolactam). *Int. J. Nanomedicine* 14, 6901–6915. doi:10.2147/ijn.s214467

Farzanfar, J., Farjadian, F., Roointan, A., Mohammadi-Samani, S., and Tayebi, L. (2021). Assessment of pH Responsive Delivery of Methotrexate Based on PHEMA-St-PEG-DA Nanohydrogels. *Macromol. Res.* 29 (1), 54–61. doi:10.1007/s13233-021-9007-6

Freag, M. S., Saleh, W. M., and Abdallah, O. Y. (2018). Exploiting Polymer Blending Approach for Fabrication of Buccal Chitosan-Based Composite Sponges with Augmented Mucoadhesive Characteristics. *Eur. J. Pharm. Sci.* 120, 10–19. doi:10.1016/j.ejps.2018.04.041

Ghasemiyeh, P., Azadi, A., Daneshamouz, S., and Mohammadi Samani, S. (2017). Cyproterone Acetate-Loaded Solid Lipid Nanoparticles (SLNs) and Nanostructured Lipid Carriers (NLCs): Preparation and Optimization. *Trends Pharm. Sci.* 3 (4), 275–286.

Ghasemiyeh, P., and Mohammadi-Samani, S. (2019). Hydrogels as Drug Delivery Systems; Pros and Cons. *Trends Pharm. Sci.* 5 (1), 7–24. doi:10.30476/TIPS.2019.81604.1002

Ghasemiyeh, P., and Mohammadi-Samani, S. (2018). Solid Lipid Nanoparticles and Nanostructured Lipid Carriers as Novel Drug Delivery Systems: Applications, Advantages and Disadvantages. *Res. Pharm. Sci.* 13 (4), 288–303. doi:10.4103/1735-5362.235156

Ghasemiyeh, P., Azadi, A., Daneshamouz, S., Heidari, R., Azarpira, N., and Mohammadi-Samani, S. (2019). Cyproterone Acetate-Loaded Nanostructured Lipid Carriers: Effect of Particle Size on Skin Penetration and Follicular Targeting. *Pharm. Dev. Technol.* 24 (7), 812–823. doi:10.1080/10837450.2019.1596133

Ghasemiyeh, P., and Mohammadi-Samani, S. (2020). Potential of Nanoparticles as Permeation Enhancers and Targeted Delivery Options for Skin: Advantages and Disadvantages. *Drug Des. Devel Ther.* 14, 3271–3289. doi:10.2147/dddt.s264648

Guo, B., and Ma, P. X. (2018). Conducting Polymers for Tissue Engineering. *Biomacromolecules* 19 (6), 1764–1782. doi:10.1021/acs.biomac.8b00276

Hamoudi-Ben Yelles, M. C., Tran Tan, V., Danede, F., Willart, J. F., and Siepmann, J. (2017). PLGA Implants: How Poloxamer/PEO Addition Slows Down or Accelerates Polymer Degradation and Drug Release. *J. Controlled Release* 253, 19–29. doi:10.1016/j.jconrel.2017.03.009

Hillmyer, M. (1999). Block Copolymer Synthesis. *Curr. Opin. Solid State. Mater. Sci.* 4 (6), 559–564. doi:10.1016/s1359-0286(00)00006-1

Hussain, M., Xie, J., Hou, Z., Shezad, K., Xu, J., Wang, K., et al. (2017). Regulation of Drug Release by Tuning Surface Textures of Biodegradable Polymer Microparticles. *ACS Appl. Mater. Inter.* 9 (16), 14391–14400. doi:10.1021/acsami.7b02002

Jones, C. D., and Lyon, L. A. (2000). Synthesis and Characterization of Multiresponsive Core–Shell Microgels. *Macromolecules* 33 (22), 8301–8306. doi:10.1021/ma001398m

Jones, S. A., Martin, G. P., Royall, P. G., and Brown, M. B. (2005). Biocompatible Polymer Blends: Effects of Physical Processing on the Molecular Interaction of Poly(vinyl Alcohol) and Poly(vinyl Pyrrolidone). *J. Appl. Polym. Sci.* 98 (5), 2290–2299. doi:10.1002/app.22390

Keogh, R., Blackman, L. D., Foster, J. C., Varlas, S., and O'Reilly, R. K. (2020). The Importance of Cooperativity in Polymer Blending: Toward Controlling the Thermoresponsive Behavior of Blended Block Copolymer Micelles. *Macromol. Rapid Commun.* 41 (6), 1900599. doi:10.1002/marc.201900599

Klouda, L. (2015). Thermoresponsive Hydrogels in Biomedical Applications. *Eur. J. Pharmaceutics Biopharmaceutics* 97, 338–349. doi:10.1016/j.ejpb.2015.05.017

Kolhe, P., and Kannan, R. M. (2003). Improvement in Ductility of Chitosan through Blending and Copolymerization with PEG: FTIR Investigation of Molecular Interactions. *Biomacromolecules* 4 (1), 173–180. doi:10.1021/bm025689+

Kong, T., Wu, J., Yeung, K. W. K., To, M. K. T., Wang, L., and Wang, L. (2013). Microfluidic Fabrication of Polymeric Core-Shell Microspheres for Controlled Release Applications. *Biomicrofluidics* 7 (4), 044128. doi:10.1063/1.4819274

Langer, R. (1993). Polymer-controlled Drug Delivery Systems. *Acc. Chem. Res.* 26 (10), 537–542. doi:10.1021/ar00034a004

Lecomte, F., Siepmann, J., Walther, M., MacRae, R. J., and Bodmeier, R. (2003). Blends of Enteric and GIT-Insoluble Polymers Used for Film Coating: Physicochemical Characterization and Drug Release Patterns. *J. controlled release* 89 (3), 457–471. doi:10.1016/s0168-3659(03)00155-x

Liechty, W. B., Kryscio, D. R., Slaughter, B. V., and Peppas, N. A. (2010). Polymers for Drug Delivery Systems. *Annu. Rev. Chem. Biomol. Eng.* 1, 149–173. doi:10.1146/annurev-chembioeng-073009-100847

Liu, J., Lin, S., Li, L., and Liu, E. (2005). Release of Theophylline from Polymer Blend Hydrogels. *Int. J. Pharmaceutics* 298 (1), 117–125. doi:10.1016/j.ijpharm.2005.04.006

Lu, K.-Y., Lin, Y.-C., Lu, H.-T., Ho, Y.-C., Weng, S.-C., Tsai, M.-L., et al. (2019). A Novel Injectable *In Situ* Forming Gel Based on Carboxymethyl Hexanoyl Chitosan/hyaluronic Acid Polymer Blending for Sustained Release of Berberine. *Carbohydr. Polym.* 206, 664–673. doi:10.1016/j.carbpol.2018.11.050

Marks, J. A., Wegiel, L. A., Taylor, L. S., and Edgar, K. J. (2014). Pairwise Polymer Blends for Oral Drug Delivery. *J. Pharm. Sci.* 103 (9), 2871–2883. doi:10.1002/jps.23991

Mohammadi, F., Mohammadi Samani, S., Tanideh, N., and Ahmadi, F. (2018). Hybrid Scaffolds of Hyaluronic Acid and Collagen Loaded with Prednisolone: An Interesting System for Osteoarthritis. *Adv. Pharm. Bull.* 8 (1), 11–19. doi:10.15171/apb.2018.002

Mohammadi-Samani, S., and Taghipour, B. (2015). PLGA Micro and Nanoparticles in Delivery of Peptides and Proteins; Problems and Approaches. *Pharm. Dev. Technol.* 20 (4), 385–393. doi:10.3109/10837450.2014.882940

Monfared, M., Taghizadeh, S., Zare-Hoseinabadi, A., Mousavi, S. M., Hashemi, S. A., Ranjbar, S., et al. (2019). Emerging Frontiers in Drug Release Control by Core-Shell Nanofibers: a Review. *Drug Metab. Rev.* 51 (4), 589–611. doi:10.1080/03602532.2019.1642912

Naseem, K., Begum, R., Wu, W., Irfan, A., and Farooqi, Z. H. (2018). Advancement in Multi-Functional Poly(styrene)-Poly(N-Isopropylacrylamide) Based Core-Shell Microgels and Their Applications. *Polym. Rev.* 58 (2), 288–325. doi:10.1080/15583724.2017.1423326

Ojah, N., Saikia, D., Gogoi, D., Baishya, P., Ahmed, G. A., Ramteke, A., et al. (2019). Surface Modification of Core-Shell Silk/PVA Nanofibers by Oxygen Dielectric Barrier Discharge Plasma: Studies of Physico-Chemical Properties and Drug Release Behavior. *Appl. Surf. Sci.* 475, 219–229. doi:10.1016/j.apsusc.2018.12.270

Perinelli, D. R., Bonacucina, G., Pucciarelli, S., Cespi, M., Casettari, L., Polzonetti, V., et al. (2014). Could Albumin Affect the Self-Assembling Properties of a Block Co-polymer System and Drug Release? an *In-Vitro* Study. *Pharm. Res.* 32 (3), 1094–1104. doi:10.1007/s11095-014-1521-1

Pillai, O., and Panchagnula, R. (2001). Polymers in Drug Delivery. *Curr. Opin. Chem. Biol.* 5 (4), 447–451. doi:10.1016/s1367-5931(00)00227-1

Roointan, A., Farzanfar, J., Mohammadi-Samani, S., Behzad-Behbahani, A., and Farjadian, F. (2018). Smart pH Responsive Drug Delivery System Based on poly(HEMA-Co-DMAEMA) Nanohydrogel. *Int. J. Pharm.* 552 (1-2), 301–311. doi:10.1016/j.ijpharm.2018.10.001

Roointan, A., Kianpour, S., Memari, F., Gandomani, M., Gheibi Hayat, S. M., and Mohammadi-Samani, S. (2018). Poly(lactic-co-glycolic Acid): The Most Ardent and Flexible Candidate in Biomedicine!. *Int. J. Polymeric Mater. Polymeric Biomater.* 67 (17), 1028–1049. doi:10.1080/00914037.2017.1405350

Salmanpour, M., Yousefi, G., Samani, S. M., Mohammadi, S., Anbardar, M. H., and Tamaddon, A. (2019). Nanoparticulate Delivery of Irinotecan Active Metabolite (SN38) in Murine Colorectal Carcinoma through Conjugation to Poly (2-ethyl 2-Oxazoline)-B-Poly (L-Glutamic Acid) Double Hydrophilic Copolymer. *Eur. J. Pharm. Sci.* 136, 104941. doi:10.1016/j.ejps.2019.05.019

Samani, S. M., Montaseri, H., and Kazemi, A. (2003). The Effect of Polymer Blends on Release Profiles of Diclofenac Sodium from Matrices. *Eur. J. pharmaceutics biopharmaceutics* 55 (3), 351–355. doi:10.1016/s0939-6411(03)00030-4

Sionkowska, A. (2011). Current Research on the Blends of Natural and Synthetic Polymers as New Biomaterials: Review. *Prog. Polym. Sci.* 36 (9), 1254–1276. doi:10.1016/j.progpolymsci.2011.05.003

Sionkowska, A., Wisniewski, M., Skopinska, J., Kennedy, C. J., and Wess, T. J. (2004). Molecular Interactions in Collagen and Chitosan Blends. *Biomaterials* 25 (5), 795–801. doi:10.1016/s0142-9612(03)00595-7

Sohrabi, A., Shaibani, P. M., Etayash, H., Kaur, K., and Thundat, T. (2013). Sustained Drug Release and Antibacterial Activity of Ampicillin Incorporated Poly(methyl Methacrylate)-Nylon6 Core/shell Nanofibers. *Polymer* 54 (11), 2699–2705. doi:10.1016/j.polymer.2013.03.046

Srikar, R., Yarin, A. L., Megaridis, C. M., Bazilevsky, A. V., and Kelley, E. (2008). Desorption-limited Mechanism of Release from Polymer Nanofibers. *Langmuir* 24 (3), 965–974. doi:10.1021/la702449k

Srivastava, A., Yadav, T., Sharma, S., Nayak, A., Kumari, A. A., and Mishra, N. (2015). Polymers in Drug Delivery. *J. Biosciences Medicines* 4 (1), 69–84. doi:10.4236/jbm.2016.41009

Taghipour, B., Yakhchali, M., Haririan, I., Tamaddon, A. M., and Samani, S. M. (2014). The Effects of Technical and Compositional Variables on the Size and Release Profile of Bovine Serum Albumin from PLGA Based Particulate Systems. *Res. Pharm. Sci.* 9 (6), 407–420.

Tiwari, S. K., Tzezana, R., Zussman, E., and Venkatraman, S. S. (2010). Optimizing Partition-Controlled Drug Release from Electrospun Core-Shell Fibers. *Int. J. Pharm.* 392 (1-2), 209–217. doi:10.1016/j.ijpharm.2010.03.021

Tran, T. H., Ramasamy, T., Choi, J. Y., Nguyen, H. T., Pham, T. T., Jeong, J. H., et al. (2015). Tumor-targeting, pH-Sensitive Nanoparticles for Docetaxel Delivery to Drug-Resistant Cancer Cells. *Int. J. Nanomedicine* 10, 5249–5262. doi:10.2147/IJN.S89584

Vaidya, U. R., and Bhattacharya, M. (1994). Properties of Blends of Starch and Synthetic Polymers Containing Anhydride Groups. *J. Appl. Polym. Sci.* 52 (5), 617–628. doi:10.1002/app.1994.070520505

Vashisth, P., Singh, R. P., and Pruthi, V. (2016). A Controlled Release System for Quercetin from Biodegradable Poly(lactide-Co-Glycolide)-Polycaprolactone

Nanofibers and its *In Vitro* Antitumor Activity. *J. Bioactive Compatible Polym.* 31 (3), 260–272. doi:10.1177/0883911515613098

Wang, C., Han, W., Tang, X., and Zhang, H. (2012). Evaluation of Drug Release Profile from Patches Based on Styrene-Isoprene-Styrene Block Copolymer: The Effect of Block Structure and Plasticizer. *Aaps Pharmscitech* 13 (2), 556–567. doi:10.1208/s12249-012-9778-3

Ward, M. A., and Georgiou, T. K. (2011). Thermoresponsive Polymers for Biomedical Applications. *Polymers* 3 (3), 1215–1242. doi:10.3390/polym3031215

Wu, T., Ding, M., Shi, C., Qiao, Y., Wang, P., Qiao, R., et al. (2020). Resorbable Polymer Electrospun Nanofibers: History, Shapes and Application for Tissue Engineering. *Chin. Chem. Lett.* 31 (3), 617–625. doi:10.1016/j.cclet.2019.07.033

Xiao, X.-C., Chu, L.-Y., Chen, W.-M., Wang, S., and Xie, R. (2004). Preparation of Submicrometer-Sized Monodispersed Thermoresponsive Core–Shell Hydrogel Microspheres. *Langmuir* 20 (13), 5247–5253. doi:10.1021/la036230j

Yin, W., Ke, W., Lu, N., Wang, Y., Japir, A. A.-W. M. M., Mohammed, F., et al. (2020). Glutathione and Reactive Oxygen Species Dual-Responsive Block Copolymer Prodrugs for Boosting Tumor Site-specific Drug Release and Enhanced Antitumor Efficacy. *Biomacromolecules* 21 (2), 921–929. doi:10.1021/acs.biomac.9b01578

Zhang, H., Chang, L., Zhang, B., Li, P., Wang, M., Yao, K. D., et al. (2008). Synthesis and Characterization of Microparticles Made of Carboxymethyloxysuccinic-Acid-Modified PLA-PEG Co-polymer. *J. Biomater. Sci. Polym. Edition* 19 (1), 99–111. doi:10.1163/156856208783227677

Zhang, L. (2007). *Thermally-responsive Core-Shell Particles*. Bethlehem, Pennsylvania: Lehigh University.

Zhang, Z., Tsai, P.-C., Ramezanli, T., and Michniak-Kohn, B. B. (2013). Polymeric Nanoparticles-Based Topical Delivery Systems for the Treatment of Dermatological Diseases. *WIREs Nanomed Nanobiotechnol* 5 (3), 205–218. doi:10.1002/wnan.1211

Zupančič, Š. (2019). Core-shell Nanofibers as Drug Delivery Systems. *Acta Pharm.* 69 (2), 131–153. doi:10.2478/acph-2019-0014

Zupančič, Š., Sinha-Ray, S., Sinha-Ray, S., Kristl, J., and Yarin, A. L. (2016). Controlled Release of Ciprofloxacin from Core-Shell Nanofibers with Monolithic or Blended Core. *Mol. Pharm.* 13 (4), 1393–1404. doi:10.1021/acs.molpharmaceut.6b00039

Conflict of Interest: The authors declare that the research was conducted in the absence of any commercial or financial relationships that could be construed as a potential conflict of interest.

Publisher's Note: All claims expressed in this article are solely those of the authors and do not necessarily represent those of their affiliated organizations, or those of the publisher, the editors and the reviewers. Any product that may be evaluated in this article, or claim that may be made by its manufacturer, is not guaranteed or endorsed by the publisher.

frontiers in Materials

ORIGINAL RESEARCH
published: 26 January 2022
doi: 10.3389/fmats.2021.803054

Hydroxyapatite Growth on Poly (Dimethylsiloxane-Block-ε-Caprolactone)/Tricalcium Phosphate Coatings Obtained by Electrophoretic Deposition

Franco Leonardo Redondo[1,2], *María Carolina Giaroli*[1,2], *Andrés Eduardo Ciolino*[3,4] *and Mario Daniel Ninago*[1,2]*

[1]Universidad Nacional de Cuyo, Facultad de Ciencias Aplicadas a La Industria, San Rafael, Mendoza, Argentina, [2]Consejo Nacional de Investigaciones Científicas y Técnicas (CONICET), Ciudad Autónoma de Buenos Aires, Buenos Aires, Argentina, [3]Planta Piloto de Ingeniería Química, PLAPIQUI (UNS-CONICET), Bahía Blanca, Argentina, [4]Departamento de Ingeniería Química, Universidad Nacional Del Sur (UNS), Bahía Blanca, Argentina

For the first time, composite coatings based on poly(dimethylsiloxane-*block*-ε-caprolactone) copolymer and tricalcium phosphate were obtained on stainless steel plates by using the electrophoretic deposition technique. The effect of different deposition times on the final characteristics of the resulting coatings was also studied. Block copolymers were obtained through a combination of anionic and ring-opening polymerization, with good homogeneity and chemical composition (Đ < 1.3 and w_{PCL} = 0.39). The composites obtained at different electrophoretic deposition times revealed a linear dependence between the deposited weight and time during assays. When immersing in simulated body fluid, a higher amount of residual solids (~ 20 %) were observed by thermogravimetric analysis after 7 days of immersion. Scanning electron microscopy micrographs revealed a porous microstructure over the metallic substrate and the absence of micro-cracks, and X-ray diffraction patterns exhibited diffraction peaks associated with a hydroxyapatite layer. Finally, energy-dispersive X-ray analysis revealed values of the Ca/P ratio between 1.40 and 1.50 in samples, which are closer to the stoichiometric hydroxyapatite values reported in hard tissues. The results obtained in this article confirm the usefulness of poly(dimethylsiloxane-*block*-ε-caprolactone) copolymer and cheaper tricalcium phosphate as precursors of compact and homogenous coatings obtained by electrophoretic deposition, which yields useful substrates for hydroxyapatite growth.

Keywords: block copolymer, tricalcium phosphate, electrophoretic deposition, bioactivity, hydroxyapatite, ring-opening polymerization

OPEN ACCESS

Edited by:
Nafisa Gull,
University of the Punjab, Pakistan

Reviewed by:
Temel Öztürk,
Giresun University, Turkey
Sixun Zheng,
Shanghai Jiao Tong University, China

***Correspondence:**
Mario Daniel Ninago
mninago@fcai.uncu.edu.ar

Specialty section:
This article was submitted to Polymeric and Composite Materials, a section of the journal Frontiers in Materials

Received: *27 October 2021*
Accepted: *27 December 2021*
Published: *26 January 2022*

Citation:
Redondo FL, Giaroli MC, Ciolino AE and Ninago MD (2022) Hydroxyapatite Growth on Poly(Dimethylsiloxane-Block-ε-Caprolactone)/Tricalcium Phosphate Coatings Obtained by Electrophoretic Deposition. Front. Mater. 8:803054. doi: 10.3389/fmats.2021.803054

1 INTRODUCTION

Biocompatible materials play an important role in the area of tissue engineering mainly because they give a new vision of the development materials destined to the repair and regeneration of tissues or the replacement of missing human bones and teeth, among other applications (Qu et al., 2019). One of the main challenges for polymer´s researchers is to develop non-toxic, biodegradable, bioactive, and osteoconductive materials with good mechanical properties at the time of application. For such a purpose, composites formed from two or more materials with excellent properties (polymers,

ceramics, and bioglasses) are widely used in tissue engineering (Yeong et al., 2010; Qu et al., 2019; Bonetti et al., 2020; Ninago et al., 2020; Redondo et al., 2020). Therefore, tissue engineering is a promising area of growing interest in the design and obtaining of polymer-based bioactive materials because of the large number of opportunities that polymeric materials offer.

The use of these materials can be explained according to their ability to be re-absorbed or degraded after a certain time of being implanted without generating toxic products in the receptor organism, and they provide more controllability on physicochemical characteristics such as pore size, porosity, solubility, biocompatibility, enzymatic reactions, and allergic response (Yang et al., 2015; Clavijo et al., 2016; Ghassemi et al., 2018; Quiroga et al., 2018; Ghalayani Esfahani et al., 2019; Taale et al., 2019). In last years, various methodologies capable of developing these new materials have appeared, such as melt mixing (Pishbin et al., 2015), dissolution-leaching (Jordan et al., 2005), and electrophoretic deposition (EPD) technique (El-Ghannam, 2005; Cabanas-Polo and Boccaccini, 2015; Redondo et al., 2020), among others.

The EPD technique is used for the fabrication of coatings because of its simplicity, versatility, and usefulness on substrates with complex geometry (Ghalayani Esfahani et al., 2019; Bonetti et al., 2020; Pereira et al., 2020). EPD is an extremely promising technique for producing organic/inorganic composite scaffolds over several substrates (magnesium, titanium, and stainless steel, among others) to avoid the release of metal ions due to corrosion phenomena (Ghalayani Esfahani et al., 2019; Joy-anne et al., 2019). In addition, a strong union between the material to be implanted and the bone tissue is achieved with this type of methodology (El-Ghannam, 2005; Cabanas-Polo and Boccaccini, 2015). In particular, EPD of soft composites is an attractive technique that can be used to produce uniform coatings with a controlled microstructure, without requiring expensive equipment (Clavijo et al., 2016; Pereira et al., 2020; Redondo et al., 2020). The use of a polymer matrix in biodegradable composites allows obtaining materials with specific geometries and provides a platform for incorporation and release of biomolecules and drugs. These materials can be used in varied applications such as implants in orthopedic surgery, scaffolds, ligament union, sutures, controlled release of drugs, flexible tubes for cardiovascular surgery, and dental repairs, among others (Zhao et al., 2008; Ghasemi-Mobarakeh et al., 2010; Ghalayani Esfahani et al., 2019; Redondo et al., 2020).

Synthetic polymers such as poly(ε-caprolactone) (PCL), poly-lactic acid (PLA), or poly (lactic-co-glycolic) acid (PLGA) are biodegradable and can be used for applications in bone tissue engineering (Boccaccini et al., 2010; Seuss et al., 2016; Pereira et al., 2020). PCL is one of the Food and Drug Administration (FDA)–approved biopolymers and has been extensively used in biomedical applications because of its inherent properties of good mechanical strength, biocompatibility, and biodegradability (Thinakaran et al., 2020). In addition, within the most prominent physicochemical properties of PCL, we can mention its good compatibility with a large variety of polymers (Miola et al., 2015; Joy-anne et al., 2019). Besides, because of being a non-toxic polymer, it is widely used in biomedical applications as long-term implantable devices, scaffolds for tissue growth, drug-delivery systems, and 3D printing or electrospinning devices, among others (Wietor et al., 2011; Liang et al., 2013; Yazdimamaghani et al., 2015; Redondo et al., 2020). PCL or PCL-based copolymers can be obtained by various polymerization techniques such as "click" chemistry, ring-opening polymerization (ROP), or hydrogen-transfer polymerization (Öztürk et al., 2016; Öztürk and Meyvacı, 2017; Savaş et al., 2021). In this sense, ROP is defined as "polymerization in which a cyclic monomer yields a monomeric unit that is either acyclic or contains fewer rings than the cyclic monomer." The technique is widely used for a lot of systems with many monomers, initiators, and catalysts, including lactones and silicones, among others (Öztürk and Meyvacı, 2017).

Silicones, or polysiloxanes, are other biocompatible polymers that are used extensively in the field of biomedicine (Danesin et al., 2012; Redondo et al., 2020). The chemical structure of these polymers has a simple sequence of atoms: polysiloxanes: Si(<)–O–Si(<)–. Usually, substituents at the Si atoms are methyl groups, thus generating the poly(dimethylsiloxane) (PDMS), which is obtained either by polycondensation of $Si(CH_3)_2(Cl)_2$ or by ROP of cyclic monomers, such as hexamethyl (cyclotrisiloxane) (D_3) or octamethyl (cyclotetrasiloxane) (D_4). In addition, PDMS derivatives are widely employed in drug-delivery systems or nanotechnology applications, among others (Nag et al., 2018a; Wolf et al., 2018; Joy-anne, et al., 2019; Luo et al., 2019). PDMS-based organic–inorganic materials have high degrees of flexibility, excellent electrical-insulating properties, and exceptional heat resistance at higher temperatures (Chen et al., 2018; Nag et al., 2018b; Raj et al., 2018; Aoki, 2020). For example, composites from PDMS and ceramic powder allow reducing the thermal stress between the metal substrate and EPD film, while achieving a high thermal conductivity and an enhanced electrical insulation without sintering (Aoki, 2020).

Ceramic materials such as calcium phosphates and silicate glasses are interesting biomaterials due to their bioactivity properties (osteoconduction and osteoinduction) and their ability to form a reactive hydroxyapatite (HA) layer. In recent years, specific compositions of them have been used to obtain hard and soft implants for tissue engineering (Zhou and Lee, 2011; Sartore et al., 2019; Wang et al., 2019; Pereira et al., 2020). The development of bioresorbable and bioactive composites for tissue engineering applications is being investigated worldwide, and many approaches have been published by including combinations of resorbable homopolymers such as PLA, PLGA, and PCL, with HA, tricalcium phosphate ($Ca_3(PO4)_2$, TCP), or bioactive glasses and glass-ceramics in different scaffold architectures (Duruncan and Brown, 2001; Ma et al., 2001; Yang et al., 2005; Ghassemi et al., 2018; Sungsee and Tanrattanakul, 2019). In the most usual approach, HA, TCP, and bioactive glass particles are combined with polymeric biodegradable substrates in order to obtain the desired scaffolds or coatings (Roether et al., 2002; Taale et al., 2019; Mondal et al., 2020; Shah Mohammadi et al., 2020).

HA particles exhibit a chemical composition and crystalline structure similar to that of living bones, and show high

osteoconductivity as well as bioresorbability in biological environments (Maeda et al., 2007; Ramezani et al., 2017). One of the main purposes for employing HA in the synthesis of biodegradable polymeric scaffolds is its ability to modify surface properties in the resulting composites, which are suitable for their use in bone-tissue engineering (Ramezani et al., 2017; Qu et al., 2019; Zhao et al., 2019). The deposition of the HA layer on polymeric materials by using a simulated body-fluid (SBF) solution is often generated by the increase in the supersaturation of inorganic ions in the medium. On the other hand, TCP excels in terms of degradability and bioactivity (two important reasons for its frequent use in clinical applications), and it has attracted much interest since it has been postulated as a precursor of HA formation (Loher et al., 2006). Consequently, it might be reasonable to use TCP as a Ca^{2+} ions–releasing source, by supplying the desired Ca^{2+} ions when immersed in SBF and by promoting HA synthesis (Yu et al., 2018; Dorozhkin, 2010).

In one of the previous work, we reported the capability of block copolymers to induce the precipitation of a HA layer (Redondo et al., 2018; Ninago et al., 2020; Redondo et al., 2020). In this sense, the effect of molecular architecture (linear or branched) of block copolymers and the use of Bioglass® on EPD tests (t = 6 min) was analyzed. It was observed that linear block copolymers promote a better HA deposition when *in vitro* assays were performed. By taking into account these results, in this work, bioactive coatings based on PDMS-*b*-PCL block copolymer and TCP as a mineral filler were employed for HA deposition by using the EPD technique. The emphasis of this work is placed on the combination of these materials for the first time, by obtaining bioactive coatings that promote HA growth. In addition, the effect of EPD time was also studied. It is envisioned that the coatings obtained from this methodology will combine PDMS-*b*-PCL and HA composites in a synergic way, which could be considered as an alternative for scaffolds in bone-tissue engineering (Chen et al., 2019; Qu et al., 2019; Mondal et al., 2020).

2 MATERIALS AND METHODS

Materials

The reagents used for anionic and ROP polymerization were purified by the traditional procedures reported in the literature (Uhrig and Mays, 2005; Redondo et al., 2020). Hexamethyl (cyclotrisiloxane) monomer (D_3, Sigma-Aldrich, 98 %) for anionic polymerization and ε-caprolactone (ε-CL, Sigma-Aldrich, 99 %) for block copolymer synthesis were purified by mixing with the calcium hydride powder (CaH_2, Sigma-Aldrich, 95 %), followed by heating and distilling under vacuum according to conventional procedures. Tetrahydrofuran (THF, Ciccarelli), cyclohexane (Dorwill), and methanol (Química Industrial) were used for the reaction (Agudelo and Pérez, 2016), and stannous octoate was used as a polymerization catalyst (Satti et al., 2017).

For EPD assays, the obtained block copolymers and TCP (CARLO ERBA Reagents) were employed (Boccaccini et al., 2007; Quiroga et al., 2018). Acetone (Sintorgan) was used as a solvent and stainless steel (AISI 316L) plates as metallic substrates. For bioactivity assessments, simulated body fluid (SBF) was prepared according to the suggestions given by Kokubo and Takadama (2006).

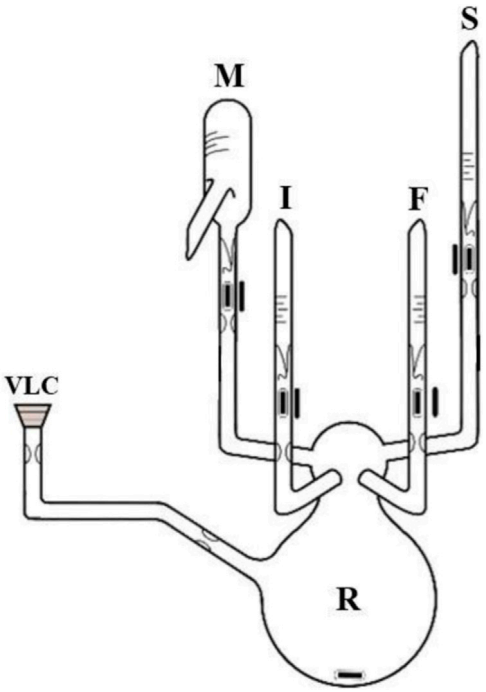

SCHEME 1 | Reactor for PDMS-OH synthesis. References: I: sec-Bu^-Li^+ ampoule; S: THF ampoule; M: D_3 monomer in a cyclohexane ampoule; F: methanol ampoule; R: main reactor; VLC: vacuum line connection.

Synthesis of PDMS-OH Macroinitiator and Linear Block Copolymer

2.1.1 PDMS-OH

The poly(dimethylsiloxane) (PDMS-OH) homopolymer was synthesized by anionic polymerization, employing hand-made polymerization reactors and high-vacuum techniques (**Scheme 1**) (Ninago et al., 2017; Redondo, 2018). In brief, the sealed ampoule of the D_3 monomer (12.5 g, previously dissolved in 40–50 ml of dry cyclohexane) was gently broken and poured into the reactor flask, followed by the addition of the sec-Bu^-Li^+ ampoule (2.9 ml, 0.28 M). The reagents were gently mixed by employing manual movements, and the reaction was left to proceed during ~ 20 h at room temperature. Then, the THF ampoule (10 ml) was broken, and polymerization was left to proceed, at room temperature, during 20 h. The reaction was finished by the addition of the well-degassed methanol ampoule (5 ml), and the resulting PDMS-OH polymer was then precipitated in cold methanol (**Scheme 1**).

2.1.2 PDMS-*B*-PCL Copolymer

The PDMS-*b*-PCL copolymer was synthesized by ROP polymerization of ε-CL monomer, according to the methodology already published by the group (Redondo et al. 2018). Copolymerization was carried out in a glass reactor under

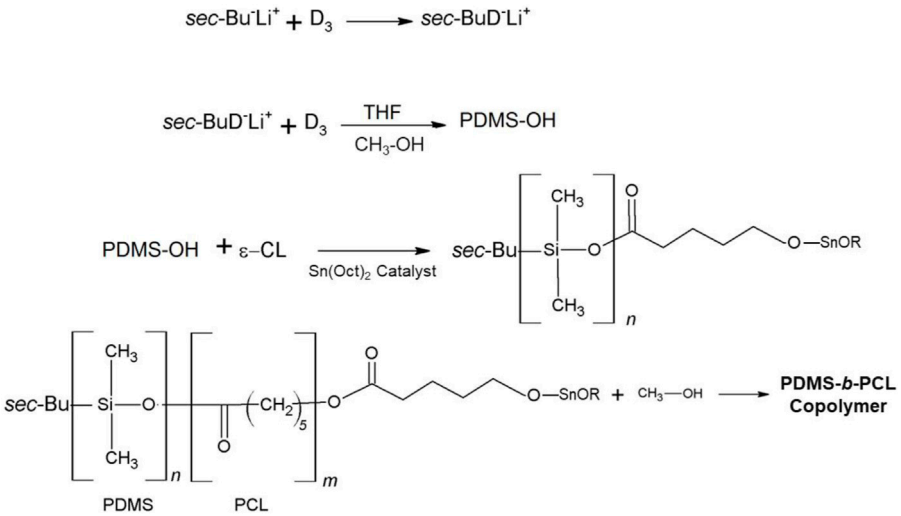

SCHEME 2 | Reaction pathway in the synthesis of PDMS-OH and PDMS-*b*-PCL copolymer.

the nitrogen atmosphere, by employing degassed toluene as a solvent and tin (II) 2-ethylhexanoate ($Sn(Oct)_2$) as a catalyst, at 110°C for 24 h (**Scheme 2**). A catalyst/PDMS-OH ratio of 0.5 was employed (Satti et al., 2017). The obtained copolymers were precipitated, filtered, and stored until their use.

Characterization of the Linear Block Copolymer and TCP Powder

2.1.3 Nuclear Magnetic Resonance (^{1}H-NMR)

The ^{1}H-NMR spectrum of PDMS-*b*-PCL copolymer was performed by using an Avance DPX 400 spectrometer (400 MHz for H and 100 MHz for C) employing $CDCl_3$ as a solvent. From the spectrum, the content of PCL in PDMS-*b*-PCL (the weight fraction of PCL in the copolymer, w_{PCL}) was determined.

2.1.4 Size-Exclusion Chromatography

The molar mass and polydispersity were determined by using an SEC-employing system, a Waters 515 HPLC pump, and a Waters model 410 differential refractometer detector. Toluene and polystyrene were employed as a solvent and standard for calibration, respectively.

2.1.5 Fourier-Transform Infrared Spectroscopy (FTIR-ATR)

Spectra of block copolymer and TCP particles were registered on a Nicolet® iS5 spectrometer, equipped with an attenuated total reflectance accessory (iD7-ATR). Samples were recorded with an accumulation of 16 scans between 3,500–550 cm^{-1} range and a resolution of 4 cm^{-1}.

2.1.6 Differential Scanning Calorimetry

Thermal transitions of PDMS-OH macroinitiator and PDMS-*b*-PCL copolymer were studied on a TA Instruments Calorimeter. Samples (~ 10 mg) were measured under an inert atmosphere of nitrogen, with a flow of 50 ml min^{-1}. First heating was performed from -90–210°C at 10°C min^{-1}. Then, samples were kept at 210°C during 5 min in order to avoid the influence of previous thermal history. After cooling at 10°C min^{-1}, they were heated again from -90–210°C at 10°C min^{-1}. Glass-transition (T_g) and melting temperature (T_m) of PDMS and PCL blocks were determined from this second heating process. With the data obtained, the percentage of crystallinity (% X_c) was obtained by following the equation reported by Yam et al. (1999).

2.1.7 Thermogravimetric Analysis

Thermal stabilities of PDMS-*b*-PCL copolymer and TCP were analyzed by using TGA equipment (Discovery TA Instruments TGA5500 balance). The tests were studied under the nitrogen atmosphere, with a flow of 25 ml min^{-1} and 2°C min^{-1} heating rate, in the 30–700°C range. The percentage of weight loss versus temperature was registered.

2.1.8 Laser Diffraction

Particle-size distribution of TCP was determined by using a Horiba Partica LA-950 Laser Diffraction Particle Size Distribution Analyzer (Kyoto, Japan).

2.1.9 X-Ray Diffraction

The crystal structure identification of TCP was determined by XRD. The patterns were obtained on an Philips PW1710 X-ray diffractometer (Philips, Holland), provided with a tube, a copper anode, and a detector operating at 45 kV and 30 mA within 2θ from 5 to 60°.

2.1.10 Scanning Electron Microscopy

The TCP particles were analyzed by SEM, by using a LEO 40XVP scanning electron microscope, operated at 10 kV. To perform this study, the samples were dispersed over 3M® aluminum

conductive tape by using air flow and coated with gold in an SPI sputter coater. From this analysis, the topographical characteristics of particles were obtained from the secondary electron signal.

Electrophoretic Co-Deposition

Electrophoretic co-deposition assays were performed by following the procedure reported in a previous work (Redondo et al., 2020). For this purpose, a mixture of TCP/copolymer was suspended into a water/acetone solution (10 % v/v) in a [copolymer]:[TCP] ratio equal to 50:50 (wt/wt). It is important to note that prior to the co-EPD deposition procedure, the suspension was stabilized through magnetic stirring and ultrasonic bath for 30 min, by following the procedure previously reported (Redondo et al., 2020). A stainless-steel sample, with rectangular geometry (20 mm × 7 mm x 0.5 mm) was used as a substrate to be coated (working electrode). EPD was carried out by employing an electrophoretic cell connected to an adjustable source (ATTEN model TPR3020S, 220 V/50 Hz). The deposition cell included two parallel stainless-steel foils as a deposition and counter electrodes. The deposition area was fixed at 15 mm × 7 mm, and the distance between electrodes was 10 mm. The deposition conditions for all samples were the following: 20 V by keeping suspension at 56°C and different deposition times: 1, 10, 20, and 30 min. Finally, the samples were removed from suspension and kept in a desiccator, at room temperature.

Characterization of Coatings

2.1.11 Thickness, Deposited Weight, and Thermal Analysis

Coating thicknesses were determined by the use of a digital coating thickness measuring instrument (Digital meter-Microprocessor). Ten values were measured in order to determine the average thickness and standard deviation values. In addition, the deposited weight (W_d) was calculated by employing gravimetric techniques according to **Equation 1**:

$$W_d = \frac{\Delta m}{S_d}, \tag{1}$$

where Δm corresponds to the weight difference between the metallic substrate and the coating, and S_d is the effective deposition area (Redondo et al., 2020).

In addition, the thermal transitions of coatings were studied by employing the aforementioned DSC calorimeter, following the procedure described previously.

In Vitro Assays

Bioactivity tests were carried out by immersion of coatings in SBF during 7 and 28 days at 37°C, replacing SBF solution every 3 days, and by following the protocol already reported by Kokubo and Takadama (2006). FTIR spectra of coatings (before and after being soaked in SBF solution) were obtained by the scratching material employing the aforementioned spectrometer.

Thermal stability of samples after incubation in SBF solution was studied by TGA analysis. Surface appearance of coatings was analyzed by SEM, by using a LEO 40XVP scanning electron microscope, operated at 10 kV. In addition, energy-dispersive X-ray detector (EDX, Model DX-4) with a UTW window was used to quantify the elementary composition of samples. From this analysis, it was possible to visualize the surface of the coatings and the Ca/P ratio. Finally, HA identification was determined by the XRD technique, employing aforementioned equipment.

3 RESULTS AND DISCUSSION

Copolymers and TCP Powder

Figure 1 and **Table 1** summarize the molar mass distribution of PDMS-OH macroinitiator and PDMS-*b*-PCL copolymer. PDMS-OH presents a low dispersity value (Đ = 1.06), which agrees with those obtained by anionic polymerization (almost a symmetric and narrow chromatogram is observed). Besides, PDMS-*b*-PCL shows Đ = 1.36. This value is similar to the values reported in the scientific literature for the synthesis of homopolymers and copolymers based of ε-CL using ROP (Duruncan and Brown, 2001; Ma et al., 2001; Redondo, 2018; Wang et al., 2019). In addition, a clear shift of the PDMS-*b*-PCL chromatogram is also observed in **Figure 1**. This fact constitutes clear evidence of the increase in molar mass due to the incorporation of the PCL block in the resulting copolymer. The PCL content in PDMS-*b*-PCL copolymer was determined by ^{1}H-NMR as w_{PCL} = 0.39 (Zhou and Lee, 2011; Sultana, 2018).

Figure 2 shows the FTIR-ATR spectra of the TCP precursor, PDMS-OH macroinitiator, and PDMS-*b*-PCL copolymer. PDMS-OH macroinitiator exhibits the typical absorption bands detected at 2,963 cm^{-1} (associated with C–H vibration bonds attached to Si atoms) (Liang and Ruckenstein, 1996; Wu et al., 2006; Redondo, 2018); 1,261 cm^{-1} (associated with out-of-phase vibrations of -Si$(CH_3)_2$- and O–Si–O groups) (Agudelo and Pérez, 2016); and 1,094, 1,024, and 801 cm^{-1} (bands associated with the vibration of the Si–O–Si and C–Si–C bonds, respectively) (Agudelo and Pérez, 2016; Ninago et al., 2017; Redondo, 2018). Regarding to PDMS-*b*-PCL copolymer, absorption bands associated to the PCL block are observed at 2,960 and 2,865 cm^{-1} (vibration bands from methylene, -CH_2, groups) and 1,724 cm^{-1} (a pronounced signal attributed to the stretching vibrations from carbonyl groups, >C=O) (Redondo, 2018). In addition, the corresponding absorption bands associated to the PDMS block are also observed at 1,260, 1,091, 1,032, and 801 cm^{-1}. On the other hand, the TCP spectrum shows absorption bands at 1,088, 561, and 600 cm^{-1} (bands associated with bending out-of-plane of the PO_4^{3-} group); 1,026 and 962 cm^{-1} (bands associated with the asymmetric vibration of the PO_4^{3-} group); and typical absorption bands of TCP (Peña and Vallet- Regı, 2003; Reid et al., 2006; Mohandes and Salavati-Niasari, 2014a; Park et al., 2014).

Figure 3 shows X-ray diffraction patterns of TCP. Twelve peaks associated to the structure of TCP are detected at 2Θ ~ 24.8°, 25.8°, 28.1°, 29.0°, 31.8°, 32.8°, 34.1°, 39.8°, 46.7°, 48.1°, 49.5°, and 53.1° (Cordero-Arias et al., 2015). The most prominent peaks in the diffractogram are the following: 2Θ ~ 25.8°, 31.8°, 39.8°, 46.7°, and 53.1°, which correspond to the planes (002), (211),

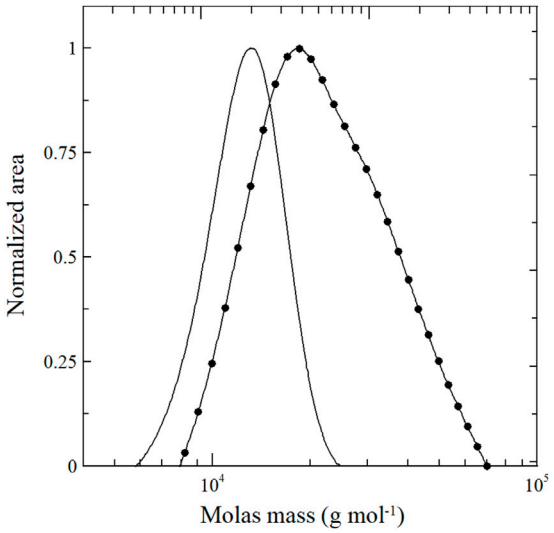

FIGURE 1 | SEC chromatograms: (-) PDMS-OH macroinitiator and (●) PDMS-*b*-PCL copolymer.

(221), (222) y, and (004), respectively (Lala et al., 2016; Aguiar et al., 2018).

The distribution of the particle size from the TCP powder is shown in **Figure 4A**. From LD analysis, an average size of 12.1 μm in a unimodal distribution with a smaller population shoulder (with an average size of 2.9 μm) was determined. The SEM micrograph of TCP shows irregular particles with conglomerates of asymmetric morphology (**Figure 4B**), in accordance with the literature reported by Ginebra et al. (2004) and Nagase et al. (1989).

The thermal characterization of synthesized polymers is shown in **Table 1** and **Figure 5**. Regarding to DSC measurements, PDMS-OH macroinitiator presents only a thermal transition (T_{mPDMS}) in the range of temperature analyzed. Besides, three thermal transitions are detected in PDMS-*b*-PCL copolymer: T_{gPCL} and T_{mPCL} of the PCL block and T_{mPDMS} of the PDMS semi-crystalline phase (Redondo et al., 2018). Besides, % crystallinity (X_c) was obtained by taking into account the PCL content and ΔH_{ref} = 136.1 J g^{-1} (Yam et al., 1999). The value of X_c is reduced in PDMS-*b*-PCL copolymer (26.3 %) when comparing to reference PCL homopolymer (44.7 %) due to the coupling of the PDMS block. Moreover, two thermal transitions were detected in PCL homopolymer: T_{gPCL} and T_{mPCL}.

On the other hand, the thermal degradation initiation temperature ($T_{0.05}$, for 5% mass loss) was calculated from TGA curves (not shown). PDMS-OH macroinitiator shows a $T_{0.05}$ value at ~ 304°C (Ninago et al., 2013; Ramezani et al., 2017; Redondo, 2018). PCL homopolymer shows a $T_{0.05}$ value at 341.5°C, becoming more noticeable after approximately 400°C (the thermal degradation event which corresponds to polyester chain decomposition) (Cai et al., 2014; Ninago et al., 2015; Redondo, 2018). On the other hand, the following degradation events in the copolymer were detected at 193°C (associated to the rupture of polyester chains through the ester pyrolysis reaction generating H_2O, CO_2, and 5-hexenoic acid); at 289°C (associated to the PCL block decomposition); and at 366°C (associated to the PDMS block degradation) (Persenaire et al., 2001; Ninago et al., 2013; Redondo et al., 2018). Regarding to TCP, no decomposition event was observed in the studied range.

Characterization of Coatings

Figure 6 shows thickness and deposited weight values for the coatings obtained at different test times: 1, 10, 20, and 30 min. A linear dependence between deposited weight and time was observed (an R^2 value of 0.98). In addition, an increase in the thickness is also observed for higher EDP times at constant deposition voltage. In accordance, higher thickness and weight values are found at 30 min of EPD assay. In order to obtain thicker coatings, it is convenient to extend the EPD time. In this sense, Bartmanski et al. (2019) and Wang et al. (2002) reported the same behavior in EPD tests obtaining a nanohydroxyapatite coating. These authors stressed that the prolongation of EPD time did not cause any adverse effects on the coating structure and resulted in a significantly higher thickness of the coatings. On the other hand, **Figure 5** includes the thermal transitions of the coatings obtained. In this sense, the glass transition and melting point of the PCL block were detected at −64.0°C and 57.5°C, respectively. Besides, the thermal transition of the PDMS block was also detected at −45.2°C. In addition, a significant reduction in the X_c value for PCL is observed: 3.3 % due to the incorporation of TCP particles interfere in the ordering of the PCL chains during the crystallization process. This phenomenon encourages the decreasing of the X_c value. Chen et al. (2014) reported a similar behavior during the study of PCL composites reinforced with bioactive particles.

TABLE 1 | Thermal characterization of synthesized polymers.

Sample	M_n [a] (g mol^{-1})	Đ [a]	w_{PCL} [b]	T_{gPCL} [c] (°C)	T_{mPDMS} [c] (°C)	T_{mPCL} [c] (°C)	X_c [c] (°C)	$T_{0.05}$ [d] (°C)
PDMS-OH	12,300	1.06	--	--	-44.9	--	n/a	304.0
PCL	26,000	1.60	1.00	−66.0	--	55.9	44.7	341.5
PDMS-*b*-PCL	21,300	1.36	0.39	−59.1	−42.4	50.4	26.3	205.1

[a] *Number average molar mass (M_n) and dispersity (Đ) determined by SEC and ^{1}H-NMR.*
[b] *Weight fraction of PCL in copolymers (w_{PCL}) determined by ^{1}H-NMR.*
[c] *Glass-transition temperature (T_g), melting temperature (T_m), and degree of crystallinity (X_c) determined by DSC.*
[d] *5 % thermal degradation temperature ($T_{0.05}$) determined by TGA.*

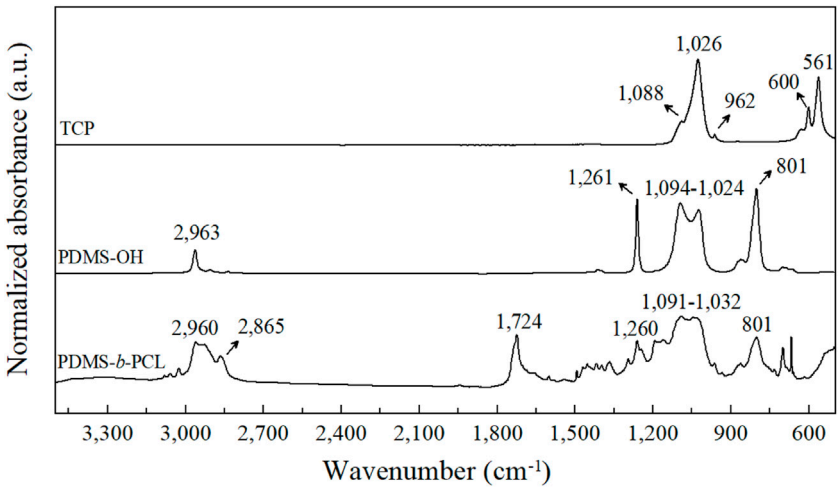

FIGURE 2 | Normalized FTIR-ATR spectra of TCP particles, PDMS-OH macroinitiator, and PDMS-*b*-PCL copolymer (spectra were shifted from the *y*-axis in order to show differences).

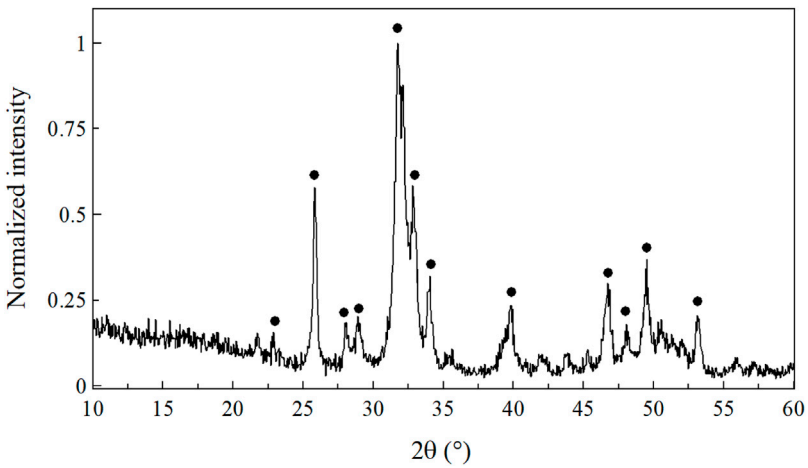

FIGURE 3 | XRD spectrum of TCP particles.

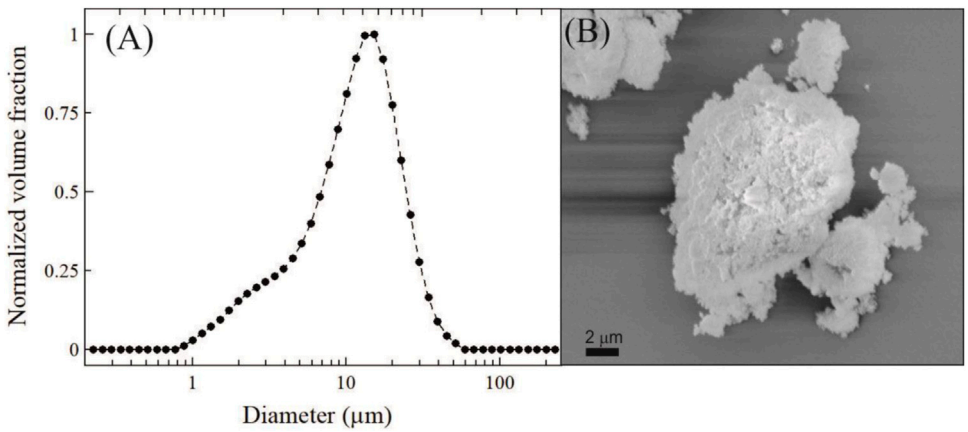

FIGURE 4 | (A) Particle size distribution of TCP by LD and **(B)** SEM micrograph of TCP particles.

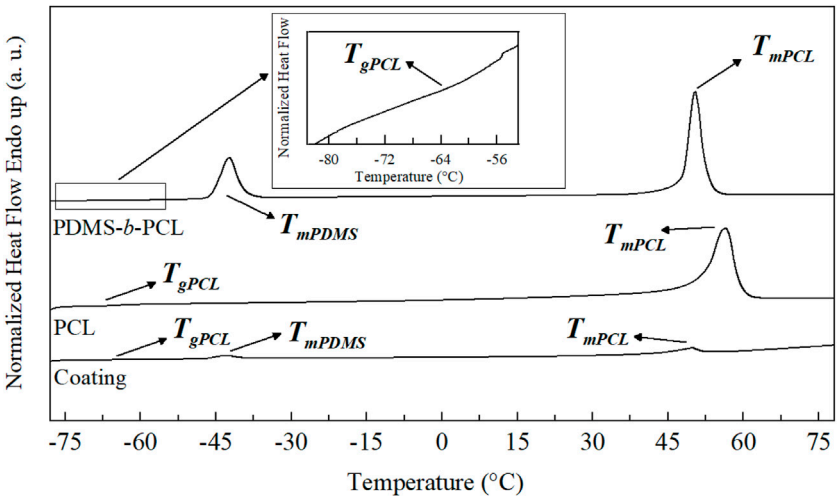

FIGURE 5 | Thermal transitions of PDMS-*b*-PCL copolymer, PCL homopolymer, and coating (before soaking in SBF solution) by DSC.

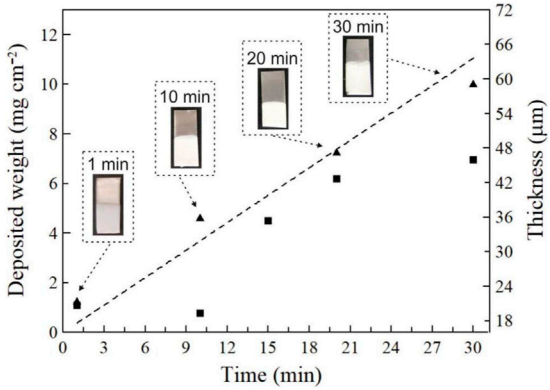

FIGURE 6 | (■) Thickness and (▲) deposited weight of coatings obtained by EPD procedures.

In Vitro Assays

In vitro assays were performed by soaking in SBF solution for 7 and 28 days. For these tests, the sample with higher thickness and weight values was selected (t = 30 min for EPD co-deposition).

Figure 7 shows the normalized FTIR-ATR spectra of the coating before and after immersion in SBF solution for 7 and 28 days, respectively. PCL and PDMS absorption bands are distinguishable in all samples as well as the absorption bands at 1,024 and 600 cm^{-1} (bands associated with the asymmetric vibration and bending out-of-plane of the PO_4^{3-} group, respectively [Peña and Vallet- Regı, 2003; Reid et al., 2006; Mohandes and Salavati-Niasari, 2014a; Park et al., 2014]) attributed to the TCP filler.

After immersion in SBF solution, new vibration bands were detected at 3,183 cm^{-1} (stretching vibration attributed to the crystal water and surface-adsorbed water molecules), 1,629 cm^{-1} (vibrations of the –COOH group), and 1,552 cm^{-1} (vibration of the CO_3^{2-} group). These results are in good agreement with those described by Mohandes and Salavati-Niasari (2014b). In addition, this fact could be explained considering the formation of carboxylic ethers in the coatings and their interaction with a new-formed HA phase on the surface (Chen et al., 2014; Mohandes and Salavati-Niasari, 2014b).

Figure 8 shows X-ray diffraction patterns of coatings after being soaked in SBF solution during 7 and 28 days. XRD patterns of coatings exhibit diffraction peaks associated to the HA phase (Chen et al., 2014). The existence of characteristic diffraction peaks associated with the HA phase are detected at 2Θ values of 26.0°, 31.9°, 33.0°, 34.1°, 39.9°, 46.8°, 49.6°, and 53.3°, corresponding to the diffraction planes (002), (211), (300), (202), (310), (222), (213), and (004), respectively (Mohandes and Salavati-Niasari, 2014a; Mohandes and Salavati-Niasari, 2014b; Miola et al., 2015; Lala et al., 2016; Redondo et al., 2020). This fact confirms the effectiveness of the mineralization process. A similar behavior was observed in a previous work, where composite coatings were obtained by employing the same copolymer and Bioglass® as an inorganic filler. The presence of HA was also detected as an acute and intense signal that appeared at 2Θ ~ 31.8° and other characteristic diffraction peaks at 2Θ ~ 25.9°, 29°, 39°, and 46.7° (Redondo et al., 2020).

In a similar analysis, Dorozhkin (2010) and Suchanek and Yoshimura (1998) stressed that chemical changes can occur in bioceramic materials when they are exposed to *in vitro* conditions. Therefore, in an acidic medium, it was found that TCP particles can be partially dissolved by causing the liberation of Ca^{2+} and PO_4^{3-} ions to the solution. Consequently, the increase of ions leads to the supersaturation of the biologic fluid by promoting the precipitation of biological HA nanocrystals. In this context, Roether et al., (2002) reported that HA is formed on PLA/Bioglass composite materials after 7 days of immersion in SBF. Zhang et al., (2004) also reported that after 7 days of immersion in SBF, PLA/Bioglass composite

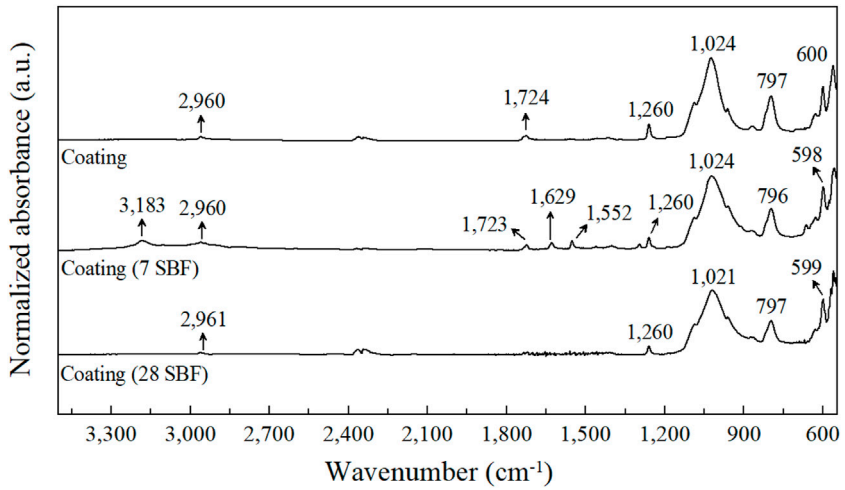

FIGURE 7 | Normalized FTIR-ATR spectra of coatings before and after soaking in SBF solution.

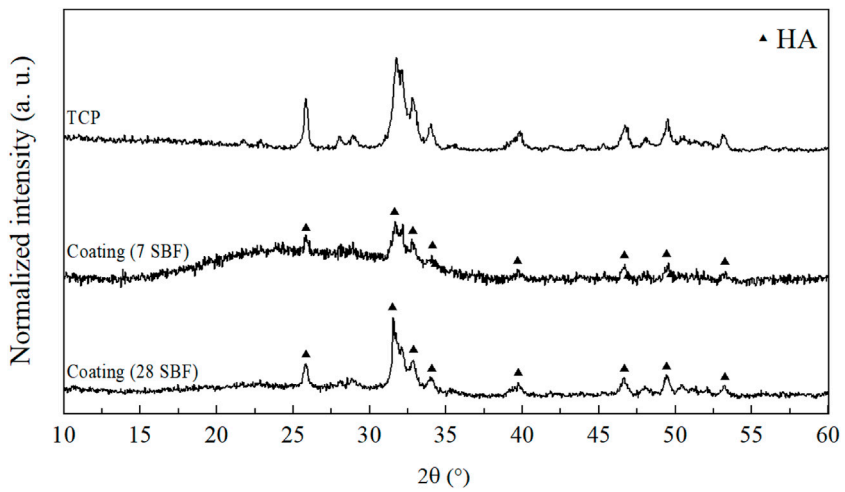

FIGURE 8 | XRD spectra of coatings after immersion in SBF solution.

materials fabricated by using thermally induced phase separation (TIPS) developed HA on their surfaces. In addition, the absence of stainless-steel substrate peaks confirms the successful co-deposition methodology employed. According to the obtained results, TCP/PDMS-*b*-PCL coatings evidenced the ability to form a HA layer onto the composite substrate (Zhang et al., 2004; Maeda et al., 2007).

Thermogravimetric tests before and after *in vitro* assessment are shown in **Figure 9**. Weight loss events in coatings before being soaked in SBF solution are undoubtedly attributed to degradation processes of polymeric chains of PDMS and PCL since TCP particles present thermal stability without degradation events at TGA test temperatures.

The coatings exhibit a slight reduction in $T_{0.05}$ temperatures (239.2°C) when comparing to their respective polymers. The TGA curve of the coating shows a weight loss event associated to the rupture of the PCL block at 236°C, while the PDMS block degradation is evidenced at 368°C (see the two peaks in the first derivative dW/dT). The TGA analysis showed the individual decomposition temperatures of the polymeric blocks that constitute the copolymer. Öztürk et al., (2013) reported the same behavior for the thermal analysis of triarm block copolymers of poly(styrene-*block*-β-butyrolactone) (PS-*b*-PBL). Regarding to the coating after being soaked in SBF solution, only an event of degradation was observed. The decomposition started at 300°C, and it is completed at 400°C, by reaching ~ 89 % weight loss. The first derivative dW/dT curve shows a single peak at 365°C.

When comparing, the weight loss percentage for the coating before immersion in SBF solution is lower than that of the coating

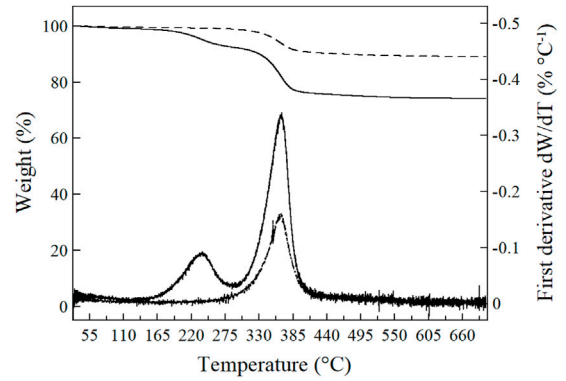

FIGURE 9 | TGA and first derivative dW/dT curves of the coating before (-) and after (--) immersion in SBF solution during 7 days.

after immersion in SBF solution. These results could be indicating that the coating after immersion in SBF solution has a higher content of the HA precipitate itself. This behavior could be attributed to a better transformation of TCP into HA by a dissolution–precipitation mechanism, which produces a new inorganic phase (Suchanek and Yoshimura, 1998; Somrani et al., 2003). Besides, it was possible to calculate the value of the experimental [Polymer]:$[TCP]_e$ wt/wt ratio. The samples tested show a higher TCP value when compared to the theoretical value (50:50 wt/wt). That is to say, coatings before and after immersion in SBF solution presented [Polymer]:$[TCP]_e$ ratios equal to 26:74 (wt/wt) and 11:89 (wt/wt), respectively. In this sense, the macromolecular structure in blocks encourages a higher TCP deposition due to higher values was obtained after soaking in SBF solution.

Figure 10 shows the SEM images of coatings after immersion in SBF solution during 7 days (**Figure 10A**) and 28 days (**Figure 10B**). In addition, EDX patterns were also included in the figure in order to analyze the elementary composition of coatings as well as the Ca/P ratio. A microporous structure is observed in the SEM micrographs, with a thin continuous layer without superficial fractures that covered the metallic substrate. Besides, a more compact and uniform coating (surface covered) is obtained for longer immersion times. **Figure 10B** reveals a more compact and smoother surface, whereas **Figure 10A** exhibits the presence of aggregates and a porous structure. Moreover, TCP particles are evenly distributed within the polymer matrix, obtaining a good mix between materials. Fauré et al., (2012) reported a similar behavior of bioactive particles during the EPD methodology: the particles that settle induce the incorporation of more particles on the coating, thus achieving surfaces with the interconnected macroporous and microporous structure.

Finally, EDX analysis revealed a value of the Ca/P ratio between 1.40 and 1.50 for both immersion times (7 and 28 days), by exhibiting values closer to those reported in the literature (Raynaud et al., 2002; Yu et al., 2018). In this sense,

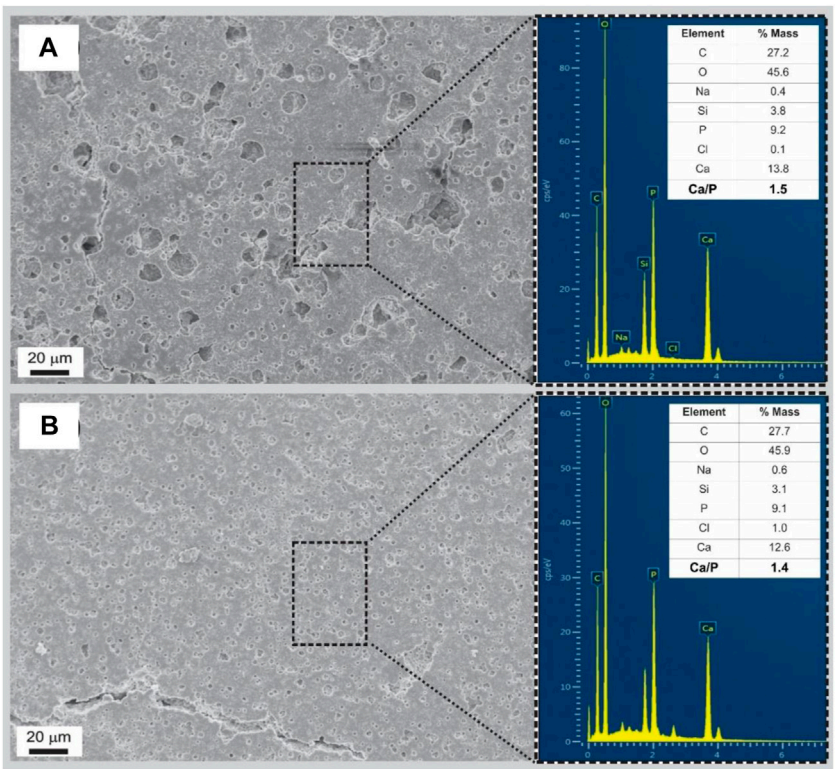

FIGURE 10 | SEM micrographs (1,000x) and EDX spectra of coatings after immersion in SBF solution during **(A)** 7 days and **(B)** 28 days.

Raynaud et al., (2002) and Yu et al., (2018) reported the same behavior by using powders of apatite calcium phosphate with the Ca/P ratio ranging from 1.50 to 1.67. These authors stressed that HA growing could be attributed to the higher diffusion rate of calcium species relative to that of phosphate anions inside the polymeric matrix, which leads to a higher release of calcium from the surface. Altogether, this induces a rapid formation of a thin HA layer owing to the large surface area over which it is distributed and significantly decreases when the PO_4^{3-} content in the solution approaches zero (Yu et al., 2018).

According to Ramezani et al., (2017), the rapid exchange of Ca^{2+} and Mg^{2+} ions with H^+ or H_3O^+ from SBF solution increases the hydroxyl concentration of the solution. This change leads to the superficial modification of the coating, which causes HA nucleation. Then, the migration of PO_4^{3-}, Ca^{2+}, and OH^- ions from the surrounding fluid to the surface of the coating accelerates the nucleation and precipitation of an HA layer (Ramezani et al., 2017; Yu et al., 2018). In this sense, it is plausible that the synergistic effects of co-EPD time + TCP/PDMS-*b*-PCL promote a coating surface that induces the further HA growth.

4 CONCLUSION

Poly(dimethylsiloxane-*block*-ε-caprolactone) copolymer was obtained by a combination of anionic and ring-opening polymerization. The resulting block copolymer showed a good compatibility with the tricalcium phosphate powder to obtain compact and potentially bioactive coatings by electrophoretic deposition. A linear dependence of deposited weight and thickness was observed for electrodeposition time. After *in vitro* assays in SBF solution, new absorption bands and new patterns assigned to tricalcium phosphate were detected by FTIR-ATR and XRD analysis, while SEM-EDX analysis revealed similar Ca/P ratio values those reported for natural bone tissues. According to these results, the coatings obtained in this work evidence an enhanced capacity to induce the precipitation of tricalcium phosphate and suggest the chemical transformation of tricalcium phosphate into HA through a dissolution–precipitation mechanism.

DATA AVAILABILITY STATEMENT

The raw data supporting the conclusions of this article will be made available by the authors, without undue reservation.

AUTHOR CONTRIBUTIONS

FR, MG, AC, and MN conceived the study, performed the experimental analysis as well as the interpretation of data, and drafted the manuscript. In addition, all authors read and approved the final manuscript.

FUNDING

This work was supported by the Fondo para la Investigación Científica y Tecnológica (FONCyT, Argentina) under grant (PICT-2016-0181) and Universidad Nacional de Cuyo (UNCuyo, Argentina) under grant (SIIP 06/L030-B; SeCTyP PROJOVIN).

ACKNOWLEDGMENTS

The authors wish to thank the Consejo Nacional de Investigaciones Científicas y Técnicas (CONICET, Argentina).

REFERENCES

Agudelo, N. A., and Pérez, L. D. (2016). Synthesis and Characterization of Polydimethylsiloxane End-Modified Polystyrene from Poly(Styrene - Co -Vinyltriethoxysilane) Copolymers. *Mat. Res.* 19 (2), 459–465. doi:10.1590/1980-5373-MR-2015-0599

Aguiar, H., Chiussi, S., López-Álvarez, M., González, P., and Serra, J. (2018). Structural Characterization of Bioceramics and Mineralized Tissues Based on Raman and XRD Techniques. *Ceramics Int.* 44 (1), 495–504. doi:10.1016/j.ceramint.2017.09.203

Aoki, Y. (2020). Superhydrophobic Coating Fabricated by Electrophoretic Deposition Using Polydimethylsiloxane-Based Organic-Inorganic Hybrid Materials and Ceramic Powders. *Mol. Cryst. Liquid Cryst.* 704 (1), 10–16. doi:10.1080/15421406.2020.1741795

Bartmanski, M., Zielinski, A., Jazdzewska, M., Głodowska, J., and Kalka, P. (2019). Effects of Electrophoretic Deposition Times and Nanotubular Oxide Surfaces on Properties of the Nanohydroxyapatite/nanocopper Coating on the Ti13Zr13Nb alloy. *Ceram. Int.* 45 (16), 20002–20010. doi:10.1016/j.ceramint.2019.06.258

Boccaccini, A. R., Chen, Q., Lefebvre, L., Gremillard, L., and Chevalier, J. (2007). Sintering, Crystallisation and Biodegradation Behaviour of Bioglass-Derived Glass-Ceramics. *Faraday Discuss.* 136, 27–44. doi:10.1039/B616539G

Boccaccini, A. R., Keim, S., Ma, R., Li, Y., and Zhitomirsky, I. (2010). Electrophoretic Deposition of Biomaterials. *J. R. Soc. Interf.* 7 (Suppl. l_5), S581–S613. doi:10.1098/rsif.2010.0156.focus

Bonetti, L., Altomare, L., Bono, N., Panno, E., Campiglio, C. E., Draghi, L., et al. (2020). Electrophoretic Processing of Chitosan Based Composite Scaffolds with Nb-Doped Bioactive Glass for Bone Tissue Regeneration. *J. Mater. Sci. Mater. Med.* 31 (5), 1–12. doi:10.1007/s10856-020-06378-6

Cabanas-Polo, S., and Boccaccini, A. R. (2015). Understanding Bioactive Glass Powder Suspensions for Electrophoretic Deposition of Bioactive Glass-Polymer Coatings. *J. Electrochem. Soc.* 162 (11), D3077–D3083. doi:10.1149/2.0211511jes

Cai, J., Xiong, Z., Zhou, M., Tan, J., Zeng, F., MeihuMa, S., et al. (2014). Thermal Properties and Crystallization Behavior of Thermoplastic Starch/Poly(ε-Caprolactone) Composites. *Carbohydr. Polym.* 102, 746–754. doi:10.1016/j.carbpol.2013.10.095

Chen, Q., Cabanas-Polo, S., Goudouri, O.-M., and Boccaccini, A. R. (2014). Electrophoretic Co-deposition of Polyvinyl Alcohol (PVA) Reinforced Alginate-Bioglass Composite Coating on Stainless Steel: Mechanical Properties and *In-Vitro* Bioactivity Assessment. *Mater. Sci. Eng. C* 40, 55–64. doi:10.1016/j.msec.2014.03.019

Chen, J., Zheng, J., Gao, Q., Zhang, J., Zhang, J., Omisore, O., et al. (2018). Polydimethylsiloxane (PDMS)-based Flexible Resistive Strain Sensors for Wearable Applications. *Appl. Sci.* 8 (3), 345. doi:10.3390/app8030345

Chen, C.-C., Lee, S.-Y., Teng, N.-C., Hu, H.-T., Huang, P.-C., and Yang, J.-C. (2019). *In Vitro* and *In Vivo* Studies of Hydrophilic Electrospun PLA95/β-TCP Membranes for Guided Tissue Regeneration (GTR) Applications. *Nanomaterials* 9 (4), 599. doi:10.3390/nano9040599

Clavijo, S., Membrives, F., Quiroga, G., Boccaccini, A. R., and Santillán, M. J. (2016). Electrophoretic Deposition of Chitosan/Bioglass® and Chitosan/Bioglass®/TiO2 Composite Coatings for Bioimplants. *Ceram. Int.* 42 (12), 14206–14213. doi:10.1016/j.ceramint.2016.05.178

Cordero-Arias, L., Cabanas-Polo, S., Goudouri, O. M., Misra, S. K., Gilabert, J., Valsami-Jones, E., et al. (2015). Electrophoretic Deposition of ZnO/alginate and ZnO-Bioactive Glass/alginate Composite Coatings for Antimicrobial Applications. *Mater. Sci. Eng. C* 55, 137–144. doi:10.1016/j.msec.2015.05.034

Danesin, R., Brun, P., Roso, M., Delaunay, F., Samouillan, V., Brunelli, K., et al. (2012). Self-assembling Peptide-Enriched Electrospun Polycaprolactone Scaffolds Promote the H-Osteoblast Adhesion and Modulate Differentiation-Associated Gene Expression. *Bone* 51 (5), 851–859. doi:10.1016/j.bone.2012.08.119

Dorozhkin, S. V. (2010). Bioceramics of Calcium Orthophosphates. *Biomaterials* 31 (7), 1465–1485. doi:10.1016/j.biomaterials.2009.11.050

Duruncan, C., and Brown, P. W. (2001). Biodegradable Hydroxyapatite–Polymer Composites. *Adv. Eng. Mater.* 3 (4), 227–231. doi:10.1002/1527-2648(200104)3:4<227::aid-adem227>3.0.co;2-1

El-Ghannam, A. (2005). Bone Reconstruction: from Bioceramics to Tissue Engineering. *Expert Rev. Med. Devices* 2 (1), 87–101. doi:10.1586/17434440.2.1.87

Fauré, J., Drevet, R., Potiron, S., Gordin, D. M., Oudadesse, H., Gloriant, T., et al. (2012). "Electrophoretic Deposition of Bioactive Glass Coatings on Ti12Mo5Ta alloy," in *Key Engineering Materials* (Switzerland: Trans Tech Publications Ltd), 135–140.

Ghalayani Esfahani, A., Soleimanzade, M., Campiglio, C. E., Federici, A., Altomare, L., Draghi, L., et al. (2019). Hierarchical Microchannel Architecture in Chitosan/bioactive Glass Scaffolds via Electrophoretic Deposition Positive-replica. *J. Biomed. Mater. Res.* 107 (7), 1455–1465. doi:10.1002/jbm.a.36660

Ghasemi-Mobarakeh, L., Prabhakaran, M. P., Morshed, M., Nasr-Esfahani, M. H., and Ramakrishna, S. (2010). Bio-functionalized PCL Nanofibrous Scaffolds for Nerve Tissue Engineering. *Mater. Sci. Eng. C* 30 (8), 1129–1136. doi:10.1016/j.msec.2010.06.004

Ghassemi, T., Shahroodi, A., Ebrahimzadeh, M. H., Mousavian, A., Movaffagh, J., and Moradi, A. (2018). Current Concepts in Scaffolding for Bone Tissue Engineering. *Arch. Bone Jt. Surg.* 6 (2), 90–99. doi:10.22038/abjs.2018.26340.1713

Ginebra, M. P., Driessens, F. C. M., and Planell, J. A. (2004). Effect of the Particle Size on the Micro and Nanostructural Features of a Calcium Phosphate Cement: A Kinetic Analysis. *Biomaterials* 25 (17), 3453–3462. doi:10.1016/j.biomaterials.2003.10.049

Jordan, J., Jacob, K. I., Tannenbaum, R., Sharaf, M. A., and Jasiuk, I. (2005). Experimental Trends in Polymer Nanocomposites-A Review. *Mater. Sci. Eng. A* 393 (1-2), 1–11. doi:10.1016/j.msea.2004.09.044

Oliver, J.-a. N., Su, Y., Lu, X., Kuo, P.-H., Du, J., and Zhu, D. (2019). Bioactive Glass Coatings on Metallic Implants for Biomedical Applications. *Bioactive Mater.* 4, 261–270. doi:10.1016/j.bioactmat.2019.09.002

Kokubo, T., and Takadama, H. (2006). How Useful Is SBF in Predicting *In Vivo* Bone Bioactivity? *Biomaterials* 27 (15), 2907–2915. doi:10.1016/j.biomaterials.2006.01.017

Lala, S., Satpati, B., and Pradhan, S. K. (2016). Sintering Behavior and Growth Mechanism of β-TCP in Nanocrystalline Hydroxyapatite Synthesized by Mechanical Alloying. *Ceramics Int.* 42 (11), 13176–13182. doi:10.1016/j.ceramint.2016.05.109

Liang, L., and Ruckenstein, E. (1996). Pervaporation of Ethanol-Water Mixtures through Polydimethylsiloxane-Polystyrene Interpenetrating Polymer Network Supported Membranes. *J. Membr. Sci.* 114 (2), 227–234. doi:10.1016/0376-7388(95)00319-3

Liang, J.-Z., Zhou, L., Tang, C.-Y., and Tsui, C.-P. (2013). Crystallization Properties of Polycaprolactone Composites Filled with Nanometer Calcium Carbonate. *J. Appl. Polym. Sci.* 128 (5), 2940–2944. doi:10.1002/app.38359

Loher, S., Reboul, V., Brunner, T. J., Simonet, M., Dora, C., Neuenschwander, P., et al. (2006). Improved Degradation and Bioactivity of Amorphous Aerosol Derived Tricalcium Phosphate Nanoparticles in Poly(lactide-Co-Glycolide). *Nanotechnology* 17 (8), 2054–2061. doi:10.1088/0957-4484/17/8/044

Luo, W., Charara, M., Saha, M. C., and Liu, Y. (2019). Fabrication and Characterization of Porous CNF/PDMS Nanocomposites for Sensing Applications. *Appl. Nanosci.* 9 (6), 1309–1317. doi:10.1007/s13204-019-00958-x

Ma, P. X., Zhang, R., Xiao, G., and Franceschi, R. (2001). Engineering New Bone Tissuein Vitro on Highly Porous Poly(?-Hydroxyl Acids)/hydroxyapatite Composite Scaffolds. *J. Biomed. Mater. Res.* 54 (2), 284–293. doi:10.1002/1097-4636(200102)54:2<284::aid-jbm16>3.0.co;2-w

Maeda, H., Maquet, V., Kasuga, T., Chen, Q. Z., Roether, J. A., and Boccaccini, A. R. (2007). Vaterite Deposition on Biodegradable Polymer Foam Scaffolds for Inducing Bone-like Hydroxycarbonate Apatite Coatings. *J. Mater. Sci. Mater. Med.* 18 (12), 2269–2273. doi:10.1007/s10856-007-3108-4

Miola, M., Verné, E., Ciraldo, F. E., Cordero-Arias, L., and Boccaccini, A. R. (2015). Electrophoretic Deposition of chitosan/45S5 Bioactive Glass Composite Coatings Doped with Zn and Sr. *Front. Bioeng. Biotechnol.* 3, 159. doi:10.3389/fbioe.2015.00159

Mohandes, F., and Salavati-Niasari, M. (2014a). *In Vitro* comparative Study of Pure Hydroxyapatite Nanorods and Novel Polyethylene Glycol/graphene Oxide/Hydroxyapatite Nanocomposite. *J. Nanopart. Res.* 16 (9), 1–12. doi:10.1007/s11051-014-2604-y

Mohandes, F., and Salavati-Niasari, M. (2014b). Freeze-Drying Synthesis, Characterization and *In Vitro* Bioactivity of Chitosan/graphene Oxide/hydroxyapatite Nanocomposite. *RSC Adv.* 4 (49), 25993–26001. doi:10.1039/C4RA03534H

Mondal, S., Nguyen, T. P., Pham, V. H., Hoang, G., Manivasagan, P., Kim, M. H., et al. (2020). Hydroxyapatite Nano Bioceramics Optimized 3D Printed Poly Lactic Acid Scaffold for Bone Tissue Engineering Application. *Ceramics Int.* 46 (3), 3443–3455. doi:10.1016/j.ceramint.2019.10.057

Nag, A., Afasrimanesh, N., Feng, S., and Mukhopadhyay, S. C. (2018a). Strain Induced Graphite/PDMS Sensors for Biomedical Applications. *Sensors Actuators A: Phys.* 271, 257–269. doi:10.1016/j.sna.2018.01.044

Nag, A., Feng, S., Mukhopadhyay, S. C., Kosel, J., and Inglis, D. (2018b). 3D Printed Mould-Based Graphite/PDMS Sensor for Low-Force Applications. *Sensors Actuators A: Phys.* 280, 525–534. doi:10.1016/j.sna.2018.08.028

Nagase, M., Chen, R.-B., Asada, Y., and Nakajima, T. (1989). Radiographic and Microscopic Evaluation of Subperiosteally Implanted Blocks of Hydrated and Hardened α-tricalcium Phosphate in Rabbits. *J. Oral Maxillofac. Surg.* 47 (6), 582–586. doi:10.1016/S0278-2391(89)80073-4

Ninago, M. D., Satti, A. J., Ciolino, A. E., and Villar, M. A. (2013). Influence of Amorphous Block on the thermal Behavior of Well-Defined Block Copolymers Based on ε-caprolactone. *J. Therm. Anal. Calorim.* 112 (3), 1277–1287. doi:10.1007/s10973-012-2673-z

Ninago, M. D., López, O. V., Lencina, M. M. S., García, M. A., Andreucetti, N. A., Ciolino, A. E., et al. (2015). Enhancement of Thermoplastic Starch Final Properties by Blending with Poly(ε-Caprolactone). *Carbohydr. Polym.* 134, 205–212. doi:10.1016/j.carbpol.2015.08.007

Ninago, M. D., Hanazumi, V., Passaretti, M. G., Vega, D. A., Ciolino, A. E., and Villar, M. A. (2017). Enhancement of Mechanical and Optical Performance of Commercial Polystyrenes by Blending with Siloxane-Based Copolymers. *J. Appl. Polym. Sci.* 134 (30), 45122. doi:10.1002/app.45122

Ninago, M. D., Ciolino, A. E., and Villar, M. A. (2020). Improvement in Poly(ε-Caprolactone) Bio-Activity. Structural Characterization and *In Vitro* Assessment. *Int. J. Polymeric Mater. Polymeric Biomater.* 69 (4), 201–210. doi:10.1080/00914037.2018.1552864

Öztürk, T., and Meyvacı, E. (2017). Synthesis and Characterization Poly(ε-Caprolactone-B-Ethylene Glycol-B-ε-Caprolactone) ABA Type Block Copolymers via "Click" Chemistry and Ring-Opening Polymerization. *J. Macromol. Sci. A* 54 (9), 575–581. doi:10.1080/10601325.2017.1309251

Öztürk, T., Atalar, M. N., Göktaş, M., and Hazer, B. (2013). One-step Synthesis of Block-Graft Copolymers via Simultaneous Reversible-Addition Fragmentation Chain Transfer and Ring-Opening Polymerization Using a Novel Macroinitiator. *J. Polym. Sci. Part. A: Polym. Chem.* 51 (12), 2651–2659. doi:10.1002/pola.26654

Öztürk, T., Yavuz, M., Göktaş, M., and Hazer, B. (2016). One-step Synthesis of Triarm Block Copolymers by Simultaneous Atom Transfer Radical and Ring-

Opening Polymerization. *Polym. Bull.* 73 (6), 1497–1513. doi:10.1007/s00289-015-1558-2

Park, C.-H., Kim, E. K., Tijing, L. D., Amarjargal, A., Pant, H. R., Kim, C. S., et al. (2014). Preparation and Characterization of LA/PCL Composite Fibers Containing Beta Tricalcium Phosphate (β-TCP) Particles. *Ceramics Int.* 40 (3), 5049–5054. doi:10.1016/j.ceramint.2013.10.016

Peña, J., and Vallet-Regı, M. (2003). Hydroxyapatite, Tricalcium Phosphate and Biphasic Materials Prepared by a Liquid Mix Technique. *J. Eur. Ceram. Soc.* 23 (10), 1687–1696. doi:10.1016/S0955-2219(02)00369-2

Pereira, H. F., Cengiz, I. F., Silva, F. S., Reis, R. L., and Oliveira, J. M. (2020). Scaffolds and Coatings for Bone Regeneration. *J. Mater. Sci. Mater. Med.* 31 (3), 1–16. doi:10.1007/s10856-020-06364-y

Persenaire, O., Alexandre, M., Degée, P., and Dubois, P. (2001). Mechanisms and Kinetics of Thermal Degradation of Poly(ε-Caprolactone). *Biomacromolecules* 2 (1), 288–294. doi:10.1021/bm0056310

Pishbin, F., Cordero-Arias, L., Cabanas-Polo, S., and Boccaccini, A. R. (2015). "Bioactive Polymer-Calcium Phosphate Composite Coatings by Electrophoretic Deposition," in *Surface Coating and Modification of Metallic Biomaterials* (United Kingdom: Woodhead Publishing), 359–377. doi:10.1016/B978-1-78242-303-4.00012-0

Qu, H., Fu, H., Han, Z., and Sun, Y. (2019). Biomaterials for Bone Tissue Engineering Scaffolds: A Review. *RSC Adv.* 9 (45), 26252–26262. doi:10.1039/C9RA05214C

Quiroga, G. A. R., Redondo, F. L., Ninago, M. D., Ciolino, A. E., Villar, M. A., and Santillán, M. J. (2018). Fabricación de Recubrimientos compuestos de Bioglass®/poli (ε-caprolactona) Obtenidos por Co-Deposición Electroforética Sobre Acero Inoxidable. *Matéria (Rio de Janeiro)* 23 (02), 1–12. doi:10.1590/s1517-707620180002.0431

Raj, A., Suthanthiraraj, P. P. A., and Sen, A. K. (2018). Pressure-Driven Flow through PDMS-Based Flexible Microchannels and Their Applications in Microfluidics. *Microfluid Nanofluid* 22 (11), 1–25. doi:10.1007/s10404-018-2150-5

Ramezani, S., Emadi, R., Kharaziha, M., and Tavangarian, F. (2017). Synthesis, Characterization and *In Vitro* Behavior of Nanostructured Diopside/biphasic Calcium Phosphate Scaffolds. *Mater. Chem. Phys.* 186, 415–425. doi:10.1016/j.matchemphys.2016.11.013

Raynaud, S., Champion, E., Bernache-Assollant, D., and Thomas, P. (2002). Calcium Phosphate Apatites with Variable Ca/P Atomic Ratio I. Synthesis, Characterisation and thermal Stability of Powders. *Biomaterials* 23 (4), 1065–1072. doi:10.1016/S0142-9612(01)00218-6

Redondo, F. L., Ninago, M. D., de Freitas, A. G. O., Giacomelli, C., Ciolino, A. E., and Villar, M. A. (2018). Tailor-Made, Linear, and "Comb-Like" Polyester-Based Copolymers: Synthesis, Characterization, and Thermal Behavior of Potential 3D-Printing/Electrospinning Candidates. *Int. J. Polym. Sci.* 2018, 1–15. doi:10.1155/2018/8252481

Redondo, F. L., Quiroga, G. A. R., de Freitas, A. G. O., Villar, M. A., Ninago, M. D., and Ciolino, A. E. (2020). Composite Coatings Based on Linear and Branched Block Copolymers for Hydroxyapatite Deposition in Simulated Body-Fluid. *Polymer-Plastics Tech. Mater.* 59 (9), 985–997. doi:10.1080/25740881.2020.1719138

Redondo, F. L. (2018). *Síntesis y caracterización de copolímeros bloque biocompatibles. Thesis, Bahía Blanca*. Argentina: Universidad Nacional del Sur. Available at: http://repositoriodigital.uns.edu.ar/handle/123456789/4168.

Reid, J. W., Tuck, L., Sayer, M., Fargo, K., and Hendry, J. A. (2006). Synthesis and Characterization of Single-phase Silicon-Substituted α-tricalcium Phosphate. *Biomaterials* 27 (15), 2916–2925. doi:10.1016/j.biomaterials.2006.01.007

Roether, J. A., Boccaccini, A. R., Hench, L. L., Maquet, V., Gautier, S., and Jérôme, R. (2002). Development and *In Vitro* Characterisation of Novel Bioresorbable and Bioactive Composite Materials Based on Polylactide Foams and Bioglass for Tissue Engineering Applications. *Biomaterials* 23 (18), 3871–3878. doi:10.1016/S0142-9612(02)00131-X

Sartore, L., Inverardi, N., Pandini, S., Bignotti, F., and Chiellini, F. (2019). PLA/PCL-based Foams as Scaffolds for Tissue Engineering Applications. *Mater. Today Proc.* 7, 410–417. doi:10.1016/j.matpr.2018.11.103

Satti, A. J., de Freitas, A. G. O., Marani, M. L. S., Villar, M. A., Vallés, E. M., Giacomelli, C., et al. (2017). Anionic Ring Opening Polymerization of ε-Caprolactone Initiated by Lithium Silanolates. *Aust. J. Chem.* 70 (1), 106–112. doi:10.1071/CH16270

Savaş, B., Çatıker, E., Öztürk, T., and Meyvacı, E. (2021). Synthesis and Characterization of Poly(α-Methyl β-alanine)-poly(ε-caprolactone) Tri Arm star Polymer by Hydrogen Transfer Polymerization, Ring-Opening Polymerization and "click" Chemistry. *J. Polym. Res.* 28 (2), 1–10. doi:10.1007/s10965-020-02367-z

Seuss, S., Heinloth, M., and Boccaccini, A. R. (2016). Development of Bioactive Composite Coatings Based on Combination of PEEK, Bioactive Glass and Ag Nanoparticles with Antibacterial Properties. *Surf. Coat. Tech.* 301, 100–105. doi:10.1016/j.surfcoat.2016.03.057

Shah Mohammadi, M., Rezabeigi, E., Bertram, J., Marelli, B., Gendron, R., Nazhat, S. N., et al. (2020). Poly(d,l-Lactic Acid) Composite Foams Containing Phosphate Glass Particles Produced via Solid-State Foaming Using CO2 for Bone Tissue Engineering Applications. *Polymers* 12 (1), 231. doi:10.3390/polym12010231

Somrani, S., Rey, C., and Jemal, M. (2003). Thermal Evolution of Amorphous Tricalcium Phosphate. *J. Mater. Chem.* 13 (4), 888–892. doi:10.1039/B210900J

Suchanek, W., and Yoshimura, M. (1998). Processing and Properties of Hydroxyapatite-Based Biomaterials for Use as Hard Tissue Replacement Implants. *J. Mater. Res.* 13 (1), 94–117. doi:10.1557/JMR.1998.0015

Sultana, N. (2018). "Mechanical and Biological Properties of Scaffold Materials," in *Functional 3D Tissue Engineering Scaffolds* (United Kingdom: Woodhead Publishing), 1–21. doi:10.1016/B978-0-08-100979-6.00001-X

Sungsee, P., and Tanrattanakul, V. (2019). Biocomposite Foams from Poly(lactic Acid) and Rubber wood Sawdust: Mechanical Properties, Cytotoxicity, and *In Vitro* Degradation. *J. Appl. Polym. Sci.* 136 (48), 48259. doi:10.1002/app.48259

Taale, M., Krüger, D., Ossei-Wusu, E., Schütt, F., Rehman, M. A. U., Mishra, Y. K., et al. (2019). Systematically Designed Periodic Electrophoretic Deposition for Decorating 3D Carbon-Based Scaffolds with Bioactive Nanoparticles. *ACS Biomater. Sci. Eng.* 5 (9), 4393–4404. doi:10.1021/acsbiomaterials.9b00102

Thinakaran, S., Loordhuswamy, A., and Venkateshwapuram Rengaswami, G. (2020). Electrophoretic Deposition of Chitosan/nano Silver Embedded Micro Sphere on Centrifugal Spun Fibrous Matrices - A Facile Biofilm Resistant Biocompatible Material. *Int. J. Biol. Macromol.* 148, 68–78. doi:10.1016/j.ijbiomac.2020.01.086

Uhrig, D., and Mays, J. W. (2005). Experimental Techniques in High-Vacuum Anionic Polymerization. *J. Polym. Sci. A. Polym. Chem.* 43 (24), 6179–6222. doi:10.1002/pola.21016

Wang, C., Ma, J., Cheng, W., and Zhang, R. (2002). Thick Hydroxyapatite Coatings by Electrophoretic Deposition. *Mater. Lett.* 57 (1), 99–105. doi:10.1016/S0167-577X(02)00706-1

Wang, L., Wang, D., Zhou, Y., Zhang, Y., Li, Q., and Shen, C. (2019). Fabrication of Open-porous PCL/PLA Tissue Engineering Scaffolds and the Relationship of Foaming Process, Morphology, and Mechanical Behavior. *Polym. Adv. Technol.* 30 (10), 2539–2548. doi:10.1002/pat.4701

Wietor, J.-L., Van Beek, D. J. M., Peters, G. W., Mendes, E., and Sijbesma, R. P. (2011). Effects of Branching and Crystallization on Rheology of Polycaprolactone Supramolecular Polymers with Ureidopyrimidinone End Groups. *Macromolecules* 44 (5), 1211–1219. doi:10.1021/ma1026065

Wolf, M. P., Salieb-Beugelaar, G. B., and Hunziker, P. (2018). PDMS with Designer Functionalities-Properties, Modifications Strategies, and Applications. *Prog. Polym. Sci.* 83, 97–134. doi:10.1016/j.progpolymsci.2018.06.001

Wu, N., Huang, L., and Zheng, A. (2006). Synthesis and Properties of Polystyrene/polydimethylsiloxane Graft Copolymers. *Front. Chem. China* 1 (3), 350–356. doi:10.1007/s11458-006-0043-4

Yam, W. Y., Ismail, J., Kammer, H. W., Schmidt, H., and Kummerlöwe, C. (1999). Polymer Blends of Poly(ε-Caprolactone) and Poly(vinyl Methyl Ether) - Thermal Properties and Morphology. *Polymer* 40 (20), 5545–5552. doi:10.1016/S0032-3861(98)00807-6

Yang, C. R., Wang, Y. J., Chen, X. F., and Zhao, N. R. (2005). Biomimetic Fabrication of BCP/COL/HCA Scaffolds for Bone Tissue Engineering. *Mater. Lett.* 59 (28), 3635–3640. doi:10.1016/j.matlet.2005.07.022

Yang, Y., Michalczyk, C., Singer, F., Virtanen, S., and Boccaccini, A. R. (2015). *In Vitro* study of Polycaprolactone/bioactive Glass Composite Coatings on Corrosion and Bioactivity of Pure Mg. *Appl. Surf. Sci.* 355, 832–841. doi:10.1016/j.apsusc.2015.07.053

Yazdimamaghani, M., Razavi, M., Vashaee, D., Pothineni, V. R., Rajadas, J., and Tayebi, L. (2015). Significant Degradability Enhancement in Multilayer Coating

of Polycaprolactone-Bioactive Glass/gelatin-Bioactive Glass on Magnesium Scaffold for Tissue Engineering Applications. *Appl. Surf. Sci.* 338, 137–145. doi:10.1016/j.apsusc.2015.02.120

Yeong, W. Y., Sudarmadji, N., Yu, H. Y., Chua, C. K., Leong, K. F., Venkatraman, S. S., et al. (2010). Porous Polycaprolactone Scaffold for Cardiac Tissue Engineering Fabricated by Selective Laser Sintering. *Acta Biomater.* 6 (6), 2028–2034. doi:10.1016/j.actbio.2009.12.033

Yu, Y., Mathew, R., and Edén, M. (2018). Quantitative Composition-Bioactivity Relationships of Phosphosilicate Glasses: Bearings from the Phosphorus Content and Network Polymerization. *J. Non-Cryst. Sol.* 502, 106–117. doi:10.1016/j.jnoncrysol.2018.07.060

Zhang, K., Wang, Y., Hillmyer, M. A., and Francis, L. F. (2004). Processing and Properties of Porous Poly(l-Lactide)/bioactive Glass Composites. *Biomaterials* 25 (13), 2489–2500. doi:10.1016/j.biomaterials.2003.09.033

Zhao, J., Guo, L. Y., Yang, X. B., and Weng, J. (2008). Preparation of Bioactive Porous HA/PCL Composite Scaffolds. *Appl. Surf. Sci.* 255 (5), 2942–2946. doi:10.1016/j.apsusc.2008.08.056

Zhao, N., Lv, Z., Ma, J., Zhu, C., and Li, Q. (2019). Fabrication of Hydrophilic Small Diameter Vascular Foam Scaffolds of Poly(ε-Caprolactone)/Polylactic Blend by Sodium Hydroxide Solution. *Eur. Polym. J.* 110, 31–40. doi:10.1016/j.eurpolymj.2018.11.011

Zhou, H., and Lee, J. (2011). Nanoscale Hydroxyapatite Particles for Bone Tissue Engineering. *Acta Biomater.* 7 (7), 2769–2781. doi:10.1016/j.actbio.2011.03.019

Conflict of Interest: The authors declare that the research was conducted in the absence of any commercial or financial relationships that could be construed as a potential conflict of interest.

Publisher's Note: All claims expressed in this article are solely those of the authors and do not necessarily represent those of their affiliated organizations, or those of the publisher, the editors, and the reviewers. Any product that may be evaluated in this article, or claim that may be made by its manufacturer, is not guaranteed or endorsed by the publisher.

frontiers in Materials

ORIGINAL RESEARCH
published: 01 February 2022
doi: 10.3389/fmats.2022.818595

Potential of Longan Seed Extract–Loaded Alginate–Chitosan Beads as Drug Delivery System

Tanawat Buntum[1], *Pattana Kakumyan*[1], *Suvimol Surassmo*[2], *Chuleeporn Thanomsilp*[1] *and Orawan Suwantong*[1,3]*

[1]School of Science, Mae Fah Luang University, Chiang Rai, Thailand, [2]National Nanotechnology Center, National Science and Technology Development Agency, Pathum Thani, Thailand, [3]Center of Chemical Innovation for Sustainability, Mae Fah Luang University, Chiang Rai, Thailand

The potential of a drug delivery system of the longan seed extract (LSE) incorporated in the alginate/chitosan (Alg/CS) beads has been studied. The LSE-loaded Alg/CS beads were prepared using the ionic gelation method *via* the interaction between protonated amino groups of CS and negatively charged carboxylic groups of Alg. Properties of the LSE-loaded Alg/CS beads were investigated including the morphology of the beads, particle sizes, encapsulation efficiency (%EE), controlled release profile, cytotoxicity, and biocompatibility. From the results, the amount of gallic acid, ellagic acid, and corilagin found in LSE was 25.61 ± 0.48,18.83 ± 3.75, and 21.92 ± 1.42 mg/g (based on the weight of LSE), respectively. The half-maximum inhibitory concentration (IC_{50}) of LSE was 24.29 ± 1.08 μg/ml. SEM images of the LSE-loaded Alg/CS beads showed spherical shapes and rough surfaces with some aggregation. The particle sizes were between 1.9 and 2.5 μm with the PDI values of 0.1503–0.3183. Encapsulation efficiencies were between 11 and 18%. The released amount of LSE from the LSE-loaded Alg/CS beads was ranging between 68 and 93%. Moreover, cytotoxicity and biocompatibility tests showed that the beads were non-toxic to both NCTC clone 929 and NHDF cells and promoted the attachment of NHDF cells. Thus, these beads could be used as polymeric drug carriers.

Keywords: longan seed extract, chitosan, alginate, ionic gelation, drug delivery system

OPEN ACCESS

Edited by:
Nafisa Gull,
University of the Punjab, Pakistan

Reviewed by:
Mohammad Alnaief,
German jordanian university, Jordan
Dhony Hermanto,
University of Mataram, Indonesia

***Correspondence:**
Orawan Suwantong
o.suwantong@gmail.com/
orawan.suw@mfu.ac.th

Specialty section:
This article was submitted to Polymeric and Composite Materials, a section of the journal Frontiers in Materials

Received: *19 November 2021*
Accepted: *04 January 2022*
Published: *01 February 2022*

Citation:
Buntum T, Kakumyan P, Surassmo S, Thanomsilp C and Suwantong O (2022) Potential of Longan Seed Extract–Loaded Alginate–Chitosan Beads as Drug Delivery System. Front. Mater. 9:818595. doi: 10.3389/fmats.2022.818595

INTRODUCTION

Polymeric carriers have been developed to control drug levels within the desired range and prolong the contact time to the specific body site. They play an important role in controlling drug delivery systems for pharmaceutical and medical applications because of their efficient carrier characteristics such as sustained, controlled, and prolonged release and reduced drug toxicity (Gagliardi et al., 2012; George et al., 2019; Venditti, 2019). Moreover, they have the ability to protect the active compound or drug from degradation.

The main properties of polymeric carriers suitable for drug delivery systems are biocompatibility, biodegradability, and non-toxicity. For that reason, alginate (Alg) and chitosan (CS) are popular materials (Kumari et al., 2010; Sun et al., 2009). Alg has numerous uses in pharmaceutical and medical applications due to its non-immunogenicity, affordability, and absorption of wound exudate (Lee and Mooney 2012; Sarei et al., 2013). CS is a cationic polysaccharide that is derived from the deacetylation of chitin. It is composed of N-acetyl-D-glucosamine linked by β-(1-4) glycosidic bonds. Many research studies illustrated CS as polymeric carriers and reported that CS has the ability to

control the release of active agents with antibacterial and hemostatic properties (Bernkop-Schnürch and Dünnhaupt 2012; Ji et al., 2011; Nguyen et al., 2017; Sinha et al., 2004).

Alg and CS can be formulated into the form of beads, which provide more benefits to controlled drug delivery systems. The Alg/CS beads could prevent rapid diffusion of the encapsulated drug in acid conditions and delay the degradation of drugs from oxidation, enzymatic degradation, and hydrolysis (Morsi et al., 2015; Nalini et al., 2019). Moreover, they could improve the stability, drug encapsulation efficiency, and the release of drug (Rajendran and Basu, 2009; Nagarwal et al., 2012). Alg and CS were used to fabricate the polymeric carriers using an ionic gelation method. This technique is a simple and mild process without the need for high temperature (De Pinho Neves et al., 2014). The attraction between protonated amino groups of CS and the negatively charged carboxylic groups of Alg creates the electrostatic interaction in the Alg/CS beads (Ahdyani et al., 2019; Nagarwal et al., 2012; Rahaiee et al., 2015; Rajendran and Basu, 2009). Rajendran and Basu prepared the nimodipine-loaded Alg/CS beads using the ionic gelation method for sustained drug release. The results showed that the nimodipine-loaded Alg/CS beads exhibited sustained drug release (Rajendran and Basu, 2009). Rahaiee et al. improved the stability of crocin by encapsulating in Alg/CS beads using a modified ionic gelation method. The results showed that Alg and CS biopolymers were the highly promising carriers for the delivery of crocin (Rahaiee et al., 2015). Moreover, Song et al. prepared Alg and CS nanoparticles loaded with curcumin. The results showed that Alg and CS nanoparticles exhibited the sustained release profiles and enhanced the uptake efficiency and cytotoxicity to cancer cells (Song et al., 2018). Thus, the Alg/CS beads have the potential for use as drug carriers.

Longan (*Dimocarpus longan* Lour.) is widely grown in Southeast Asia, China, and Taiwan. Chinese medicinal formulation uses longan for medication as an agent in the relief of neural pain (Yang et al., 2011). Due to the high content of polyphenolic compounds mainly corilagin, gallic acid, and ellagic acid (Worasuttayangkurn et al., 2012; Zhang et al., 2020), the longan seed extract (LSE) has several biological activities such as antioxidant ability, anti-tyrosinase, and anticancer activities (Lim 2013). Corilagin showed good antimicrobial, antitumor, and antioxidant activities. Gallic acid and ellagic acid were reported to be potent antioxidant and anticarcinogenic agents (Li et al., 2018; Tang et al., 2019).

This study aimed to fabricate the LSE-loaded Alg/CS beads for use as the drug delivery system. The LSE-loaded Alg/CS beads were prepared using the ionic gelation method. Various stirring methods, including the magnetic stirrer, homogenizer, and ultrasonicator, were employed for preparing the beads. High-performance liquid chromatography (HPLC) was used to determine the chemical compounds in LSE (i.e., gallic acid, ellagic acid, and corilagin). The antioxidant activity of LSE was investigated by 2,2-diphenyl-1-picrylhydrazyl (DPPH) assay. The LSE-loaded Alg/CS beads were characterized for their morphology, particle size, polydispersity index (PDI), and encapsulation efficiency (%EE). The release profiles of LSE from the LSE-loaded Alg/CS beads, cytotoxicity, and biocompatibility were also investigated.

MATERIALS AND METHODS

Materials

Materials for the polymeric carrier, alginate acid sodium salt (viscosity: 15-25 cP), and chitosan (Mw = 20–30 kDa, degree of deacetylation ≥95%) were obtained from Sigma-Aldrich (United States) and Bio 21 Co., Ltd. (Thailand), respectively. 2,2-Diphenyl-1-picrylhydrazyl (DPPH) and Span 80 (viscosity: 1,000–200 mPa s) were purchased from Sigma-Aldrich (United States). L-Ascorbic acid was bought from Chem-Supply Pty Ltd. (Australia). Glacial acetic acid was bought from Merck KGaA (Germany). Ethanol, methanol, propan-2-ol, and dimethyl sulfoxide were purchased from RCI LabScan Limited (Bangkok, Thailand). Anhydrous sodium carbonate (Na_2CO_3), sodium chloride (NaCl), anhydrous disodium hydrogen orthophosphate (Na_2HPO_4), and paraffin oil were purchased from Ajax Finechem (Australia).

Methods

Extraction of Longan Seed

Edor cultivar longan seeds from a farm in Lamphun Province, Thailand, were selected for this study. The extraction procedures were carried out following Pankongadisak and Suwantong's method with slight modification (Pankongadisak and Suwantong 2018). The dried longan seeds (approximately 10 g) were ground using mortar and pestle and then soaked in 600 ml of distilled water. The extraction process was carried out at room temperature for 72 h. After that, the mixture was filtered using a filter paper (Whatman No. 1). The extracted solution was then dried using lyophilization. Finally, the longan seed extract (LSE) was obtained and stored in a desiccator before use.

High-Performance Liquid Chromatography (HPLC) Analysis

The amounts of gallic acid, corilagin, and ellagic acid in LSE were analyzed using the HPLC technique. HPLC analysis was performed using a Waters Acquity Arc HPLC System. The chromatographic conditions were as follows: a column (Cortecs®C18 2.7 μm 4.6 × 50 mm, Waters); 0.1% v/v formic acid in Milli-Q water (solvent A), and acetonitrile (solvent B) for gradient elution were used as a mobile phase; and a total run time is 10 min. The sample injection volume was 1 μl/injection at a flow rate of 1.0 ml/min with a PDA detector-type HPLC 2998 detector used at a wavelength of 270 nm.

LSE solutions were prepared by dissolving LSE powder in Milli-Q water. The sample was filtered using a 0.22-μm membrane filter before injection. The standard solutions with concentrations varied as 25, 50, 100, 150, 200, 250, and 300 ppm were used to evaluate the amounts of gallic acid, ellagic acid, and corilagin in LSE. Quantitative analysis of polyphenolic compounds of gallic acid, ellagic acid, and corilagin was conducted by evaluating the peak area based on a standard curve.

Antioxidant Activity of Longan Seed Extract

The antioxidant activity of LSE was analyzed by DPPH assay according to the method of Blois with some modifications (Blois 1958). First, the test solutions were prepared by dissolving LSE powder in distilled water to make various concentrations as 3.125, 6.25, 12.5, 25, and 50 μg/ml. L-Ascorbic acid was used as a standard compound, and the solutions were prepared by using distilled water to make the same concentrations as LSE test solutions. Next, 50 μl of each solution was mixed with 150 μl of 100 μM DPPH solution. After that, the reaction mixture was kept in the dark at room temperature for 30 min. The antioxidant activity of LSE and L-ascorbic acid against DPPH radicals was determined by measuring the absorbance at 517 nm using a microplate reader (BioTek Instruments, United States). The percentage antioxidant activity (%AA) was calculated according to the following equation:

$$\mathrm{AA}\,(\%) = \frac{\mathrm{A_{control}} - \mathrm{A_{sample}}}{\mathrm{A_{control}}} \times 100, \quad (1)$$

where $A_{control}$ and A_{sample} are the absorbance values of the testing solution without and with LSE or L-ascorbic acid, respectively.

Indirect Cytotoxicity of Longan Seed Extract

The indirect cytotoxicity of LSE was investigated using NCTC clone 929 and normal human dermal fibroblast (NHDF) cells. NCTC clone 929 (16th passage) and NHDF (16th passage) cells were cultured at 37°C in a humidified atmosphere of 95% air and 5% CO_2 using Dulbecco's modified Eagle medium (DMEM; GIBCO, United States). The DMEM contains 10% fetal bovine serum (FBS; GIBCO, United States) and 1% antibiotic and antimycotic formulation (GIBCO, United States). LSE powder was dissolved in a serum-free medium (SFM; containing DMEM and 1% antibiotic agent) to produce various concentration solutions as 5, 2.5, 1.25, 0.625, 0.313, 0.156, 0.078, 0.039, and 0.02 mg/ml. The LSE solutions were sterilized before testing by 0.22-μm Minisart syringe filters (Sartorius, Germany). Four replicates were performed in 96-well tissue culture plates (TCPS; SPL Life Science, Korea). The plates were seeded with cell suspension at 8,000 cells/well and incubated for 24 h at a 37°C humidified incubator with 5% CO_2. Then, the cells were starved with SFM for 24 h. After 24 h, the medium was changed to LSE solution, and the cells were re-incubated for 24 h. Then 3-(4,5-dimethylthiazol-2-yl)-2,5-diphenyltetrazolium bromide (MTT; AMRESCO, United States) assay was used to determine the viability of cells cultured with LSE solution. The assay was carried out in triplicate (n = 3) with an Epoch Microplate Spectrophotometer (BioTek Instruments, United States) at the wavelength of 570 nm.

Preparation of LSE-Loaded Alg/CS Beads

The LSE-loaded Alg/CS beads were prepared by using the ionic gelation method. First, 4.5% w/v of Alg solution was prepared by dissolving 0.225 g of Alg in 5 ml of distilled water at room temperature. After that, 0.2 g (2% w/w, based on the weight of Alg and CS powder) of LSE was added to the Alg solution with stirring. The mixture (aqueous phase) was added dropwise into an oil phase that contained 25 ml of paraffin oil and 1.25 ml of Span 80 with a stirring speed of 1,200 rpm for 30 min. Then, 1% w/v of chitosan solution was prepared by dissolving chitosan in 1% v/v of acetic acid at room temperature for 24 h. After that, the LSE-loaded Alg/CS beads were obtained by adding 1% w/v CS solution (pH of 4) drop by drop to the mixture at different stirring conditions (see **Table 1**). A total of 10% w/v of $CaCl_2$ solution was then added to the mixture with stirring at room temperature for 2 h. Then 10 ml of propan-2-ol was added to harden the beads. The LSE-loaded Alg/CS beads were collected by centrifugation at room temperature and subsequently washed several times with propan-2-ol and distilled water, respectively. The LSE-loaded Alg/CS beads were lyophilized for 1 day. Finally, the LSE-loaded Alg/CS beads were collected and stored in a desiccator before use.

Morphology and Particle Size of LSE-Loaded Alg/CS Beads

Morphology characterization of the LSE-loaded Alg/CS beads was carried out using an LEO 1450 VP Scanning Electron Microscope (SEM) with an accelerating voltage of 20 kV. The dry beads were deposited on a thin aluminum plate and then coated with a thin layer of gold. The SEM images of the LSE-loaded Alg/CS beads were obtained.

The particle size and PDI of the LSE-loaded Alg/CS beads were determined by dynamic light scattering (DLS) using a particle size analyzer (Zetasizer nano series, Malvern instrument, United Kingdom). The LSE-loaded Alg/CS bead diameter was determined after the dispersion of beads with distilled water in the ultrasonic bath for 2 min. The results were reported as the mean value and performed in triplicate.

Fourier Transform Infrared Spectroscopy (FTIR)

The LSE-loaded Alg/CS beads were mixed with KBr and prepared as a pellet to identify the structure of the LSE-loaded Alg/CS beads by FTIR (PerkinElmer, United States) in the range of 4,000–400 cm^{-1}, with a resolution of 32 cm^{-1}. The spectra are shown in **Figure 4**.

Encapsulation Efficiency of LSE-Loaded Alg/CS Beads

The LSE-loaded Alg/CS beads were first dissolved in phosphate-buffered solution (PBS) at 37°C for 1 day. The amount of LSE in PBS was determined by a UV–Vis spectrophotometer at the wavelength of 277 nm. The amounts of LSE in the beads were calculated using a calibration curve. The encapsulation efficiency (%EE) was calculated following **Eq. 2**.

$$\%\mathrm{EE} = \frac{\text{Weight of the loaded LSE}}{\text{Weight of the initial LSE}} \times 100. \quad (2)$$

Release Study

The LSE release profiles from the LSE-loaded Alg/CS beads were analyzed by using the total immersion method at 37°C for two days. Using a dialysis bag (molecular weight cut-off 12,000–14,000), the LSE/Alg/CS beads were loaded in a bag followed by 10 ml of PBS. The dialysis bag was then immersed

TABLE 1 | Preparation of LSE-loaded Alg/CS beads with different stirring methods.

Code	Instrument	Stirring condition
LSE/Alg/CS-S	Magnetic stirrer	Speed of 1,200 rpm for 60 min
LSE/Alg/CS-H	Homogenizer (T25 digital ULTRA-URRAX®)	Speed of 5,000 rpm for 30 min
LSE/Alg/CS-U	Ultrasonicator (Vibra-Cell™ VC750)	Pulse on 3 s pulse off 1 s for 10 min

in 20 ml of PBS. The release profiles were performed by collecting the sample solution at a specified time. Once the sample solution was collected, the same amount of fresh PBS was added. The UV–Vis spectrophotometer (Perkin-Elmer, United States) was used to analyze the amount of LSE released. The released amount of LSE was calculated using the calibration curve of LSE at 277 nm.

Indirect Cytotoxicity of LSE-Loaded Alg/CS Beads

NCTC clone 929 (14th passage) and NHDF (13th passage) cells were cultured at 8,000 cells/well in DMEM containing 10% FBS and 1% antibiotic and antimycotic formulation at 37°C in a humidified atmosphere of 95% air and 5% CO_2 for 24 h to enable cell attachment. The LSE-loaded Alg/CS beads were immersed in SFM at 37°C for 24 h to produce various concentrations of the extraction media (i.e., 0.5, 5, and 10 mg/ml). This assay was performed in four replicate wells in 96-well plates. Before investigation, the extraction media were sterilized using 0.22-μm Minisart syringe filters. After that, the cultured cells were then starved with the serum-free medium (SFM) for 24 h. The medium was then replaced with the extraction media, and the cells were re-incubated for 24 h. Finally, the cell viability was determined by MTT assay. The viability of cells cultured with fresh SFM was used as a control.

Biocompatibility Evaluation of LSE-Loaded Alg/CS Beads

The biocompatibility evaluation of the LSE-loaded Alg/CS beads was performed with NHDF cells. First, NHDF cells (density of 25,000 cells/well) were allowed to grow in 24-well tissue culture polystyrene plates (TCPS; SPL Life Science, Korea) for 24 h. The LSE-loaded Alg/CS beads (2.5 mg) were sterilized under UV for 1 h and then added into each well. NHDF cells cultured with the LSE-loaded Alg/CS beads were allowed to grow for 2, 24, and 72 h. At each time point, the cell viability was investigated by MTT assay.

The morphology of cells cultured with the LSE-loaded Alg/CS beads was observed by using a SEM. NHDF cells (cell density of 25,000 cells/well) were seeded on a cover glass in 24-well plates and then cultured for 24 h to allow cell attachment. After that, the sterilized LSE-loaded Alg/CS beads were added to each well of 24-well plates. After 24 h, the culture medium in each well was removed and washed with PBS. The cells cultured with the beads were then fixed with 3% v/v glutaraldehyde for 30 min. After that, the cells were dehydrated with different concentrations (30, 50, 70, 90, and 100% v/v) of ethanol solution for two min each. The cells were immersed with 500 μl of 100% hexamethyldisilazane for five min and then left to dry in a desiccator at room temperature for 24 h. Finally, the cells were coated with gold before SEM observation.

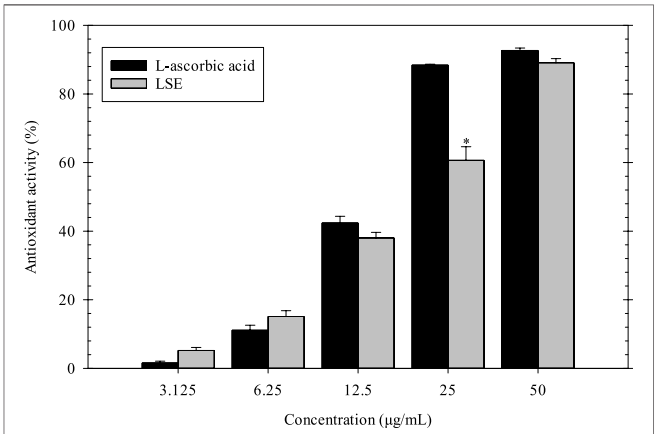

FIGURE 1 | Antioxidant activity of LSE and L-ascorbic acid. *$p < 0.05$ compared with L-ascorbic acid at each concentration.

Statistical Analysis

The experiments were represented as means ± standard derivation (SD). Analysis of variance (one-way ANOVA) and Tukey's *post hoc* test in SPSS were carried out (IBM SPSS statistics 24, United States). The statistical significance was accepted at $p < 0.05$.

RESULTS AND DISCUSSION

Extraction of Longan Seed Extract

The bioactive compounds in longan seeds such as phenolic acid, flavonoids, and polysaccharides showed antimicrobial, antioxidant, and anti-inflammatory activities (Rangkadilok et al., 2007). In this study, the ground longan seeds were extracted with distilled water. The percent yield of LSE was 7.46 ± 0.17%. The amount of gallic acid, ellagic acid, and corilagin, which are the major polyphenolic compounds found in the longan seed, was 25.61 ± 0.48, 18.83 ± 3.75, and 21.92 ± 1.42 mg/g (based on the weight of LSE), respectively. These values are in the same order with the results reported by Pankongadisak and Suwantong (Pankongadisak and Suwantong 2018).

Antioxidant Activity of Longan Seed Extract

The antioxidant activity of LSE as compared with L-ascorbic acid was determined by DPPH assay. In **Figure 1**, the antioxidant activity of LSE and L-ascorbic acid increased with increasing concentration. The maximum antioxidant activity of LSE and L-ascorbic acid at a concentration of 50 μg/ml was 89.10 and 92.71%, respectively. The half-maximum inhibitory concentration (IC_{50}) of LSE was 24.63 ± 0.71 μg/ml, which is close to the standard drug (L-ascorbic acid) of 15.12 ± 0.09 μg/ml.

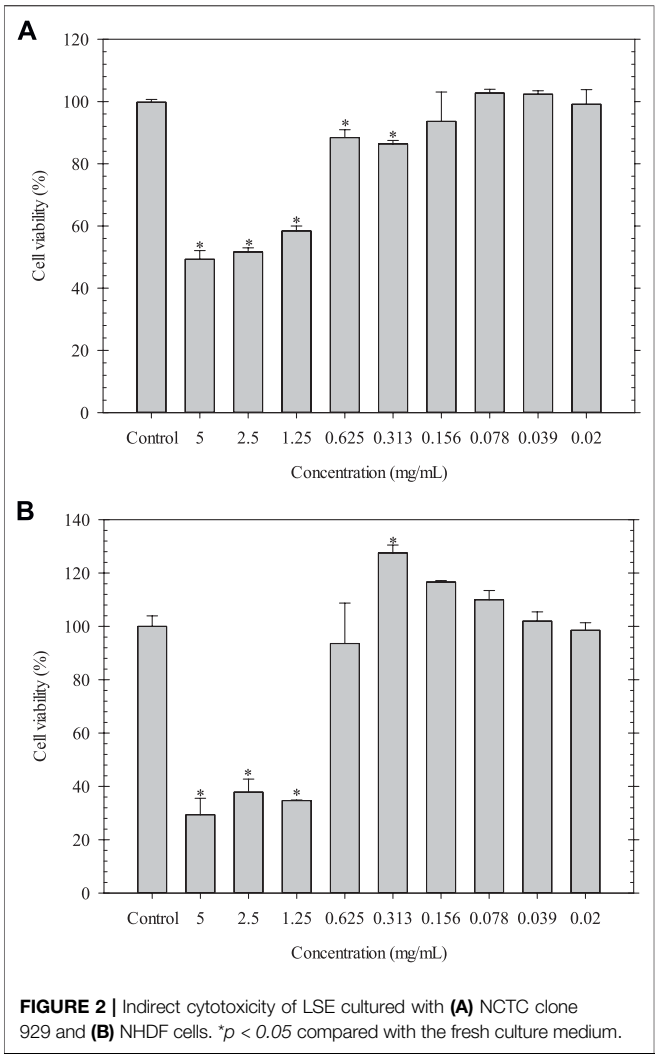

FIGURE 2 | Indirect cytotoxicity of LSE cultured with **(A)** NCTC clone 929 and **(B)** NHDF cells. *$p < 0.05$ compared with the fresh culture medium.

Thus, the polyphenolic compounds such as gallic acid, ellagic acid, and corilagin in LSE showed strong antioxidant activity.

Indirect Cytotoxicity of Longan Seed Extract

The indirect cytotoxicity of LSE was carried out by MTT assay using NCTC clone 929 and NHDF cells. The cell viability was measured after 24 h of incubation (**Figure 2**). The results showed that the viability of NCTC clone 929 cells cultured with LSE ranged between ~86 and ~103%, while that of NHDF cells cultured with LSE ranged between ~93 and ~128% at a concentration of 0.02–0.625 mg/ml. These results confirmed that LSE at concentrations of 0.02–0.625 mg/ml was non-toxic to the cells and had potential use for further study.

Morphology, Size, and PDI of LSE-Loaded Alg/CS Beads

The LSE-loaded Alg/CS beads were prepared by using the ionic gelation method. The negatively charged carboxylic groups of Alg interacted with the protonated amino groups of CS to form the Alg/CS beads (Nagarwal et al., 2012; Rahaiee et al., 2015). **Figure 3** shows that LSE/Alg/CS-S and LSE/Alg/CS-H exhibited more spherical shapes and dispersed particles. In contrast, LSE/Alg/CS-U showed an aggregation between particles because the shear force and time from the ultrasonicator were not enough to separate the particles completely. Besides, the merging of the polymer network during freeze-drying caused the aggregation of particles (Rahaiee et al., 2015). Moreover, the sizes of LSE/Alg/CS-S, LSE/Alg/CS-H, and LSE/Alg/CS-U were 1.88 ± 0.40, 2.41 ± 0.21, and 2.54 ± 0.15 μm, respectively. The PDIs of LSE/Alg/CS-S, LSE/Alg/CS-H, and LSE/Alg/CS-U were 0.198 ± 0.142, 0.150 ± 0.104, and 0.318 ± 0.048, respectively, as shown in **Table 2**.

FTIR Analysis

Figure 4 shows the FTIR spectra for LSE, Alg, CS, and LSE-loaded Alg/Cs beads. FTIR spectra of all samples between 3,000 and 3,600 cm^{-1} showed broad absorption bands indicating the O–H stretching and N–H stretching frequencies in the structure. For the spectrum of LSE, the peaks at 1,706 and 1,609 cm^{-1} were attributed to C–H aromatic and C=C alkene stretching, respectively. The peaks at 1,522 cm^{-1} represented N–O stretching. The peak at 1,050 cm^{-1} showed the strong intensity of C–O stretching of ether (Aziz et al., 2018; Chollakup et al., 2021). For Alg, the FTIR spectrum represented the carboxyl anion stretching vibrations (asymmetric and symmetric) at 1,610 and 1,423 cm^{-1}. The FTIR spectrum of CS showed the peak at 1,663 attributing to C=O stretching in amide I. The peaks at 1,592 cm^{-1} were assigned to N–H bending in amide II. In addition, the spectrum of CS showed the peak at 1,323 cm^{-1} which was assigned to N–H stretching in amide III (Bajpai 2019; Butt et al., 2019; Pereira et al., 2019). The LSE-loaded Alg/CS beads showed the shifted band intensity of 3,382 cm^{-1} (O–H, N–H) and 2,924 cm^{-1} (C–H). Moreover, the peak at 1,610 cm^{-1} of Alg was shifted to 1,606 cm^{-1}. The peaks at 1,422 cm^{-1} were observed. This might be due to the shifting of asymmetrical and symmetrical stretching of -COO^- of Alg. The peak at 1,530 cm^{-1} due to the protonation of amine groups of CS was not observed. This might be due to the overlap with the peak at 1,606 cm^{-1}. From these results, it could be proved that the carboxylate groups of Alg reacted with the protonated amino groups of CS by intermolecular or electrostatic interactions to form the LSE-loaded Alg/CS beads (Butt et al., 2019; Rahaiee et al., 2015). Moreover, the absorption band of the O–H stretching and N–H stretching was shifted to 3,382 cm^{-1} due to the interaction of the hydroxyl group of LSE with Alg and CS. The disappearance of the peaks at 1,706, 1,609, and 1,522 cm^{-1} of LSE was due to the interaction of LSE with Alg and CS. The results confirmed that LSE was loaded in the Alg/CS beads successfully. In addition, the %EE of the LSE-loaded Alg/CS beads was another investigation to confirm that LSE was successfully loaded into the beads.

Encapsulation Efficiency

The % EE is the percentage of LSE that successfully entrapped into the Alg/CS beads. The %EE was quantified by the UV–Vis spectrophotometer at a wavelength of 277 nm. The %EE of the LSE-loaded Alg/CS beads is shown in **Table 1**. The %EE of LSE/Alg/CS-S, LSE/Alg/CS-H, and LSE/Alg/CS-U was 11.97 ± 0.91, 13.80 ± 2.99, and 18.42 ± 0.79%, respectively. The LSE/Alg/CS-U showed the highest value of %EE. This result showed that the

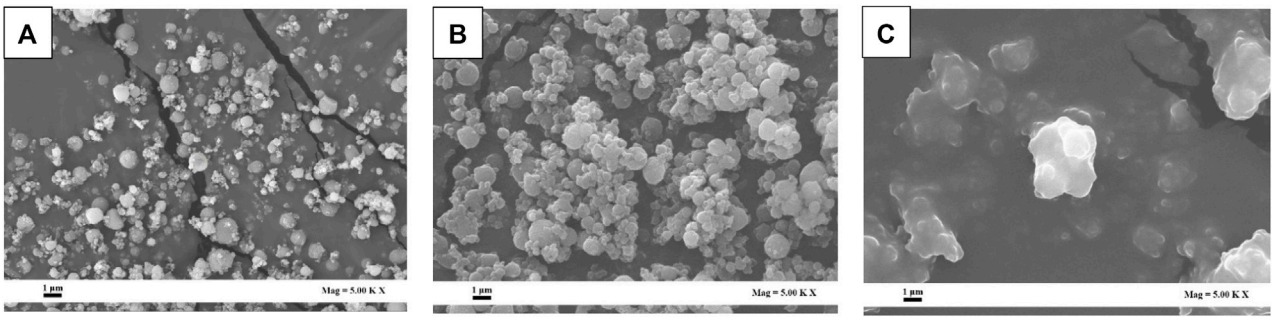

FIGURE 3 | SEM images of **(A)** LSE/Alg/CS-S, **(B)** LSE/Alg/CS-H, and **(C)** LSE/Alg/CS-U.

TABLE 2 | Particle size, PDI, and EE (%) of LSE-loaded Alg/CS beads.

Sample	Particle size (μm)	PDI	EE (%)
LSE/Alg/CS-S	1.88 ± 0.40	0.198 ± 0.142	11.97 ± 0.91
LSE/Alg/CS-H	2.41 ± 0.21	0.150 ± 0.104	13.80 ± 2.99
LSE/Alg/CS-U	2.54 ± 0.15	0.318 ± 0.048	18.42 ± 0.79*

large particle size of LSE/Alg/CS-U increased the ability to entrap LSE in high amounts (Lecaroz et al., 2006). Moreover, after freeze-drying, LSE/Alg/CS-U showed the merging of the polymer network caused by the formation of irregular shapes and particle aggregates.

Release Study

The release characteristics of LSE from the LSE-loaded Alg/CS beads were investigated by using the total immersion method for two days, and the results are shown in **Figure 5**. All samples showed similar profiles of the cumulative released amount. The release rate was fastest between 0 and 120 min. After that the cumulative released amounts were gradually increased and reached a plateau at the longest immersion time. The maximum cumulative released amount of LSE from LSE/Alg/CS-S, LSE/Alg/CS-H, and LSE/Alg/CS-U was 93, 86, and 68%, respectively. LSE/Alg/CS-U showed the lowest released amount of LSE, whereas LSE/Alg/CS-S and LSE/Alg/CS-H showed similar values. The low released amount of LSE observed from LSE/Alg/CS-U could be the merging of the beads that caused the formation of irregular shapes of the beads after the freeze-drying method. The merging of the beads makes the beads have large size with the low surface area. Thus, this can cause the lower released amount of LSE from the LSE/Alg/CS-U than the others. While, LSE/Alg/CS-S and LSE/Alg/CS-H showed the small spherical shape without the merging of the beads, resulting in the higher released amount of LSE from LSE/Alg/CS-S and LSE/Alg/CS-H.

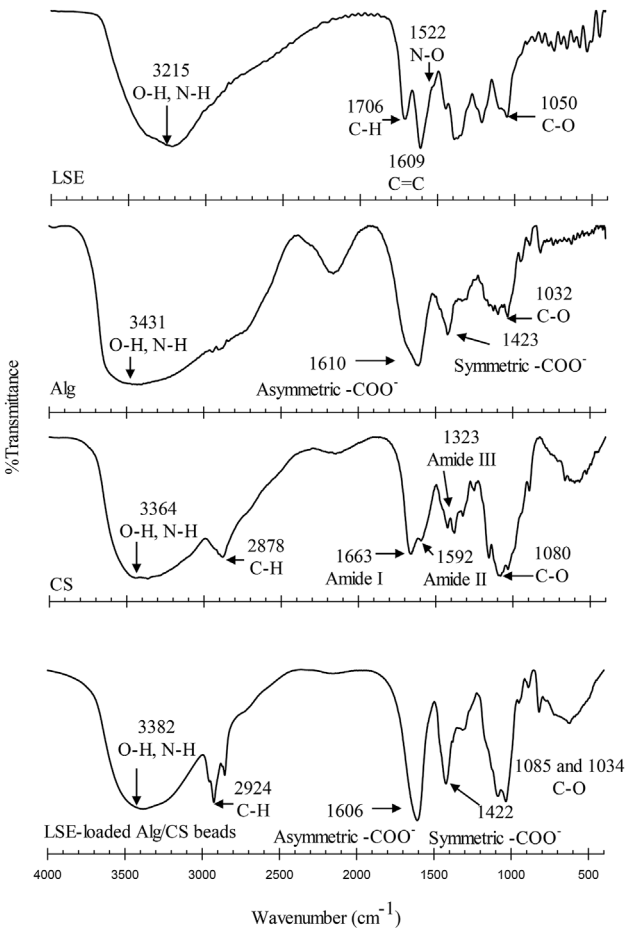

FIGURE 4 | FTIR spectra of LSE, Alg, CS, and LSE-loaded Alg/CS beads.

Indirect Cytotoxicity of LSE-Loaded Alg/CS Beads

The indirect cytotoxicity of the LSE-loaded Alg/CS beads was carried out by MTT assay using NCTC clone 929 cells and NHDF cells. The viability of cells was measured after 24 h incubation with different concentrations (0.5, 5, and 10 mg/ml) of extraction media from the LSE-loaded Alg/CS beads (**Figure 6**). The results showed that the viability of NCTC clone 929 cells cultured with the extraction media from LSE/Alg/CS-S, LSE/Alg/CS-H, and LSE/Alg/CS-U ranged between

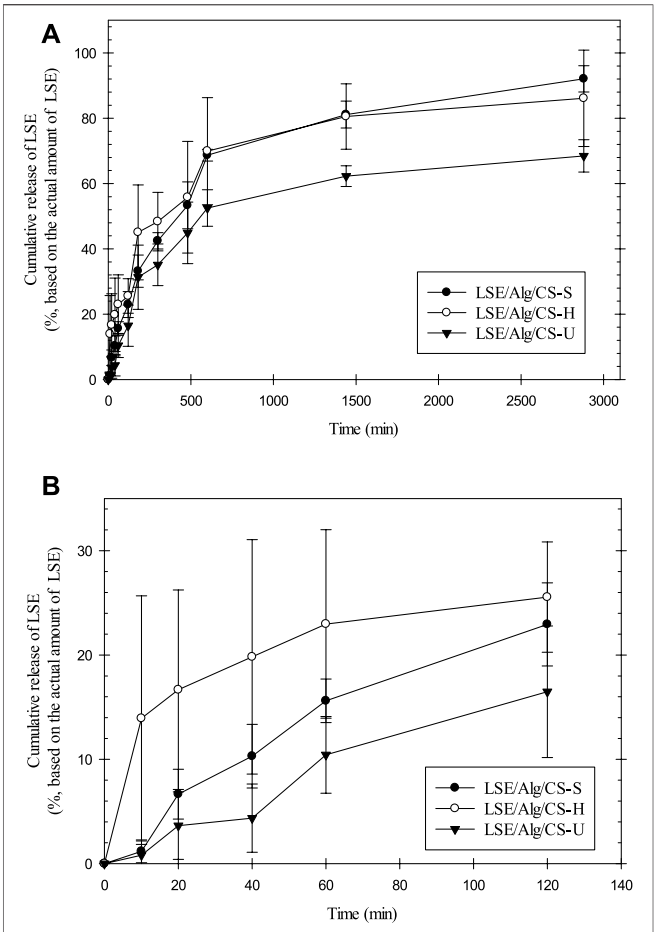

FIGURE 5 | (A) Release profiles of LSE from LSE-loaded Alg/CS beads and **(B)** expanded figure of the release profile at first 120 min.

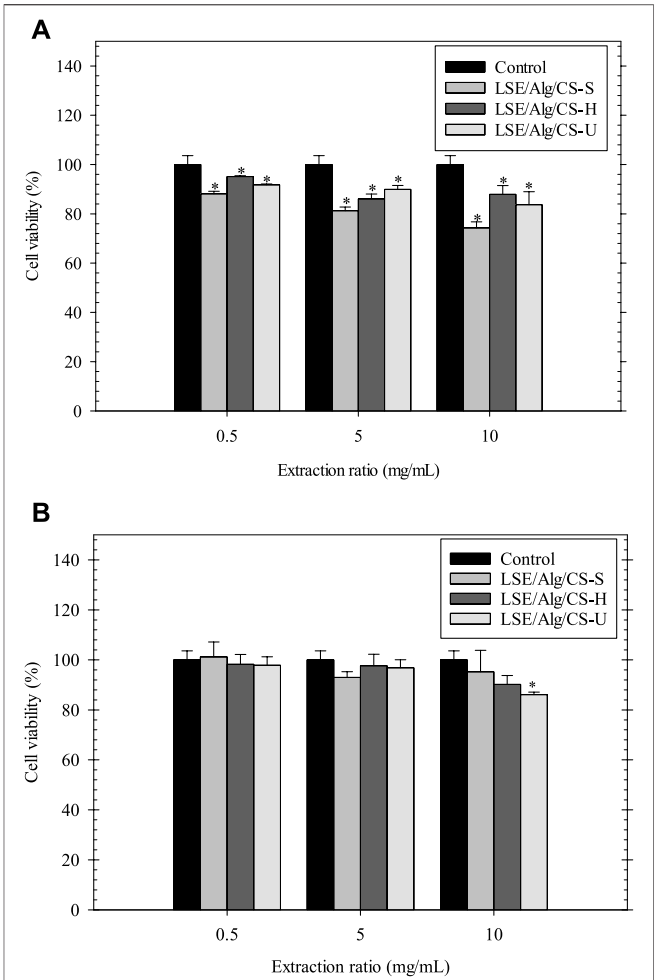

FIGURE 6 | Indirect cytotoxicity of LSE-loaded Alg/CS beads cultured with **(A)** NCTC clone 929 and **(B)** NHDF cells (n = 3). *$p < 0.05$ compared with the fresh culture medium.

74 and 95%, while the viability of NHDF cells ranged between 86 and 101%. According to the ISO 10993-5 cytotoxicity standard, if the percent cell viability is increased to >70%, it has a non-cytotoxic potential. Thus, these beads were non-toxic to both NCTC clone 929 cells and NHDF cells and had the potential for use in biomedical applications.

Biocompatibility

For use in biomedical applications, materials must exhibit good biocompatibility, non-toxic, and support cell growth (Kim et al., 2008). Thus, the biocompatibility of cells cultured with the LSE-loaded Alg/CS beads was carried out. The viability of NHDF cells cultured with the fresh culture medium was the control. The Alg/CS beads without the loading of LSE were designated as Alg/CS. **Figure 7** demonstrates the viability of NHDF cells cultured with samples at different incubation times (2, 24, and 72 h). After incubation, the viability of cells was determined by MTT assay. The viability of NHDF cells cultured with all samples was between 97 and 126%. The viability of NHDF cells was more than 70% after treatment with samples at different time points, indicating these beads were non-toxic and compatible with the cells.

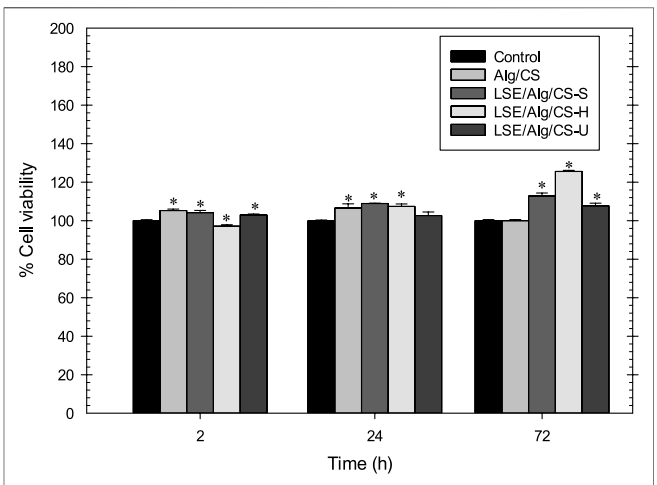

FIGURE 7 | Cell biocompatibility of LSE-loaded Alg/CS beads with NHDF cells. *$p < 0.05$ compared with the fresh culture medium.

TABLE 3 | Morphology of NHDF cells cultured with LSE-loaded Alg/CS beads after 24 h.

Condition	100x	500x
Control	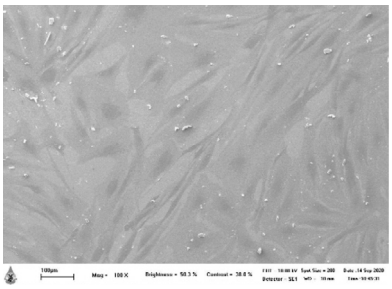	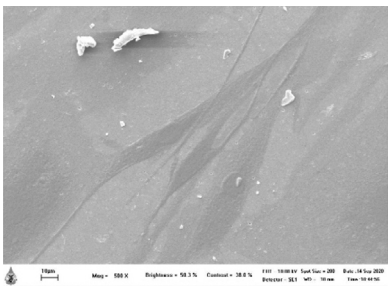
Alg/CS	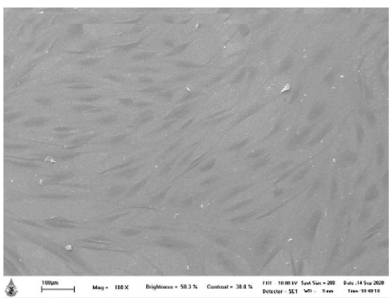	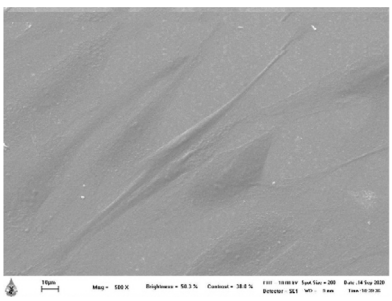
LSE/Alg/CS-S	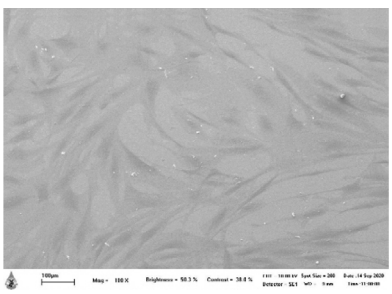	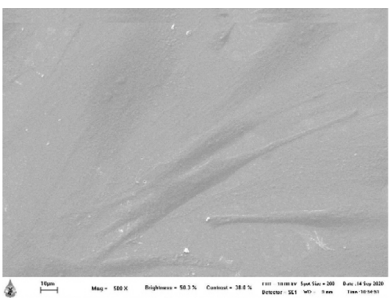
LSE/Alg/CS-H	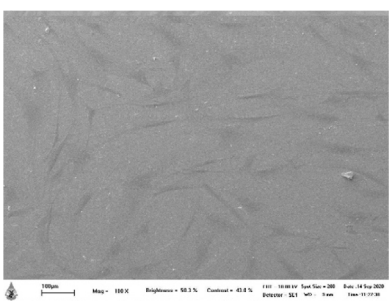	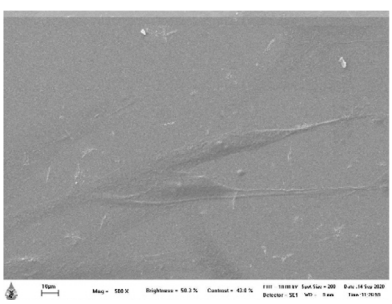
LSE/Alg/CS-U	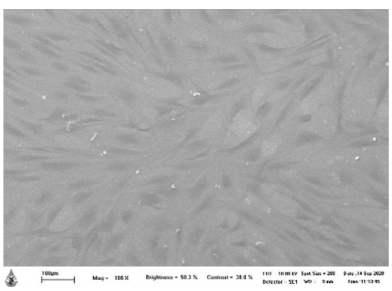	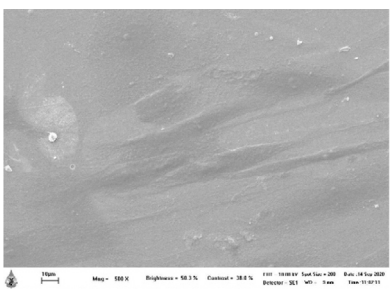

The morphology of NHDF cells cultured with LSE-loaded Alg/CS beads was observed by using a SEM (see **Table 3**). From the results, the NHDF cells cultured with all samples showed good attachment on the cover glass and exhibited a spindle shape on the surface. Therefore, these LSE-loaded Alg/CS beads had the potential for use in biomedical applications.

CONCLUSION

In this study, the LSE-loaded Alg/CS beads were successfully prepared. The polymeric carriers were made from Alg and CS using the ionic gelation method. The LSE was added as an active ingredient. The LSE-loaded Alg/CS beads showed the spherical shape with some aggregation. The particle sizes of the LSE-loaded Alg/CS beads were ranging between ~1.9 and ~2.5 μm. PDI ranged between 0.150 and 0.318. LSE/Alg/CS-S had the smallest sizes, while LSE/Alg/CS-U showed the highest %EE. The cumulative released amount of LSE from LSE/Alg/CS-S had the highest value. Finally, these beads were non-toxic to both NCTC clone 929 and NHDF cells and promoted the attachment of NHDF cells. These results suggested that these beads can be used as drug carriers for biomedical applications.

DATA AVAILABILITY STATEMENT

The raw data supporting the conclusion of this article will be made available by the authors, without undue reservation.

AUTHOR CONTRIBUTIONS

TB contributed to methodology, acquisition of data, analysis and interpretation of data, and drafting the manuscript; PK contributed to reviewing and editing the manuscript; SS helped with methodology and reviewing and editing the manuscript; CT assisted with reviewing and editing the manuscript; and OS involved in conceptualization, methodology, funding acquisition, analysis and interpretation of data, and reviewing and editing the manuscript.

ACKNOWLEDGMENTS

The authors would like to acknowledge Mae Fah Luang University for funding. The authors gratefully acknowledge the National Nanotechnology Center (NANOTEC), the National Science and Technology Development Agency (NSTDA), Scientific and Technological Instruments Center (STIC), and Mae Fah Luang University for laboratory facilities.

REFERENCES

Ahdyani, R., Novitasari, L., Martien, R., and Danarti, R. E. T. N. O. (2019). Formulation and Characterization of Timolol Maleate-Loaded Nanoparticles Gel by Ionic Gelation Method Using Chitosan and Sodium Alginate. *Int. J. App Pharm.* 11, 48–54. doi:10.22159/ijap.2019v11i6.34983

Aziz, H., Rahim, N., Ramli, S., Alazaiza, M., Omar, F., and Hung, Y.-T. (2018). Potential Use of *Dimocarpus Longan* Seeds as a Flocculant in Landfill Leachate Treatment. *Water* 10, 1672. doi:10.3390/w10111672

Bajpai, A. K. (2019). Facile Preparation of Ionotropically Crosslinked Chitosan-Alginate Nanosorbents by Water-In-Oil (W/O) Microemulsion Technique: Optimization and Study of Arsenic (V) Removal. *J. Water Process Eng.* 32, 100920. doi:10.1016/j.jwpe.2019.100920

Bernkop-Schnürch, A., and Dünnhaupt, S. (2012). Chitosan-based Drug Delivery Systems. *Eur. J. Pharmaceutics Biopharmaceutics* 81, 463–469. doi:10.1016/j.ejpb.2012.04.007

Blois, M. S. (1958). Antioxidant Determinations by the Use of a Stable Free Radical. *Nature* 181, 1199–1200. doi:10.1038/1811199a0

Butt, A., Jabeen, S., Nisar, N., Islam, A., Gull, N., Iqbal, S. S., et al. (2019). Controlled Release of Cephradine by Biopolymers Based Target Specific Crosslinked Hydrogels. *Int. J. Biol. Macromolecules* 121, 104–112. doi:10.1016/j.ijbiomac.2018.10.018

Chollakup, R., Kongtud, W., Sukatta, U., Premchookiat, M., Piriyasatits, K., Nimitkeatkai, H., et al. (2021). Eco-friendly rice Straw Paper Coated with Longan (*Dimocarpus Longan*) Peel Extract as Bio-Based and Antibacterial Packaging. *Polymers* 13, 3096. doi:10.3390/polym13183096

De Pinho Neves, A. L., Milioli, C. C., Müller, L., Riella, H. G., Kuhnen, N. C., and Stulzer, H. K. (2014). Factorial Design as Tool in Chitosan Nanoparticles Development by Ionic Gelation Technique. *Colloids Surf. A: Physicochemical Eng. Aspects* 445, 34–39. doi:10.1016/j.colsurfa.2013.12.058

Gagliardi, M., Bardi, G., and Bifone, A. (2012). Polymeric Nanocarriers for Controlled and Enhanced Delivery of Therapeutic Agents to the CNS. *Ther. Deliv.* 3, 875–887. doi:10.4155/tde.12.55

George, A., Shah, P. A., and Shrivastav, P. S. (2019). Natural Biodegradable Polymers Based Nano-Formulations for Drug Delivery: A Review. *Int. J. Pharmaceutics* 561, 244–264. doi:10.1016/j.ijpharm.2019.03.011

Ji, J., Hao, S., Wu, D., Huang, R., and Xu, Y. (2011). Preparation, Characterization and *In Vitro* Release of Chitosan Nanoparticles Loaded with Gentamicin and Salicylic Acid. *Carbohydr. Polym.* 85, 803–808. doi:10.1016/j.carbpol.2011.03.051

Kim, I.-Y., Seo, S.-J., Moon, H.-S., Yoo, M.-K., Park, I.-Y., Kim, B.-C., et al. (2008). Chitosan and its Derivatives for Tissue Engineering Applications. *Biotechnol. Adv.* 26, 1–21. doi:10.1016/j.biotechadv.2007.07.009

Kumari, A., Yadav, S. K., and Yadav, S. C. (2010). Biodegradable Polymeric Nanoparticles Based Drug Delivery Systems. *Colloids Surf. B: Biointerfaces* 75, 1–18. doi:10.1016/j.colsurfb.2009.09.001

Lecaroz, C., Gamazo, C., Renedo, M. J., and Blanco-Prieto, M. J. (2006). Biodegradable Micro- and Nanoparticles as Long-Term Delivery Vehicles for Gentamicin. *J. Microencapsulation* 23, 782–792. doi:10.1080/02652040600946886

Lee, K. Y., and Mooney, D. J. (2012). Alginate: Properties and Biomedical Applications. *Prog. Polym. Sci.* 37, 106–126. doi:10.1016/j.progpolymsci.2011.06.003

Li, X., Deng, Y., Zheng, Z., Huang, W., Chen, L., Tong, Q., et al. (2018). Corilagin, a Promising Medicinal Herbal Agent. *Biomed. Pharmacother.* 99, 43–50. doi:10.1016/j.biopha.2018.01.030

Lim, T. K. (2013). "Dimocarpus Longan Subsp. Malesianus Var. Malesianus," in *Edible Medicinal and Non-medicinal Plants* (Springer), 33–38. doi:10.1007/978-94-007-5628-1_6

Morsi, N., Ghorab, D., Refai, H., and Teba, H. (2015). Preparation and Evaluation of Alginate/chitosan Nanodispersions for Ocular Delivery. *Int. J. Pharm. Pharm. Sci.* 7, 234–240.

Nagarwal, R. C., Kumar, R., and Pandit, J. K. (2012). Chitosan Coated Sodium Alginate-Chitosan Nanoparticles Loaded with 5-FU for Ocular Delivery: *In Vitro* Characterization and *In Vivo* Study in Rabbit Eye. *Eur. J. Pharm. Sci.* 47, 678–685. doi:10.1016/j.ejps.2012.08.008

Nalini, T., Basha, S. K., Mohamed Sadiq, A. M., Kumari, V. S., and Kaviyarasu, K. (2019). Development and Characterization of Alginate/Chitosan Nanoparticulate System for Hydrophobic Drug Encapsulation. *J. Drug Deliv. Sci. Tech.* 52, 65–72. doi:10.1016/j.jddst.2019.04.002

Nguyen, T. V., Nguyen, T. T. H., Wang, S.-L., Vo, T. P. K., and Nguyen, A. D. (2017). Preparation of Chitosan Nanoparticles by TPP Ionic Gelation Combined with spray Drying, and the Antibacterial Activity of Chitosan Nanoparticles and a Chitosan Nanoparticle-Amoxicillin Complex. *Res. Chem. Intermed.* 43, 3527–3537. doi:10.1007/s11164-016-2428-8

Pankongadisak, P., and Suwantong, O. (2018). The Potential Use of Thermosensitive Chitosan/silk Sericin Hydrogels Loaded with Longan Seed Extract for Bone Tissue Engineering. *RSC Adv.* 8, 40219–40231. doi:10.1039/C8RA07255H

Pereira, A. D. S., Diniz, M. M., De Jong, G., Gama Filho, H. S., Dos Anjos, M. J., Finotelli, P. V., et al. (2019). Chitosan-alginate Beads as Encapsulating Agents for Yarrowia Lipolytica Lipase: Morphological, Physico-Chemical and Kinetic Characteristics. *Int. J. Biol. Macromolecules* 139, 621–630. doi:10.1016/j.ijbiomac.2019.08.009

Rahaiee, S., Shojaosadati, S. A., Hashemi, M., Moini, S., and Razavi, S. H. (2015). Improvement of Crocin Stability by Biodegradeble Nanoparticles of Chitosan-Alginate. *Int. J. Biol. Macromolecules* 79, 423–432. doi:10.1016/j.ijbiomac.2015.04.041

Rajendran, A., and Basu, S. (2009). Alginate-chitosan Particulate System for Sustained Release of Nimodipine. *Trop. J. Pharm. Res.* 8, 433–440. doi:10.4314/tjpr.v8i5.48087

Rangkadilok, N., Sitthimonchai, S., Worasuttayangkurn, L., Mahidol, C., Ruchirawat, M., and Satayavivad, J. (2007). Evaluation of Free Radical Scavenging and Antityrosinase Activities of Standardized Longan Fruit Extract. *Food Chem. Toxicol.* 45, 328–336. doi:10.1016/j.fct.2006.08.022

Sarei, F., Zolfagharian, H., Khaki, P., Bidhendi, S., and Dounighi, N. (2013). Alginate Nanoparticles as a Promising Adjuvant and Vaccine Delivery System. *Indian J. Pharm. Sci.* 75, 442–449. doi:10.4103/0250-474X.119829

Sinha, V. R., Singla, A. K., Wadhawan, S., Kaushik, R., Kumria, R., Bansal, K., et al. (2004). Chitosan Microspheres as a Potential Carrier for Drugs. *Int. J. Pharmaceutics* 274, 1–33. doi:10.1016/j.ijpharm.2003.12.026

Song, W., Su, X., Gregory, D., Li, W., Cai, Z., and Zhao, X. (2018). Magnetic Alginate/chitosan Nanoparticles for Targeted Delivery of Curcumin into Human Breast Cancer Cells. *Nanomaterials* 8, 907. doi:10.3390/nano8110907

Sun, L., Zhou, S., Wang, W., Li, X., Wang, J., and Weng, J. (2009). Preparation and Characterization of Porous Biodegradable Microspheres Used for Controlled Protein Delivery. *Colloids Surf. A: Physicochemical Eng. Aspects* 345, 173–181. doi:10.1016/j.colsurfa.2009.04.053

Tang, Y.-Y., He, X.-M., Sun, J., Li, C.-B., Li, L., Sheng, J.-F., et al. (2019). Polyphenols and Alkaloids in Byproducts of Longan Fruits (*Dimocarpus Longan* Lour.) and Their Bioactivities. *Molecules* 24 (6), 1186. doi:10.3390/molecules24061186

Venditti, I. (2019). Morphologies and Functionalities of Polymeric Nanocarriers as Chemical Tools for Drug Delivery: A Review. *J. King Saud Univ. - Sci.* 31, 398–411. doi:10.1016/j.jksus.2017.10.004

Worasuttayangkurn, L., Watcharasit, P., Rangkadilok, N., Suntararuks, S., Khamkong, P., and Satayavivad, J. (2012). Safety Evaluation of Longan Seed Extract: Acute and Repeated Oral Administration. *Food Chem. Toxicol.* 50, 3949–3955. doi:10.1016/j.fct.2012.07.068

Yang, B., Jiang, Y., Shi, J., Chen, F., and Ashraf, M. (2011). Extraction and Pharmacological Properties of Bioactive Compounds from Longan (Dimocarpus Longan Lour.) Fruit - A Review. *Food Res. Int.* 44, 1837–1842. doi:10.1016/j.foodres.2010.10.019

Zhang, X., Guo, S., Ho, C.-T., and Bai, N. (2020). Phytochemical Constituents and Biological Activities of Longan (*Dimocarpus Longan* Lour.) Fruit: A Review. *Food Sci. Hum. Wellness* 9, 95–102. doi:10.1016/j.fshw.2020.03.001

Conflict of Interest: The authors declare that the research was conducted in the absence of any commercial or financial relationships that could be construed as a potential conflict of interest.

Publisher's Note: All claims expressed in this article are solely those of the authors and do not necessarily represent those of their affiliated organizations, or those of the publisher, the editors, and the reviewers. Any product that may be evaluated in this article, or claim that may be made by its manufacturer, is not guaranteed or endorsed by the publisher.

frontiers in Materials

ORIGINAL RESEARCH
published: 28 February 2022
doi: 10.3389/fmats.2022.823545

Novel Stimuli-Responsive Pectin-PVP-Functionalized Clay Based Smart Hydrogels for Drug Delivery and Controlled Release Application

Shabnam Rehmat[1,2], Nayab Batool Rizvi[1], Saba Urooge Khan[3], Abdul Ghaffar[4], Atif Islam[3]*, Rafi Ullah Khan[3], Azra Mehmood[5], Hira Butt[5] and Muhammad Rizwan[6]*

[1]School of Chemistry, University of the Punjab, Lahore, Pakistan, [2]HEJ Research Institute of Chemistry, International Center for Chemical and Biological Sciences, University of Karachi, Karachi, Pakistan, [3]Institute of Polymer and Textile Engineering, University of the Punjab, Lahore, Pakistan, [4]Department of Chemistry, University of Engineering and Technology, Lahore, Pakistan, [5]Center of Excellence in Molecular Biology, University of the Punjab, Punjab, Pakistan, [6]Department of Biomedical Engineering, Michigan Technological University, Houghton, MI, United States

OPEN ACCESS

Edited by:
Wenbo Wang,
Inner Mongolia University, China

Reviewed by:
Maria Emilia Villanueva,
Consejo Nacional de Investigaciones Científicas y Técnicas (CONICET), Argentina
Mohamed El-Aassar,
Jouf University, Saudi Arabia

***Correspondence:**
Shabnam Rehmat
shabnamrehmat123@gmail.com
Atif Islam
dratifislam@gmail.com

Specialty section:
This article was submitted to Polymeric and Composite Materials, a section of the journal Frontiers in Materials

Received: *27 November 2021*
Accepted: *05 January 2022*
Published: *28 February 2022*

Citation:
Rehmat S, Rizvi NB, Khan SU, Ghaffar A, Islam A, Khan RU, Mehmood A, Butt H and Rizwan M (2022) Novel Stimuli-Responsive Pectin-PVP-Functionalized Clay Based Smart Hydrogels for Drug Delivery and Controlled Release Application. Front. Mater. 9:823545. doi: 10.3389/fmats.2022.823545

Stimuli-responsive drug delivery systems are urgently required for injectable site-specific delivery and release of drugs in a controlled manner. For this purpose, we developed novel pH-sensitive, biodegradable, and antimicrobial hydrogels from bio-macromolecule pectin, polyvinylpyrrolidone (PVP), 3-aminopropyl (diethoxy)methyl silane (3-APDEMS), and sepiolite clay via blending and solution casting technique. The purified sepiolite (40 um) was functionalized with 3-APDEMS crosslinker (*ex-situ* modification) followed by hydrogels fabrication. FTIR and SEM confirmed crosslinked structural integrity and rod-like morphology of hydrogels respectively. The swelling properties of hydrogels could be controlled by varying the concentration of modified clay in pectin/PVP blends. Moreover, the decrease in pH increased the swelling of hydrogels indicating the pH-responsiveness of hydrogels. All hydrogels were degraded after 21 days in phosphate buffer saline pH 7.4 (human blood pH). *In-vitro* cytotoxicity against 3T3 mouse fibroblast cell line analysis confirmed cytocompatibility of all hydrogels. Ceftriaxone sodium (CTX-S) was selected as a model drug. The release profile of the hydrogel showed 91.82% release in PBS for 2 h in a consistent and controlled manner. The chemical structure of the drug remained intact during and after release confirmed through UV-Visible spectroscopy. Overall, these hydrogels could be used as potential scaffolds for future biomedical applications.

Keywords: hydrogel, pectin, 3-aminopropyl (diethoxy) methylsilane, polyvinylpyrrolidone, drug delivery, pH-responsive

1 INTRODUCTION

Conventional methods of drug delivery lead to the diffusion of drugs evenly throughout the body causing considerable damage to normal cells while reducing bioavailability. To overcome unfavorable actions, site-specific distribution of therapeutic medicine is essential. The smart hydrogel-based drug carriers can offer distinct advantages as targeted delivery (Raza et al., 2021), site-specificity, slow release of the drug, drug stability, optimized drug absorption, physiochemical compatibility with drug, non-

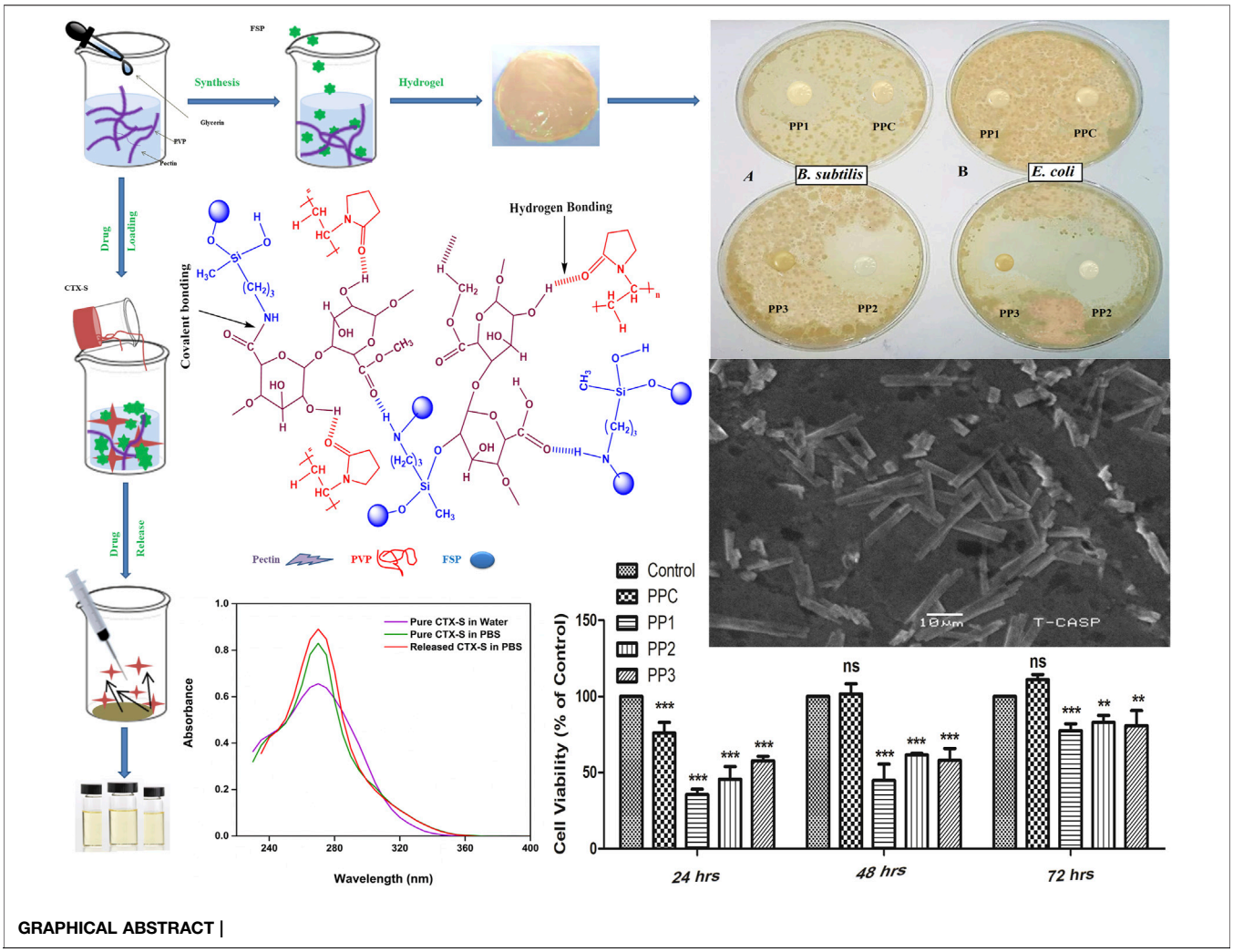

GRAPHICAL ABSTRACT |

toxicity, and biodegradability (Veronovski et al., 2014; Rasool et al., 2019; Peers et al., 2020; Ko et al., 2021; Liu et al., 2021). A variety of polymer-based stimuli-responsive (pH, temperature, light, enzymes, electricity, ultrasound, glucose) hydrogels have been synthesized (Yang et al., 2009; Peers et al., 2020; Liu et al., 2021; Song et al., 2021) due to their high swelling rate, soft tissue compatibility, and capability to prevent chemical and enzyme degradation (Islam and Yasin, 2012; Iglesias et al., 2020; Shirazi et al. 2021). Polymeric chains crosslink to develop microporous three-dimensional semi-interpenetrating networks (semi-IPNs) called hydrogel by penetrating at least one suitable linear or branched polymer (Liu et al., 2003; Mishra et al., 2008; Sivagangi Reddy et al., 2016; Rinoldi et al., 2021). Polysaccharides and their derivatives are among the ideal candidates for smart hydrogel formation due to stimuli-responsive behavior, reducing dose frequency, nontoxicity, stability, biocompatibility, biodegradability, easy availability, and cost-effectiveness (Roy et al., 2010; Sharma and Ahuja, 2011).

Pectin is an anionic, acidic, water-soluble, pH-sensitive, and fruit extracted polysaccharide (Mishra et al., 2008; Sriamornsak et al., 2008; Pierce et al., 2020). Its ability to naturally turn into gel, stabilize and thicken makes it a promising candidate for drug delivery application (Sharma and Ahuja, 2011; Veronovski et al., 2014). Pectin polysaccharide-based drug carriers direct the controlled release of therapeutic agents to achieve efficient treatment (Li et al., 2020; Li et al., 2021). However, pectin is a great choice for hydrogel formation however they show instant release of the drug, low thermal stability, and poor mechanical properties (Mishra et al., 2008; Li et al., 2020). Blending pectin with polymer like polyvinylpyrrolidone (PVP) offers the solution to these obstacles (Ghasemiyeh and Mohammadi-Samani, 2021). It is a hydrophilic synthetic polymer with tremendous solubility, low toxicity, biological compatibility (Eid et al., 2012; Singh and Singh, 2020), and excellent hydrogel film-forming properties. It has been reported to improve the mechanical characteristics of the hydrogel for various biomedical applications (Sizílio et al., 2018; Saeedi Garakani et al., 2020; Kumar et al., 2020).

Mishra et al. (2008) developed and examined the efficiency of pectin-based hydrogels prepared with different PVP ratios *via*

solution casting method for salicylic acid drug release (Mishra et al., 2008). Hussain et al. (2018) reported pH-dependent pectin-based nano-carriers functionalized with nano-graphene oxide for delivery of paclitaxel with better stability, higher drug loading efficiency, and non-toxicity (Hussien et al., 2018).

To improve hydrogel properties we used sepiolite (SP); a porous, lightweight reactive mineral clay (Nieto-Suárez et al., 2009) that has been reported as a reinforcing filler. It has been used as a pharmaceutical and medicinal ingredient for therapeutic purposes (Hun Kim et al., 2016; Darder et al., 2017; Dutta and Devi, 2021). It has also been used for tissue engineering, bio-medicines, and drug delivery applications (Ruiz-Hitzky et al., 2010; Gülmen, Güvel, and Kızılcan 2015; Tanc and Orakdogen 2019). Pectin and PVP have enormous potential for chemical/physical modifications using crosslinking agents like silane-based cross-linkers (Marandi et al., 2008; Yasin et al., 2008; Mirzaei B et al., 2013). In this study we choose 3-aminopropyl (diethoxy)methylsilane crosslinker (Khramov et al., 2003). Its bifunctional property makes it appropriate for crosslinking the polymers (Sanaeepur et al., 2019; Zu et al., 2019). In the current report, ceftriaxone sodium (CTX-S) has been used as a model drug. It is a third-generation cephalosporin (Bali et al., 2018) antibiotic used to treat various bacterial infections including tuberculosis, cholera, pneumonia, urinary tract, and pelvic inflammatory infections.

Various methods have been reported for hydrogel formation including freeze thawing, complex coacervation, radiation grating, and solution casting (Gulrez et al., 2011). Solution casting method is easy, cost effective, and requires shorter time of preparation. It is convenient to control reaction conditions in this technique (Rahman et al., 2018). Pectin-PVP based hydrogels have been used for delivery of various drugs other than ceftriaxone sodium (Mishra et al., 2008).

In this work, the functionalization of sepiolite clay with bifunctional 3-amino (diethoxy) methyl silane (3-APDEMS) was performed to produce novel functionalized sepiolite clay (FSP) using crosslinker and its use to produce novel pectin/PVP/functionalized clay based hydrogel blends for the delivery of ceftriaxone sodium. According to the best of our knowledge, the modification of sepiolite with 3-APDEMS, development of pectin/PVP/modified clay based hydrogels and their use particularly for the delivery and controlled release of ceftriaxone sodium (CTX-S) has not been reported yet. The physical blending and solution casting technique was adapted to develop novel pH-responsive hydrogels composed of pectin/PVP/3-APDEMS-sepiolite. The effects of variant concentrations of functionalized clay (FSP) on the characteristics of fabricated hydrogel were analyzed through FTIR and SEM. The swelling response of all the hydrogels was examined in water, ionic solutions (NaCl, $CaCl_2$), and buffers of varying pH. Biodegradation was observed in PBS for 21 days along with the antimicrobial activity. *In-vitro* toxicology for all hydrogels was assessed through XTT assay against 3T3 mouse fibroblast cell line. The chemical activity was performed to check the drug stability as well. The drug release pattern of CTX-S was investigated in phosphate buffer saline (PBS), simulated gastric fluid (SGF), and simulated intestinal fluid (SIF) via UV-vis spectroscopy.

2 EXPERIMENTAL WORK

2.1 Materials

Pectin (M. W = 1,61, 254, 94 g/mol) (low methoxy content), PVP (M. W = 40,000–70,000 g/mol), 3-aminopropyl (diethoxy) methylsilane (97%; MW = 191.34 g/mol) and sepiolite were obtained from Sigma Aldrich. Glycerin and ceftriaxone sodium were obtained locally. NaCl (sodium chloride), $CaCl_2$ (calcium chloride), Na_2HPO_4 (Disodium hydrogen phosphate), KH_2PO4 (potassium dihydrogen phosphate), and KCl (potassium chloride) were also purchased from Sigma-Aldrich. NaOH (sodium hydroxide) and $C_3H_2NaO_2$ (sodium acetate) were obtained from Riedel-de Haen. Ethanol and hydrochloric acid were purchased from BDH laboratory supplies and J.T. Baker, respectively. XTT (Cytotoxicity Detection assay kit II) was purchased from Roche, Germany. *B. subtilis* MH-4 (G+) strain, *E. coli* BL-21 (G-) strain, and LB agar were obtained from and Institute of Biochemistry and Biotechnology, University of the Punjab Lahore.

2.2 Modification of Sepiolite With 3-APDEMS

The *ex-situ* modification of clay was done according to the previously reported method (Shafiq et al., 2012). Sepiolite clay was purified by the mechanical stirring of the clay suspension (10 g/700 ml) for 24 h around 760 rpm. The resulting suspension was filtered and desiccated overnight at 105°C. The purified clay was grounded and sieved through 40 μm sieves. 5 g of purified raw sepiolite clay (RSP) was dispersed in 250 ml of isopropanol followed by mechanical stirring in the glass reactor. 500 μL of 3-APDEMS was solvated in 20 ml ethanol and added to RSP/isopropanol mixture. The suspension was stirred mechanically in a glass reactor for 2 h at 60°C. The functionalized clay was filtered followed by washing with ethanol. The *ex-situ* functionalized sepiolite clay (FSP) was dried up in a vacuum oven. The proposed reaction of sepiolite with 3-APDEMS is presented in **scheme 1**.

2.3 Fabrication of Hydrogels

Pectin (0.6 g) was solvated in double-distilled water (60 ml) at 60°C by magnetic stirring. PVP (0.4 g) was solvated in double-distilled water (20 ml) by magnetic stirring using a hot plate at 95°C. PVP solution was blended with the pectin solution with constant stirring for 2 h at 60°C. 200 μL of glycerin was added to the pectin-PVP blend upon stirring in order to prevent brittleness in the hydrogel. For crosslinking, varying amounts of FSP (3-APDEMS-sepiolite clay) ranging from 0.05–0.15 wt% were dispersed in 10 ml water and sonicated for 1 hour at an ambient temperature. Sonicated clay was poured into a pre-blended mixture drop wise and stirred magnetically for 2 h at 60°C. The fabricated hydrogels were cast in plates and desiccated using a desiccating oven (LVO-2040, Lab Tech, Korea) at 60°C under vacuum. Depending upon the concentration of modified functionalized clay (FSP), the hydrogels were referred to as control blend PPC (0 wt%), PP1 (0.05 wt%), PP2 (0.10 wt%), and PP3 (0.15 wt%). The treated hydrogels with sepiolite were: PP1, PP2, PP3 while the untreated was PPC which was controlled

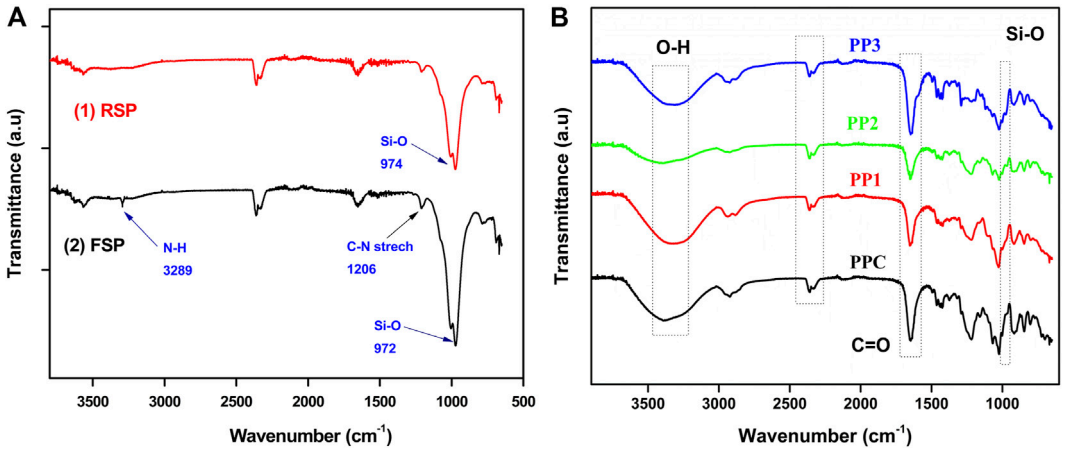

FIGURE 1 | (A) FTIR spectral analysis of modification of sepiolite clay with 3-APDEMS **(B)** FTIR spectral analysis of PPC, PP1, PP2, and PP3 semi-IPNs.

sample. The overall fabrication of hydrogels is shown in **scheme 2**.

2.4 Swelling Studies

To determine the swelling properties of prepared semi-IPNs, pre-weighed dried hydrogel samples were submerged in distilled water, NaCl and $CaCl_2$ salt solutions (0.1, 0.3, 0.5, 0.7, 0.9, and 1 M) and buffer solutions (pH 2, 4, 7, 7.4, and 8). The pH of all NaCl and $CaCl_2$ salt solutions was kept neutral. At a pre-set time interval, the swollen hydrogel was removed; the surplus solution was blotted gently and hydrogel was weighed using a sensitive weighing balance. This procedure was repeated in triplicates for all hydrogel samples in each solution.

The swelling rate was calculated using **Equation (1)**.

$$\text{Swelling } \% = (W_s - W_d/W_d)\times 100 \quad (1)$$

Where W_s = weight of swollen sample at time t and W_d = weight of sample in the dried state.

Buffer solutions of pH 2, 4, 7, 7.4, and eight were prepared to investigate the pH-dependent swelling response of hydrogels. To prepare buffer solutions of pH 2, 25 ml of 0.2 M KCl was mixed with 6.5 ml of 0.2 M HCl. For pH 4 solution, 50 ml of 0.1 M kH phthalate was mixed with 3 ml of 0.1 M NaOH. For pH 7 solution, 50 ml of 0.1 M KH_2PO_4 was mixed with 29.1 ml of 0.1 M NaOH. For pH 7.4 solution, 50 ml of 0.1 M KH_2PO_4 was mixed with 39.1 ml of 0.1 M NaOH. For pH eight solution, 50 ml of 0.1 M KH_2PO_4 was mixed with 46.1 ml of 0.1 M NaOH. All solutions were diluted up to 100 ml using distilled water.

2.5 FTIR Analysis

Spectroscopic structural elucidation of hydrogels, raw sepiolite (RSP), and functionalized sepiolite (FSP) was obtained on Shimadzu I. R–prestige-21, Kyoto, Kyoto prefecture, Japan with ATR mode. All films were vacuum dried before analysis and the scanning range was set as 4,000–650 cm^{-1}. Regular scans and resolution were maintained as 150 and 2.0 cm^{-1}, respectively.

2.6 Morphological Studies

The morphology of pectin/PVP (PPC) and pectin PVP/modified clay-based hydrogels (PP1, PP2, and PP3) was analyzed using model JEOL/EO JSM-6480 SEM Akishima, Tokyo, Japan. The images were recorded at different magnifications.

2.7 In-vitro Degradation

The biodegradation of all hydrogel samples was investigated in PBS (pH 7.4). Pre-weighed samples were placed for 21 days in PBS. All samples were weighed on days one, three, five, seven, fourteen, and twenty-one, respectively. The experiment was performed in triplicates. The percentage of degradation was measured using **Equation (2)**.

$$\text{Degradation}\,(\%) = (W_i - W_f/W_i)\times 100 \quad (2)$$

Where W_i = initial weight and W_f = final weight.

2.8 Antimicrobial Analysis

Agar disc diffusion assay (Mathew, 2018) was performed to investigate the anti-bacterial potential of all hydrogels against *B. subtilis* MH-4 and *E. coli* BL-21. Approximately, 5 mm disc-shaped sample of each hydrogel was cut. Bacterial culture was grown over 24 h in the form of suspension. 100 µL of bacterial suspension was transferred to sterilized LB agar plates. Aseptically, the hydrogel samples were transported to agar plates. Air was considered as negative control. The culture plates were incubated in the static incubator at 37°C for the next 24 h. The inhibition zones (clear zone) acted as an indicator for restricted bacterial growth around samples. The diameter of inhibition zones was recorded and measured.

2.9 Cytotoxicity Studies

The cytocompatibility of all hydrogels was investigated using Cytotoxicity Detection Kit II (XTT); Roche, Germany (XTT; sodium 3-[1- (phenylaminocarbonyl)- 3,4- tetrazolium]-bis (4-methoxy6-nitro) benzene sulfonic acid hydrate) (Jacob et al.,

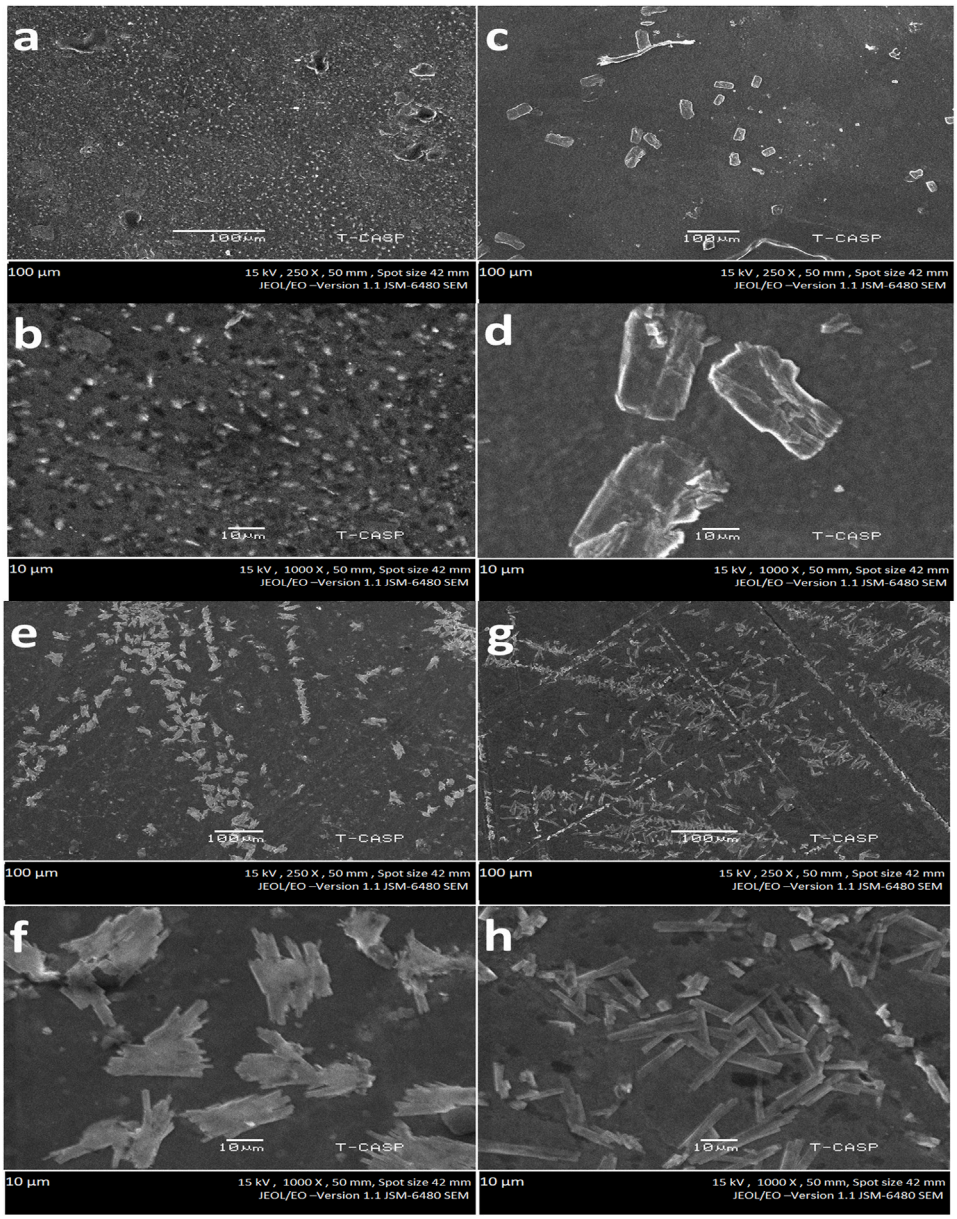

FIGURE 2 | Morphology of hydrogels at different magnifications **(A,B)**. PPC (Functionalized Sepiolite clay = 0 wt%) **(C,D)**. PP1(Functionalized Sepiolite clay = 0.05 wt%) **(E,F)** PP2 (Functionalized Sepiolite clay = 0.1 wt%) **(G,H)** PP3 (Functionalized Sepiolite clay = 0.15 wt%).

2020). The hydrogels were cut into the size of ~0.30 cm^2 and sterilized. After soaking the gel in a culture medium for half an hour, the cells at the density of 8,000 cells per well were seeded on the hydrogels. The cultured cells without hydrogel were used as control. XTT and PMS (electron coupling reagent) were mixed in a 50:1 ratio to form the labeling mixture. The cultured cells were incubated with 50 ul of labeling mixture and 100 ul of DMEM (containing 5% FBS) in 96-well plates for 24, 48, and 72 h under standardized conditions. Absorbance readout was determined at 450 and 630 nm (reference wavelength) using a microplate reader (Spectramax PLUS, United States) (Aguiar et al., 2017). The cell viability over time (24, 48, and 72 h) was measured in terms of percentage. The test was performed in triplicate.

2.10 Ceftriaxone Sodium (CTX-S Antibiotic Drug) Loading and Release Analysis

To investigate the release of drug from hydrogels the PBS, SGF, and SIF buffers were prepared. PBS (phosphate buffer saline pH 7.4) was synthesized by solvating NaCl (8 g), KCl (0.2 g), Na_2HPO_4 (1.44 g), and KH_2PO_4 (0.24 g) in 700 ml of distilled water and the volume was raised to 1 L. The pH was adjusted to

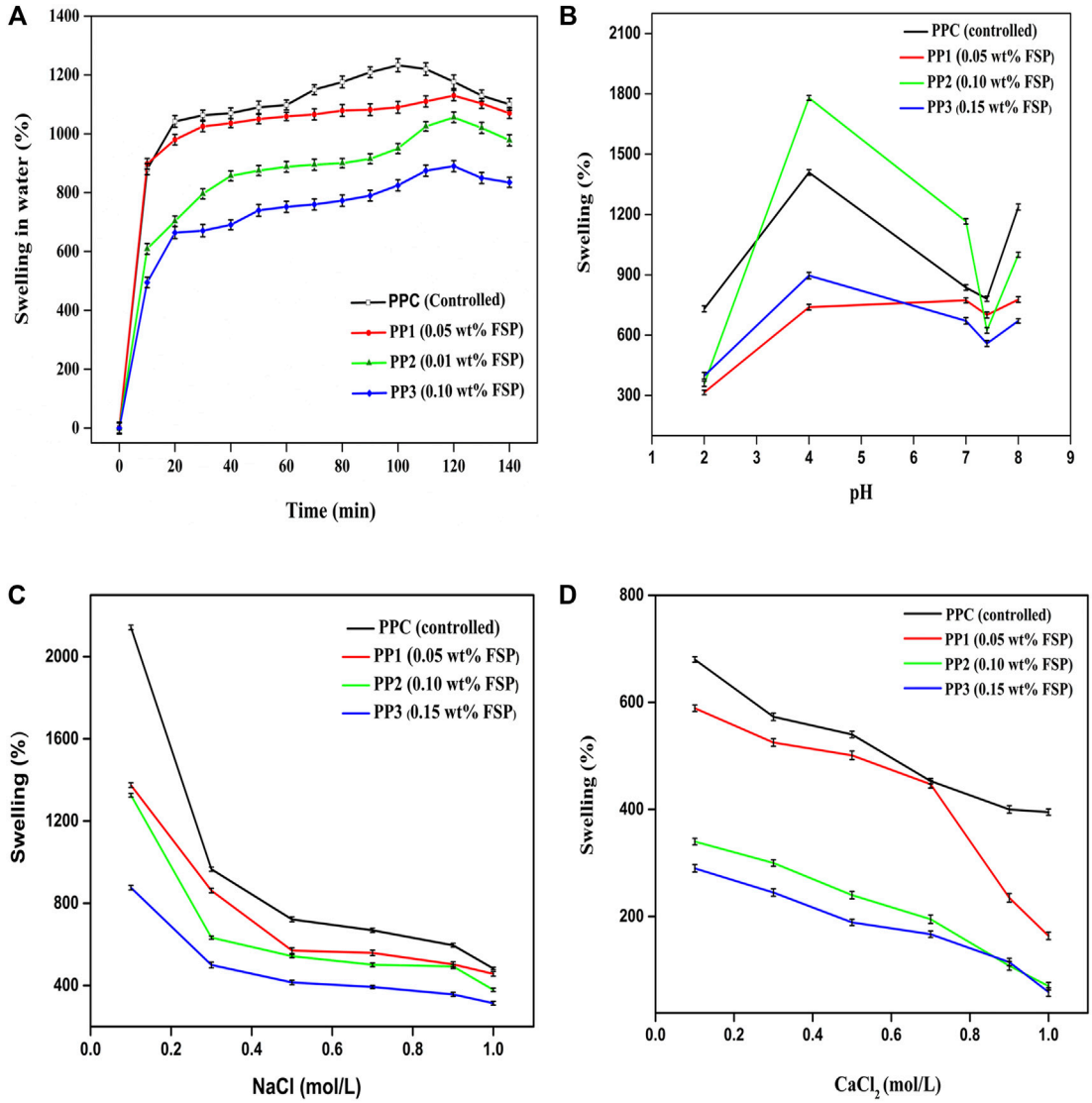

FIGURE 3 | (A) Time-dependent swelling behavior of PP hydrogel in water **(B)** pH-sensitive swelling response of PP hydrogels **(C)** swelling response of PP hydrogels against NaCl **(D)** swelling response of PP hydrogels against $CaCl_2$.

7.4. NaCl (1 g) and HCl (3.5 ml) were solvated in 100 ml of distilled water to prepare SGF (simulated gastric fluid pH 1.2). To adjust the pH to 1.2, the total volume was raised to 500 ml. To prepare SIF (simulated intestinal fluid pH 6.8), 0.1 M NaOH and 0.2 M KH_2PO_4 were mixed by 118 ml: 250 ml ratio. The pH of SIF was adjusted to 6.8.

CTX-S (50 mg) was liquefied in 5 ml H_2O and poured into the pectin-PVP mixture upon continuous stirring. The mixture was stirred for 1 h. The pectin-PVP/CTX-S mixture was crosslinked by the addition of 0.10g/10 ml sonicated suspension of 3-APDEMS-sepiolite (FSP). The antibiotic-containing solutions were cast and dried in an oven at 40°C. To examine the discharge pattern of CTX-S, the dried CTX-S-loaded hydrogels were immersed separately in 100 ml of solutions of PBS (pH 7.4), SGF (pH 1.2), and SIF (pH 6.8) at 37°C. At an equal interval of 10 min, 5 ml of release medium was collected in the glass vial and replaced with 5 ml of stock solution. Similar process was repeated over 4 h. The release of CTX-S was investigated at 241 nm (Ayushi and Mansi, 2018) using a V-730 UV-visible spectrophotometer (JASCO).

2.11 Chemical Activity

To investigate the effect of hydrogel on the chemical integrity of CTX-S before loading into the hydrogel and after release from hydrogel, the chemical activity of CTX-S was performed according to the previously described method (Bashir et al., 2018). The UV spectra of pure CTX-S in water, pure CTX-S in PBS, and CTX-S released in PBS, were obtained using a UV-Vis spectrophotometer (Model T90, Pg Instrumental) at the wavelength range 200–400 nm.

3 RESULTS AND DISCUSSION

Pectin has been used in drug delivery applications due to its antimicrobial potential, biocompatibility, nontoxicity, biodegradability, and swelling properties. Pectin produces physically crosslinked gel by hydrogen bonding, ionic association, or hydrophobic interactions (Ahrabi et al., 2000; Andrews et al., 2009). Sepiolite was functionalized with 3-APDEMS before addition to the pectin-PVP blends. The diverse effects of variant concentrations of 3-APDEMS-sepiolite (FSP) on the properties of fabricated semi-IPNs were investigated.

3.1 FTIR Analysis of Functionalized Sepiolite Clay and Fabricated Hydrogels

Previously reported method has been followed to modify sepiolite clay with 3-APDEMS (Shafiq et al., 2012). 3-APDEMS was used as the characteristic bifunctional crosslinker; its silanol groups reacted with -OH of sepiolite during modification and -NH_2 (amino) with polymer matrix during hydrogel fabrication via condensation. The proposed reaction of sepiolite with 3-APDEMS is presented in **scheme 1**. The addition of ethanol to 3-APDEMS activated the molecule by generating silanol sites (Si-OH) which reacted with sepiolite via condensation process to produce 3-APEMS functionalized sepiolite clay (FSP).

To investigate the modification of sepiolite the FTIR spectra of raw sepiolite (RSP) and functionalized sepiolite (FSP) were obtained. **Figure 1A** 1) represents the spectra of RSP and **Figure 1A** 2) shows spectra of FSP. In FSP, a characteristic peak appeared at 3,289 cm^{-1} which could be ascribed to the -NH stretch of 3-APDEMS confirming the modification of RSP (Xu et al., 1997). Another characteristic peak in FSP spectra at 1,210–1,150 cm^{-1} appeared which could be ascribed to the C-N stretch (Nandiyanto et al., 2019). The Si-O bond stretch can be seen at 974 cm^{-1} in RSP which was shifted to lower wavenumber 972 cm^{-1} in FSP (Shafiq et al., 2012). The increased intensity of the Si-O peak in FSP can also be observed. This increased intensity of the Si-O peak could be ascribed to the formation of new Si-O bonds during modification.

The varied concentration of FSP was added to polymer blends to fabricate hydrogels. **Scheme 3** presented the proposed crosslinking of FSP with pectin/PVP polymer matrix. FSP developed hydrogen bonding with pectin and PVP majorly through–OH and–NH_2 groups. The COOH of pectin could form covalent linkage with–NH_2 of FSP through condensation reaction.

To investigate the incorporation of polymers into the hydrogel polymer matrix, FTIR spectra of all hydrogels were recorded. Spectral analysis of all functional groups of hydrogels is presented in **Figure 1B**. The spectral analysis showed a band at 3,366–3,300 cm^{-1} indicated vibrations of polymer boneded -OH groups (Mishra et al., 2008; Naeem et al., 2017). Peaks at 1,420–1,460 cm^{-1} indicated the C-H bending vibrations. The peeks at 1,023–1,042 cm^{-1} showed the starching vibration of C-N of PVP within the hydrogel networks (Mishra et al., 2008; Kumar et al., 2010).

The distinctive doublet that appeared around 2,360–2,330 cm^{-1} might be due to adsorbed CO_2. However, Basha (2010) and Bryaskova et al. (2011) separately reported this distinctive doublet as characteristic peaks of pure PVP IR spectrum (Basha, 2010; Bryaskova et al., 2011) which indicated the incorporation of PVP in all hydrogels. The peaks around 2,970 cm^{-1} could be ascribed to the -CH_2 vibrations of PVP chain (Song et al., 2014) while the peaks at 1,625–1,660 cm^{-1} indicated the presence of C=O stretching vibrations in all hydrogels (Fares et al., 2010; Sohail et al., 2014). The Si-O stretching vibrations can be observed in PP1, PP2, and PP3 around 970 cm^{-1} (Shafiq et al., 2012) which shows the incorporation of modified sepiolite clay.

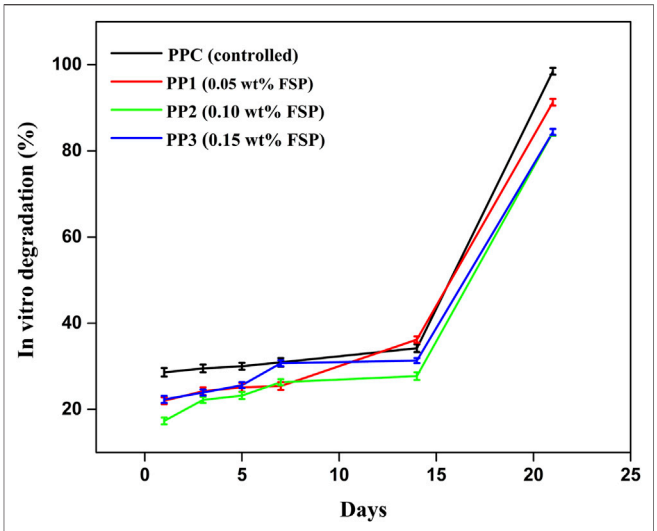

FIGURE 4 | *In-vitro* degradation analysis of PP hydrogels in PBS (pH 7).

3.2 Morphological Analysis of Hydrogels via SEM

The morphological properties of fabricated hydrogels are highly dependent on the polymers and incorporated clay (Liu et al., 2020). Raw sepiolite clay (SP) exhibits rod/fiber-like morphology as evident from reported data (Abrougui et al., 2019). Evident from the work of Palem et al. (2021), a small concentration of raw sepiolite (fibrous clay) affects the morphology of composites by enhancing the interfacial interactions between the polymers and–OH of sepiolite layers (Palem et al., 2021; Liu et al., 2020). In this study, the sepiolite was first functionalized with bifunctional 3-APDEMS moiety then incorporated into the polymer matrix. The modified sepiolite clay (FSP) has both–NH_2 (from 3-APDEMS) and–OH groups (from 3-APDEMS and sepiolite) which can enhance the crosslinking density by a greater degree as compared to raw sepiolite, hence causing the drastic change in shape and size of the hydrogel. To investigate the possible effect of the reinforcement of FSP on the morphology of hydrogels with respect to the varied concentrations of FSP, SEM analysis was conducted. **Figures 2A–H** shows SEM micrographs of pectin/PVP control hydrogel (PPC with 0 wt%) and pectin/PVP/modified clay-based hydrogels (PP1, PP2, and PP3). Pure

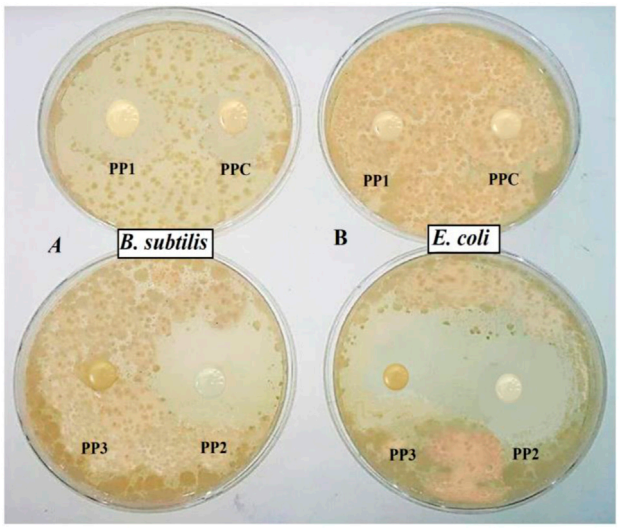

FIGURE 5 | Antimicrobial activity of fabricated hydrogels after 24 h against **(A)** *Bacillus subtilis* MH-4 (G+) **(B)** *Escherichia coli* BL-21 (G-).

pectin shows the elongated granular structure and pure PVP shows spherical granular shapes as it seems in literature (Kumar et al., 2010; Mishra et al., 2008). In our study the PPC (0 wt% FSP) is composed of pectin and PVP only thus spherical granular structures of PPC can be observed from the micrographs of PPC. While the SEM images of PP1 (0.05wt % FSP) and PP2 (0.1wt% FSP) showed capsule-type structures (10–50 μm) separated from one another. SEM micrographs of PP3 (0.15wt% FSP) showed a large population of refined, compact rod-like structures (10 μm). Moving from PPC to PP1 (**Figures 3A–D**), a clear change in the shape of particles from granular to capsule can be observed after the addition of 0.05 wt% FSP. The change in morphology from PP1 (0.05 wt% FSP) capsule structure to PP2 (0.10 wt% FSP) rod-like structure with a reduction in size of particle can be seen (**Figures 3C–F**). This change in morphology can be attributed to the increased concentration of FSP and the interfacial interactions between FSP and polymer networks. From PP2 (0.05 wt% FSP) to PP3 (0.15 wt% SP) (**Figures 3E–H**), the amount of clay, as well as the number of interfacial bonds, increased in PP3 caused the rod-like compact structure and increased shrinkage in particle size. This change in morphology of hydrogels with an increase in the concentration of FSP could be attributed to fibrous structure of FSP and enhanced covalent linkages and hydrogen bonding due to NH_2 and–OH of FSP throughout the hydrogel (Liu et al., 2020; Palem et al., 2021).

TABLE 1 | Antimicrobial potential of hydrogels in terms of inhibition zones.

Bacterial cultures	Diameter (d) of hollow zones formed (mm)			
—	PPC	PP1	PP2	PP3
E.coli BL-21	2	3	18	23
B.subtilis MH-4	5	9	16	0

3.3 Swelling Kinetics

To obtain a comprehensive understanding of swelling characteristics of newly developed hydrogels we tested swelling kinetics of all hydrogels in different media.

3.3.1 Swelling Response of Hydrogels in Water

The swelling response of PP hydrogel in water to time is demonstrated in **Figure 3A**. All the hydrogels presented different responses against water. The hydrogels exhibited an increase in swelling over time. The amount of crosslinker affected the swelling behavior of all films differently. In the controlled sample, maximum swelling (1,233%) was observed after 100 min while FSP incorporated samples showed maximum swelling as; PP1 (1,130%), PP2 (1,056%), PP3 (890%) after 120 min. All films started to dwell after reaching the respective equilibrium time.

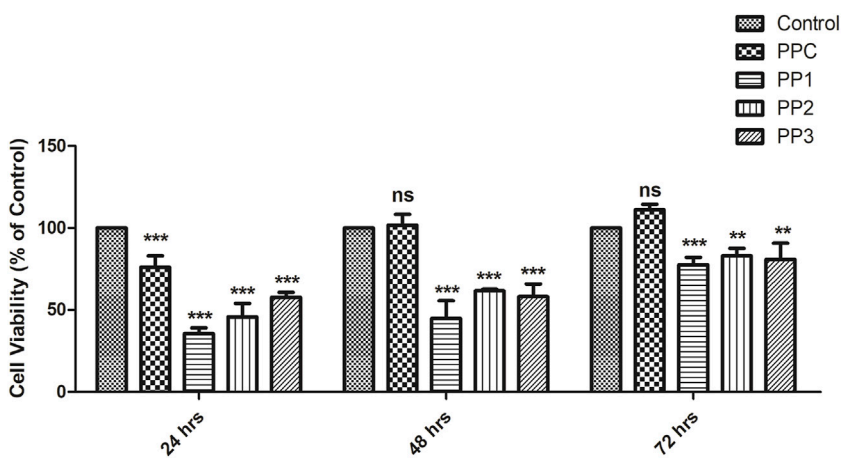

FIGURE 6 | Viability of 3T3 fibroblasts cells seeded in different groups of hydrogels determined by XTT assay. The control group (doted bar) represents 3T3 fibroblasts cells seeded without any hydrogel. Cells exhibit high viability indicating absence of cytotoxic effect of hydrogels. *p denotes statistical significance: *$p < 0.05$; **$p < 0.01$; ***$p < 0.001$.

Maximum swelling was exhibited by PPC and minimum swelling was shown by PP3. The decrease in swelling from PPC to PP3 could be attributed to the decreasing number of free pendent carboxyl and hydroxyl groups upon increasing the amount of crosslinker. The crosslinker might have caused the shrinkage of pores by increasing the crosslinking density and high chain interconnectivity leaving a fewer number of pores for diffusion of solvent into hydrogel matrix (Butt et al., 2019). With an increase in the amount of FSP, a clear decrease in the swelling trend was noticed.

3.3.2 Effect of pH on Swelling of Hydrogels

Different stimuli can cause unusual alterations in hydrogel swelling behavior, structure, and mechanical properties. The swelling extent of fabricated films is critically affected by the nature of base polymers, pH, and the type of buffer medium. For pH-dependent controlled release of the drug, the response of hydrogel swelling due to change in pH of medium particularly needs to be studied. The behavior of all hydrogels was checked in different pH solutions (pH 2, 4, 7, 7.4, and 8). **Figure 3B** depicts the pH-dependent swelling trend of all hydrogels. All hydrogels showed a minimum swelling rate at pH 2. With an increase in pH, an increase in swelling was observed, while at neutral pH the swelling was decreased. The swelling was again increased at basic pH. This was due to the charge imbalance caused by the pH of the buffer solution. At the pH value (pH 2) lower than the pKa value (3.55–4.10) of pectin, the pendent -COOH group of pectin did not lose its proton and remained uncharged resulting in low swelling. Furthermore, the hydrogen bonds were developed between the -OH of pectin and -C=O of PVP which instigated less swelling at said pH (Mishra et al., 2008). At pH (pH 4) equal to pKa of pectin, a few -COOH in the pectin backbone might be ionized by losing protons. This ionization caused intra-chain repulsive forces inducing hydrophilicity and increase in pore size causing the inward movement of solvent into the hydrogel through the process of diffusion resulting in an increase in swelling. (Butt et al., 2019). Maximum swelling of PPC (1,409%), PP1 (739%), PP2 (1780%), and PP3 (896%) was noted at the pH value equal to the pKa value of pectin. The increased extent of swelling in PP2 specifically at pH 4 might be due to the increased diffusion rate caused by the influence of salt concentration, type of salts present in the medium, and ionization of -COOH group at the pH value equal to the pKa value of pectin. Moving to neutral pH, the swelling of PP2 again decreased and minimized at pH 7.4 followed by a rise at basic pH. At basic pH 8) where the pH value of medium was much higher than the pKa value of pectin, the dissociation of hydrogen bonds and ionization of–COOH groups of pectin caused an increase in the swelling rate. The fabricated hydrogel films showed pH-dependent swelling. These films responded to the slight change in pH of the medium which can result in a change in hydrogel characteristics.

3.3.3 Effect of Ionic Concentration on Swelling of Hydrogels

The swelling response of hydrogels could be affected by the concentration of ions (Na^+ and Ca^{2+}) present in the blood. To investigate the possible effect of these ions on the swelling response of hydrogel was studied *in vitro* against different concentrations of sodium chloride and calcium chloride salt solutions under neutral pH conditions. The sodium chloride and calcium chloride are neutral salts. Upon dissolution in water both of these salts dissociated into cations (Na^+ and Ca^{2+}) and anions (Cl^-). **Figures 3C,D** depict the swelling response of all hydrogels in NaCl and $CaCl_2$ respectively. Both the NaCl and $CaCl_2$ electrolytes contain the same anion (Cl^-) but different cations; monovalent sodium ions and divalent calcium ions, respectively. **Figures 3C,D** indicated an observable decrease in the swelling rate of hydrogels with the rise in the electrolyte concentration. An increase in concentration increased the

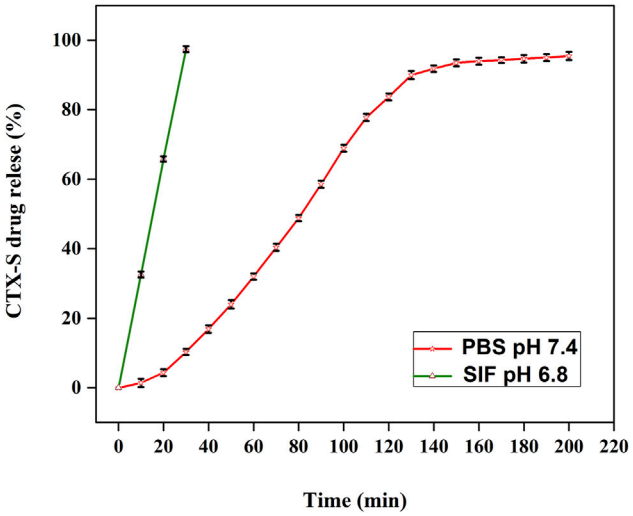

FIGURE 7 | The controlled *in vitro* release of CTX-S in PBS (pH 7.4) and SIF (pH 6.8).

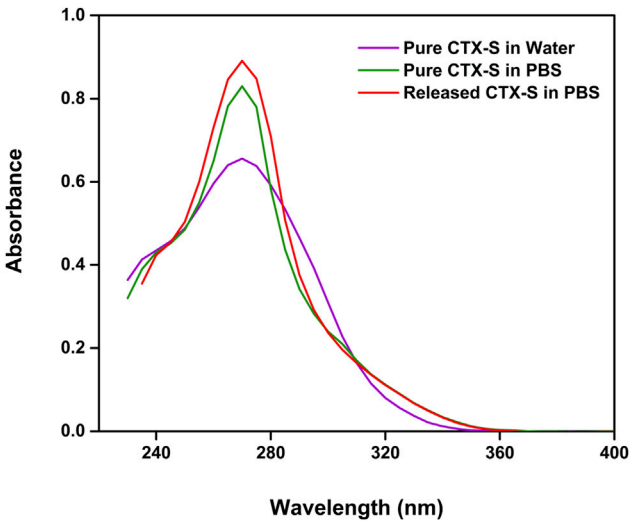

FIGURE 8 | The chemical activity of the pure CTX-S and after release from the hydrogel.

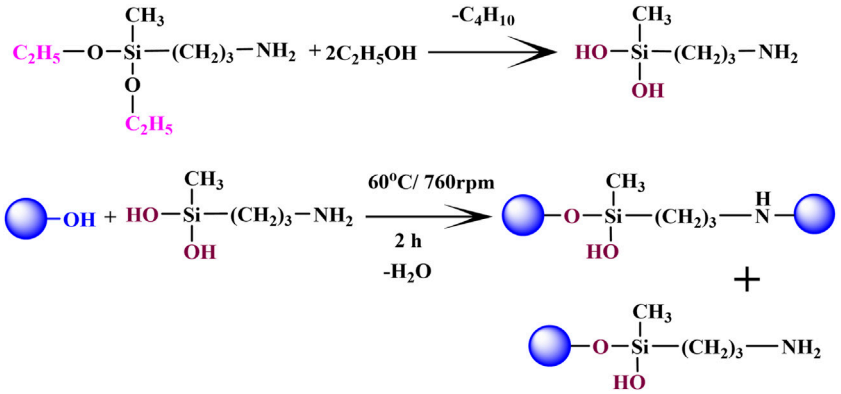

FIGURE 9 | Proposed reaction for modification of sepiolite with 3-APDEMS

osmotic pressure within the polymeric network. This osmotic pressure hindered the movement of solvent into the gel hence decreasing the swelling extent (Rasool et al., 2010; Rasool et al., 2019). The second factor affecting the swelling trend of films observed was the net charge of ions. The ionic charge on cations influenced the swelling of hydrogels in an inverse manner. As the ionic charge Ca^{+2} is higher than the charge on Na^{+1} thus all the hydrogels showed less swelling in calcium chloride solution in comparison with swelling in sodium chloride solutions. The inter-chain complexes caused the hydrogel to attain a more compact structure hindering the diffusion of the solvent into the hydrogel which decreased the swelling rate (Muller et al., 2003). The swelling of all hydrogels decreased with an increase in ionic concentration as well as ionic charge.

3.4 In-vitro Degradation

The fabricated hydrogels are mainly composed of pectin. The monomers of pectin are linked via glycosidic linkages which can be easily broken by various enzymes resulting in small polysaccharide chains. These chains are further broken down to incorporate into biological metabolic pathways. In this analysis, the *in-vitro* biodegradation of all semi-IPNs was examined in a PBS solution of pH 7.4 for 21 days. The outcomes are presented in **Figure 4** which depicted the extent of degradation of PP films (PPC = 98.5%, PP1 = 91.3%, PP2 = 84.3% and PP3 = 84.4%) with respect to time. The biodegradation of all PP hydrogels depended on the nature and concentration of pectin, PVP, and FSP crosslinker. **Figure 4** showed that with an increase in the amount of FSP, the extent of degradation was decreased which can be attributed to the increased inter and intra-molecular forces of attraction among the polymers and FSP (Giri et al., 2013). The PPC hydrogel without FSP exhibited a higher degree of degradation (lower % remaining weights) as compared to hydrogels crosslinked with FSP (PP1, PP2, and PP3). The FSP (functionalized sepiolite clay) hindered the diffusion of solvent through the polymer matrix in PP1, PP2, and PP3. Thus, an increase in crosslinking density upon an increase of FSP concentration impeded the degradation of semi-IPNs.

The *in vitro* degradation results of all hydrogels also depicted the stabilizing effect of modified clay on the pectin-PVP polymer matrix. **Figure 4** presents the PP3 (0.15 wt% FSP) showed the highest stability while PPC (0 wt% FSP) showed minimum stability in PBS over time. The stability of hydrogel increased with an increase in the concentration of modified clay which could be referred to the increased inter-chain crosslinking density of polymer matrix.

3.5 Antimicrobial Analysis

The antimicrobial activity was examined by measuring the inhibition zones generated around the hydrogel (Nešić et al., 2017). The antimicrobial activity of all hydrogels is presented in **Figure 5** while in **Table 1**, the inhibition zone diameters (d in mm) are described. The antimicrobial activity of all hydrogels was investigated against *B. subtilis* MH-4 (G+) and *E. coli* BL-21 (G-) via the disc diffusion method and air was considered as the negative control. The PPC (0 wt% FSP) and PP1 (0.05 wt% FSP) showed less activity (5ays and 9days, respectively) against *B. subtilis* and negligible activity (2ays and 3 days respectively) against *E. coli*. The PP2 (0.10wt% FSP) showed remarkable antimicrobial activity against both strains. In contrast, PP3 (0.15wt% FSP) showed the highest activity (23 days) against *E. coli*. However, PP3 did not show any considerable activity against *B. subtilis* which could be attributed to the thickness of the cell wall of *B. subtilis*. *B. subtilis* exhibited a relatively denser outer membrane in contrast to *E. coli*. This possibly is the fact that *B. subtilis* showed greater resistance to the antimicrobial activity of hydrogels as compared to *E. coli* which exhibited a considerably greater sensitivity towards pectin-PVP/3-APDEMS sepiolite based hydrogels. The hydrogels generated pores in the cytoplasmic membrane of bacteria which caused the leakage of cytoplasmic material leading to cell death (Carson et al., 2002; Guerra-Rosas et al., 2017). The hydrogels possibly caused cell surface disintegration and irregular cellular boundaries. This restricted the growth of microbes around the hydrogel samples (**Figure 5**). The carboxylic group (-COOH) of pectin deprotonated when interacted with the bacterial cells. The -COOH was converted into carboxylate ion (COO^-) and H^+ ions. The H^+ ions caused the change in pH of the bacterial cells. This change in pH disrupted the bacterial cell wall while carboxylate ions inhibited cellular activities by binding with positive species of

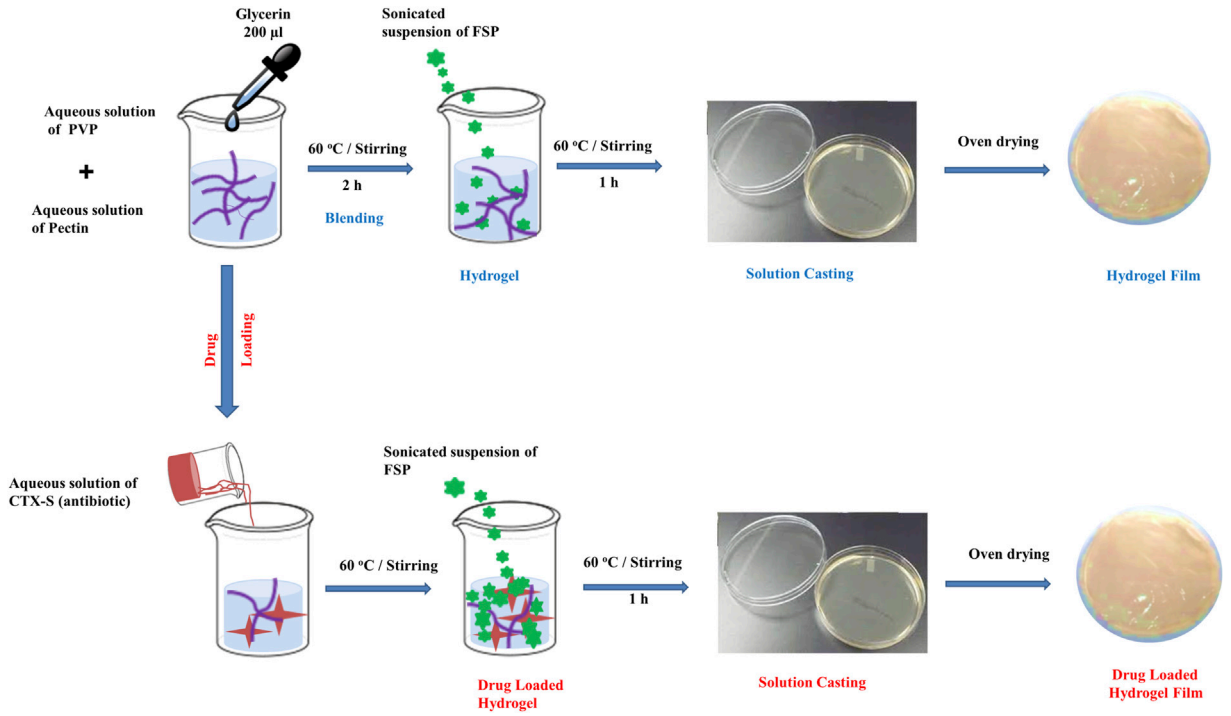

FIGURE 10 | Fabrication of hydrogel films

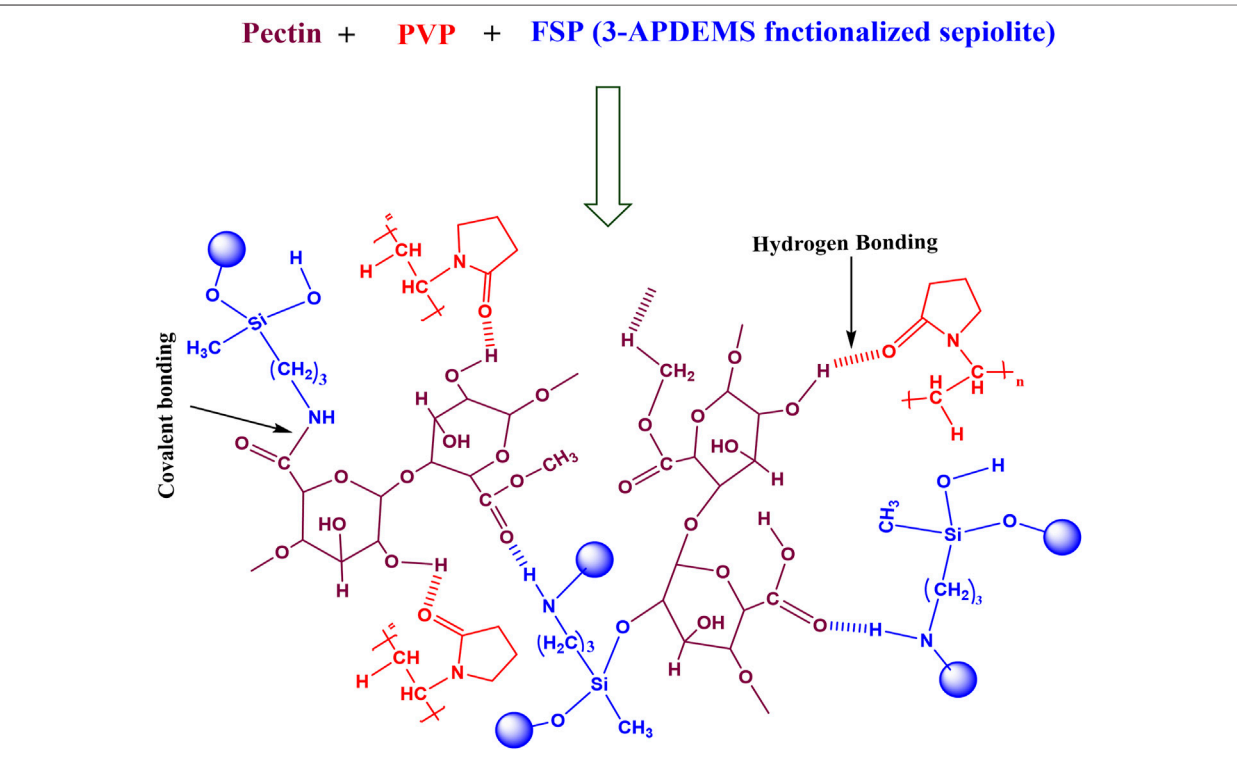

FIGURE 11 | Proposed crosslinked Pectin-PVP-FSP hydrogel matrix

bacterial cell (Kundukad et al., 2017). Overall, the films with large amount of modified clay possessed a higher antimicrobial potential. This property indicates that these hydrogels would enhance the anti-microbial potential of anti-biotics and could be used for wound healing applications.

3.6 Cytotoxicity Studies

To determine the impact of hydrogel on cell survival XTT assay was performed on 3T3 mouse fibroblast cell line. Hydrogel cytotoxicity was assessed by cell viability after 12, 48, and 72 hrs. ANOVA paired with Tukey's test was performed using SPSS software (version 17.0) for the validation of results. The results are presented in **Figure 6** which showed cell viability in PPC (75.87 ± 7.0%), PP1 (35.59 ± 3.44%), PP2 (45.64 ± 8.32%), and PP3 (57.67 ± 2.98%) groups as compared to control group (3T3 mouse fibroblast cells seeded without hydrogels) which is presented as doted bar (100 ± 0.0%) after 24 h. However, the viability of cells in different groups progressively increased with time (after 48 and 72 h). After 72 h, cell viability was significantly increased up to (111.08 ± 3.31%) in PPC (77.61 ± 4.46%) in PP1 (82.93 ± 4.59%) in PP2, and (80.85 ± 9.85%) in PP3. Furthermore, the results indicated that hydrogel supports the proliferation of cells even after 48 and 72 h as depicted by progressive increase in the percentage of viable cells in all groups (PPC, PP1, PP2, and PP3). The cell viability of all hydrogels was above 75% after 72 h (considered as non-cytotoxic) which indicated that PPC, PP1, PP2, and PP3 hydrogels are cytocompatible (Mishra et al., 2008).

Hydrogels have been used to efficiently deliver the seeded cells to the wound bed in a sustained and controlled manner (da Silva et al., 2019; Zhou et al., 2020). Hydrogel scaffolds allow sufficient transference of gases, nutrients, and growth factors to promote adhesion, retention, and survival of cells while reduce the microenvironmental shock and attack by host immune response in order to maximize the therapeutic capacity of cells (Garg et al., 2012; Nezhad-Mokhtari et al., 2019). Hydrogel is considered biodegradable, cytologically compatible, non-antigenic, ECM mimic, anti-microbial, and has the ability to maintain cellular potential (Xu et al., 2018).

The increase in cell proliferation after 72 h indicates that hydrogels understudy can play a crucial role in tissue engineering application as well.

3.7 Release Analysis of CTX-S

The pH-dependent release of drug was studied by immersing the CTX-S loaded hydrogel in PBS (pH 7.4), SIF (pH 6.8), and SGF (pH 1.2) to investigate the use of hydrogel for injectable drug delivery and controlled release application. PP2 was chosen as the host drug carrier over other hydrogels due to good swelling behavior in the buffer, good antimicrobial potential, and optimum biodegradability. The host drug carrier PP2 (0.10wt % FSP) was loaded with CTX-S and its release profile was examined in PBS (pH 7.4), SGF (pH 1.2), and SIF (pH 6.8) with time at 37°C according to the method described by Butt, et al. (2019) (Islam and Yasin, 2012; Butt et al., 2019). **Figure 7** demonstrated the drug release results showing a linear release of CTX-S in PBS. The drug release was remained steady as 91.82% drug was released in 2 h and 20 min. **Figure 7** demonstrates that release of drug was dependent on pH of buffer media, as the release of CTX-S was found consistent in PBS (pH 7.4) as compared to SIF (pH 6.8) and SGF (pH 1.2) which was in agreement with the pH-dependent swelling data (**section 3.3.2**). The results indicated that swelling has a dominating role in the release of drug via diffusion. In accordance with pH swelling results (**section 3.3.2**), the hydrogel showed higher swelling in SIF (pH 6.8) resulted in the creation of larger pore size and osmotic pressure inside of hydrogel matrix hence, facilitating faster diffusion rate of drug from hydrogel to medium (Bukhari et al., 2015; Mahdavinia et al., 2017; Sabzi et al., 2020). In SIF, more than 90% drug was released in first 30 min. The hydrogel showed lower swelling (**section 3.3.2**) at pH 7.4 (PBS) than that of swelling at pH 6.8. The decreased swelling at pH 7.4 resulted in the slower and consistent diffusion rate of drug from hydrogel to medium with respect to time. **Figure 7** indicated the sustained release of drug in PBS at pH 7.4 (blood pH).

Three different drug release mechanisms have been reported in literature i.e. swelling, erosion, and diffusion. The swelling, and diffusion work in conjugation when the polymer matrix was placed in a solution with a huge concentration difference (Benita, 2005). In this study, the drug release followed the process of diffusion in a controlled manner. In SGF, 28.4% drug was released in the first 10 min which was not in conformity with the US pharmacopeia standard as reported that the release of the drug in SGF must not be >10% in the first 30 min. In SIF 97.4%, the drug was released in 30 min. The CTX-S release in PBS and SIF was accordant with US pharmacopeia standard which confirmed the release in PBS and SIF must be >80%.

The results show that by controlling the type of polymer used for hydrogel preparation and its response to the change in pH, the release of drug can be controlled. The present hydrogel is suitable for injectable delivery and controlled release of drug.

3.8 Chemical Activity

To investigate the effect of hydrogel on the chemical integrity of loaded drug, the chemical activity of pure CTX-S (in PBS as well as water) and after release from hydrogel (in PBS) was observed using a double beam UV-vis spectrophotometer (Bashir et al., 2018). **Figure 8** shows recorded UV-vis scan spectra of pure ceftriaxone sodium antibiotic drug (CTX-S) before and after release from the hydrogel. The maximum absorbance for all three samples was observed at wavelength 270 nm which was characteristic (lambda maximum) of CTX-S. A similar pattern of all spectral lines indicated that the respective model drug did not show any chemical bonding with the hydrogel matrix and has retained its chemical configuration after being released from the host carrier. Thus, the fabricated hydrogel proved to be an effective carrier for antibiotics and hydrophilic drugs.

4 CONCLUSION

The macro-porous structure composed of different entities offers a novel multifunctional system with desired properties capable to develop suitable drug delivery carriers. The pectin-PVP-FSP based novel biodegradable semi-IPN drug carriers

with varying amounts of FSP (3-APDEMS functionalized sepiolite clay) was successfully developed by the solution casting method. FTIR study demonstrated the modification of clay with 3-APDEMS and SEM revealed rod-like morphology of hydrogels with size ranging 10–50 μm. With an increase in the amount of crosslinker, the degree of water swelling decreased. PP2 and PP3 showed the least swelling rate in water and electrolytes (NaCl and $CaCl_2$). The formulations PP2 and PP3 with an increased amount of crosslinker showed less degree of biodegradation. Both PP2 and PP3 showed remarkable antimicrobial activity against *E. coli* with hollow zone diameter 23 and 18 mm respectively. While for *B. subtilis* PP2 showed the best antimicrobial activity with a hollow zone diameter of 16 mm. This depicted that PP2 was effective against G+ and G-bacteria. All the hydrogels proved to be cytocompatible. In buffer solutions, all hydrogels less swelling at pH 2 which comparatively increased with increase in pH of medium. The *in vitro* drug release study of CTX-S loaded in phosphate buffer saline (pH 7.4) indicated 91.82% release in 2 h and 20 min in a controlled manner. Both pure CTX-S and released CTX-S drug showed maximum absorbance at 270 nm illustrating no chemical interaction between carrier and loaded drug. These hydrogels provide a better profile for pH-dependent injectable delivery and controlled release of ceftriaxone sodium. The fabricated hydrogels exhibited pH sensitivity for controlled drug release behavior, biodegradability, low-cost fabrication route, and antimicrobial potential. These characteristics make these hydrogels an ideal applicant for the slow release of drugs in a controlled manner, injectable drug delivery, and wound healing and wound dressing applications. With slight modification, these could be considered as promising materials for delivery of polar compounds, scaffolding, tissue engineering, and cancer therapeutics in the future.

DATA AVAILABILITY STATEMENT

The original contributions presented in the study are included in the article/supplementary material, further inquiries can be directed to the corresponding authors.

AUTHOR CONTRIBUTIONS

SR: Investigation; Experimental work, Methodology, Conceptualization; Data curation, Roles/Writing—original draft. NR: Project administration; Resources. SK: Supervision, validation, software. AG: Formal analysis. AI: Supervision; Validation; Investigation; Visualization; Writing—review andamp; editing; Software. RK: Formal analysis. AM: Cytotoxicity analysis. HB: Cytotoxicity analysis. DH: Supervision; Validation; Visualization, review. MR: Validation; Visualization, review, editing.

ACKNOWLEDGMENTS

The author is highly obliged to the School of Chemistry, Institute of Polymer and Textile Engineering, and Institute of Biochemistry and Biotechnology, University of the Punjab, Lahore for providing lab facilities.

REFERENCES

Abrougui, M. M., Lopez-Lopez, M. T., and Duran, J. D. G (2019). Mechanical Properties of Magnetic Gels Containing Rod-like Composite Particles. *Phil. Trans. R. Soc. A.* 377 (2143):20180218. doi:10.1098/rsta.2018.0218

Aguiar, P. H. N., Fernandes, N. M. G. S., Zani, C. L., and Mourão, M. M. (2017). A High-Throughput Colorimetric Assay for Detection of Schistosoma Mansoni Viability Based on the Tetrazolium Salt XTT. *Parasit Vectors* 10 (1), 300–310. doi:10.1186/s13071-017-2240-3

Ahrabi, S. F., Madsen, G., Dyrstad, K., Sande, S. A., and Graffner, C. (2000). Development of Pectin Matrix Tablets for Colonic Delivery of Model Drug Ropivacaine. *Eur. J. Pharm. Sci.* 10 (1), 43–52. doi:10.1016/s0928-0987(99)00087-1

Andrews, G. P., Laverty, T. P., and Jones, D. S. (2009). Mucoadhesive Polymeric Platforms for Controlled Drug Delivery. *Eur. J. Pharmaceutics Biopharmaceutics* 71 (3), 505–518. doi:10.1016/j.ejpb.2008.09.028

Ayushi, V. M., and Mansi, U. P. (2018). Development and Validation of UV Spectrophotometric Method for the Estimation of Ceftriaxone Sodium in Nanoparticles. *Res. Article - Der. Pharma. Chemica.* 10 (3)

Bali, G. K., Singla, S., Kashyap, Y., Dumka, V. K., and Kalia, A. (2018). Preparation, Physico-Chemical Characterization and Pharmacodynamics of Ceftriaxone Loaded BSA Nanoparticles. *J. Nanomed Nanotechnol* 9 (509), 2. doi:10.4172/2157-7439.1000509

Basha, M. A.-F. (2010). Magnetic and Optical Studies on Polyvinylpyrrolidone Thin Films Doped with Rare Earth Metal Salts. *Polym. J.* 42 (9), 728–734. doi:10.1038/pj.2010.60

Bashir, S., Teo, Y. Y., Ramesh, S., and Ramesh, K. (2018). Synthesis and Characterization of Karaya Gum-G- Poly (Acrylic Acid) Hydrogels and *in vitro* Release of Hydrophobic Quercetin. *Polymer* 147, 108–120. doi:10.1016/j.polymer.2018.05.071

Benita, S. (2005). *Microencapsulation: Methods and Industrial Applications*. Florida, USA: CRC Press.

Bryaskova, R., Pencheva, D., Nikolov, S., and Kantardjiev, T. (2011). Synthesis and Comparative Study on the Antimicrobial Activity of Hybrid Materials Based on Silver Nanoparticles (AgNps) Stabilized by Polyvinylpyrrolidone (PVP). *J. Chem. Biol.* 4 (4), 185–191. doi:10.1007/s12154-011-0063-9

Bukhari, S. M. H., Khan, S., Rehanullah, M., and Ranjha, N. M. (20152015). Synthesis and Characterization of Chemically Cross-Linked Acrylic Acid/Gelatin Hydrogels: Effect of pH and Composition on Swelling and Drug Release. *Int. J. Polym. Sci.* 2015, 1–15. doi:10.1155/2015/187961

Butt, A., Jabeen, S., Nisar, N., Islam, A., Gull, N., Iqbal, S. S., et al. (2019). Controlled Release of Cephradine by Biopolymers Based Target Specific Crosslinked Hydrogels. *Int. J. Biol. Macromolecules* 121, 104–112. doi:10.1016/j.ijbiomac.2018.10.018

Carson, C. F., Mee, B. J., and Riley, T. V. (2002). Mechanism of Action of Melaleuca Alternifolia (tea Tree) Oil on *Staphylococcus aureus* Determined by Time-Kill, Lysis, Leakage, and Salt Tolerance Assays and Electron Microscopy. *Antimicrob. Agents Chemother.* 46 (6), 1914–1920. doi:10.1128/aac.46.6.1914-1920.2002

da Silva, L. P., Reis, R. L., Correlo, V. M., and Marques, A. P. (2019). Hydrogel-based Strategies to advance Therapies for Chronic Skin Wounds. *Annu. Rev. Biomed. Eng.* 21, 145–169. doi:10.1146/annurev-bioeng-060418-052422

Darder, M., Matos, C. R. S., Aranda, P., Gouveia, R. F., and Ruiz-Hitzky, E. (2017). Bionanocomposite Foams Based on the Assembly of Starch and Alginate with Sepiolite Fibrous clay. *Carbohydr. Polym.* 157, 1933–1939. doi:10.1016/j.carbpol.2016.11.079

Dutta, J., and Devi, N. (2021). Preparation, Optimization, and Characterization of Chitosan-Sepiolite Nanocomposite Films for Wound Healing. *Int. J. Biol. Macromolecules* 186, 244–254. doi:10.1016/j.ijbiomac.2021.07.020

Eid, M., El-Arnaouty, M. B., Salah, M., Soliman, E.-S., and Hegazy, E.-S. A. (2012). Radiation Synthesis and Characterization of Poly(vinyl alcohol)/poly(N-Vinyl-2-Pyrrolidone) Based Hydrogels Containing Silver Nanoparticles. *J. Polym. Res.* 19 (3), 9835. doi:10.1007/s10965-012-9835-3

Fares, M. M., Assaf, S. M., and Abul-Haija, Y. M. (2010). Pectin Grafted poly(N-Vinylpyrrolidone): Optimization Andin Vitrocontrollable Theophylline Drug Release. *J. Appl. Polym. Sci.* 117 (4), 1945–1954. doi:10.1002/app.32172

Garg, T., Singh, O., Arora, S., and Murthy, R. (2012). Scaffold: a Novel Carrier for Cell and Drug Delivery. *Crit. Rev. Ther. Drug Carrier Syst.* 29 (1), 1–63. doi:10.1615/critrevtherdrugcarriersyst.v29.i1.10

Ghasemiyeh, P., and Mohammadi-Samani, S. (2021). Polymers Blending as Release Modulating Tool in Drug Delivery. *Front. Mater.* 8, 752813. doi:10.3389/fmats.2021.752813

Giri, T. K., Thakur, D., Alexander, A., Ajazuddin, H., Badwaik, H., Tripathy, M., et al. (2013). Biodegradable IPN Hydrogel Beads of Pectin and Grafted Alginate for Controlled Delivery of Diclofenac Sodium. *J. Mater. Sci. Mater. Med.* 24 (5), 1179–1190. doi:10.1007/s10856-013-4884-7

Guerra-Rosas, M. I., Morales-Castro, J., Cubero-Márquez, M. A., Salvia-Trujillo, L., and Martín-Belloso, O. (2017). Antimicrobial Activity of Nanoemulsions Containing Essential Oils and High Methoxyl Pectin during Long-Term Storage. *Food Control* 77, 131–138. doi:10.1016/j.foodcont.2017.02.008

Gülmen, S. S. T., Güvel, E. A., and Kızılcan, N. (2015). Preparation and Characterization of Chitosan/polypyrrole/sepiolite Nanocomposites. *Procedia-Social Behav. Sci.* 195, 1623–1632. doi:10.1016/j.sbspro.2015.06.219

Gulrez, S. K. H., Al-Assaf, S., and Phillips, G. O. (2011). Hydrogels: Methods of Preparation, Characterisation and Applications. *Prog. Mol. Environ. Bioengineering-from Anal. Model. Tech. Appl.* 2, 117–150. doi:10.5772/24553

Hun Kim, M., Choi, G., Elzatahry, A., Vinu, A., Bin Choy, Y., and Choy, J.-H. (2016). Review of clay-drug Hybrid Materials for Biomedical Applications: Administration Routes. *Clays Clay Miner.* 64 (2), 115–130. doi:10.1346/ccmn.2016.0640204

Hussien, N. A., Işıklan, N., and Türk, M. 2018. Pectin-conjugated Magnetic Graphene Oxide Nanohybrid as a Novel Drug Carrier for Paclitaxel Delivery. *Artif. Cell Nanomedicine, Biotechnol.* 46 (Suppl. 1): 264–273. doi:10.1080/21691401.2017.1421211

Iglesias, N., Galbis, E., Valencia, C., Díaz-Blanco, M. J., Lacroix, B., and de-Paz, M.-V. (2020). Biodegradable Double Cross-Linked Chitosan Hydrogels for Drug Delivery: Impact of Chemistry on Rheological and Pharmacological Performance. *Int. J. Biol. Macromolecules* 165, 2205–2218. doi:10.1016/j.ijbiomac.2020.10.006

Islam, A., and Yasin, T. (2012). Controlled Delivery of Drug from pH Sensitive Chitosan/poly (Vinyl Alcohol) Blend. *Carbohydr. Polym.* 88 (3), 1055–1060. doi:10.1016/j.carbpol.2012.01.070

Jacob, B., Kloss, N., Böhle, S., Kirschberg, J., Zippelius, T., Heinecke, M., et al. (2020). Tranexamic Acid Is Toxic on Human Chondrocytes, *in vitro*. *J. Orthopaedics* 20, 1–5. doi:10.1016/j.jor.2019.12.008

Khramov, A. N., Balbyshev, V. N., Voevodin, N. N., and Donley, M. S. (2003). Nanostructured Sol–Gel Derived Conversion Coatings Based on Epoxy-And Amino-Silanes. *Prog. Org. Coat.* 47 (3-4), 207–213. doi:10.1016/s0300-9440(03)00140-1

Ko, W-K., Lee, S. J., Kim, S. J., Han, G. H., Han, I-b., Hong, J. B., et al. (2021). Direct Injection of Hydrogels Embedding Gold Nanoparticles for Local Therapy after Spinal Cord Injury. *Biomacromolecules* 22(7), 2887–2901. doi:10.1021/acs.biomac.1c00281

Kumar, M., Mishra, R. K., and Banthia, A. K. (2010). Development of Pectin Based Hydrogel Membranes for Biomedical Applications. *Int. J. Plast. Technol.* 14 (2), 213. doi:10.1007/s12588-011-0019-5

Kumar, R., Rahman, H., Ranwa, S., Kumar, A., and Kumar, G. (2020). Development of Cost Effective Metal Oxide Semiconductor Based Gas Sensor over Flexible Chitosan/PVP Blended Polymeric Substrate. *Carbohydr. Polym.* 239, 116213. doi:10.1016/j.carbpol.2020.116213

Kundukad, B., Schussman, M., Yang, K., Seviour, T., Yang, L., Rice, S. A., et al. (2017). Mechanistic Action of Weak Acid Drugs on Biofilms. *Sci. Rep.* 7 (1), 4783–4812. doi:10.1038/s41598-017-05178-3

Li, D-q., Li, J., Dong, H-l., Li, X., Zhang, J-q., Ramaswamy, S., et al. (2021). Pectin in Biomedical and Drug Delivery Applications: A Review. *Int. J. Biol. Macromolecules* 185, 49–65. doi:10.1016/j.ijbiomac.2021.06.088

Li, D.-q., Wang, S.-y., Meng, Y.-j., Li, J.-f., and Li, J. (2020). An Injectable, Self-Healing Hydrogel System from Oxidized Pectin/chitosan/γ-Fe2O3. *Int. J. Biol. Macromolecules* 164, 4566–4574. doi:10.1016/j.ijbiomac.2020.09.072

Liu, L., Fishman, M. L., Kost, J., and Hicks, K. B. (2003). Pectin-based Systems for colon-specific Drug Delivery via Oral Route. *Biomaterials* 24 (19), 3333–3343. doi:10.1016/s0142-9612(03)00213-8

Liu, P., Du, M., Clode, P., Li, H., Liu, J., and Leong, Y.-K. (2020). Surface Chemisty, Microstructure, and Rheology of Thixotropic 1-D Sepiolite Gels. *Clays Clay Miner.* 68 (1), 9–22. doi:10.1007/s42860-019-00050-z

Liu, S., Qamar, S. A., Qamar, M., Basharat, K., and Bilal, M. (2021). Engineered Nanocellulose-Based Hydrogels for Smart Drug Delivery Applications. *Int. J. Biol. Macromolecules* 181, 275–290. doi:10.1016/j.ijbiomac.2021.03.147

Mahdavinia, G. R., Mosallanezhad, A., Soleymani, M., and Sabzi, M. (2017). Magnetic- and pH-Responsive κ-carrageenan/chitosan Complexes for Controlled Release of Methotrexate Anticancer Drug. *Int. J. Biol. Macromolecules* 97, 209–217. doi:10.1016/j.ijbiomac.2017.01.012

Marandi, G. B., Esfandiari, K., Biranvand, F., Babapour, M., Sadeh, S., and Mahdavinia, G. R. (2008). pH Sensitivity and Swelling Behavior of Partially Hydrolyzed Formaldehyde-Crosslinked Poly(acrylamide) Superabsorbent Hydrogels. *J. Appl. Polym. Sci.* 109 (2), 1083–1092. doi:10.1002/app.28205

Mathew, S. (2018). Comparative Evaluation of Antimicrobial Efficacy of Neem and Ginger, to Prove its Effectiveness in Decontaminating "Gutta Percha Cones"-An *in vitro* Study. *Int. J. Contemp. Res. Rev.* 9 (01). doi:10.15520/ijcrr/2018/9/01/400

Mirzaei B., E., Ramazani S. A., A., Shafiee, M., and Danaei, M. (2013). Studies on Glutaraldehyde Crosslinked Chitosan Hydrogel Properties for Drug Delivery Systems. *Int. J. Polymeric Mater. Polymeric Biomater.* 62 (11), 605–611. doi:10.1080/00914037.2013.769165

Mishra, R. K., Datt, M., and Banthia, A. K. (2008). Synthesis and Characterization of Pectin/PVP Hydrogel Membranes for Drug Delivery System. *Aaps Pharmscitech* 9 (2), 395–403. doi:10.1208/s12249-008-9048-6

Muller, M. J., Hollyoak, M. A., Moaveni, Z., Brown, T. L. H., Herndon, D. N., and Heggers, J. P. (2003). Retardation of Wound Healing by Silver Sulfadiazine Is Reversed by Aloe Vera and Nystatin. *Burns* 29 (8), 834–836. doi:10.1016/s0305-4179(03)00198-0

Naeem, F., Khan, S., Jalil, A., Ranjha, N. M., Riaz, A., Haider, M. S., et al. (2017). pH Responsive Cross-Linked Polymeric Matrices Based on Natural Polymers: Effect of Process Variables on Swelling Characterization and Drug Delivery Properties. *Bioimpacts* 7 (3), 177–192. doi:10.15171/bi.2017.21

Nandiyanto, A. B. D., Oktiani, R., and Ragadhita, R. (2019). How to Read and Interpret FTIR Spectroscope of Organic Material. *Indonesian J. Sci. Technol.* 4 (1), 97–118. doi:10.17509/ijost.v4i1.15806

Nešić, A., Onjia, A., Davidović, S., Dimitrijević, S., Errico, M. E., Santagata, G., et al. (2017). Design of Pectin-Sodium Alginate Based Films for Potential Healthcare Application: Study of Chemico-Physical Interactions between the Components of Films and Assessment of Their Antimicrobial Activity. *Carbohydr. Polym.* 157, 981–990. doi:10.1016/j.carbpol.2016.10.054

Nezhad-Mokhtari, P., Ghorbani, M., Roshangar, L., and Soleimani Rad, J. (2019). A Review on the Construction of Hydrogel Scaffolds by Various Chemically Techniques for Tissue Engineering. *Eur. Polym. J.* 117, 64–76. doi:10.1016/j.eurpolymj.2019.05.004

Nieto-Suárez, M., Palmisano, G., Ferrer, M. L., Gutiérrez, M. C., Yurdakal, S., Augugliaro, V., et al. (2009). Self-assembled Titania–Silica–Sepiolite Based Nanocomposites for Water Decontamination. *J. Mater. Chem.* 19 (14), 2070–2075. doi:10.1039/B813864H

Palem, R. R., Rao, K. M., Shimoga, G., Saratale, R. G., Shinde, S. K., Ghodake, G. S., et al. (2021). Physicochemical Characterization, Drug Release, and Biocompatibility Evaluation of Carboxymethyl Cellulose-Based Hydrogels Reinforced with Sepiolite Nanoclay. *Int. J. Biol. Macromolecules* 178, 464–476. doi:10.1016/j.ijbiomac.2021.02.195

Peers, S., Montembault, A., and Ladavière, C. (2020). Chitosan Hydrogels for Sustained Drug Delivery. *J. Controlled Release* 326, 150–163. doi:10.1016/j.jconrel.2020.06.012

Pierce, A., Zheng, Y., Wagner, W. L., Scheller, H. V., Mohnen, D., Ackermann, M., et al. (2020). Visualizing Pectin Polymer-Polymer Entanglement Produced by Interfacial Water Movement. *Carbohydr. Polym.* 246, 116618. doi:10.1016/j.carbpol.2020.116618

Rahman, M. R., Chang Hui, J. L., and Hamdan, S. b. (2018). "Introduction and Reinforcing Potential of Silica and Various clay Dispersed Nanocomposites," in *Silica and Clay Dispersed Polymer Nanocomposites* (Amsterdam, Netherlands: Elsevier), 1–24. doi:10.1016/b978-0-08-102129-3.00001-4

Rasool, A., Ata, S., and Islam, A. (2019). Stimuli Responsive Biopolymer (Chitosan) Based Blend Hydrogels for Wound Healing Application. *Carbohydr. Polym.* 203, 423–429. doi:10.1016/j.carbpol.2018.09.083

Rasool, N., Yasin, T., Heng, J. Y. Y., and Akhter, Z. (2010). Synthesis and Characterization of Novel pH-, Ionic Strength and Temperature- Sensitive Hydrogel for Insulin Delivery. *Polymer* 51 (8), 1687–1693. doi:10.1016/j.polymer.2010.02.013

Raza, M. A., Jeong, J.-O., and Park, S. H. (2021). State-of-the-Art Irradiation Technology for Polymeric Hydrogel Fabrication and Application in Drug Release System. *Front. Mater.* 8, 769436. doi:10.3389/fmats10.3389/fmats.2021.769436

Rinoldi, C., Lanzi, M., Fiorelli, R., Nakielski, P., Zembrzycki, K., Kowalewski, T., et al. (2021). Three-Dimensional Printable Conductive Semi-Interpenetrating Polymer Network Hydrogel for Neural Tissue Applications. *Biomacromolecules* 22(7), 3084–3098. doi:10.1021/acs.biomac.1c00524

Roy, N., Saha, N., Kitano, T., and Saha, P. (2010). Novel Hydrogels of PVP–CMC and Their Swelling Effect on Viscoelastic Properties. *J. Appl. Polym. Sci.* 117 (3), 1703–1710. doi:10.1002/app.32056

Ruiz-Hitzky, E., Aranda, P., Darder, M., and Rytwo, G. (2010). Hybrid Materials Based on Clays for Environmental and Biomedical Applications. *J. Mater. Chem.* 20 (42), 9306–9321. doi:10.1039/c0jm00432d

Sabzi, M., Afshari, M. J., Babaahmadi, M., and Shafagh, N. (2020). pH-Dependent Swelling and Antibiotic Release from Citric Acid Crosslinked Poly(vinyl Alcohol) (PVA)/nano Silver Hydrogels. *Colloids Surf. B: Biointerfaces* 188, 110757. doi:10.1016/j.colsurfb.2019.110757

Saeedi Garakani, S., Davachi, S. M., Bagher, Z., Heraji Esfahani, A., Jenabi, N., Atoufi, Z., et al. (2020). Fabrication of Chitosan/polyvinylpyrrolidone Hydrogel Scaffolds Containing PLGA Microparticles Loaded with Dexamethasone for Biomedical Applications. *Int. J. Biol. Macromolecules* 164, 356–370. doi:10.1016/j.ijbiomac.2020.07.138

Sanaeepur, H., Mashhadikhan, S., Mardassi, G., Ebadi Amooghin, A., Van der Bruggen, B., and Moghadassi, A. (2019). Aminosilane Cross-Linked Poly Ether-Block-Amide PEBAX 2533: Characterization and CO2 Separation Properties. *Korean J. Chem. Eng.* 36 (8), 1339–1349. doi:10.1007/s11814-019-0323-x

Shafiq, M., Yasin, T., and Saeed, S. (2012). Synthesis and Characterization of Linear Low-Density Polyethylene/sepiolite Nanocomposites. *J. Appl. Polym. Sci.* 123 (3), 1718–1723. doi:10.1002/app.34633

Sharma, R., and Ahuja, M. (2011). Thiolated Pectin: Synthesis, Characterization and Evaluation as a Mucoadhesive Polymer. *Carbohydr. Polym.* 85 (3), 658–663. doi:10.1016/j.carbpol.2011.03.034

Shirazi, N. M., Eslahi, N., and Gholipour-Kanani, A. (2021). Production and Characterization of Keratin/Tragacanth Gum Nanohydrogels for Drug Delivery in Medical Textiles. *Front. Mater* 8, 371. doi:10.3389/fmats.2021.720385

Singh, B., and Singh, B. (2020). Graft Copolymerization of Polyvinylpyrollidone onto Azadirachta indica Gum Polysaccharide in the Presence of Crosslinker to Develop Hydrogels for Drug Delivery Applications. *Int. J. Biol. Macromolecules* 159, 264–275. doi:10.1016/j.ijbiomac.2020.05.091

Sivagangi Reddy, N., Madhusudana Rao, K., Sudha Vani, T. J., Krishna Rao, K. S. V., and Lee, Y. I. (2016). Pectin/poly(acrylamide-co-acrylamidoglycolic Acid) pH Sensitive Semi-IPN Hydrogels: Selective Removal of Cu2+and Ni2+, Modeling, and Kinetic Studies. *Desalination Water Treat.* 57 (14), 6503–6514. doi:10.1080/19443994.2015.1008053

Sizílio, R. H., Galvão, J. G., Trindade, G. G. G., Pina, L. T. S., Andrade, L. N., Gonsalves, J. K. M. C., et al. (2018). Chitosan/pvp-based Mucoadhesive Membranes as a Promising Delivery System of Betamethasone-17-Valerate for Aphthous Stomatitis. *Carbohydr. Polym.* 190, 339–345.

Sohail, K., Khan, I. U., Shahzad, Y., Hussain, T., and Ranjha, N. M. (2014). pH-Sensitive Polyvinylpyrrolidone-Acrylic Acid Hydrogels: Impact of Material Parameters on Swelling and Drug Release. *Braz. J. Pharm. Sci.* 50 (1), 173–184. doi:10.1590/s1984-82502011000100018

Song, F., Gong, J., Tao, Y., Cheng, Y., Lu, J., and Wang, H. (2021). A Robust Regenerated Cellulose-Based Dual Stimuli-Responsive Hydrogel as an Intelligent Switch for Controlled Drug Delivery. *Int. J. Biol. Macromolecules* 176, 448–458. doi:10.1016/j.ijbiomac.2021.02.104

Song, Y.-J., Wang, M., Zhang, X.-Y., Wu, J.-Y., and Zhang, T. (2014). Investigation on the Role of the Molecular Weight of Polyvinyl Pyrrolidone in the Shape Control of High-Yield Silver Nanospheres and Nanowires. *Nanoscale Res. Lett.* 9 (1), 17. doi:10.1186/1556-276x-9-17

Sriamornsak, P., Thirawong, N., Nunthanid, J., Puttipipatkhachorn, S., Thongborisute, J., and Takeuchi, H. (2008). Atomic Force Microscopy Imaging of Novel Self-Assembling Pectin-Liposome Nanocomplexes. *Carbohydr. Polym.* 71 (2), 324–329. doi:10.1016/j.carbpol.2007.05.027

Tanc, B., and Orakdogen, N. (2019). Insight into (Alkyl)methacrylate-based Copolymer/sepiolite Nanocomposite Cryogels Containing Amino and Sulfonic Acid Groups: Optimization of Network Properties and Elasticity via Cryogelation Process. *Reactive Funct. Polym.* 140, 31–47. doi:10.1016/j.reactfunctpolym.2019.03.022

Veronovski, A., Tkalec, G., Knez, Ž., and Novak, Z. (2014). Characterisation of Biodegradable Pectin Aerogels and Their Potential Use as Drug Carriers. *Carbohydr. Polym.* 113, 272–278. doi:10.1016/j.carbpol.2014.06.054

Xu, Y., Li, Y., Chen, Q., Chen, Q., Fu, L., Tao, L., et al. (2018). Injectable and Self-Healing Chitosan Hydrogel Based on Imine Bonds: Design and Therapeutic Applications. *Int. J. Mol. Sci.* 19 (8), 2198. doi:10.3390/ijms19082198

Xu, Z., Liu, Q., and Finch, J. A. (1997). Silanation and Stability of 3-aminopropyl Triethoxy Silane on Nanosized Superparamagnetic Particles: I. Direct Silanation. *Appl. Surf. Sci.* 120 (3-4), 269–278. doi:10.1016/s0169-4332(97)00234-1

Yang, X., Chen, L., Huang, B., Bai, F., and Yang, X. (2009). Synthesis of pH-Sensitive Hollow Polymer Microspheres and Their Application as Drug Carriers. *Polymer* 50 (15), 3556–3563. doi:10.1016/j.polymer.2009.06.027

Yasin, T., Rasool, N., and Akhter, Z. (2008). Synthesis of Carboxymethyl-Chitosan/acrylic Acid Hydrogel Using Silane Crosslinker. *e-Polymers* 8 (1). doi:10.1515/epoly.2008.8.1.1636

Zhou, S., Wang, Y., Zhang, K., Cao, N., Yang, R., Huang, J., et al. (2020). The Fabrication and Evaluation of a Potential Biomaterial Produced with Stem Cell Sheet Technology for Future Regenerative Medicine. *Stem Cells Int* 2020, 9567362. doi:10.1155/2020/9567362

Zu, G., Kanamori, K., Nakanishi, K., Lu, X., Yu, K., Huang, J., et al. (2019). Superelastic Multifunctional Aminosilane-Crosslinked Graphene Aerogels for High thermal Insulation, Three-Component Separation, and Strain/pressure-Sensing Arrays. *ACS Appl. Mater. Inter.* 11 (46), 43533–43542. doi:10.1021/acsami.9b16746

Conflict of Interest: The authors declare that the research was conducted in the absence of any commercial or financial relationships that could be construed as a potential conflict of interest.

Publisher's Note: All claims expressed in this article are solely those of the authors and do not necessarily represent those of their affiliated organizations, or those of the publisher, the editors and the reviewers. Any product that may be evaluated in this article, or claim that may be made by its manufacturer, is not guaranteed or endorsed by the publisher.

frontiers in Materials

MINI REVIEW
published: 18 March 2022
doi: 10.3389/fmats.2022.845700

Polymeric Organo-Hydrogels: Novel Biomaterials for Medical, Pharmaceutical, and Drug Delivery Platforms

Nahit Aktas[1,2]*, *Duygu Alpaslan*[2] and *Tuba Erşen Dudu*[2]

[1]Department of Chemical Engineering, Faculty of Engineering, Kyrgyz-Turkish Manas University, Bishkek, Kyrgyzstan,
[2]Department of Chemical Engineering, Institute Natural and Applied Sciences, Van Yüzüncü Yıl University, Van, Turkey

In the recent two decades, tremendous devices and materials such as stents, biomimetic organs, scaffolds, and vessels have been developed for medical purposes. When such devices are utilized in the body, the side effects or biocompatibility of the materials have to be studied extensively. Interdisciplinary studies have reviled numerous strategies to overcome adverse body reactions against implanted devices. Besides naturally occurring materials such as collagen, chitosan, hyaluronic acid, and dextran, various synthetic and modified materials such as poly(lactic acid), poly(ethylene glycol), poly(vinyl alcohol), and poly(acrylamide) have been accomplished. In this context, progress in polymer science makes hydrogels a valuable candidate for those utilizations. Moreover, hydrogels received enormous attention as drug delivery devices because of their unique properties, such as soft structure and responsive capabilities based on the functional group attached. Particularly, the developments in synthetic materials have brought out numerous materials for medical and pharmaceutical applications. In recent studies, organo-hydrogels, a branch of hydrogels, have drawn considerable attention over hydrogels because of superior properties such as the coexistence of organic and aqueous phases and viscoelastic bi-phasic natures. They were prepared in bulk forms and nano-scale dimensions, which allow them to be utilized more extensively. These incredible structures provide them with extensive features to be utilized from head to toe in every aspect of health care application. In this short review, we will focus on some of the pioneering perspectives of organo-hydrogels particularly accomplished in clinical therapy and the use of their biodegradable, target-responsive properties as sensing components in novel microscale apertures.

Keywords: biomaterials, organogel, drug delivery, hydrogels, medical application, responsive polymers, smart materials

OPEN ACCESS

Edited by:
Nafisa Gull,
University of the Punjab, Pakistan

Reviewed by:
Dursun Saraydin,
Cumhuriyet University, Turkey
Musa Kamaci,
Piri Reis University, Turkey
Abdullah Turan,
Yüzüncü Yıl University, Turkey

***Correspondence:**
Nahit Aktas
nahit.aktas@manas.edu.kg

Specialty section:
This article was submitted to Polymeric and Composite Materials, a section of the journal Frontiers in Materials

Received: *30 December 2021*
Accepted: *24 February 2022*
Published: *18 March 2022*

Citation:
Aktas N, Alpaslan D and Dudu TE (2022) Polymeric Organo-Hydrogels: Novel Biomaterials for Medical, Pharmaceutical, and Drug Delivery Platforms. Front. Mater. 9:845700. doi: 10.3389/fmats.2022.845700

INTRODUCTION

Developments in health care and pharmaceutical science are dependent on variations of novel drugs and rely significantly on drug carriers, which deliver drugs through the living organisms from the first step up to reach the targeted organs. In this perspective, drug carriers have drawn gradually increasing importance and had an enormous impact on interdisciplinary studies, as summarized in

reviews on relevant areas (Sadtler et al., 2020; Bernhard and Tibbitt, 2021; Mitchell et al., 2021; Sadeghi et al., 2021). The complex structure of the drug delivery through the human body requires closer collaborations between disciplines such as clinical medicine, biology, immunology, chemistry, and chemical and biological engineering (Langer and Peppas, 1983; Peer et al., 2007; Sahiner et al., 2011; Garner et al., 2020; Alpaslan et al., 2021a). It is well known that each drug has an intake level above which it is toxic and below which it is insufficient, whereas available drug concentration in a body at a defined time is an important prescribed routine in the therapy. The drug delivery systems' objective is the sum of the use of strategies and methodologies of synthesis, preparations, and modifications of drug carriers by the collaboration of chemistry, biology, and relevant engineering disciplines, which improve the fraction of drug that reaches its targeted tissues. Webber and Langer described the properties that drug delivery systems must have as follows: therapeutic efficacy, drug exposure/toxicity, dose frequency, therapeutic adherence, and patient-specific therapeutic function (Webber and Langer, 2017). From the clinicians and patients' perspectives, maintaining the drug in the range and the required dosage is important. The utilization of the drug carriers for *in vivo* cases relies on many properties to be adopted by the complex physiology within living organisms, even though they were previously optimized throughout *ex vivo* studies (Langer and Peppas, 1981; Uhrich et al., 1999; Sagbas et al., 2015; Kakkar et al., 2017; Sahiner et al., 2018; Alpaslan et al., 2021b). Drug carriers need to overcome many tests prior to clinical implementation. As the first step, biocompatibility is only a very tiny part of those tests. Research has focused on case-sensitive delivery systems with responsive behavior to physiological environments, which must address biocompatibility, specific targeting, and transport. In the light of the above context, hydrogels and organogels have drawn considerable attention in the preparation of those materials (Peppas, 1982; Langer and Peppas, 1983; Jabbari and Peppas, 1994; Webber and Langer, 2017). Since the first time hydrogels appeared for biomedical applications in 1959 (Wichterle and Lim, 1960), they have drawn tremendous attention. Hundreds of studies are published every year on their utilization for specific purposes in medical applications. As described in common definitions, hydrogels are three-dimensional structures consisting of polymeric units and swollen in water or biological liquids (Uhrich et al., 1999; Koetting et al., 2015). Hydrogels have favorable properties that allow them to be used as biomaterials for drug delivery, implants, and engineered tissue platforms. Having a highly hydrophilic nature let them have water uptake properties that make them similar to cells in the biological environment and provide them with excellent properties to be used as biomaterials (Bell et al., 1995; Peppas et al., 2006; Koetting and Peppas, 2014; Sahiner et al., 2017; Zhang et al., 2020). Since Wichterle and Lim introduced gels prepared from polyvinyl alcohol or glycol monomethacrylate, which are exceptions among the polymers used in biomedical applications (Wichterle and Lím, 1960), numerous studies have been published to introduce novel materials in this context. Nowadays, hydrogels in bulk or particle form are used in numerous medical applications such as ophthalmology, biosensors, membranes, and drug carriers (Langer and Peppas, 1983; Bell et al., 1995; Hassan et al., 2000; Peppas et al., 2006; Suner et al., 2019; Sadtler et al., 2020; Vichare et al., 2020). Most known hydrogels and their utilization purposes in medicine are extensively studied and listed in review literature (Uhrich et al., 1999; Peppas et al., 2000). The polymeric backbone and the composition of the atomic structures are various, which makes those polymeric structures unique for the targeted applications. For instance, poly(vinyl alcohol) (PVA), polyacrylamide (PAAm), poly(N-vinyl pyrrolidone) (PNVP), poly(hydroxyethyl methacrylate) (PHEMA), poly(ethylene glycol) monomethyl ether (PEGME), and cellulose were used as intravascular carriers (Ronneberger et al., 1996; Ronneberger et al., 1997; Tsai et al., 2002; Dalsin et al., 2003; Anderson and Shive, 2012). Poly(hydroxyethyl methacrylate), methacrylic acid, butyl methacrylate, poly(hydroxyethyl methacrylate) and poly(ethylene terephthalate) are applied in contact lenses. Cellulose acetate, polyvinyl alcohol, thermo-polymers of HEMA, MMA, and p(HEMA-b-siloxane) were used for artificial tendons, artificial skin, and ophthalmic applications. Poly(glycolic acid), poly(lactic acid), chitosan, hyaluronate, and dextran are biodegradable hydrogels and used in controlled drug delivery (Draye et al., 1998; Vercruysse and Prestwich, 1998; Uhrich et al., 1999; Peppas et al., 2000; Borchard and Junginger, 2001; Cadée et al., 2001; Khor and Lim, 2003; Peppas et al., 2006; Sahiner et al., 2011; Uchegbu et al., 2011; Suner et al., 2018; Sahiner, 2021).

This short review focuses on recent advances of engineered organogels for medical, pharmaceutical, and drug delivery platforms and their utilization. Therefore, it will not cover important studies relevant to significant drug delivery materials and methods that have been tremendously studied recently.

Biocompatibility of Materials Used for Medication, Standard Tests, and Regulations

A living organism always reacts protectively regardless of the kind of material implanted, which is the natural reaction of all living organisms. As various controlled drug delivery devices are available commercially, it is important to consider the biocompatibility parameters for these systems. Since the acceptance of the Medical Devices Amendments in 1976, the biocompatibility of the materials for medical issues has been increasing (Park and Park, 1996). Biocompatibility is commonly defined as the absence of cytotoxicity of implant material and the material's functionality, which provides it to support cell-implant material interactions where it is applied. In this regard, biocompatibility tests are the tests carried out at conditions similar to the biological environment to evidently predict whether a biomaterial or an implant presents a potential danger for the applied body. In this context, the first step to improving any material as an implant or drug delivery is to test its biocompatibility prior to studying its bio-adhesion behaviors through biological environments, as the body's reaction to implanted devices adversely affects patients'

health. On top of all these, the body's response to an antipathetic material in a particular application may not be antipathetic for that material in another application (Onuki et al., 2008).

In fact, an adverse response, for instance, inflammation, is induced when any foreign material such as an implant or biomaterial treats the living organisms (Fournier et al., 2003; Anderson et al., 2008). Moreover, the magnitude of the response varies according to the properties of the biomaterials and depends on chemical composition to the surface of the biomaterials, shape, morphology, sterility, and degradation of the materials (Peppas, 1982; Fournier et al., 2003; Sagbas et al., 2015). The body response is created after implantation, nonspecific absorption of blood and defensive tissue fluids is induced, and immune and inflammatory cells are produced by the body to protect it from biomaterials (Downes and Mishra, 2011). The 10993 protocol of the International Organization for Standardization (ISO) describes a series of standards for determining materials as biocompatible prior to initiating clinical investigations. European and Asian countries accepted the ISO 10993 standards, whereas FDA required more strict requirements in addition to the ISO requirements published in Blue Book Memorandum G95-1 (Required Biocompatibility Training and Toxicology Profiles for Evaluation of Medical Devices). These issues have been extensively discussed in the relevant literature (Onuki et al., 2008; Kohane and Langer, 2010; Bernard et al., 2018).

In the first step of improving a medical device, some inexpensive *in vitro* tests are applied to the materials to evaluate useful information prior to animal tests. These tests reduce risks and save time and resources early in choosing the best materials for *in vivo* studies. As the surface of a biomaterial is in contact with the cell at a molecular level, properties such as surface roughness, chemical structure, hydrophilicity, smoothness, swelling, tensile strength, hardness, durability, and interaction with proteins become more important (Angelova and Hunkeler, 1999; Wang et al., 2004; Thevenot et al., 2008; Akkas et al., 2013). Wettability is an important property of the materials as hydrophilic surfaces reduce interfacial free energy, making protein adsorption and cell contact easier. In this context, the hydrophilicity of the polymeric biomaterials is increased by various chemical and physical techniques. Several characterization techniques such as atomic force microscopy, X-ray diffraction, infrared spectroscopy, X-ray photoelectron spectroscopy, and scanning electron microscopy are widely accomplished to characterize the materials (Sagbas et al., 2015; Sahiner et al., 2019; Vichare et al., 2020). These tests generally consist of cytotoxicity, irritation, and hemocompatibility (Peppas and Sahlin, 1996; Onuki et al., 2008; Bernard et al., 2018).

Bernard et al. (2018) presented a detailed investigation on the biocompatibility of polymer-based biomaterials and clinical devices. Although the biocompatibility tests are in evaluation, useful studies are available to decide the final product. Regarding that study, biocompatibility assessment must be carried out in three steps as follow:

i) Polymer granules or bland: determining being extractable and leachable (antioxidants, plasticizers, stabilizers, pigment, lubricants, catalysts, and contaminants), toxicological evaluation, and degradation profile.
ii) Polymer films and sheets or generation by spin coating technique: surface functional group, microstructure (wettability, surface roughness, swelling, and electrostatic effect), protein adsorption, cell viability, cytotoxicity, primary evaluation of sterilization impacts, and chemical and lipid resistance.
iii) Specimen representative of the final product: protein adhesion, cell viability, cytotoxicity, hemocompatibility, *in vivo* studies, and being leachable (Bernard et al., 2018).

Organogels: Novel Biomaterials in Medication and Pharmaceutical Utilizations

There is evidence that medicinal plants and herbs were extensively used by primitive tribal shamans, mages, and sorcerers to treat disease or pain since ancient ages (Finlayson, 1893). Organogels are biomaterials produced by the combination of essential oils and polymeric hydrogels *via* chemical and physical methods (Alpaslan et al., 2021a; Alpaslan et al., 2021b; Alpaslan et al., 2021c). Additional to their natural abundance, organogels have superior properties in the eye of biocompatibility, making them valuable materials in controlled drug delivery and medical applications (Tokuyama and Kato, 2010; Alsaab et al., 2016; Esposito et al., 2018).

We investigate recent studies on the application of organogels; this area provides opportunities for future research on controlled drug delivery and medical utilizations (**Table 1**).

In the study on pluronic lecithin organogels (PLO gels), Alsaab et al. (2016) stated that, with the advancement of topical and transdermal drug delivery, organogels are one of the most effective bases for drugs that need to be administered orally or by injection. In the early years of PLO production, there was an increase in research into possible application areas. PLO gels are widely used as transdermal medicine for systemic and local effects. Several research articles have questioned the effectiveness of PLO gel-containing drugs in percutaneous absorption. This may be due to inappropriate synthesis and combination of transdermal PLO gels with drugs (an appropriate drug with ideal molecular weight, log *p*-value, and potency). PLO gels should be preferred primarily as transdermal application, and attention should be paid to the suitability of the drugs (physicochemical properties, dose, and application site) to be used. Alsaab et al. stated that further advanced research (based on blind and placebo-controlled studies and concrete results) should be conducted to evaluate the optimum efficacy of drug-loaded PLO gels for patient care and therapeutic applications of PLO gels (Alsaab et al., 2016). PLO and sorbitan monostearate organogels (SMO) containing ketorolac tromethamine were synthesized. Sustained-release ketorolac tromethamine (KT) niosomal organogels were synthesized to increase skin permeability and drug efficacy. There are unbiased variables in hydrophilic-lipophilic balance value (HLB), which is the ratio of cholesterol in total lipid (Chol. Ratio) and the ratio of total lipid to the drug (L:D ratio)) for sufficient concentrations. The response surface technique was used to investigate the effect of these

TABLE 1 | Summary of papers describing drug delivery application of materials.

Materials	Functional monomer	Cross-linker	Drugs	Amount of drug released	Ref.
Poly(agar-co-glycerol-co-thyme oil)	Thyme oil	MBA/GA	5-Fluorouracil	84.3%	Olak et al. (2020)
Poly(agar-co-glycerol-co-peppermint oil)	Peppermint oil	MBA/GA	Paracetamol; carboplatin	99.7%; 100% (pH 7.4)	Alpaslan et al. (2021c)
Poly(agar-co-glycerol-co-castor oil)	Castor oil	MBA/GA	Oxaliplatin; D_3 vitamin	100% (pH 7.4); 49.43 (pH 2)	Alpaslan et al. (2021b)
Agar-co-glycerol-co-sweet almond oil)	Sweet almond oil	MBA/GA	Oxaliplatin; ceftriaxone	100% (pH 7.4); 29.34% (pH 7.4)	Ersen Dudu et al. (2021)
Poly(agar-co-glycerol-co-onion oil-based)	Onion oil	MBA/GA	Carboplatin; ceftriaxone	99.96% (pH 7.4); 33.17% (pH 8)	Alpaslan et al. (2021a)
Poly(agar-co-glycerol-co-garlic oil)	Garlic oil	MBA/GA	Carboplatin; ceftriaxone	95.4% (pH 7.4); 37.8% (pH 8)	Alpaslan et al. (2021d)
Poly(agar-co-glycerol-co-coconut oil)	Coconut oil	MBA/GA	5-Fluorouracil; D_3 vitamin	29.92% (pH 7.4); 89.09% (pH 2)	Alpaslan et al. (2021e)
Bis(PhAlaOH)/LEE	—	—	Ibuprofen	2.90% (pH 7.4)	Uzan et al. (2016)
HAS (12-hydroxystearic acid)	Castor oil	—	Ketoconazole	90% (p H1.2); 75% (pH 4); 30% (pH 6); 25% (pH 6.8)	Martin et al. (2017)
HAS (12-hydroxystearic acid)	Castor oil	—	Indomethacin	20% (pH 6.8)	Martin et al. (2017)
VRC-OA-PL407	Oleic acid	—	Voriconazole	100%	Querobino et al. (2019)
Organogel-FNZ	Soybean oil stearic acid	—	Flunarizine hydrochloride	100%	Dai et al. (2020)
G/W nano-dispersion	—	—	Paclitaxel	66% (pH 7.4)	Fardous et al. (2022)
PEG4000-HDI	—	PEG4000	Norfloxacin	0.8% (pH 7.4)	Liu et al. (2018)
PEG4000-HDI-CD	—	PEG4000	Norfloxacin	0.7% (pH 7.4)	Liu et al. (2018)

variables on the cumulative release percentages. The capture efficiency of KT niosomes was 40.13%, whereas the cumulative release percentage of KT after 6 and 12 h reached 52.3% and 74.5%, respectively. The niosomal organogel showed an 85% pow edema inhibition effect, positively correlated with the *in vitro* results. The sustained-release niosomal organogel of KT is an effective alternative to oral-dosage forms with fewer systemic side effects and high drug bioavailability (Elsayed et al., 2019).

Studies reviewed by Esposito et al. (2018) indicate that physicochemical properties (thermodynamic behavior, viscoelasticity, and versatility) have important effects on the synthesis and stabilization of organogels. These properties can be easily adjusted with formulations. Organogels obtained by hybridization with the materials in the formulation become ideal matrices, providing effective drug concentration over a long period of time, thereby increasing the chances of patients adapting to therapeutic applications. Although the biocompatibility properties of organogels have been reported in recent studies, they have not been studied to a large extent compared to other gel systems. Further studies should also focus on very prolonged releases with biomolecules such as peptides, proteins, or immunoglobulins from organogel-forming matrices at the application site. Further research on solvent and electrolyte diffusion, matrix degradation, and by-product elimination is required for a more effective use of organogels in effective drug delivery systems (Zeng et al., 2021).

Moreover, organogels are applied in dermal application and cosmetic industry. Fatty acid ethyl and isopropyl esters (FAEs) and bis-(aminoalcohol) oxalamides (BAOAs) with different chain lengths (ethyl laurate, ethyl myristate, ethyl palmitate, isopropyl laurate, isopropyl myristate, isopropyl palmitate) are biocompatible biochemical utilized for those purposes while ibuprofen is widely used as a model drug. In pharmaceutical liquids, BOA gelators and bisphenylglycinol oxalamide do not have organogelation properties in FAEs. Others show good gelling ability with the same solvents. Organogelation depends on the nature of the amino alcohol moiety. Compounds containing the phenylalanine group bis(PhAlaOH)benzyl were good organogelators. Compounds with isobutyl, sec-butyl, and isopropyl groups have low thermal stability due to the sterically hindered branched alkyl groups, while having high stability in all gelling solvents tested and the lowest minimum gel concentrations. It is seen that bis(PhAhaOH)benzyl has high thermal stability and good gelling properties compared to other gelling solvents. The bis(PhAhaOH)benzyl/FAEs gel network also interacts with gelator molecules due to van der Waals interactions, the benzylic groups at the hydrogen bond, and amino alcohol moieties. The release rates of ibuprofen from organogels depend on the pH of their solutions and the amino alcohol groups in the oxalamide binder. In addition, ibuprofen release rates were dependent on gelator concentration and the fraction of drug (%w) in the gel matrix. BOA organogels may also be a viable alternative to human skin cancer if anti-cancer agents are delivered through them. The release of ibuprofen from organogels is compatible with Fickian diffusion control, and the retention of small drug molecules in the LMWG gel can be accomplished in simple ways (Uzan et al., 2016). Castor oil organogel loaded with two lipophilic compounds (ketoconazole or indomethacin) with different ionization behaviors was prepared by hot emulsification in water (above gelation

temperature) and cooling at room temperature. It was stated that drug loading did not affect the particle size and stability of the dispersions and did not inhibit the gelation process. Encapsulation efficiency is also good for ketoconazole and indomethacin. Stability results have been reported, with very limited drug leakage occurring during storage. Dissolution of the drug appears to allow rapid diffusion from the vehicle. Thus, the gel network of 12-hydroxystearic acid fibers will not inhibit drug release. In addition, the increased solubility of the drug in the oil phase may lead to better bioavailability as more drug is available for diffusion. Although the sustained release was not achieved, immobilization of the oil in a gelled matrix was likely responsible for the improved stability of the dispersions and limited escape of drug during storage. These systems can provide alternatives to nanoemulsions or solid lipid nanoparticles for biocompatibility, stability, or delivery of lipophilic compounds. The stickiness of the lipid-based nanoparticle, which was determined to facilitate drug tissue permeability, shows the alternativity of organogel nanoparticles in the field of oral administration (Martin et al., 2017; Alpaslan et al., 2021b). For treating *Candida albicans* infections, organogels have been developed using an oil phase of oleic acid (OA) and an aqueous phase of poloxamer (PL) PL407, alone or in combination with PL188, and 0.25–1% sodium alginate (SA). Moreover, the voriconazole (VRC) release system is targeted intravaginal. For OA-PL407-188 systems, the inclusion of SA was observed to have a concentration-dependent effect on the modulation of the VRC release rate. OA-PL407-188-SA organogels showed promising *in vitro* performance due to their antifungal activities and low cytotoxicity against HeLa and Vero cell lines. In conclusion, the findings of this study indicated that OA-PL407-188-SA organogels could provide the basis for new VRC delivery systems for use in future vaginal applications (Querobino et al., 2019).

In another study using the quality by design (QbD) paradigm, egg oil-based (EO) organogels (SSD-EOOG) were synthesized and used for the distribution of silver sulfadiazine (SSD), an effective antibacterial agent in treating burns. The prepared organogels were evaluated for *in vivo* efficacy and stability. The developed formulations were characterized for particle size, drug content, morphology, *in vitro* drug release, skin safety studies, *ex vivo* permeation, skin retention, tissue analysis, and pharmacodynamic studies in a murine burn wound model. The optimized formulation exhibited improved permeability (72.33 ± 1.73%) and retention (541.20 ± 22.16 μg/cm^2) across the skin barrier with a particle size of 256.5 nm compared to SSD-MKT. Pharmacodynamic results proved the superior therapeutic efficacy of SSD-EOOG in topical burn wounds caused by MRSA bacteria. Results showed a rate of wound shrinkage (78.23 ± 5.65%) and faster re-epithelialization in the SSD-EOOG-treated group. This study concluded that egg oil-based organogel supports the therapeutic efficacy of SSD for burn wound treatment (Thakur et al., 2020).

A new bigel was synthesized by mixing guar gum hydrogel and sorbitan monostearate-sesame oil-based organogel and evaluated as a controlled drug release system (Singh et al., 2014). Macro-scale deformation studies, viscometric analysis, shear-thinning, and viscoelastic structure of bigels were investigated. With the increase in oleogel content, bigels were smooth, stable, and biocompatible, with higher viscosity and hardness. In *in vitro* drug release experiments, it was observed that the amount of ciprofloxacin drug release increased with the decrease in organogel content. In addition, it has been found that drug release from all bigels conforms to the desired zero-order diffusion kinetics for a controlled release system. When drug-loaded bigels were examined in terms of antimicrobial activity, they had a good effect against *Bacillus subtilis*, and it was predicted that they could be considered a drug release system.

Zeng et al. (2021) found that the effective interfacial function of organogels can maintain low adhesion for months, even under harsh outdoor conditions. Superior surface property is critically dependent on the continuous renewal of the liquid layer from the matrix to the surface, creating unique micro-/nano-structures in the matrix, achieving a structural gradient, making them a superior surface for droplet manipulation. With their low modulus, organogels are widely researched for practical application as anti-icing and anti-fouling coatings. The biocompatibility, biodegradability, and functionality of organogelators and solvents enable the hybridization and stabilization of organogels with bioactive substances in microporous matrices, imparting thermodynamic behavior rheological properties for drug release and cosmetic potentials. Edible artificial organogels structured with vegetable oils for fat replacement in food processing have been developed by utilizing the solid-like physicochemical property. Organogels have an obvious disadvantage due to organic solvent. Its main component, the high-priced organic solvent, is costly in organogel production, leaving it out of various practical applications. Furthermore, interface interactions are considered weak if they act as interface material due to their low adhesive strength to substrates, especially organogels with low viscosity solvent. Amphiphilic organogels and the addition of a binder coating may be suitable options for strong binding to different materials. Poor mechanical performance limits organogels for use in various applications (Zeng et al., 2021).

A new *in situ* gel system was prepared using soybean oil, stearic acid, and N-methyl-2-pyrrolidinone (10:1:3, v/w/v). The gel was in a low viscosity sol when applied to the conjunctival sac and then quickly gelled in the eye, and *in vivo* experiments have shown that organogel-flunarizine hydrochloride has bioavailability, low ocular irritation, and biocompatibility, properties suitable for intraocular administration. The release of the organogel-flunarizine hydrochloride can be prolonged by 48 h. Pharmacokinetics in rats showed that the organogel helped maintain the effective organogel concentration in the body and slowed the rate of drug clearance compared to flunarizine hydrochloride solution. Organogel-flunarizine hydrochloride is a promising drug delivery system with therapeutic efficacy for treating brain diseases by intraocular administration (Dai et al., 2020).

An organogel-based nanoemulsion has been developed to effectively deliver hydrophobic drugs with organogel droplets that can gel *in situ*. A combination of G/W nanoemulsion, lipiodol, and organogelator 12-hydroxystearic acid (12-HSA) was used, stabilized with polyoxyethylene hydrogenated castor

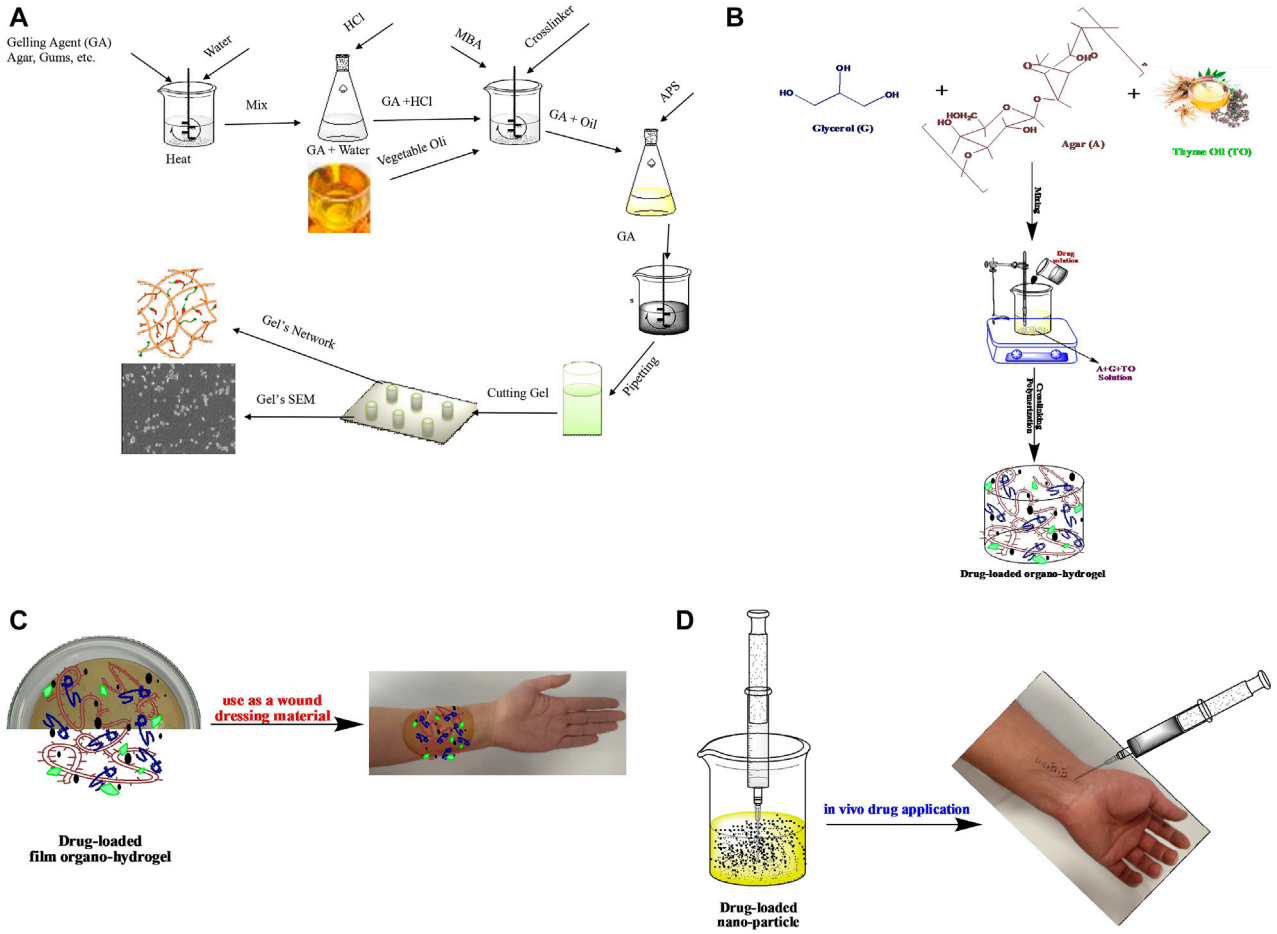

FIGURE 1 | (A) Schematic representation of organogels preparation. **(B)** Schematic representation of drug loading to organogels. **(C)** Application of drug-loaded organogels in a film form. **(D)** Application of drug-loaded organogels in an injectable form (in nano-scale).

oil (HCO-60) as a surfactant. The prepared nanoemulsion has a high drug loading efficiency (~97%) with an average diameter of 206 nm. This drug delivery system was novel in terms of organogel structure with thermo-reversible property and stability over a long period of time. The prepared nanoemulsion can effectively encapsulate and deliver hydrophobic drugs at the application site. The physicochemical properties of the organogel-based nanoemulsion were not affected by the storage temperature, and the *in vitro* study did not affect the mitochondrial and metabolic activities of primary rat hepatocytes. Both *in vitro* and *in vivo* studies determined the cytotoxicity of paclitaxel-containing organogel-based nanoemulsion against skin cancer. Therefore, organogel-based nanoemulsion can be a drug carrier in the body, and organogel-based nanoemulsion can be used to treat melanoma with fewer side effects and site-specificity (Fardous et al., 2021). A transdermal drug delivery system (TDDS) for circulatory organogels was recently developed with new evaluation in propylene glycol. The G′ value of the poly(VbNMDG)-Aq gel is 950 Pa, and the poly(VbNMDG)-PG gel is suitable for use as a transdermal depot. In permeability, the auxiliary aid limonene has a synergistic effect on limonene/PG. The poly(VbNMDG) gel can be evaluated for optimal testability for 24 h depending on the conditions. Overall, the poly(VbNMDG)-PG gel formed possible polymer–polymer interaction with the new organogel, which can improve the permeability of transdermal testosterone and be compatible with the penetration enhancing system (Charoensumran and Ajiro, 2020). The *in situ* organogels based on amino acid (the four amino-based gelator: N-icosanoyl-L-alanine methyl ester (C20-Ala-Me) N-icosanoyl-L-glutamate dimethyl ester (C20-Glu-Me), N-icosanoyl-L-serine methyl ester (C20-Ser-Me), and N-arachidonoyl-L-alanine ethyl ester (C20-Ala-Et)) derivatives were synthesized as biocompatible and biodegradable, the optimal formulation was investigated based on the central composite design experiments, and the risperidone-loaded organogel was prepared. It showed that risperidone-organogel could provide a release for up to 20 days. Compared with the drug oil solution, the drug concentration in the blood was prolonged from 1 day to 7 days, showing that the release of risperidone-organogel conforms to the Ritger–Peppas model and is a combined action of drug diffusion and erosion (Hu et al., 2020).

A new magnetic micro-organogel with a protein shell and oil core was prepared. The magnetic micro-organogel synthesized by utilizing the hydrophilicity and flexibility of the protein shell has a suitable dispersibility in water. In this study, superparamagnetism of OA-Fe_3O_4 in the oil core showed the easily accessible mobility of the magnetic micro-organogel for targeted drug delivery. The high loading efficiency of the magnetic micro-organogel for hydrophobic drugs is demonstrated by the high encapsulation rate of Coumarin 6. The magnetic micro-organogel exhibited thermosensitive and GSH-sensitive behavior. Release mechanisms included erosion, diffusion, and degradation. The magnetic micro-organogel was shown to be a potential material for high-efficiency delivery and stimuli-responsive release of hydrophobic drugs (Dong et al., 2021). The carrier property of organogel-based nanogel disperse (NGD) with 12-hydroxystearic acid and lipiodol for paclitaxel anti-cancer drug was investigated *in vitro* and *in vivo*. Organogel gel (G/W) nano-dispersion in water with 12-hydroxystearic acid and lipiodol was synthesized by the ultrasonication method and stabilized with a non-ionic surfactant. Paclitaxel-loaded NGDs were found to be biocompatible with mouse hepatocytes and fibroblast cells *in vitro*, while paclitaxel-loaded G/W nano-dispersion showed cytotoxicity ($p < 0.05$) against lung cancer (A549) cell lines. Intravenous administration of paclitaxel-loaded NGDs shows an anti-cancer effect against lung cancer *in vivo* with a significant reduction in tumor volume ($p < 0.05$). Paclitaxel-loaded NGDs may be a promising carrier for sustained drug release and chemotherapy agents (Fardous et al., 2022).

Sagiri et al. (2015) used the ionotropic gelation method to synthesize organogel-entrapped core-shell (organogel-alginate) type new microparticles. It has been used in controlled drug release applications. The encapsulation of the organogels was confirmed by microscopic, XRD, FTIR, and DSC studies. Encapsulation of the organogel in microparticles prevented the leakage of the inner phase and increased the efficiency of drug encapsulation. In *in vitro* drug release studies, ciprofloxacin was used as a model drug and was continuously released from the organogel containing microparticles. In addition, the biocompatibility of the microparticles was tested by hemocompatibility and cytocompatibility studies and found to have antimicrobial activity against *Escherichia coli*. Drug release data showed that the release occurred by super case-II diffusion. The developed core-shell type hybrid microparticles are thought to be promising for controlled drug release systems (Sagiri et al., 2015).

In a study by Kodela et al. (2017), bigels containing different ratios of agar gel and stearyl alcohol were prepared as oleogel type in the hydrogel. Thus, the inherent stability of bigel-based formulations, biphasic formulations, and gel-based formulations is combined. In addition, the increase in oleogel ratio caused the formation of microscopic structures similar to biphasic formulations, greatly reducing the hydrogen bonding in the formulations and the electrical stability of the formulations. The mechanical properties of bigels increased with the addition of oleogel into the agar hydrogel until the critical concentration was reached and started to decrease after reaching this critical point. The inherent electrical stability of bigels was found to be lower compared to hydrogels. Ciprofloxacin hydrochloride drug release from bigels was analyzed by the Korsmeyer–Pappas and Peppas–Sahlin models, and Fickian diffusion was found dominant in general. The results suggest that the mechanical, electrical, and drug-release properties of drugs can be improved by changes in their composition and can be used in food and pharmaceutical applications (Kodela et al., 2017).

In this study, bigels were synthesized using an oleogel based on stearic acid/rice bran oil and tamarind gum hydrogel. The oleogel portion was prepared by mixing stearic acid and rice bran oil, whereas the hydrogel portion was prepared from the mixture of tamarind gum and hydroethanol solution. Analysis showed that bigels exhibited the presence of stearic acid melting endotherm (oleogel associated) and water evaporation endotherm (hydrogel associated), and the hydrogel had the lowest bulk resistivity compared to other formulations. It has been observed that the bulk electrical resistance of bigels is controlled by the oleogel phase and there is an increase in the diffusion of moxifloxacin HCl from the formulations with the increase of the hydrogel ratio. It has been predicted that the bigels with the developed formulations can be used as a potential drug release material (Paul et al., 2018). A schematic representation of organogel preparation, drug loading step, and implementation in film and injectable forms are given in **Figure 1**.

CONCLUSION

In this mini-review, we have focused on some recent developments of drug delivery platforms, particularly organogels based applications. We tried to give a point of view of state of the art. It is expected that organogels will be utilized at a gradually increasing level in the coming years because of their unique characteristics such as biocompatibility, being easily tunable, tailoring by chemical modifications. These properties enable organogels to be applied with enormous potential applications in drug delivery, anti-icing, anti-fouling, food processing, and more.

AUTHOR CONTRIBUTIONS

All authors listed have made a substantial, direct, and intellectual contribution to the work and approved it for publication.

REFERENCES

Akkas, T., Citak, C., Sirkecioglu, A., and Güner, F. S. (2013). Which Is More Effective for Protein Adsorption: Surface Roughness, Surface Wettability or Swelling? Case Study of Polyurethane Films Prepared from castor Oil and Poly(ethylene Glycol). *Polym. Int.* 62 (8), 1202–1209. doi:10.1002/pi.4408

Alpaslan, D., Erşen Dudu, T. E., and Aktaş, N. (2021c). Synthesis and Characterization of Novel Organo-Hydrogel Based agar, Glycerol and Peppermint Oil as a Natural Drug Carrier/release Material. *Mater. Sci. Eng. C* 118, 111534. doi:10.1016/j.msec.2020.111534

Alpaslan, D., Erşen Dudu, T., and Aktas, N. (2021a). Development of Onion Oil-Based Organo-Hydrogel for Drug Delivery Material. *J. Dispersion Sci. Technol.*, 1–13. doi:10.1080/01932691.2021.1974869

Alpaslan, D., Ersen Dudu, T., and Aktas, N. (2021b). Evaluation of poly(agar-co-glycerol-co-castor Oil) Organo-Hydrogel as a Controlled Release System Carrier Support Material. *Polym. Bull.*, 9. doi:10.1007/s00289-021-03777-9

Alpaslan, D., Olak, T., Turan, A., Ersen Dudu, T., and Aktas, N. (2021d). A Garlic Oil-Based Organo-Hydrogel for Use in pH-Sensitive Drug Release. *Chem. Pap.* 75, 5759–5772. doi:10.1007/s11696-021-01760-2

Alpaslan, D., Olak, T., Turan, A., Ersen Dudu, T., and Aktas, N. (2021e). Use of Coconut Oil-Based Organo-Hydrogels in Pharmaceutical Applications. *J. Polym. Environ.* 30, 666–680. doi:10.1007/s10924-021-02219-x

Alsaab, H., Bonam, S. P., Bahl, D., Chowdhury, P., Alexander, K., and Boddu, S. H. (2016). Organogels in Drug Delivery: A Special Emphasis on Pluronic Lecithin Organogels. *J. Pharm. Pharm. Sci.* 19 (2), 252–273. doi:10.18433/J3V89W

Anderson, J. M., Rodriguez, A., and Chang, D. T. (2008). Foreign Body Reaction to Biomaterials. *Semin. Immunol.* 20 (2), 86–100. doi:10.1016/j.smim.2007.11.004

Anderson, J. M., and Shive, M. S. (2012). Biodegradation and Biocompatibility of PLA and PLGA Microspheres. *Adv. Drug Deliv. Rev.* 64, 72–82. doi:10.1016/j.addr.2012.09.004

Angelova, N., and Hunkeler, D. (1999). Rationalizing the Design of Polymeric Biomaterials. *Trends Biotechnol.* 17 (10), 409–421. doi:10.1016/s0167-7799(99)01356-6

Bell, C. L., and Peppas, N. A. (1995). "Biomedical Membranes from Hydrogels and Interpolymer Complexes," in *Biopolymers Ii*. Editors N. A. Peppas&R and S. Langer (Berlin/Heidelberg: Springer-Verlag), Advences in Polymer Science, Vol. 122. doi:10.1007/3540587888_15

Bernard, M., Jubeli, E., Pungente, M. D., and Yagoubi, N. (2018). Biocompatibility of Polymer-Based Biomaterials and Medical Devices - Regulations,in Vitroscreening and Risk-Management. *Biomater. Sci.* 6 (8), 2025–2053. doi:10.1039/c8bm00518d

Bernhard, S., and Tibbitt, M. W. (2021). Supramolecular Engineering of Hydrogels for Drug Delivery. *Adv. Drug Deliv. Rev.* 171, 240–256. doi:10.1016/j.addr.2021.02.002

Borchard, G., and Junginger, H. E. (2001). Modern Drug Delivery Applications of Chitosan. *Adv. Drug Deliv. Rev.* 52 (2), 103. doi:10.1016/s0169-409x(01)00188-0

Cadée, J. A., Brouwer, L. A., den Otter, W., Hennink, W. E., and van Luyn, M. J. (2001). A Comparative Biocompatibility Study of Microspheres Based on Crosslinked Dextran or Poly(lactic-Co-Glycolic)acid after Subcutaneous Injection in Rats. *J. Biomed. Mater. Res.* 56 (4), 600–609. doi:10.1002/1097-4636(20010915)56:4<600::aid-jbm1133>3.0.co;2-i

Charoensumran, P., and Ajiro, H. (2020). Controlled Release of Testosterone by Polymer-Polymer Interaction Enriched Organogel as a Novel Transdermal Drug Delivery System: Effect of Limonene/PG and Carbon-Chain Length on Drug Permeability. *Reactive Funct. Polym.* 148, 104461. doi:10.1016/j.reactfunctpolym.2019.104461

Dai, M., Bai, L., Zhang, H., Ma, Q., Luo, R., Lei, F., et al. (2020). A Novel Flunarizine Hydrochloride-Loaded Organogel for Intraocular Drug Delivery *In Situ*: Design, Physicochemical Characteristics and Inspection. *Int. J. Pharmaceutics* 576, 119027. doi:10.1016/j.ijpharm.2020.119027

Dalsin, J. L., Hu, B.-H., Lee, B. P., and Messersmith, P. B. (2003). Mussel Adhesive Protein Mimetic Polymers for the Preparation of Nonfouling Surfaces. *J. Am. Chem. Soc.* 125 (14), 4253–4258. doi:10.1021/ja0284963

Dong, J., Du, X., Zhang, Y., Zhuang, T., Cui, X., and Li, Z. (2021). Thermo/glutathione-sensitive Release Kinetics of Heterogeneous Magnetic Micro-organogel Prepared by Sono-Catalysis. *Colloids Surf. B: Biointerfaces* 208, 112109. doi:10.1016/j.colsurfb.2021.112109

Downes, S., and Mishra, A. A. (2011). Tissue-biomaterial Interactions. *Adv. Wound Repair Therapies*, 174–185. doi:10.1533/9780857093301.2.174

Draye, J.-P., Delaey, B., Van de Voorde, A., Van Den Bulcke, A., De Reu, B., and Schacht, E. (1998). *In Vitro* and *In Vivo* Biocompatibility of Dextran Dialdehyde Cross-Linked Gelatin Hydrogel Films. *Biomaterials* 19 (18), 1677–1687. doi:10.1016/s0142-9612(98)00049-0

Elsayed, M. M. A., El Rasoul, S. A., Ramadan, A. E. h., and Hussein, A. K. (2019). Response Surface Methodology as a Useful Tool for Development and Optimization of Sustained Release Ketorolac Tromethamine Niosomal Organogels. *J. Pharm. Innov.* 15 (4), 664–677. doi:10.1007/s12247-019-09421-4

Ersen Dudu, T., Alpaslan, D., and Aktas, N. (2021). Application of Poly (Agar-Co-Glycerol-Co-Sweet Almond Oil) Based Organo-Hydrogels as a Drug Delivery Material. *J. Polym. Environ.* 30, 483–493. doi:10.1007/s10924-021-02212-4

Esposito, C. L., Kirilov, P., and Roullin, V. G. (2018). Organogels, Promising Drug Delivery Systems: an Update of State-Of-The-Art and Recent Applications. *J. Controlled Release* 271, 1–20. doi:10.1016/j.jconrel.2017.12.019

Fardous, J., Omoso, Y., Joshi, A., Yoshida, K., Patwary, M. K. A., Ono, F., et al. (2021). Development and Characterization of Gel-In-Water Nanoemulsion as a Novel Drug Delivery System. *Mater. Sci. Eng. C* 124, 112076. doi:10.1016/j.msec.2021.112076

Fardous, J., Omoso, Y., Yoshida, K., Ono, F., Patwary, M. K. A., and Ijima, H. (2022). Gel-in-water Nanodispersion for Potential Application in Intravenous Delivery of Anticancer Drugs. *J. Biosci. Bioeng.* 133, 174–180. doi:10.1016/j.jbiosc.2021.10.001

Finlayson, J. (1893). Ancient Egyptian Medicine: [A Bibliographical Demonstration in the Library of the Faculty of Physicians and Surgeons, Glasgow, January 12th, 1893.]. *BMJ* 1 (1684), 748–752. doi:10.1136/bmj.1.1684.748

Fournier, E., Passirani, C., Montero-Menei, C. N., and Benoit, J. P. (2003). Biocompatibility of Implantable Synthetic Polymeric Drug Carriers: Focus on Brain Biocompatibility. *Biomaterials* 24 (19), 3311–3331. doi:10.1016/s0142-9612(03)00161-3

Garner, I., Vichare, R., Paulson, R., Appavu, R., Panguluri, S. K., Tzekov, R., et al. (2020). Carbon Dots Fabrication: Ocular Imaging and Therapeutic Potential. *Front. Bioeng. Biotechnol.* 8, 8. doi:10.3389/fbioe.2020.573407

Hassan, C. M., and Peppas, N. A. (2000). "Structure and Applications of Poly(vinyl Alcohol) Hydrogels Produced by Conventional Crosslinking or by Freezing/thawing Methods," in *Biopolymers/Pva Hydrogels/Anionic Polymerisation Nanocomposites*. Editor A. Abe (Cham, Switzerland: Springer International Publishing AG).

Hu, B., Yan, H., Sun, Y., Chen, X., Sun, Y., Li, S., et al. (2020). Organogels Based on Amino Acid Derivatives and Their Optimization for Drug Release Using Response Surface Methodology. *Artif. Cell Nanomedicine, Biotechnol.* 48 (1), 266–275. doi:10.1080/21691401.2019.1699833

Jabbari, E., and Peppas, N. A. (1994). Polymer-polymer Interdiffusion and Adhesion. *J. Macromolecular Sci. C: Polym. Rev.* 34 (2), 205–241. doi:10.1080/15321799408009635

Kakkar, A., Traverso, G., Farokhzad, O. C., Weissleder, R., and Langer, R. (2017). Evolution of Macromolecular Complexity in Drug Delivery Systems. *Nat. Rev. Chem.* 1 (8). doi:10.1038/s41570-017-0063

Khor, E., and Lim, L. Y. (2003). Implantable Applications of Chitin and Chitosan. *Biomaterials* 24 (13), 2339–2349. doi:10.1016/s0142-9612(03)00026-7

Kodela, S. P., Pandey, P. M., Nayak, S. K., Uvanesh, K., Anis, A., and Pal, K. (2017). Novel agar-stearyl Alcohol Oleogel-Based Bigels as Structured Delivery Vehicles. *Int. J. Polymeric Mater. Polymeric Biomater.* 66 (13), 669–678. doi:10.1080/00914037.2016.1252362

Koetting, M. C., and Peppas, N. A. (2014). Stimuli-responsive Hydrogels for Oral Delivery of High Isoelectric point-exhibiting Therapeutic Proteins. *Abstr. Pap. Am. Chem. Soc.* 247, 247.

Koetting, M. C., Peters, J. T., Steichen, S. D., and Peppas, N. A. (2015). Stimulus-responsive Hydrogels: Theory, Modern Advances, and Applications. *Mater. Sci. Eng. R: Rep.* 93, 1–49. doi:10.1016/j.mser.2015.04.001

Kohane, D. S., and Langer, R. (2010). Biocompatibility and Drug Delivery Systems. *Chem. Sci.* 1 (4), 441–446. doi:10.1039/c0sc00203h

Langer, R., and Peppas, N. (1983). Chemical and Physical Structure of Polymers as Carriers for Controlled Release of Bioactive Agents: A Review. *J. Macromolecular Sci. C* 23 (1), 61–126. doi:10.1080/07366578308079439

Langer, R., and Peppas, N. (1981). Present and Future Applications of Biomaterials in Controlled Drug Delivery Systems. *Biomaterials* 2 (4), 201–214. doi:10.1016/0142-9612(81)90059-4

Liu, D.-E., Chen, Q., Long, Y.-B., Ma, J., and Gao, H. (2018). A Thermo-Responsive Polyurethane Organogel for Norfloxacin Delivery. *Polym. Chem.* 9 (2), 228–235. doi:10.1039/c7py01803g

Martin, B., Brouillet, F., Franceschi, S., and Perez, E. (2017). Evaluation of Organogel Nanoparticles as Drug Delivery System for Lipophilic Compounds. *Aaps Pharmscitech* 18 (4), 1261–1269. doi:10.1208/s12249-016-0587-y

Mitchell, M. J., Billingsley, M. M., Haley, R. M., Wechsler, M. E., Peppas, N. A., and Langer, R. (2021). Engineering Precision Nanoparticles for Drug Delivery. *Nat. Rev. Drug Discov.* 20 (2), 101–124. doi:10.1038/s41573-020-0090-8

Olak, T., Turan, A., Alpaslan, D., Dudu, T. E., and Aktaş, N. (2020). Developing poly(Agar-co-Glycerol-co-Thyme Oil) Based Organo-Hydrogels for the Controlled Drug Release Applications. *J. Drug Deliv. Sci. Technol.* 60, 102088. doi:10.1016/j.jddst.2020.102088

Onuki, Y., Bhardwaj, U., Papadimitrakopoulos, F., and Burgess, D. J. (2008). A Review of the Biocompatibility of Implantable Devices: Current Challenges to Overcome Foreign Body Response. *J. Diabetes Sci. Technol.* 2 (6), 1003–1015. doi:10.1177/193229680800200610

Park, H., and Park, K. (1996). Biocompatibility Issues of Implantable Drug Delivery Systems. *Pharm. Res.* 13 (12), 1770–1776. doi:10.1023/a:1016012520276

Paul, S. R., Qureshi, D., Yogalakshmi, Y., Nayak, S. K., Singh, V. K., Syed, I., et al. (2018). Development of Bigels Based on Stearic Acid-Rice Bran Oil Oleogels and Tamarind Gum Hydrogels for Controlled Delivery Applications. *J. Surfactants Deterg* 21 (1), 17–29. doi:10.1002/jsde.12022

Peer, D., Karp, J. M., Hong, S., FaroKhzad, O. C., Margalit, R., and Langer, R. (2007). Nanocarriers as an Emerging Platform for Cancer Therapy. *Nat. Nanotech* 2 (12), 751–760. doi:10.1038/nnano.2007.387

Peppas, N. A., Hilt, J. Z., Khademhosseini, A., and Langer, R. (2006). Hydrogels in Biology and Medicine: From Molecular Principles to Bionanotechnology. *Adv. Mater.* 18 (11), 1345–1360. doi:10.1002/adma.200501612

Peppas, N. A., Huang, Y., Torres-Lugo, M., Ward, J. H., and Zhang, J. (2000). Physicochemical Foundations and Structural Design of Hydrogels in Medicine and Biology. *Annu. Rev. Biomed. Eng.* 2, 9–29. doi:10.1146/annurev.bioeng.2.1.9

Peppas, N. A., and Sahlin, J. J. (1996). Hydrogels as Mucoadhesive and Bioadhesive Materials: A Review. *Biomaterials* 17 (16), 1553–1561. doi:10.1016/0142-9612(95)00307-x

Peppas, N. A. (1982). Structure, Testing, and Applications of Biomaterials. *Adv. Chem. Ser.* 199, 465–473. doi:10.1021/ba-1982-0199.ch028

Querobino, S. M., de Faria, N. C., Vigato, A. A., da Silva, B. G. M., Machado, I. P., Costa, M. S., et al. (2019). Sodium Alginate in Oil-Poloxamer Organogels for Intravaginal Drug Delivery: Influence on Structural Parameters, Drug Release Mechanisms, Cytotoxicity and *In Vitro* Antifungal Activity. *Mater. Sci. Eng. C* 99, 1350–1361. doi:10.1016/j.msec.2019.02.036

Ronneberger, B., Kao, W. J., Anderson, J. M., and Kissel, T. (1996). *In Vivo* biocompatibility Study of ABA Triblock Copolymers Consisting of poly(L-Lactic-Co-Glycolic Acid) A Blocks Attached to central Poly(oxyethylene) B Blocks. *J. Biomed. Mater. Res.* 30 (1), 31–40. doi:10.1002/(sici)1097-4636(199601)30:1<31::aid-jbm5>3.0.co;2-s

Ronneberger, B., Kissel, T., and Anderson, J. M. (1997). Biocompatibility of ABA Triblock Copolymer Microparticles Consisting of poly(L-Lactic-Co-Glycolic-Acid) A-Blocks Attached to central Poly(oxyethylene) B-Blocks in Rats after Intramuscular Injection. *Eur. J. Pharmaceutics Biopharmaceutics* 43 (1), 19–28. doi:10.1016/s0939-6411(96)00006-9

Sadeghi, I., Byrne, J., Shakur, R., and Langer, R. (2021). Engineered Drug Delivery Devices to Address Global Health Challenges. *J. Controlled Release* 331, 503–514. doi:10.1016/j.jconrel.2021.01.035

Sadtler, K., Collins, J., Byrne, J. D., and Langer, R. (2020). Parallel Evolution of Polymer Chemistry and Immunology: Integrating Mechanistic Biology with Materials Design. *Adv. Drug Deliv. Rev.* 156, 65–79. doi:10.1016/j.addr.2020.06.021

Sagbas, S., Aktas, N., and Sahiner, N. (2015). Modified Biofunctional P(tannic Acid) Microgels and Their Antimicrobial Activity. *Appl. Surf. Sci.* 354, 306–313. doi:10.1016/j.apsusc.2015.06.163

Sagiri, S. S., Singh, V. K., Banerjee, I., Pramanik, K., Basak, P., and Pal, K. (2015). Core-shell-type Organogel-Alginate Hybrid Microparticles: A Controlled Delivery Vehicle. *Chem. Eng. J.* 264, 134–145. doi:10.1016/j.cej.2014.11.032

Sahiner, N., Ozay, O., and Aktas, N. (2011). 4-Vinylpyridine-Based Smart Nanoparticles with N-Isopropylacrylamide, 2-Hydroxyethyl Methacrylate, Acrylic Acid, and Methacrylic Acid for Potential Biomedical Applications. *Cnano* 7 (3), 453–462. doi:10.2174/157341311795542507

Sahiner, N., Sagbas, S., Sahiner, M., Blake, D. A., and Reed, W. F. (2018). Polydopamine Particles as Nontoxic, Blood Compatible, Antioxidant and Drug Delivery Materials. *Colloids Surf. B: Biointerfaces* 172, 618–626. doi:10.1016/j.colsurfb.2018.09.019

Sahiner, N., Sagbas, S., Sahiner, M., and Silan, C. (2017). P(TA) Macro-, Micro-, Nanoparticle-Embedded Super Porous P(HEMA) Cryogels as Wound Dressing Material. *Mater. Sci. Eng. C* 70, 317–326. doi:10.1016/j.msec.2016.09.025

Sahiner, N. (2021). Self-Crosslinked Ellipsoidal Poly(Tannic Acid) Particles for Bio-Medical Applications. *Molecules* 26 (9), 2429. doi:10.3390/molecules26092429

Sahiner, N., Suner, S. S., and Ayyala, R. S. (2019). Mesoporous, Degradable Hyaluronic Acid Microparticles for Sustainable Drug Delivery Application. *Colloids Surf. B: Biointerfaces* 177, 284–293. doi:10.1016/j.colsurfb.2019.02.015

Suner, S. S., Demirci, S., Yetiskin, B., Fakhrullin, R., Naumenko, E., Okay, O., et al. (2019). Cryogel Composites Based on Hyaluronic Acid and Halloysite Nanotubes as Scaffold for Tissue Engineering. *Int. J. Biol. Macromolecules* 130, 627–635. doi:10.1016/j.ijbiomac.2019.03.025

Suner, S. S., Sahiner, M., Sengel, S. B., Rees, D. J., Reed, W. F., and Sahiner, N. (2018). Responsive Biopolymer-Based Microgels/nanogels for Drug Delivery Applications. *Stimuli Responsive Polymeric Nanocarriers Drug Deliv. Appl. Types Triggers* 1, 453–500. doi:10.1016/b978-0-08-101997-9.00021-7

Thakur, K., Mahajan, A., Sharma, G., Singh, B., Raza, K., Chhibber, S., et al. (2020). Implementation of Quality by Design (QbD) Approach in Development of Silver Sulphadiazine Loaded Egg Oil Organogel: An Improved Dermatokinetic Profile and Therapeutic Efficacy in Burn Wounds. *Int. J. Pharmaceutics* 576, 118977. doi:10.1016/j.ijpharm.2019.118977

Thevenot, P., Hu, W., and Tang, L. (2008). Surface Chemistry Influences Implant Biocompatibility. *Curr. Top. Med. Chem.* 8 (4), 270–280. doi:10.2174/156802608783790901

Tokuyama, H., and Kato, Y. (2010). Preparation of Thermosensitive Polymeric Organogels and Their Drug Release Behaviors. *Eur. Polym. J.* 46 (2), 277–282. doi:10.1016/j.eurpolymj.2009.10.016

Tsai, W.-B., Grunkemeier, J. M., McFarland, C. D., and Horbett, T. A. (2002). Platelet adhesion to polystyrene-based surfaces preadsorbed with plasmas selectively depleted in fibrinogen, fibronectin, vitronectin, or von Willebrand's factor. *J. Biomed. Mater. Res.* 60 (3), 348–359. doi:10.1002/jbm.10048

Uchegbu, I. F., Schätzlein, A. G., Tetley, L., Gray, A. I., Sludden, J., Siddique, S., et al. (2011). Polymeric Chitosan-Based Vesicles for Drug Delivery. *J. Pharm. Pharmacol.* 50 (5), 453–458. doi:10.1111/j.2042-7158.1998.tb06185.x

Uhrich, K. E., Cannizzaro, S. M., Langer, R. S., and Shakesheff, K. M. (1999). Polymeric Systems for Controlled Drug Release. *Chem. Rev.* 99 (11), 3181–3198. doi:10.1021/cr940351u

Uzan, S., Barış, D., Çolak, M., Hoşgören, H., and Hosgoren, H. (2016). Organogels as Novel Carriers for Dermal and Topical Drug Delivery Vehicles. *Tetrahedron* 72 (47), 7517–7525. doi:10.1016/j.tet.2016.10.009

Vercruysse, K. P., and Prestwich, G. D. (1998). Hyaluronate Derivatives in Drug Delivery. *Crit. Rev. Ther. Drug Carrier Syst.* 15 (5), 513–555. doi:10.1615/critrevtherdrugcarriersyst.v15.i5.30

Vichare, R., Garner, I., Paulson, R. J., Tzekov, R., Sahiner, N., Panguluri, S. K., et al. (2020). Biofabrication of Chitosan-Based Nanomedicines and its Potential Use for Translational Ophthalmic Applications. *Appl. Sci.* 10 (12), 4189. doi:10.3390/app10124189

Wang, Y.-X., Robertson, J. L., Spillman, Jr., W. B., and Claus, R. O. (2004). Effects of the Chemical Structure and the Surface Properties of Polymeric Biomaterials on Their Biocompatibility. *Pharm. Res.* 21 (8), 1362–1373. doi:10.1023/b:pham.0000036909.41843.18

Webber, M. J., and Langer, R. (2017). Drug Delivery by Supramolecular Design. *Chem. Soc. Rev.* 46 (21), 6600–6620. doi:10.1039/c7cs00391a

Wichterle, O., and Lim, D. (1960). Hydrophilic Gels for Biological Use. *Nature* 185 (4706), 2. doi:10.1038/185117a0

Wichterle, O., and Lím, D. (1960). Hydrophilic Gels for Biological Use. *Nature* 185 (4706), 117–118. doi:10.1038/185117a0

Zeng, L., Lin, X., Li, P., Liu, F.-Q., Guo, H., and Li, W.-H. (2021). Recent Advances of Organogels: from Fabrications and Functions to Applications. *Prog. Org. Coat.* 159, 106417. doi:10.1016/j.porgcoat.2021.106417

Zhang, Z., Suner, S. S., Blake, D. A., Ayyala, R. S., and Sahiner, N. (2020). Antimicrobial Activity and Biocompatibility of Slow-Release Hyaluronic Acid-Antibiotic Conjugated Particles. *Int. J. Pharmaceutics* 576, 119024. doi:10.1016/j.ijpharm.2020.119024

Conflict of Interest: The authors declare that the research was conducted in the absence of any commercial or financial relationships that could be construed as a potential conflict of interest.

The reviewer AT declared a shared affiliation, with collaboration, with the authors to the handling editor at the time of the review.

Publisher's Note: All claims expressed in this article are solely those of the authors and do not necessarily represent those of their affiliated organizations or those of the publisher, the editors, and the reviewers. Any product that may be evaluated in this article, or claim that may be made by its manufacturer, is not guaranteed or endorsed by the publisher.

frontiers | Frontiers in Materials

ORIGINAL RESEARCH
published: 07 April 2022
doi: 10.3389/fmats.2022.826251

Novel Silane Crosslinked Chitosan Based Electrospun Nanofiber for Controlled Release of Benzocaine

Mehwish Naz[1], Sehrish Jabeen[2], Nafisa Gull[2], Abdul Ghaffar[1], Atif Islam[1,2], Muhammad Rizwan[3], Huda Abdullah[4], Atta Rasool[2], Shahzad Khan[2] and Rafi Khan[2]*

[1]*Department of Chemistry, University of Engineering and Technology, Lahore, Pakistan,* [2]*Institute of Polymer and Textile Engineering, University of the Punjab, Lahore, Pakistan,* [3]*Department of Chemistry, The University of Lahore, Lahore, Pakistan,* [4]*Electrical and Electronic Engineering Programme, Faculty of Engineering and Built Environment, Universiti Kebangsaan Malaysia, Bangi, Malaysia*

Nanofibers mats of chitosan (CTS)/polyvinyl alcohol (PVA)/halloysite nanoclay and drug loaded CTS/PVA/halloysite nanoclay//3-glycidyoxypropyl trimethoxysilane were fabricated using the electrospinning method. Electrospun nanofiber samples were characterized by Fourier transform infrared spectroscopy (FTIR), scanning electron microscopy (SEM), and thermogravimetric analysis (TGA). FTIR confirmed the chemical and physical bonding among ingredients such as CTS, PVA, nanoclay and crosslinker in the nanofibers. SEM images showed the development of uniform nanofibers. The average nanofiber diameter was observed in the range of 50–200 nm. Antimicrobial activity was examined against *E. coli* and *S. aurus* bacteria. The results obtained indicated that all nanofiber samples showed significant antimicrobial activity against the Gram-positive as well as Gram-negative bacteria. TGA results indicated that the thermal stability of nanofibers increased with the addition of the crosslinker. The drug release was studied in phosphate buffer saline (PBS) solution (pH 7.4) at 37°C and was released from nanofibers in 2.5 h. Hence, these prepared nanofibers can be used in medication where the drug is required for a long duration.

Keywords: chitoan, controlled release, crosslinked, nanofiber, silane

OPEN ACCESS

Edited by:
Wenbo Wang,
Inner Mongolia University, China

Reviewed by:
Alaa Fahmy,
Al-Azhar University, Egypt
Ratiram Gomaji Chaudhary,
Seth Kesarimal Porwal College, India

****Correspondence:***
Atif Islam
dratifislam@gmail.com

Specialty section:
This article was submitted to Polymeric and Composite Materials, a section of the journal Frontiers in Materials

Received: *30 November 2021*
Accepted: *18 January 2022*
Published: *07 April 2022*

Citation:
Naz M, Jabeen S, Gull N, Ghaffar A, Islam A, Rizwan M, Abdullah H, Rasool A, Khan S and Khan R (2022) Novel Silane Crosslinked Chitosan Based Electrospun Nanofiber for Controlled Release of Benzocaine. Front. Mater. 9:826251. doi: 10.3389/fmats.2022.826251

1 INTRODUCTION

Nanotechnology has been utilized extensively with different compositions and biological properties in medicine for therapeutic drug delivery, tissue engineering applications, and the development of treatments for a variety of diseases and disorders. The high surface are a to volume ratio of nanomaterials can also be used in composites, chemical reactions, and energy storage applications (Suri et al., 2007; Shi et al., 2010; Safari and Zarnegar, 2014; Sutradhar and Amin, 2014). A fiber is an elongated, slender, and thread-like structure. The term "nanofiber" means that the fibers have a diameter in the nanometer range. These nanofibers are referred to as superfine, ultrafine, and submicron fibers (Adam et al., 2013). The electrospun nanofibers are very small in size, and they have many distinctive properties that allow them to be used in many small places. They also have a high surface area to volume ratio which significantly changes the physical, chemical, and morphological properties of the nanofiber mats (Mishra et al., 2019). The large surface area of nanofibers makes them appropriate for use in new technologies which need a smaller size and smaller environments to take place the chemical reactions. Chemical reactions speed up with increasing the surface area.

Nanofibers can be produced by using several methods, such as self-assembly, phase separation technique, drawing method, electrospinning, and template synthesis. Electrospinning is a unique, easy, flexible, efficient, and cost-effective process for the fabrication of continuous nanofibers using a high potential electric field with a diameter range from 10 nm to several hundreds nanometers. Compared to other techniques, electrospinning is the most efficient method to produce nano or microscale nanofiber from a polymer solution using a high voltage electrical field that induces charges to the polymer solution. An electrically charged jet is expelled from the needle tip when the surface tension of the polymer solution is overcome by the electrostatic forces and nonwoven nanofibers mat are formed and collected on the collector (Yu et al., 2009; Sirin et al., 2013).

Biopolymers show good biocompatibility but poor mechanical properties and high production cost (Gull et al., 2019a). Natural polymers are highly sensitive to change in pH and temperature and lose their basic structure immediately. To overcome this drawback many strategies have been used (Rafique et al., 2016). Polymer blending is an attractive method that has been extensively used for providing new desirable characteristics (Gull et al., 2020a). Polymer blends are prepared by various methods including solution blending, which is very simple and rapid because it only requires simple equipment and does not involve any complicated process. This is mainly due to its simplicity, the availability of a wide range of synthetic and natural polymers for blending, and its effectiveness for practical utilization. The blending of polymers may result in the reduction of their basic cost, the improvement of their processing, and the maximization of their important properties. Polymer blends are physical mixtures of two or more structurally different homopolymers or copolymers and they interact through secondary forces with out covalent bonding (Mudigoudra et al., 2012).

Chitosan (CTS) is the most abundant natural polymer distributed widely in nature. The main source of the CTS and chitin are crabs shells, fungi, and shrimps shells. Its molecular weight (MW) varies in the ranges of 300–1,000 kDa depending on the chitin source (Mahdavi et al., 2013; Pokhrel et al., 2015). CTS has several properties which make it useful for many applications like drug delivery, wound healing, immunology, and hematology (Gull et al., 2020b). The MW and degree of deacetylation are the main factors that affect the properties of CTS. Reactions of CTS are more versatile because of the existence of -NH_2 groups (Gull et al., 2019b). Nitrogen present in the CTS depends on the degree of deacetylation and mostly in the form of primary aliphatic amine which makes it more reactive (Dutta et al., 2004). It shows good antimicrobial activity and inhibits microbial growth. This antibacterial activity is due to the binding of cationic amino groups of CTS with the microorganisms' anionic groups which inhibit the growth of microorganisms. In agriculture, CTS hinders bacterial growth and infection and stimulates the natural defenses and growth of plants (Ding et al., 2013).

Polyvinyl alcohol (PVA) is non-carcinogenic, biocompatible, biodegradable, nontoxic, and hydrophilic polymer. It has good film-forming properties, processing ability, and good chemical resistance (Fahmy et al., 2020; Fahmy et al., 2021). It is used in agriculture to deliver fertilizers, pesticides, herbicides, and fungicides, as well as to coat seeds. Such prepared seeds are ready for germination only under adequate temperature and humidity conditions (Reis et al., 2006; Haweel and Ammar, 2008; Ranjha and Khan, 2013; Gaaz et al., 2015; Swapna et al., 2015). 3-Glycidoxypropyl trimethoxysilane (3-GPTMS) is a colorless transparent liquid that is soluble in a variety of organic solvents, undergoes hydrolysis easily and condensation reaction to form polysiloxanes. It polymerizes easily in the presence of light, heat, and peroxides (Sapic et al., 2009).

Controlled drug delivery systems offer numerous advantages compared to conventional dosage forms including enhanced effectiveness, condensed toxicity, site-specificity to reduce the side effects of the drug, improved concentration maintenance, and controlled duration of drug release (Coelho et al., 2010; Baptista et al., 2013; Hu et al., 2014). Controlled targeted delivery of the drug is attained by utilizing the material, composed of either non-degradable or biodegradable polymer. The drug release is reliant on polymer nanofibers degradation. A broad range of polymer materials are used as drug delivery media or sources. The polymer medium for drug delivery is determined according to the requirements of the application. The type of polymer, solvent, and compatibility of the drug are important processing variables when trying to attain reproducible and stable drug delivery. Several drugs have been incorporated into electrospun nanofibers and transported to the desired target site in the body (Gholipour-Kanani and Bharami, 2010). The aim of this study was to prepare the novel electrospun nanofibers comprised of polymer blend which was crosslinked with silane crosslinker and used for controlled drug release system.

2 MATERIALS AND METHODS

2.1 Materials

Chitosan $(C_8H_{13}NO_5)_n$ was purchased from Biolog (GmbH) Trademark, Germany. Polyvinyl alcohol $(C_2H_4O)_n$ and formic acid were bought from Sigma-Aldrich. Potassium dihydrogen phosphate (KH_2PO_4), sodium dihydrogen phosphate (NaH_2PO_4), and sodium chloride (NaCl) were procured from Merck, Germany, and potassium chloride (KCl) was procured from Fisher chemicals. All chemicals were used without any further treatment.

2.2 Fabrication of Nanofibers

CTS (0.5 g) weighed on the electronic balance and dissolved in 1% formic acid solution with continuous stirring on a magnetic hot plate. PVA (3.5 g) was added to the pre-heated water at 90°C while creating a shear well and stirred until it completely dissolved. The PVA solution was added to the CTS solution and stirred for 1.5 h. Then, 100 µL 3-GPTMS was dissolved into methanol and added in the blended solution dropwise while creating a continuous shear well by stirring on a magnetic plate for 2 h, and then the blended solution was sonicated for a further 1 h. The blended solution was stirred again, and the solvent was

evaporated till the solution becomes viscous for electrospinning. CPC-1 was a controlled nanofiber sample containing CTS and PVA without crosslinker. CPC-2 was a nanofiber sample containing 100 µL crosslinker (3-GPTMS). CPC-3 was a benzocaine-loaded sample.

3 CHARACTERIZATIONS

3.1 Fourier Transformer Infrared Spectroscopy

Fourier Transformer Infrared Spectroscopy (FTIR) spectra of the nanofiber samples were analyzed by using Agilent technology. The FTIR of electrospun nanofibers were analyzed over the wavenumber range of 4,000–650 cm^{-1} at a resolution of 4 cm^{-1}.

3.2 Thermogravimetric Analysis

Thermogravimetric characterization of electrospun nanofibers was carried out by using star^{e} sw 12.10 model. The heating rate was kept at 10°C/min from room temperature to 600°C and nitrogen flow was maintained at (10 ml/min).

3.3 Scanning Electron Microscopy

The morphology and diameter of the electrospun nanofiber were analyzed using nano nova SEM 450. The SEM images results were obtained at different resolutions.

3.4 Antibacterial Activity

The antimicrobial activity of prepared nanofibers was determined using the disc diffusion method. A nutrient agar medium was prepared to grow the bacterial culture on a petri dish in the form of a slant. It was prepared by adding the respective amount of water and mixing it thoroughly. Then the agar containing vessels were heated in a water bath for 30–45 min to produce a transparent medium. After 45 min, the vessels were removed from the water bath and cooled. After maintaining the pH, the vessel was covered with aluminum foil and placed in an autoclave for sterilization at 15 psi and 121°C for 20 min. This semi-hot agar media was spread on petri dishes which were placed in an incubator at 37°C for 24 h. These petri dishes had clear agar medium, which means that there was no contamination. Nutrient broth medium was also prepared, and 10–15 ml autoclaved nutrient broth was poured into sterilized test tubes to be used for bacterial growth. A platinum loop was heated to red hot to sterilize it, then some strains were taken from pure and transferred to a test tube containing nutrient broth, covered with a sterilized cotton plug, and placed in an incubator for 24 h at 37°C. The prepared agar plates and bacteria-containing nutrient broth test tubes were kept in laminar flow. The petri dishes containing nutrient agar media were uncovered, and the nutrient broth was poured into each and spread across the whole petri dish. Samples were placed on the petri dish containing the bacterial culture. The petri dishes were placed in an incubator for 24 h at 37°C and then the zone of inhibition was measured with the help of a measuring scale in mm.

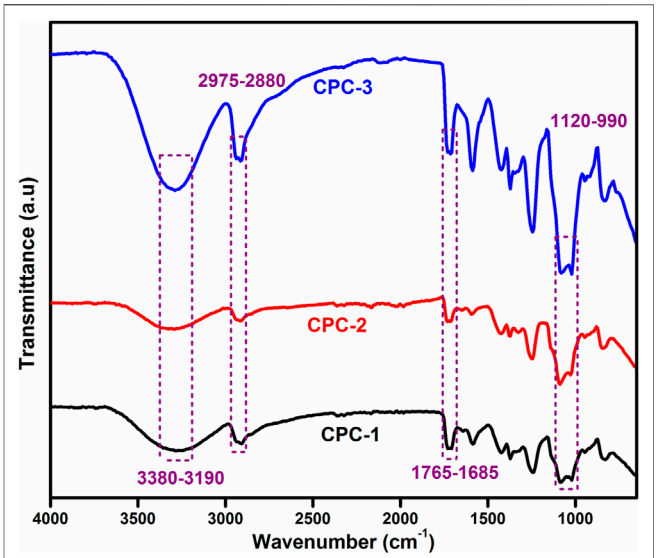

FIGURE 1 | FTIR spectra of CTS and PVA blend CPC-1 and crosslinked blend solution CPC-2 and drug-loaded sample CPC-3.

3.5 Drug Loading and Release Study

50 mg benzocaine was dissolved in ethanol and added to the CPC-2 blended solution. This solution was stirred for 1 h and then crosslinker was added dropwise and stirred for a further 2 h. The blended solution was sonicated for 1 h and then stirred and evaporated till the solution became viscous.

Electrospun nanofiber drug release study was carried out in phosphate buffer saline (PBS) solution. PBS solution was prepared by dissolving 8 g NaCl, 0.24 g KCL, 1.44 g NaH_2PO_4, and KH_2PO_4 in 800 ml distilled water. The pH of the solution was adjusted to 7.4 by the addition of a few drops of sodium chloride solution. Finally, distilled water was added up to mark.

CPC-2 loaded with a drug was placed in PBS solution separately at 37°C. After every 20 min, 5 ml solution was taken out from the beaker through a syringe and a fresh solution of PBS was added to keep the volume same. Samples were collected for 3 h from the PBS solution and the amount of released drug was determined using an ultraviolet-visible spectrophotometer at 294 nm for CPC-2. The amount of drug released from nanofibers was calculated with reference to a standard solution (100 ppm of benzocaine in PBS solution).

4 RESULT AND DISCUSSION

4.1 Fourier Transforms Infrared Spectroscopy

FTIR analysis was performed to confirm the possible physical and chemical interactions among CTS, PVA, nanoclay, and crosslinker in the nanofibers. FTIR spectra of all nanofiber samples are shown in **Figure 1**. A broad band was observed in the range of 3,380–3,190 cm^{-1} in all samples due to the stretching vibration of the–OH group of PVA and the –NH_2 of CTS indicating the intensity of the hydrogen bonding. This broad

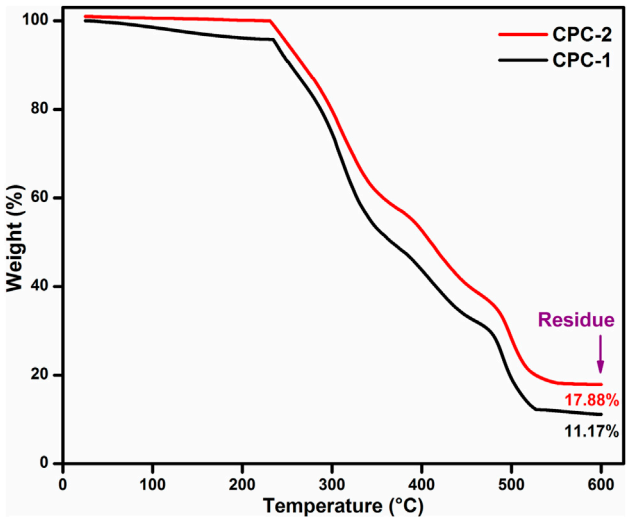

FIGURE 2 | Thermograms of nanofiber mats from room temperature to 600°C.

band is due to the merging of -OH and -NH_2 frequencies (Chaudhary et al., 2013a; Chaudhary et al., 2015; Chaudhary et al., 2019). The peak at 2,975–2,880 cm^{-1} was observed due to the vibrational frequency of -CH of alkyl groups. The sharp band at 1765–1,685 cm^{-1} is ascribed to the carbonyl group of acetylated groups of CTS. The band observed in the range of 1,120–990 cm^{-1} indicated the C-O-C group of CTS and siloxane linkage (–Si–O–C and–Si–O–Si) in the crosslinked nanofiber (Wang et al., 2016).

4.2 Thermogravimetric Analysis

The thermal stability of nanofibers was studied by thermogravimetric analysis (TGA) and the results of the crosslinked nanofibers are shown in **Figure 2**, which shows the multistep degradation. The first thermal degradation step was observed from room temperature to 225°C, which is corresponded to the moisture evaporation of bound water and H-bonded water due to the highly absorption nature of CTS and PVA (Yeh et al., 2006; Chaudhary et al., 2013b; Society C.A.M., 2013). The next degradation step is due to the oxygen-containing pendent groups, depolymerization, oxidation, and the release of gases from organic molecules like CTS and PVA, and the next degradation was due to the pyrolysis of the main carbon chain. The widening of decomposition is due to the proper blending of PVA and CTS with the crosslinker which forms chemical and hydrogen bonds (Gull et al., 2019c). **Table 1** shows the $T_{50\%}$ and residue. $T_{50\%}$ was 361°C for CPC-1 and 406°C for the crosslinked nanofiber which means that with crosslinking, the thermal stability of the nanofiber sample was increased and a high temperature was required to degrade the crosslinked sample.

4.3 Scanning Electron Microscopy

Figure 3 shows the SEM micrographs of uncrosslinked and crosslinked nanofibers and the drug-loaded sample. The surface morphology of the prepared nanofibers represents more crosslinking with an increase in the concentration of crosslinker (Potbhare et al., 2019). By crosslinking, and with all other parameters of the electrospinning kept constant, more uniform nanofibers were obtained and the average diameter of the nanofiber was in the range of 50–100 nm. CPC-1 showed a crosslinked structure which was due to the physical group of PVA and the crosslinking among all ingredients of nanofibers, but this crosslinking was more dense and compact in CPC-2 with more crosslinked mesh-like structure, due to the addition of crosslinker (Gull et al., 2020a).

4.4 Antimicrobial Analysis

The antimicrobial activity of the prepared nanofibers was determined using the disc diffusion method using Gram-negative bacteria, i.e., *E. coli* and Gram-positive bacteria i.e., *S. aurus*. The antibacterial activity of the samples was determined by measuring inhibition zones on a culture medium after 24 h of incubation. The resistance of bacterial growth was due to the cationic nature of CTS, which interacts with the anionic cell wall of bacteria. This opposite charge interaction caused the osmotic imbalance of cells and led to the cell lysis of bacteria. Another suggested mechanism is due to the interaction of CTS with bacterial DNA and penetrated bacterial nuclei, thus retarding the alteration of DNA into mRNA which eventually inhibited the growth of bacteria. Results have shown that the antimicrobial activity of the sample increased as compared to the controlled sample (**Table 2**).

4.5 *In-vitro* Release Study of Benzocaine

The release of benzocaine in CPC-2 was analyzed in PBS solution at 37°C in **Figure 4**. It was observed that the drug was released in 2.5 h which is according to the US Pharmacopeia standard. At neutral pH, CTS does not undergo protonation, which enables it to make physical interaction to develop a network which subsequently caused the controlled release of the drug from the nanofibers. From this result, it is concluded that such crosslinked nanofibers can be used for the controlled release of drugs in the biomedical field (Abbaspour et al., 2015).

4.5.1 Kinetic Study of Drug Release Analysis

To evaluate the transport mechanism of benzocaine from CPC-2, data were modeled by Ritger-Peppa's model as shown in **Eq. 1**:

TABLE 1 | Thermogravimetric data of the nanofibers.

Sample code	($T_{50\%}$)	Residue (%)
CPC-1	366.33°C	11.17
CPC-2	409.83°C	17.88

TABLE 2 | Antimicrobial results against *E. coli* and *S. aurus* bacteria.

Sample code	Gram (+)	Gram (-)
C (mm) PC-1	37 mm	38
CPC-2	40 mm	39

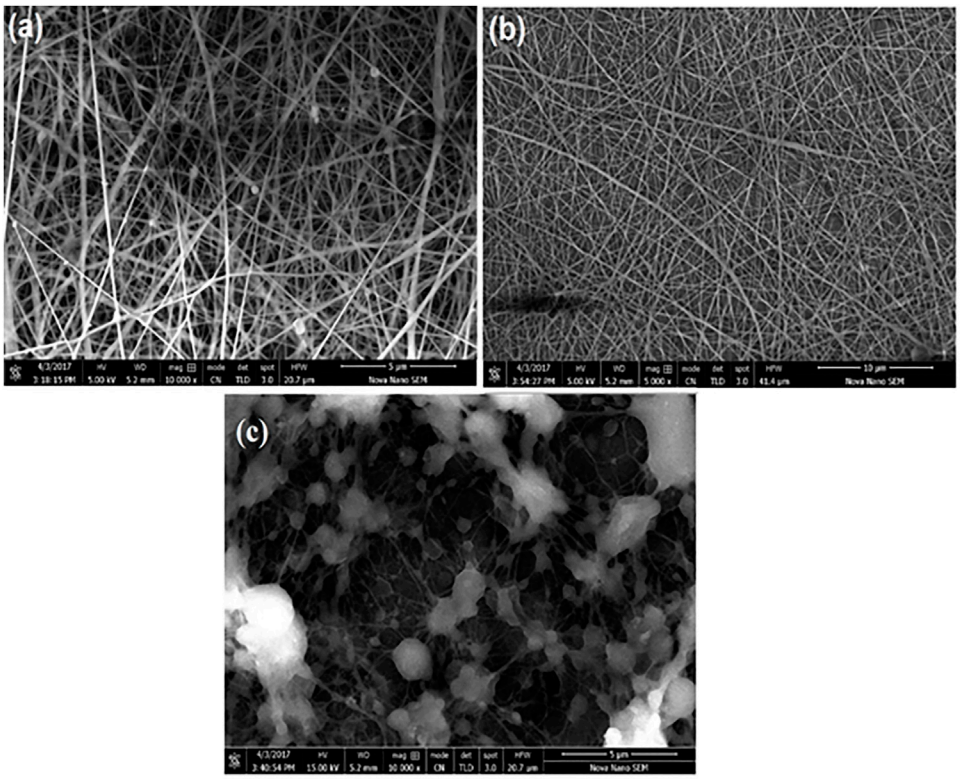

FIGURE 3 | SEM micrographs of nanofibers CPC-1 **(A)**, CPC-2 **(B)**, CPC-3**(C)**.

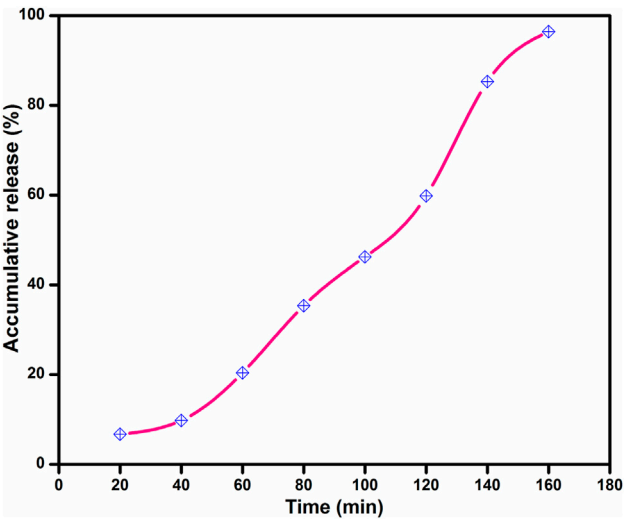

FIGURE 4 | Accumulative release of benzocaine in CPC-2.

$$\frac{M_t}{M_\infty} = Kt^n \quad (1)$$

M_t is the amount of drug released at time t, M ∞ is the total drug load, and k is the kinetic constant which does not depend upon the structural and geometrical properties of the polymer matrix. If the value of n is 0.5, it corresponds to the Fickian diffusion mechanism, if n is 1, then it is a non-Fickian mechanism. $n < 0.5 < 1$ shows the anomalous transport mechanism and $n < 0.5$ exhibit the Pseudo-Fickian behavior (Huang et al., 2007). The results of the kinetic analysis of drug release analysis are shown in **Figure 4** and **Table 3**. The lower value of n shows the Pseudo-Fickian mechanism of drug release in the drug-loaded nanofiber sample.

TABLE 3 | Kinetic parameters of accumulative drug release of benzocaine from CPC-2.

Kinetic parameters	Value
N	0.7
Intercept	−0.164
K	0.8487
Regression	96.60

5 CONCLUSION

In this study, electrospun nanofibers were prepared using a simple and cost-effective electrospinning technique. Nanofibers were prepared by using CTS, PVA, and halloysite nanoclay which is crosslinked with 3-GPTMS. Electrospun nanofibers were characterized by using FTIR,

TGA, and SEM. FTIR analysis results confirmed the bonding between the polymer chains and siloxane linkage in nanofibers. SEM micrographs showed that the continuous and long nanofibers formed and with crosslinking more uniform nanofibers were obtained. The antimicrobial activity of the nanofiber was studied against *E. coli* and *S. aureus* and results indicated that all the samples showed significant antimicrobial behavior. TGA results indicated that the thermal strength of the nanofibers increased with crosslinking. A drug release study was conducted in PBS solution (pH 7.4) at 37°C using ultraviolet-visible spectroscopy and results showed that the drug was released completely in 2.5 h in a controlled manner. Hence, it is concluded that such drug-loaded nanofibers can be used in different clinical applications.

DATA AVAILABILITY STATEMENT

The raw data supporting the conclusion of this article will be made available by the authors, without undue reservation.

AUTHOR CONTRIBUTIONS

MN performed experimental work and physical analyses. SJ assisted in manuscript writing. NG contributed in writing, editing proof reading of manuscript. AI conceived and designed the project. AG supervised the project. MR and HA contributed in interpretation of results. AR performed antibacterial analysis. SK guided in data curation. RK guided in overall direction and planning of project.

REFERENCES

Abbaspour, M., Sharif Makhmalzadeh, B., Rezaee, B., Shoja, S., and Ahangari, Z. (2015). Evaluation of the Antimicrobial Effect of Chitosan/Polyvinyl Alcohol Electrospun Nanofibers Containing Mafenide Acetate. *Jundishapur J. Microbiol.* 8, e24239–6. doi:10.5812/jjm.24239

Adam, P., Sasikanth, K., Nama, S., Suresh, P., and Brahmaiah, B. (2013). Nanofiber - A New Trend in Nano Drug Delivery System. *Int. J. Pharm. Res. Anal.* 3, 47–55.

Baptista, A. C., Ferreira, I. F., Ferreira, I., and Borges, J. P. (2013). Electrospun Fibers in Composite Materials for Medical Applications. *J. Compos. Biodegradable Polym.* 1, 56–65. doi:10.12974/2311-8717.2013.01.01.7

Chaudhary, R. G., Ali, P., Gandhare, N. V., Tanna, J. A., and Juneja, H. D. (2019). Thermal Decomposition Kinetics of Some Transition Metal Coordination Polymers of Fumaroyl Bis (Paramethoxyphenylcarbamide) Using DTG/DTA Techniques. *Arabian J. Chem.* 12, 1070–1082. doi:10.1016/j.arabjc.2016.03.008

Chaudhary, R. G., Juneja, H. D., and Gandhare, N. V. (2013). Evaluation of Kinetic Parameters from TG/DTG Data of Chelate Polymer Compounds of Isophthaoylbis(paramethoxyphenylcarbamide). *J. Chin. Adv. Mater. Soc.* 1, 305–316. doi:10.1080/22243682.2013.871210

Chaudhary, R. G., Juneja, H. D., and Gharpure, M. P. (2013). Thermal Degradation Behaviour of Some Metal Chelate Polymer Compounds with Bis(bidentate) Ligand by TG/DTG/DTA. *J. Therm. Anal. Calorimjournal Therm. Anal. Calorim.* 112, 637–647. doi:10.1007/s10973-012-2616-8

Chaudhary, R. G., Juneja, H. D., Pagadala, R., Gandhare, N. V., and Gharpure, M. P. (2015). Synthesis, Characterisation and thermal Degradation Behaviour of Some Coordination Polymers by Using TG-DTG and DTA Techniques. *J. Saudi Chem. Soc.* 19, 442–453. doi:10.1016/j.jscs.2014.06.002

Coelho, J. F., Ferreira, P. C., Alves, P., Cordeiro, R., Fonseca, A. C., Góis, J. R., et al. (2010). Drug Delivery Systems: Advanced Technologies Potentially Applicable in Personalized Treatments. *EPMA J.* 1, 164–209. doi:10.1007/s13167-010-0001-x

Ding, F., Deng, H., Du, Y., Shi, X., and Wang, Q. (2013). Emerging Chitin and Chitosan Nanofibrous Materials for Biomedical Applications. *Nanoscale* 6, 1–47. doi:10.1039/C4NR02814G

Dutta, P. K., Dutta, J., and Tripathi, V. S. (2004). Chitin and Chitosan: Chemistry, Properties and Applications. *J. Scientific Ind. Res.* 63, 20–31.

Fahmy, A., Abu-Saied, M., Helaly, H., El-Dessoki, F., and Mohamed, T. A. (2021). Novel PVA/Methoxytrimethylsilane Elastic Composite Membranes: Preparation, Characterization and DFT Computation. *J. Mol. Struct.* 1235, 130173. doi:10.1016/j.molstruc.2021.130173

Fahmy, A., Mohamed, T. A., Abu-Saied, M., Helaly, H., and El-Dossoki, F. (2020). Structure/property Relationship of Polyvinyl Alcohol/dimethoxydimethylsilane Composite Membrane: Experimental and Theoretical Studies. *Spectrochim Acta A. Mol. Biomol. Spectrosc.* 228, 117810. doi:10.1016/j.saa.2019.117810

Gaaz, T., Sulong, A., Akhtar, M., Kadhum, A., Mohamad, A., and Al-Amiery, A. (2015). Properties and Applications of Polyvinyl Alcohol, Halloysite Nanotubes and Their Nanocomposites. *Molecules* 20, 22833–22847. doi:10.3390/molecules201219884

Gholipour-Kanani, A., and Bharami, H. (2010). Scaffold and Biomedical Application:Review on Electrospun Nanofibers Scaffold and Biomedical Applications. *Trends Biomater. Artif. organs* 24, 93–115.

Gull, N., Khan, S. M., Butt, M. T. Z., Zia, S., Khalid, S., Islam, A., et al. (2019). Hybrid Cross-linked Hydrogels as a Technology Platform for *In Vitro* Release of Cephradine. *Polym. Adv. Technol.* 30, 2414–2424. doi:10.1002/pat.4688

Gull, N., Khan, S. M., Butt, O. M., Islam, A., Shah, A., Jabeen, S., et al. (2020). Inflammation Targeted Chitosan-Based Hydrogel for Controlled Release of Diclofenac Sodium. *Int. J. Biol. Macromolecules* 162, 175–187. doi:10.1016/j.ijbiomac.2020.06.133

Gull, N., Khan, S. M., Islam, A., and Butt, M. T. Z. (2019). "Hydrogels Used for Biomedical Applications," in *Bio Monomers for Green Polymeric Composites Materials*. Editors O. B. P.M. Visakh and G Menon (Hoboken: Wiley-blackwell), 175–199. doi:10.1002/9781119301714.ch9

Gull, N., Khan, S. M., Khalid, S., Zia, S., Islam, A., Sabir, A., et al. (2020). Designing of Biocompatible and Biodegradable Chitosan Based Crosslinked Hydrogel for *In Vitro* Release of Encapsulated Povidone-Iodine: A Clinical Translation. *Int. J. Biol. Macromolecules* 164, 4370–4380. doi:10.1016/j.ijbiomac.2020.09.031

Gull, N., Khan, S. M., Zahid Butt, M. T., Khalid, S., Shafiq, M., Islam, A., et al. (2019). *In Vitro* study of Chitosan-Based Multi-Responsive Hydrogels as Drug Release Vehicles: A Preclinical Study. *RSC Adv.* 9, 31078–31091. doi:10.1039/c9ra05025f

Haweel, C. K., and Ammar, S. H. (2008). Preparation of Polyvinyl Alcohol from Local Raw Material. *Iraqi J. Chem. Pet. Eng.* 9, 15–21.

Hu, J., Zeng, F., Wei, J., Chen, Y., and Chen, Y. (2014). Novel Controlled Drug Delivery System for Multiple Drugs Based on Electrospun Nanofibers Containing Nanomicelles. *J. Biomater. Sci. Polym. Edition* 25, 257–268. doi:10.1080/09205063.2013.852367

Huang, Y., Yu, H., and Xiao, C. (2007). pH-Sensitive Cationic Guar Gum/poly (Acrylic Acid) Polyelectrolyte Hydrogels: Swelling and *In Vitro* Drug Release. *Carbohydr. Polym.* 69, 774–783. doi:10.1016/j.carbpol.2007.02.016

Mahdavi, H., Mirzadeh, H., Zohuriaan, J., and Talebnezhad, F. (2013). Poly (Vinyl Alcohol)/chitosan/clay Nano-Composite Films. *J. Am. Sci.* 9, 203–214.

Mishra, R. K., Mishra, P., Verma, K., Mondal, A., Chaudhary, R. G., Abolhasani, M. M., et al. (2019). Electrospinning Production of Nanofibrous Membranes. *Environ. Chem. Lett.* 17, 767–800. doi:10.1007/s10311-018-00838-w

Mudigoudra, B. S., Masti, S. P., and Chougale, R. B. (2012). Thermal Behavior of Poly (Vinyl Alcohol)/Poly (Vinyl pyrrolidone)/Chitosan Ternary Polymer Blend Films. *Res. J. Recent Sci.* 1, 83–86.

Pokhrel, S., Yadav, P. N., and Adhikari, R. (2015). Applications of Chitin and Chitosan in Industry and MedicalScience: A Review. *Nepal J. Sci. Tech.* 16, 99–104. doi:10.3126/njst.v16i1.14363

Potbhare, A. K., Chaudhary, R. G., Chouke, P. B., Yerpude, S., Mondal, A., Sonkusare, V. N., et al. (2019). Phytosynthesis of Nearly Monodisperse CuO

Nanospheres Using Phyllanthus Reticulatus/Conyza Bonariensis and its Antioxidant/antibacterial Assays. *Mater. Sci. Eng. C* 99, 783–793. doi:10.1016/j.msec.2019.02.010

Rafique, A., Mahmood Zia, K., Zuber, M., Tabasum, S., and Rehman, S. (2016). Chitosan Functionalized Poly(vinyl Alcohol) for Prospects Biomedical and Industrial Applications: A Review. *Int. J. Biol. Macromolecules* 87, 141–154. doi:10.1016/j.ijbiomac.2016.02.035

Ranjha, N. M., and Khan, S. (2013). Chitosan/Poly (Vinyl Alcohol) Based Hydrogels for Biomedical Applications: A Review. *J. Pharm. Altern. Med.* 2, 30–41.

Reis, E. F. D., Campos, F. S., Lage, A. P., Leite, R. C., Heneine, L. G., Vasconcelos, W. L., et al. (2006). Synthesis and Characterization of Poly (Vinyl Alcohol) Hydrogels and Hybrids for rMPB70 Protein Adsorption. *Mat. Res.* 9, 185–191. doi:10.1590/s1516-14392006000200014

Safari, J., and Zarnegar, Z. (2014). Advanced Drug Delivery Systems: Nanotechnology of Health Design A Review. *J. Saudi Chem. Soc.* 18, 85–99. doi:10.1016/j.jscs.2012.12.009

Sapic, I. M., Bistricić, L., Volovsek, V., Dananic, V., and Furic, K. (2009). DFT Study of Molecular Structure and Vibrations of 3-glycidoxypropyltrimethoxysilane. *Spectrochimica Acta A: Mol. Biomol. Spectrosc.* 72, 833–840. doi:10.1016/j.saa.2008.11.032

Shi, J., Votruba, A. R., Farokhzad, O. C., and Langer, R. (2010). Nanotechnology in Drug Delivery and Tissue Engineering: From Discovery to Applications. *Nano Lett.* 10, 3223–3230. doi:10.1021/nl102184c

Sirin, S., Cetiner, S., and Sarac, A. S. (2013). Polymer Nanofibers via Electrospinning: Factors Affecting Nanofiber Quality. *J. Eng. Sci.* 16, 1–12.

Society C.A.M. (2013). *Journal of the Chinese Advanced Materials Society*. Milton Park: Taylor & Francis Group.

Suri, S. S., Fenniri, H., and Singh, B. (2007). Nanotechnology-based Drug Delivery Systems. *J. Occup. Med. Toxicol.* 2, 1–16. doi:10.1186/1745-6673-2-16

Sutradhar, K. B., and Amin, M. L. (2014). Nanotechnology in Cancer Drug Delivery and Selective Targeting. *ISRN Nanotechnology* 2014, 1–12. doi:10.1155/2014/939378

Swapna, V. P., Selvin Thomas, P., Suresh, K. I., Saranya, V., Rahana, M. P., and Stephen, R. (2015). Thermal Properties of Polyvinyl Alcohol (PVA)/Halloysite Nanotubes Reinforced Nanocomposites. *Int. J. Plast. Tech.* 19, 124–136. doi:10.1007/s12588-015-9106-3

Wang, D., Liu, W., Feng, Q., Dong, C., Liu, Q., Duana, L., et al. (2016). Effect of Inorganic/organic Ratio and Chemical Coupling on the Performance of Porous Silica/chitosan Hybrid Scaffolds. *Mater. Sci. Eng. C* 70, 1–7. doi:10.1016/j.msec2016.04.010

Yeh, J.-T., Chen, C.-L., Huang, K. S., Nien, Y. H., Chen, J. L., and Huang, P. Z. (2006). Synthesis, Characterization, and Application of PVP/chitosan Blended Polymers. *J. Appl. Polym. Sci.* 101, 885–891. doi:10.1002/app.23517

Yu, D.-G., Zhu, L.-M., White, K., and Branford-White, C. (2009). Electrospun Nanofiber-Based Drug Delivery Systems. *Health* 01, 67–75. doi:10.4236/health.2009.12012

Conflict of Interest: The authors declare that the research was conducted in the absence of any commercial or financial relationships that could be construed as a potential conflict of interest.

Publisher's Note: All claims expressed in this article are solely those of the authors and do not necessarily represent those of their affiliated organizations, or those of the publisher, the editors and the reviewers. Any product that may be evaluated in this article, or claim that may be made by its manufacturer, is not guaranteed or endorsed by the publisher.

frontiers | Frontiers in Materials

ORIGINAL RESEARCH
published: 22 June 2022
doi: 10.3389/fmats.2022.835507

Cellulose Derivative-Based Bioadhesive Blend Patch for Transdermal Drug Delivery

Sreejan Manna[1], Dadala Dhanalakshmi[2], Manas Bhowmik[3], Sougata Jana[4] and Subrata Jana[5]**

[1]Department of Pharmaceutical Technology, Brainware University, Kolkata, India, [2]Koringa College of Pharmacy, Kakinada, India, [3]Department of Pharmaceutical Technology, Jadavpur University, Kolkata, India, [4]Department of Pharmaceutics, Gupta College of Technological Sciences, Asansol, India, [5]Department of Chemistry, Indira Gandhi National Tribal University, Amarkantak, India

In this study, matrix-type transdermal patches of glibenclamide were developed using a combination of hydrophilic and hydrophobic polymers for investigating the efficacy of transdermal carriers. A cellulose derivative, HPMC E50, was used as a hydrophilic matrix-forming polymer, and Eudragit RS 100 was used as a hydrophobic polymer. The solvent casting technique was employed to develop a transdermal blend patch formulation using chloroform and methanol as the casting solvent. No drug–polymer interaction was observed by the FTIR study. The membrane permeation study exhibited a sustained release of glibenclamide up to 12 h within a range of 76.15 ± 2.80% to 101.01 ± 0.33% depending on the polymeric ratio. The increased concentration of Eudragit RS 100 in different formulations has gradually decreased the amount of drug penetration through the membrane. The kinetic analysis showed the release is best explained by zero-order kinetics, followed by Higuchi and first order. The release exponent suggested shifting of non-Fickian diffusion to the super case II transport drug release mechanism when Eudragit RS 100 concentration was increased. It is concluded that the developed formulations may be a better alternative to the conventional oral delivery of glibenclamide.

Keywords: transdermal patch, films, glibenclamide, HPMC E50, Eudragit RS 100

OPEN ACCESS

Edited by:
Nafisa Gull,
University of the Punjab, Pakistan

Reviewed by:
Fatima Ali,
University of Karachi, Pakistan
Muhammad Asim Raza,
University of Science and Technology, South Korea

****Correspondence:***
Sreejan Manna
manna.sreejan@gmail.com
Subrata Jana
jana.s.oc@gmail.com

Specialty section:
This article was submitted to Polymeric and Composite Materials, a section of the journal Frontiers in Materials

Received: *14 December 2021*
Accepted: *16 May 2022*
Published: *22 June 2022*

Citation:
Manna S, Dhanalakshmi D, Bhowmik M, Jana S and Jana S (2022) Cellulose Derivative-Based Bioadhesive Blend Patch for Transdermal Drug Delivery. Front. Mater. 9:835507. doi: 10.3389/fmats.2022.835507

1 INTRODUCTION

Since the emergence of transdermal patches, it has been considered one of the prime delivery systems for therapeutics. Transdermal drug delivery systems (TDDS) are presently regarded as a traditional means of avoiding hepatic first-pass metabolism and delivering lipophilic drugs. The transdermal application also prevents enzymatic degradation and acid-mediated decomposition of drugs (Al Hanbali et al., 2019). This technique is also useful for transporting low-molecular-weight drugs over a prolonged time span (Mutalik and Udupa 2004; Davis et al., 2020). Other major advantages of transdermally administered systems are self-administration, patient compliance, controlled release of therapeutics, and instant cessation of drug uptake by removing the patch (Alkilani et al., 2015). Continuous penetration of drugs also facilitates lowering the dose minimizing the side effects caused due to higher plasma concentration of the drug. Despite having numerous advantages, there are few drawbacks to transdermal films, that is, delivering ionic and macromolecular drugs, skin irritability, and patients with decreased peripheral blood circulation (Murphy and Carmichael 2000). According to the current scenario, transdermal uptake of a drug depends on the molecular weight of the drug, partition coefficient, degree of ionization, and hydrophilic–lipophilic balance of polymers

(Chandrashekar and Shobha Rani, 2008; Saoji et al., 2015). The highly selective barrier nature of skin limits the passage of drugs and acts as a dominant factor in transdermal absorption. The release of the medicament from a transdermal polymeric matrix can depend on the polymer ratio and permeation enhancer. According to the recent trend in transdermal delivery, drugs can also be incorporated into the adhesive layer of transdermal films (Davis et al., 2020). This approach has many advantages, including the lightweight, thin and flexible delivery system which increases patient compliance. It also minimizes the chance of drug leakage with respect to reservoir-type transdermal patches (Li et al., 2010).

Cellulose derivatives found unparalleled application as excipients in the field of pharmaceutical research and the manufacturing industry. Hydroxypropyl methylcellulose (HPMC) is one of the widely applied cellulose-based pharmaceutical excipients. This hydrophilic matrix forming polymer found extensive application in developing oral, mucosal, and transdermal delivery systems. The swellable nature and excellent safety profile, along with its enzymatic and pH-independent stability have made it an automatic choice as a hydrophilic matrix-forming agent (Mašková et al., 2020). In the molecular structure of HPMC, hydroxypropyl and methoxyl groups are attached to the linear chain of cellulose (Ford, 2014). Depending on the ratio and degree of substitution, variations in molecular weight are observed. The insignificant influence of pH and non-ionic behavior of the polymer ensures reproducible release of drug and nominal drug interaction (Nokhodchi et al., 2012; Mašková et al., 2020). The availability of various grades of HPMC has contributed to the need of designing individual drug delivery systems. This bioadhesive matrix forming agent is being widely applied in developing TDDS. A relatively less viscous grade, HPMC E50 (Hydroxypropyl methylcellulose E50- E type 2910; M.W.: 90000 Da), was selected as one of the matrices forming agents for the developed TDDS.

Eudragit was introduced as a pharmaceutical excipient in 1954 and since then it has revolutionized the concept of drug targeting. Chemically, Eudragits are polymethacrylates which are non-ionic, anionic, and cationic polymers of methacrylic acid, methacrylic acid esters, and diethylaminoethyl methacrylates in changing ratios (Yoshida et al., 2013). Eudragits are generally considered non-irritant and non-toxic in nature. It is commonly applied as a film-forming polymer in site-specific gastrointestinal delivery of drugs. The solubility of the films can be altered depending on the need for dosage forms by changing the grades of the polymer. It has also found application in pH-dependent drug release, formulation of mucoadhesive films, colon specific drug targeting, and enteric coating for enhancing stability and oral bioavailability of therapeutics (Thakral et al., 2013). Over the years, as various grades of eudragit became available, it has found widespread application in the field of drug delivery. The application of Eudragit in TDDS was extensively reported by various researchers. The transparent and elastic film forming ability of the polymer has been attributed to the development of transdermal patches (Tran and Tran, 2019). The adhesive property of the polymer helps in bioadhesion. Wrinkle free pale yellowish transdermal matrix can be developed which undergoes erosion to release the entrapped drug. Eudragit RS100 (ethyl prop-2-enoate; methyl 2-methylprop-2-enoate; trimethyl-[2-(2-methylprop-2-enoyloxy) ethyl] azanium; chloride; M.W.: 407.9 Da) having low permeability and sustained release ability which was utilized to formulate matrix based transdermal patches (Jafri et al., 2019).

Glibenclamide is chemically known as 5-chloro-N-{4-[N-(cyclohexyl-carbamoyl) sulfamoyl] phenethyl}-2-methoxy benzamide (Maiti et al., 2014). The plasma half-life of glibenclamide is about 4–6 h which leads to repeated dosing for maintaining therapeutic concentration *in vivo* (Nayak et al., 2012). This second-generation sulfonylurea is used in the therapy of non-insulin-dependent diabetes mellitus (NIDDM). Glibenclamide can stimulate insulin secretion by closing the ATP-sensitive ion channels which elevate the intracellular concentration of potassium and calcium ions in beta cells (Davis and Granner, 1996). The increased concentration of calcium ions can enhance the secretion of insulin causing hypoglycemia. Various sulfonylureas, including glibenclamide, are associated with serious hypoglycemia, and gastric side effects including vomiting, heartburn, nausea, and anorexia (Reynolds, 1993). Glibenclamide and its metabolites are reported to show hypoglycemic effects on humans owing to the increased secretion of insulin (Rydberg et al., 1994). Furthermore, Glibenclamide is reported to worsen Indomethacin-induced gastric injury and infiltration of neutrophils into the gastrointestinal mucosa (Akar et al., 1999). Oral therapy of glibenclamide can also result in increased appetite. Due to the hypoglycemic effect of glibenclamide, the use of the drug is not recommended for patients suffering from renal impairment (Mutalik and Udupa 2004). Glibenclamide is highly lipophilic and weakly acidic in nature. The use of polymeric blends in the field of drug delivery is gaining interest amongst researchers (Ghasemiyeh and Mohammadi-Samani 2021; Raza et al., 2021). Considering the adverse effects of the drug, an alternative approach to deliver glibenclamide at a controlled rate could be an acceptable approach for achieving a therapeutic level with reduced adverse effects. In this study, we have designed a novel polymeric blended transdermal system for delivering glibenclamide. A combination of hydrophilic and hydrophobic polymers including HPMC E50 and Eudragit RS 100, respectively in varying concentrations was used in order to achieve sustained release of glibenclamide through the skin. The study also aimed to investigate the effect of polymeric concentrations on physicochemical properties of the patch and drug release patterns. Various *in vitro* evaluations were performed for the characterization and optimization of the formulations.

2 MATERIALS AND METHODS

2.1 Materials

Glibenclamide was obtained from TCI Chemicals India Pvt., Ltd. HPMC E50 and Eudragit RS 100 were commercially procured from Nice Chemicals Ltd., Bangalore. PEG 400 and propylene

TABLE 1 | Composition of transdermal patches of glibenclamide.

Sl. no.	Ingredients	F_1	F_2	F_3	F_4	F_5	F_6	F_7	F_8
1	Glibenclamide (mg)	50	50	50	50	50	50	50	50
2	HPMC E50 (mg)	675	650	625	600	575	550	525	500
3	Eudragit RS 100 (mg)	25	50	75	100	125	150	175	200
4	Propylene glycol (ml)	0.2	0.2	0.2	0.2	0.2	0.2	0.2	0.2
5	PEG 400 (ml)	0.3	0.3	0.3	0.3	0.3	0.3	0.3	0.3
6	Methanol (ml)	5	5	5	5	5	5	5	5
7	Chloroform (ml)	5	5	5	5	5	5	5	5
8	Sodium benzoate (mg)	20	20	20	20	20	20	20	20

glycol were purchased from SD Fine Chemicals Ltd. Methanol and chloroform were procured from Molychem Chemicals Ltd. All the chemicals used were of analytical grades.

2.2 Methods

2.2.1 Fourier Transform-Infrared Spectroscopy

The IR spectra of pure glibenclamide, HPMC E50, Eudragit RS 100, and a physical mixture of glibenclamide with polymers were obtained after scanning of KBr mixed pellets using Shimadzu FTIR spectrophotometer (IRPrestige- 21). The samples were scanned within the wave number range of 4000–400 cm^{-1} with a scanning speed of 2 mm/s.

2.2.2 Preparation of Glibenclamide-Loaded Transdermal Patch

The transdermal patches of glibenclamide were prepared by solvent casting technique by dissolving the polymers in chloroform and methanol (Cherukuri et al., 2017). HPMC E50 and Eudragit RS100 were dissolved in chloroform and methanol (1:1 ratio) as a casting solvent mixture. The required quantity of the drug was separately dispersed in casting solvent. The two phases were mixed and PEG 400 was incorporated as a plasticizer. Propylene glycol was added as a permeation enhancer which was mixed homogeneously. A specific amount of sodium benzoate was added and uniformly mixed. The polymeric patches were cast in petri plates and the solvent was allowed to evaporate. An inverted funnel was placed on a petri plate to slow down the solvent evaporation rate and for avoiding dust accumulation. The arrangement was kept undisturbed for 24 h and then the dried films were carefully removed from the petri plates. The formed patches were cut to a uniform size, glued to the backing membrane, and stored in a desiccator wrapped in the wax paper sheet. The composition of developed transdermal patches was shown in **Table 1**.

2.2.3 Thickness

The patches were selected randomly from each batch and subjected to thickness measurement by using slide calipers. The thicknesses of the developed films were measured in three different areas, and the mean thickness was calculated for individual formulation batches.

2.2.4 Drug Content

A specific patch area (1 cm^2) was taken and dissolved in 100 ml of pH 5.6 phosphate buffer solution and stirred for 6 h. Then the solution was kept undisturbed for up to 24 h for complete solubilization of glibenclamide. After 24 h, the solution was filtered and the filtrate was scanned by using a UV-Visible spectrophotometer [(UV-2540, SHIMADZU)] at 228 nm. The concentration of dissolved glibenclamide was determined for all the formulations using the following equation:

$$\%\ Drug\ content = \frac{Actual\ glibenclamide\ content\ in\ selected\ patch}{Theoretical\ amount\ of\ glibenclamide\ in\ selected\ patch} \times 100.$$

2.2.5 Folding Endurance

Folding endurance for the developed transdermal patches of glibenclamide was determined by repeated folding of film at the same point until it breaks. It helps to determine the efficacy of plasticizers and also to measure the strength of the developed patches. The number of folding was noted up to which the specific strip of film resisted breaking (Singh and Bali, 2016). The experiment was carried out in triplicate to obtain mean folding endurance for the respective formulation.

2.2.6 % Moisture Content

Randomly selected transdermal patches of specific surface area were weighed individually and placed inside desiccators containing activated silica beads at room temperature (Madan et al., 2015). The initial weight (W_i) of the patches was recorded. The films were weighed at regular intervals until a constant final weight (W_d) was obtained. The percentage of moisture content was calculated by using the following equation:

$$\%\ Moisture\ content\ = \frac{(W_i - W_d)}{W_d} 100.$$

2.2.7 Moisture Uptake Capacity

The percentage of moisture uptake for the developed glibenclamide patches was determined by placing them initially in a desiccator for 24 h in presence of silica gel beads (Madan et al., 2015). Then the patches were removed, and the weight of individual patches was noted as initial weight (W_0). The patches were then kept in another desiccator containing saturated sodium chloride to maintain high humidity conditions. The films were removed every 7 days at the interval and weighed until obtaining constant weight (W_F). The increase in weight due to moisture uptake was determined and the percentage of moisture uptake was calculated by using the following formula:

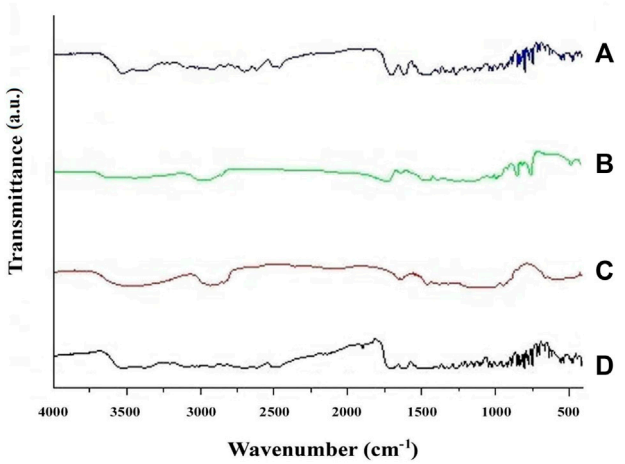

FIGURE 1 | FTIR spectrum of **(A)** pure glibenclamide; **(B)** HPMC E50; **(C)** Eudragit RS 100; and **(D)** a physical mixture of glibenclamide with polymers.

$$\%Moisture\ uptake = \frac{(W_F - W_0)}{W_0} 100.$$

2.2.8 *In Vitro* Membrane Permeation Study

In vitro membrane permeation study was carried out by using a Franz diffusion cell through a dialysis membrane (LA390, approximate capacity—1.99 ml/cm, average diameter—15.9 mm, average flat width—25.27 mm). The dialysis membrane was soaked overnight prior to use in dissolution fluid (phosphate buffer of pH 5.6). The transdermal films were cut according to the diameter of the donor cell and the dialysis membrane was placed over it and tied to one end. The donor cell was placed in such a way that the dissolution medium just touches the surface of the membrane covering the transdermal patch of glibenclamide. The stirring speed and the medium temperature were maintained at 50 rpm and 37 ± 0.5°C, respectively. 1 ml of aliquots was withdrawn at regular time intervals up to 12 h with an equal volume of fresh buffer replacement each time. The collected aliquots were filtered and spectrophotometrically analyzed for glibenclamide content at 228 nm by using a UV-visible spectrophotometer (UV-2540, SHIMADZU) (Jana et al., 2010).

2.2.9 Kinetic Analysis of Drug Release

The release behavior of glibenclamide from the developed transdermal polymer matrix can be predicted by fitting the *in vitro* drug release data into various mathematical models. Different mathematical models followed for this purpose are zero order, first order, Korsmeyer–Peppas, and Higuchi models (Korsmeyer et al., 1983; Peppas and Sahlin, 1989). The correlation coefficient obtained from each model has been noted from which the highest value indicates the best-fit mathematical model for drug release.

3 RESULTS AND DISCUSSION

3.1 FTIR Study

The FTIR of glibenclamide, HPMC E50, Eudragit RS 100, and physical mixture of drug and polymers was shown in **Figure 1**. The FTIR spectrum of pure glibenclamide (**Figure 1A**) shows a peak for symmetric S=O stretching at 1144.80 cm^{-1} which was observed at the same frequency in the spectrum of physical mixture. Pure glibenclamide shows asymmetric S=O stretching for the–SO_2NH group at 1343.48 cm^{-1} which was found in the physical mixture at exactly the same frequency. The characteristic peak for N–H stretching for–C=O–NH–was observed at 3372.68 cm^{-1}. A similar peak for N–H stretching was observed in the physical mixture of (**Figure 1D**) at 3374.61 cm^{-1}. The peak for N–H deformation and–C–O stretching vibration of–C–O–NH–was observed at 1720.58 cm^{-1} which persisted in the physical mixture without significant shift at 1707.08 cm^{-1}. The peak for asymmetric S–O stretching was found at 1384.95 cm^{-1} which was observed at 1383.98 cm^{-1} in the physical mixture (Bakshi et al., 2015). The characteristic peaks appearing in the FTIR spectrum of glibenclamide have also appeared in the spectrum of physical mixtures of the drug without any significant shifting of peaks, indicating the absence of any chemical interaction during and after preparation.

3.2 Thickness of the Film

The thickness of glibenclamide-loaded transdermal films was measured with the help of a digital slide caliper at different points and the average thickness was calculated. Almost uniform thickness was observed for the developed patches of glibenclamide as shown in **Table 2**. The result indicated that there was not much variation in the thickness between the formulation and it was found to be within the range of 0.846 ± 0.020 mm–0.913 ± 0.020 mm without considerable variation similar to other study reports (Ofokansi et al., 2015).

3.3 Drug Content

The percentage of drug content was determined with respect to the incorporated amount of glibenclamide into the specific area (1 cm^2) of the transdermal formulation. The drug content for all the formulations was observed between 96.47 ± 1.58% and 98.93 ± 1.19% (**Table 2**).

3.4 Folding Endurance

The folding endurance for the developed transdermal films was measured by repeated folding on either side of it. The matrix-based films were reported to have folding endurance within the range of 116.3 ± 4.50–162 ± 4.35 (**Table 2**). The obtained folding endurance values indicated good elasticity and strength of the designed transdermal patches. The values were roughly found to decrease with increasing Eudragit RS 100 concentration in the transdermal matrix.

3.5 % Moisture Content

The percentage of moisture content was determined in presence of activated silica beads. The % moisture content

TABLE 2 | Thickness, drug content, folding endurance, moisture content, and moisture absorbed for the developed patches.

Formulation code	Thickness* (mm)	Drug content* (%)	Folding endurance* (no. of foldings)	Moisture content* (%)	Moisture absorbed* (%)
F1	0.886 ± 0.030	98.31 ± 1.82	162 ± 4.35	6.81 ± 0.47	11.31 ± 0.60
F2	0.876 ± 0.047	97.07 ± 1.60	151.6 ± 5.13	5.55 ± 0.40	10.58 ± 0.33
F3	0.860 ± 0.043	96.52 ± 1.82	147.6 ± 3.51	5.39 ± 0.46	10.30 ± 0.66
F4	0.896 ± 0.030	97.30 ± 1.41	149 ± 6.24	4.86 ± 0.55	9.48 ± 0.41
F5	0.863 ± 0.025	96.47 ± 1.58	138 ± 3.60	4.55 ± 0.55	9.52 ± 0.53
F6	0.846 ± 0.020	98.58 ± 1.28	132.3 ± 4.04	4.32 ± 0.42	8.06 ± 0.67
F7	0.883 ± 0.037	97.38 ± 1.32	122.6 ± 7.57	3.50 ± 0.40	7.12 ± 0.76
F8	0.913 ± 0.020	98.93 ± 1.19	116.3 ± 4.50	3.21 ± 0.45	6.38 ± 0.44

**The values indicate the mean ± standard deviation of three determinations.*

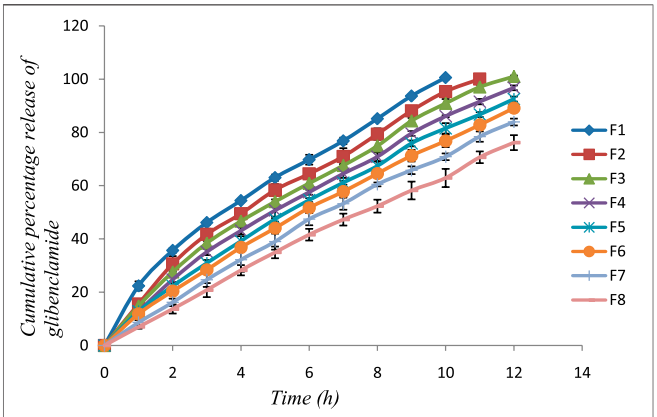

FIGURE 2 | *In vitro* membrane permeation profile of glibenclamide from the developed patches (F1-F8) in phosphate buffer of pH 5.6.

for all the transdermal films was determined within the range of 3.21 ± 0.45 to 6.81 ± 0.47 (**Table 2**). The obtained data clearly showed a gradual decrease in moisture content as the HPMC E50 concentration decreased with an increase in Eudragit RS 100 in the formulations. The minimum moisture content was observed for F8 as it contained a relatively lower concentration of HPMC E50 and a higher concentration of Eudragit RS 100 out of all the developed formulations. Similar results were observed in other matrix-type transdermal patches containing HPMC and Eudragit (Peddapalli et al., 2018).

3.6 Moisture Uptake Capacity

The moisture uptake ability was performed in a desiccator maintaining 75% relative humidity. A maximum of 11.31 ± 0.60 was observed for F1 whereas the least moisture content was found at 6.38 ± 0.44 for F8 (**Table 2**). The gradual decrease in % moisture uptake was observed due to the gradual lowering of hydrophilic HPMC E50. Minimum moisture uptake ability helps to reduce bulkiness, and also minimizes the chance of microbial contamination. Similar results were reported by Eudragit and HPMC-based transdermal films (Vijaya and Ruckmani 2011).

3.7 *In Vitro* Membrane Permeation of Glibenclamide

The release of glibenclamide from the developed transdermal films was performed in Franz diffusion cells through a dialysis membrane using pH 5.6 phosphate buffer as receptor medium. **Figure 2** demonstrates the percentage of drug permeated through the dialysis membrane over 12 h of time. The membrane permeation of F1, showed complete permeation of glibenclamide after 10 h, whereas F2 exhibited complete release of drug after 11 h. For the remaining batches of formulation, the permeation study was continued for 12 h and the percentage of the permeated drug was found to vary between 76.15 ± 2.80% and 101.01 ± 0.33%. The data obtained clearly suggest the influence of polymer ratio in % of the permeated drug. An increase in Eudragit RS 100 concentration gradually reduces the water penetration into the developed patches, as a result, the release of glibenclamide decreases through the dialysis membrane. The simultaneous decrease in HPMC E50 concentration may also be responsible for retarding the release of glibenclamide. Being a hydrophilic polymer, HPMC E50 can easily uptake water and swelling occurs which facilitates a relatively rapid release of the drug. It has been observed that when Eudragit RS 100 concentration is gradually increased, leading to a reduction in water uptake, and the percentage of drug release is significantly reduced. A similar observation was reported by other HPMC E50 and Eudragit-based transdermal films (Yamsani et al., 2017).

3.8 Kinetic Analysis of Glibenclamide Release

The kinetic modeling of all the developed transdermal matrix films was performed. The data obtained from membrane permeation of glibenclamide incorporated patches were kinetically analyzed by zero order, first order, Higuchi, and Korsemeyer–Peppas models for explaining the release of the drug (**Table 3**). The release is best explained by zero order kinetic as (r^2 > 0.977) for all the developed formulations except F1 followed by Higuchi and first order kinetics. The drug release kinetic data were analyzed by Korsemeyer–Peppas equation and the release exponent n from the developed

TABLE 3 | Kinetic analysis of *in vitro* membrane permeation of glibenclamide-loaded transdermal patch.

Formulation code	R^2 zero order	R^2 first order	R^2 Higuchi	Korsmeyer–Peppas	
				R^2	*n*
F1	0.910	0.921	0.985	0.998	0.64
F2	0.977	0.885	0.974	0.991	0.75
F3	0.982	0.861	0.972	0.996	0.76
F4	0.985	0.885	0.968	0.994	0.79
F5	0.989	0.937	0.964	0.995	0.81
F6	0.991	0.949	0.957	0.998	0.88
F7	0.993	0.976	0.945	0.993	0.92
F8	0.997	0.973	0.939	0.998	0.96

formulations is found to vary from 0.64 to 0.96 indicating that the release mechanism is following non-Fickian diffusion and shifted gradually towards Super case II transport mechanism when Eudragit concentration is increased gradually. A similar observation was noticed in other Eudragit-based transdermal formulations (Chandak and Prasad Verma, 2010; Jana et al., 2014).

4 CONCLUSION

The present investigation has demonstrated a transdermal approach to delivering glibenclamide through polymeric transdermal patches. The matrix-type transdermal patches were developed by following the solvent casting technique dissolving a hydrophilic and a hydrophobic polymer. HPMC E50 was selected as a hydrophilic matrix forming polymer to combine with a hydrophobic Eudragit RS 100. The FTIR study ensured no significant interaction between the drug and polymers. The thickness of the patches was almost uniform without significant variation. The % moisture content and moisture uptake capacity were found to depend on the polymeric ratio of transdermal films. The decrease in hydrophilic polymer concentration exhibited reduced moisture content and reduced moisture uptake ability. The membrane permeation study demonstrated a sustained release of glibenclamide over 12 h depending on polymeric composition. The decrease in hydrophilic polymer (HPMC E50) concentration reduces the % water uptake and retards the diffusion of drug molecules through the transdermal matrix. Among all the formulations, the least percentage of glibenclamide permeated was 76.15 ± 2.80% from F8 after 12 h. Finally, it is concluded that the developed transdermal patches for sustained delivery of glibenclamide can be a useful alternative in terms of avoiding the adverse effects associated with oral delivery of the drug.

DATA AVAILABILITY STATEMENT

The original contributions presented in the study are included in the article/Supplementary Material; further inquiries can be directed to the corresponding authors.

AUTHOR CONTRIBUTIONS

All authors listed have made a substantial, direct, and intellectual contribution to the work and approved it for publication.

REFERENCES

Akar, F., Uydeş-Doğan, B. S., Buharalioğlu, C. K., Abban, G., Heinemann, A., Holzer, P., et al. (1999). Protective Effect of Cromakalim and Diazoxide, and Proulcerogenic Effect of Glibenclamide on Indomethacin-Induced Gastric Injury. *Eur. J. Pharmacol.* 374, 461–470. doi:10.1016/s0014-2999(99)00277-0

Al Hanbali, O. A., Khan, H. M. S., Sarfraz, M., Arafat, M., Ijaz, S., and Hameed, A. (2019). Transdermal Patches: Design and Current Approaches to Painless Drug Delivery. *Acta Pharm.* 69, 197–215. doi:10.2478/acph-2019-0016

Alkilani, A., McCrudden, M. T., and Donnelly, R. (2015). Transdermal Drug Delivery: Innovative Pharmaceutical Developments Based on Disruption of the Barrier Properties of the Stratum Corneum. *Pharmaceutics* 7, 438–470. doi:10.3390/pharmaceutics7040438

Bakshi, P., Sadhukhan, S., and Maiti, S. (2015). Design of Modified Xanthan Mini-Matrices for Monitoring Oral Discharge of Highly Soluble Soluplus -glibenclamide Dispersion. *Mater. Sci. Eng. C* 54, 169–175. doi:10.1016/j.msec.2015.05.014

Chandak, A. R., and Prasad Verma, P. R. (2010). Eudragit-based Transdermal Delivery System of Pentazocine: Physico-Chemical, *In Vitro* and *In Vivo* Evaluations. *Pharm. Dev. Technol.* 15, 296–304. doi:10.3109/10837450903188501

Chandrashekar, N. S., and Shobha Rani, R. H. (2008). Physicochemical and Pharmacokinetic Parameters in Drug Selection and Loading for Transdermal Drug Delivery. *Indian J. Pharm. Sci.* 70, 94–96. doi:10.4103/0250-474x.40340

Cherukuri, S., Batchu, U. R., Mandava, K., Cherukuri, V., and Ganapuram, K. R. (2017). Formulation and Evaluation of Transdermal Drug Delivery of Topiramate. *Int. J. Pharm. Investig.* 7, 10–17. doi:10.4103/jphi.JPHI_35_16

Davis, D. A., Martins, P. P., Zamloot, M. S., Kucera, S. A., Williams, R. O., 3rd, Smyth, H. D. C., et al. (2020). Complex Drug Delivery Systems: Controlling Transdermal Permeation Rates with Multiple Active Pharmaceutical Ingredients. *AAPS PharmSciTech* 21, 165. doi:10.1208/s12249-020-01682-4

Davis, S. N., and Granner, D. K. (1996). "Insulin, Oral Hypoglycemic Agents, and the Pharmacology of the Endocrine Pancreas," in *Goodman and Gilman's the Pharmacological Basis of Therapeutics*. Editor A. G. Gilman (New York: McGraw-Hill), 1487–1518.

Ford, J. L. (2014). "Design and Evaluation of Hydroxypropyl Methylcellulose Matrix Tablets for Oral Controlled Release: A Historical Perspective," in *Hydrophilic Matrix Tablets for Oral Controlled Release*. Editors P. Timmins, S. R. Pygall, and C. D. Melia (New York: Springer-Verlag), 17–51. doi:10.1007/978-1-4939-1519-4_2

Ghasemiyeh, P., and Mohammadi-Samani, S. (2021). Polymers Blending as Release Modulating Tool in Drug Delivery. *Front. Mat.* 8, 752813. doi:10.3389/fmats.2021.752813

Jafri, I., Shoaib, M. H., Yousuf, R. I., and Ali, F. R. (2019). Effect of Permeation Enhancers on *In Vitro* Release and Transdermal Delivery of Lamotrigine from EudragitRS100 Polymer Matrix-type Drug in Adhesive Patches. *Prog. Biomater.* 8, 91–100. doi:10.1007/s40204-019-0114-9

Jana, S., Lakshman, D., Sen, K. K., and Basu, S. K. (2010). Development and Evaluation of Epichlorohydrin Cross-Linked Mucoadhesive Patches of Tamarind Seed Polysaccharide for Buccal Application. *Int. J. Pharm. Sci. Drug Res.* 2, 193–198.

Jana, S., Manna, S., Nayak, A. K., Sen, K. K., and Basu, S. K. (2014). Carbopol Gel Containing Chitosan-Egg Albumin Nanoparticles for Transdermal Aceclofenac Delivery. *Colloids Surfaces B Biointerfaces* 114, 36–44. doi:10.1016/j.colsurfb.2013.09.045

Korsmeyer, R. W., Gurny, R., Doelker, E., Buri, P., and Peppas, N. A. (1983). Mechanisms of Solute Release from Porous Hydrophilic Polymers. *Int. J. Pharm.* 15, 25–35. doi:10.1016/0378-5173(83)90064-9

Li, L., Fang, L., Xu, X., Liu, Y., Sun, Y., and He, Z. (2010). Formulation and Biopharmaceutical Evaluation of a Transdermal Patch Containing Letrozole. *Biopharm. Drug Dispos.* 31, 138–149. doi:10.1002/bdd.698

Madan, J. R., Argade, N. S., and Dua, K. (2015). Formulation and Evaluation of Transdermal Patches of Donepezil. *Recent Pat. Drug Deliv. Formul.* 9, 95–103. doi:10.2174/1872211308666141028213615

Maiti, S., Mukherjee, S., and Datta, R. (2014). Core-shell Nano-Biomaterials for Controlled Oral Delivery and Pharmacodynamic Activity of Glibenclamide. *Int. J. Biol. Macromol.* 70, 20–25. doi:10.1016/j.ijbiomac.2014.06.031

Mašková, E., Kubová, K., Raimi-Abraham, B. T., Vllasaliu, D., Vohlídalová, E., Turánek, J., et al. (2020). Hypromellose - A Traditional Pharmaceutical Excipient with Modern Applications in Oral and Oromucosal Drug Delivery. *J. Control. Rel.* 324, 695–727. doi:10.1016/j.jconrel.2020.05.045

Murphy, M., and Carmichael, A. J. (2000). Transdermal Drug Delivery Systems and Skin Sensitivity Reactions. Incidence and Management. *Am. J. Clin. Dermatology* 1, 361–368. doi:10.2165/00128071-200001060-00004

Mutalik, S., and Udupa, N. (2004). Glibenclamide Transdermal Patches: Physicochemical, Pharmacodynamic, and Pharmacokinetic Evaluations. *J. Pharm. Sci.* 93, 1577–1594. doi:10.1002/jps.20058

Nayak, A. K., Das, B., and Maji, R. (2012). Calcium Alginate/gum Arabic Beads Containing Glibenclamide: Development and *In Vitro* Characterization. *Int. J. Biol. Macromol.* 51 (5), 1070–1078. doi:10.1016/j.ijbiomac.2012.08.021

Nokhodchi, A., Raja, S., Patel, P., and Asare-Addo, K. (2012). The Role of Oral Controlled Release Matrix Tablets in Drug Delivery Systems. *BioImpacts* 2, 175–187. doi:10.5681/bi.2012.027

Ofokansi, K. C., Kenechukwu, F. C., and Ogwu, N. N. (2015). Design of Novel Miconazole Nitrate Transdermal Films Based on Eudragit RS100 and HPMC Hybrids: Preparation, Physical Characterization, *In Vitro* and *Ex Vivo* Studies. *Drug Deliv.* 22 (8), 1078–1085. doi:10.3109/10717544.2013.875604

Peddapalli, H., Ganta, R. P., and Boggula, N. (2018). Formulation and Evaluation of Transdermal Patches for Antianxiety Drug. *Asian J. Pharm.* 12, 127–136. doi:10.22377/ajp.v12i02.2325

Peppas, N. A., and Sahlin, J. J. (1989). A Simple Equation for the Description of Solute Release. III. Coupling of Diffusion and Relaxation. *Int. J. Pharm.* 57, 169–172. doi:10.1016/0378-5173(89)90306-2

Raza, M. A., Jeong, J.-O., and Park, S. H. (2021). State-of-the-Art Irradiation Technology for Polymeric Hydrogel Fabrication and Application in Drug Release System. *Front. Mat.* 8, 769436. doi:10.3389/fmats.2021.769436

Reynolds, J. E. F. (1993). *Martindale—The Extra Pharmacopoeia*. 30th ed. London: The Pharmaceutical Press.

Rydberg, T., Jönsson, A., Røder, M., and Melander, A. (1994). Hypoglycemic Activity of Glyburide (Glibenclamide) Metabolites in Humans. *Diabetes Care* 17, 1026–1030. doi:10.2337/diacare.17.9.1026

Saoji, S. D., Atram, S. C., Dhore, P. W., Deole, P. S., Raut, N. A., and Dave, V. S. (2015). Influence of the Component Excipients on the Quality and Functionality of a Transdermal Film Formulation. *AAPS PharmSciTech* 16, 1344–1356. doi:10.1208/s12249-015-0322-0

Singh, A., and Bali, A. (2016). Formulation and Characterization of Transdermal Patches for Controlled Delivery of Duloxetine Hydrochloride. *J. Anal. Sci. Technol.* 7, 25. doi:10.1186/s40543-016-0105-6

Thakral, S., Thakral, N. K., and Majumdar, D. K. (2013). Eudragit: a Technology Evaluation. *Expert Opin. Drug Deliv.* 10, 131–149. doi:10.1517/17425247.2013.736962

Tran, T. T. D., and Tran, P. H. L. (2019). Controlled Release Film Forming Systems in Drug Delivery: The Potential for Efficient Drug Delivery. *Pharmaceutics* 11, 290. doi:10.3390/pharmaceutics11060290

Vijaya, R., and Ruckmani, K. (2011). *In Vitro* and *In Vivo* Characterization of the Transdermal Delivery of Sertraline Hydrochloride Films. *Daru* 19, 424–432.

Yamsani, V. V., Mudulaghar, M. K., Afreen, S., Wajid, S., Ravula, S. K., and Babelghaith, S. D. (2017). Formulation Design and *In Vitro Ex Vivo* Evaluation of Transdermal Patches of Cinnarizine. *Pak. J. Pharm. Sci.* 30, 2075–2083.

Yoshida, T., Lai, T. C., Kwon, G. S., and Sako, K. (2013). pH- and Ion-Sensitive Polymers for Drug Delivery. *Expert Opin. Drug Deliv.* 10, 1497–1513. doi:10.1517/17425247.2013.821978

Conflict of Interest: The authors declare that the research was conducted in the absence of any commercial or financial relationships that could be construed as a potential conflict of interest.

Publisher's Note: All claims expressed in this article are solely those of the authors and do not necessarily represent those of their affiliated organizations, or those of the publisher, the editors, and the reviewers. Any product that may be evaluated in this article, or claim that may be made by its manufacturer, is not guaranteed or endorsed by the publisher.

Advantages of publishing in Frontiers

OPEN ACCESS
Articles are free to read for greatest visibility and readership

FAST PUBLICATION
Around 90 days from submission to decision

HIGH QUALITY PEER-REVIEW
Rigorous, collaborative, and constructive peer-review

TRANSPARENT PEER-REVIEW
Editors and reviewers acknowledged by name on published articles

Frontiers
Avenue du Tribunal-Fédéral 34
1005 Lausanne | Switzerland

Visit us: www.frontiersin.org
Contact us: frontiersin.org/about/contact

REPRODUCIBILITY OF RESEARCH
Support open data and methods to enhance research reproducibility

DIGITAL PUBLISHING
Articles designed for optimal readership across devices

FOLLOW US
@frontiersin

IMPACT METRICS
Advanced article metrics track visibility across digital media

EXTENSIVE PROMOTION
Marketing and promotion of impactful research

LOOP RESEARCH NETWORK
Our network increases your article's readership